1047

INVESTIGATION OF THE VAPOUR PHASE GROWTH OF OXIDE FILMS FROM METAL ALKOXIDES

by

Penelope Anne Lane

A Thesis submitted for the degree of Doctor of Philosophy of the University of London and for the Diploma of Membership of the Imperial College.

October 1988

Department of Materials
Royal school of Mines
Imperial College.

ABSTRACT

An investigation into the chemical vapour deposition of titanium dioxide and mixed oxide films of titanium and vanadium has been carried out. The oxides were grown in the temperature range 25-400^{o}C from titanium isopropoxide and vanadium triisopropoxide oxide.

The apparatus built for depositing the thin oxide films was a horizontal design which featured a liquid injection system, electrostatic atomisation of the precursor and provision for photolytic enhancement of growth.

The growth rate of titanium dioxide was determined as a function of substrate temperature, alkoxide injection rate and gas flow rate. A strong dependence on substrate temperature was observed; at lower temperatures the growth was kinetically controlled and at higher temperatures it was mass transport controlled. Increasing the alkoxide injection rate increased the growth rate especially in the mass transport controlled regime. Photolysis enhanced the oxide growth rate only in the kinetically controlled regime and reduced the activation energy by 0.16eV.

The crystal structure of the titanium dioxide films was identified as anatase and at growth temperatures below approximately 190^{o}C the structure was less crystalline and there was evidence from diffraction that the titanium isopropoxide had not completely decomposed to the oxide. Thermal analysis of the titanium isopropoxide gave results which were consistent with this explanation. Increasing the growth temperature resulted in a highly crystalline deposit which grew with preferred orientation.

The low temperature film characteristics were low refractive indices, unstable dielectric properties and high etching rates. At higher growth temperatures, higher refractive indices, stable dielectric properties and low etching rates were obtained.

The addition of vanadium oxide to titanium dioxide at a growth temperature of 250^{o}C led to a more amorphous crystal structure with higher refractive index, electrical conductivity and etching rate.

ACKNOWLEDGEMENTS

During the course of this PhD I have received both technical and moral support from many people. In particular I would like to thank my supervisor Dr B.A.Unvala, who started the present research group and enabled me to work in the field. The diverse nature of the work has meant that help and advice has come from a number of different sources. In particular I would like to thank Professor R.M.Hill of Kings College who has very generously allowed me to use the FRA on numerous occasions and has given me considerable guidance on the subject; my thanks are also extended to his group who have always been very kind and helpful to me. The measurement of droplet size was carried out at the Plant Protection Division of ICI with the kind permission of Dr R.A.Coffee and Mr Ian Pavey and useful discussions with Professor D.W.Pashley on the electron microscopy, Professor D.C.Bradley on alkoxide chemistry and Dr E.A.D. White on crystal growth are gratefully acknowledged. The project has involved a lot of apparatus building which would not have been possible without the technical support in the department. I would also like to thank my brother, Mr Stephen Lane who has carried out many ellipsometry measurements for me and has given me invaluable help with the photolysis side of the project. Finally to my collegues in the group, Mr Adam Wojcik and Mr Kevin Quick with whom working has been a very happy experience.

CONTENTS

Chapter 1 : INTRODUCTION

1.1 Uses of oxide films. 27

1.2 Methods of deposition. 27

1.2.1 Evaporation. 27

1.2.2 Sputtering. 28

1.2.3 Anodisation. 28

1.2.4 Sol gel. 29

1.2.5 Chemical vapour deposition. 29

1.3 Alkoxide compounds. 30

1.3.1 Properties of metal alkoxides. 30

1.3.2 Pyrolysis of metal alkoxides. 32

1.4 Reactor design. 34

1.4.1 Fluid dynamics of a horizontal reactor. 36

1.4.1.1 Reynolds number. 36

1.4.1.2 Rayleigh number. 37

1.4.1.3 Grashof number. 38

1.4.1.4 Entrance Effects. 39

1.4.1.5 Carrier gases. 41

1.4.2 Reactor design:experimental observations. 41

1.5 Growth of films. 48

1.6 Atomisation. 51

1.7 Photolysis. 56

1.7.1 Sources of UV. 56

1.7.2 Effect of UV. 57

1.7.3 Growth of oxide layers by photolysis. 57

CHAPTER 2 : LITERATURE SURVEY ON THE GROWTH OF TITANIUM DIOXIDE AND VANADIUM OXIDE FILMS.

2.1 Introduction. 61

2.2 Titanium dioxide. 61

2.2.1 Introduction to titanium dioxide. 61

2.2.2 Chemical vapour deposition of titanium dioxide films grown from metal alkoxide precursors. 65

2.2.3 Chemical vapour deposition of titanium dioxide films from titanium tetrachloride. 80

2.3 Vanadium oxide. 89

CHAPTER 3 : APPARATUS

3.1 Introduction. 93

3.2 Liquid injection. 94

3.2.1 Practical details. 94

3.2.1.1 Syringe operation. 94

3.2.1.2 Atomisation. 97

3.3 Vaporisation. 101

3.4 Reaction chamber. 102

3.5 Susceptor. 103

3.6 Susceptor heating. 104

3.7 Photolysis. 105

3.8 Characterisation of reactor. 107

3.8.1 Substrate temperature measurement. 107

3.8.2 Film uniformity as a function of gas flow rate. 108

3.8.3. Calculation of dimensionless numbers. 109

3.8.3.1 Calculation of Reynolds number. 112

3.8.3.2 Calculation of Rayleigh number. 112

3.8.3.3 Entrance lengths. 113

3.8.3.4 Ratio of Gr/Re^2. 113

3.9 Comparison with CVD growth by other workers. 114

CHAPTER 4 : CHARACTERISATION OF TITANIUM ISOPROPOXIDE AND VANADIUM TRIISOPROPOXIDE OXIDE

4.1 Thermal characterisation. 116

4.1.1 Thermal decomposition of titanium isopropoxide. 116

4.1.2 Thermal decomposition of vanadium triisopropoxide oxide. 119

4.2 Discussion of results. 121

4.3 Response of liquid alkoxide to UV illumination. 124

CHAPTER 5 : EXPERIMENTAL SECTION : INVESTIGATION INTO THE DEPENDENCE OF TITANIUM DIOXIDE GROWTH RATE ON SUBSTRATE TEMPERATURE, CONCENTRATION OF TITANIUM ISOPROPOXIDE AND GAS FLOW RATE.

5.1 Introduction. 127

5.2 Experimental details. 127

5.2.1 Thickness measurement. 127

5.2.1.1 Talystep. 128

5.2.1.2 Ellipsometry. 128

5.2.1.3 Interference colours. 128

5.2.2 Preparation for growth. 130

5.3.1 Growth rate as a function of substrate temperature and UV illumination. 130

5.3.2 Results of growth rate as a function of substrate temperature. 131

5.4.1 Growth rate as a function of precursor injection rate. 136

5.4.2.1 Results of growth rate as a function of precursor injection rate. 137

5.4.2.2 Effect of UV illumination. 142

5.5.1 Growth rate as a function of gas flow rate. 142

5.5.2 Results of growth rate as a function of gas flow rate. 143

CHAPTER 6 : CHARACTERISATION OF TITANIUM DIOXIDE FILMS AND OF MIXED TITANIUM AND VANADIUM OXIDE FILMS.

6.1 Introduction. 145

6.2 Oxide layers analysed. 146

6.2.1 Titanium dioxide films. 146

6.2.2 Mixed oxide films of titanium and vanadium. 146

6.2.2.1 Analysis of titanium and vanadium content in mixed oxide films 147

6.3 Experimental details. 148

6.3.1 X-ray diffraction. 148

6.3.2 Transmission Electron Microscopy. 149

6.3.3 Ellipsometry. 150

6.3.4 Electrical measurements of samples using a Frequency Response Analyser. 150

6.3.5 Etching. 153

CHAPTER 7 : RESULTS OF CHARACTERISATION OF OXIDE FILMS.

7.1 X-ray diffraction. 155

7.2 Transmission electron microscopy. 158

7.2.1 Microstructures of titanium films grown on sodium chloride substrates. 158

7.2.2 Electron diffraction of titanium dioxide films. 165

7.2.2.1 Analysis of diffraction patterns. 167

7.2.3 Diffraction patterns of mixed titanium-vanadium oxide films. 176

7.3 Ellipsometry 178

7.3.1 Ellipsometry of titanium dioxide films. 178

7.3.2 Ellipsometry of mixed titanium-vanadium oxide films. 183

7.4 Dielectric measurements of oxide films. 184

7.4.1 Introduction to dielectric behaviour. 184

7.4.1.1 Definitions. 184

7.4.1.2 The Debye model. 186

7.4.1.3 Limitations of Debye model. 187

7.4.1.4 Behaviour of dielectric response as a function of temperature. 189

7.4.1.5 Many body model. 190

7.4.2 Results of dielectric measurements. 192

7.4.2.1 Results of dielectric measurements of titanium dioxide films. 192

7.4.2.2 Results of dielectric measurements of titanium-vanadium mixed oxide films. 197

7.5 Etching 208

7.5.1 Etching of titanium dioxide films. 208

7.5.2 Etching of titanium-vanadium mixed oxide films. 210

CHAPTER 8 : DISCUSSION

8.1 Introduction. 211

8.2 Process details. 211

8.2.1 Efficiency of process. 211

8.2.2 Effect of illuminating the substrate during growth. 213

8.3 Properties of titanium dioxide films as a function of growth conditions. 217

8.3.1 Crystal structure of titanium dioxide films. 218

8.3.2 The change in film properties with growth temperature. 220

8.4 Titanium-vanadium mixed oxide films. 226

8.4.1 Introduction. 226

8.4.2 Structure of titanium-vanadium mixed oxide films. 227

8.4.3 Properties of titanium-vanadium mixed oxide films. 228

CONCLUSIONS 232

SUGGESTIONS FOR FURTHER WORK 235

REFERENCES 237

TABLES

page

Table 2.1 Temperature conditions of growth for amorphous, anatase and rutile forms of titanium dioxide. 64

Table 3.1 Summary of carrier gases and reactor types used in growth of titanium dioxide. 115

Table 5.1 Activation energies for titanium dioxide growth. 133

Table 7.1 Values of refractive index of titanium dioxide thin films. 181

Table 7.2 Summarising dielectric results. 207

Table 7.3 Summary of etching behaviour of titanium dioxide films. 209

FIGURES

CHAPTER 1 : INTRODUCTION

page

Figure 1.1 Pressure of zirconium tetra tert amyloxide as a function of time at 218.4°C after Bradley and Faktor (1959). 32

Figure 1.2 Schematic representation of conventional epitaxial reactors. 35

Figure 1.3 Development of flow and temperature profiles upon entering a top cooled CVD reactor after Giling (1983). 40

Figure 1.4 Interference fringes of an air cooled cylindrical cell with helium carrier gas, high flow velocity (70 $cmsec^{-1}$) and susceptor temperature of 1350K, after Giling (1982). 44

Figure 1.5 Isotherms in a horizontal reactor after Ban (1978). 45

Figure 1.6 A qualitative depiction of a transport model suggested by Ban (1978). 45

Figure 1.7 Computed variation in growth rate, V, expressed as a percentage of the maximum growth rate across the width of the tube for different tube geometries, after Andrews et al., (1969). 46

Figure 1.8 Optimized horizontal reactor, after Giling (1982). 47

Figure 1.9 Fringe pattern of optimized horizontal reactor of figure 1.8, after Giling (1982). 47

Figure 1.10 Effect of temperature on deposition in the absence of thermodynamic limitations, after Powell (1964). 49

Figure 1.11 Theoretical curves for growth flux as a function of temperature for kinetically controlled growth (A), transport controlled growth (B), and overall growth (C), after Hitchman (1981). 50

Figure 1.12 Stages of dispersion of liquid observed by increasing the applied potential, after Drozin (1955). 51

Figure 1.13 The charge to mass ratio of oil droplets as a function of droplet radius after Hendricks (1962). 53

Figure 1.14 Histogram showing distribution of droplet radii in electrostatically atomised spray after Hendricks (1962). 54

Figure 1.15 Di-isopropoxy aluminium diketonate, after Brierley (1987). 59

CHAPTER 2 : LITERATURE SURVEY

Figure 2.1 Anatase-rutile transformation against time at four temperatures, after Shannon and Pask (1965). 62

Figure 2.2a Crystal structure of anatase. 63

Figure 2.2b Crystal structure of rutile. 63

Figure 2.3 Apparatus for film preparation by CVD, after Feuersanger (1964). 66

Figure 2.4 Temperature dependence of titanium dioxide deposition rate from titanium isopropoxide for various oxygen concentrations, after Yokozawa et al., (1968). 67

Figure 2.5a Injection system used by Sladek and Gibert (1972) for oxide growth. 68

Figure 2.5b Rectangular duct reactor, after Sladek and Gibert (1972). 68

Figure 2.6 Alkoxide vapour pressures after Sladek and Gibert (1972). 69

Figure 2.7 Refractive index at 632.8nm as a function of deposition temperature after Hovel (1978). 71

Figure 2.8 Apparatus for thin film deposition, after Wang et al., (1970). 72

Figure 2.9 Temperature dependence of titanium dioxide deposition from titanium isopropoxide, after Takahashi et al., (1985). 75

Figure 2.10 Time dependence of titanium dioxide growth and rutile content for different oxygen concentrations, after Takahashi et al., (1985). 75

Figure 2.11 The dependence of deposition rate of titanium dioxide on water vapour at growth temperatures of 200 and 400°C, after Fuyuki et al., (1988). 76

Figure 2.12 The dependence of refractive index of titanium dioxide on water vapour concentration at growth temperatures of 200 and 400°C, after Fuyuki et al., (1988). 77

Figure 2.13 The dependence of etching rate of titanium dioxide films on growth temperatures of 200 and 400°C , after Fuyuki et al., (1988). 78

Figure 2.14 The dependence of dielectric constants of titanium dioxide on water vapour concentration during growth, after Fuyuki et al., (1988). 79

Figure 2.15 The densities of titanium dioxide films deposited by Hayashi and Hirai (1976), compared with other workers. 82

Figure 2.16 The temperature dependence of deposition rate of titanium dioxide films from titanium tetrachloride and 83

water vapour, after Hayashi and Hirai (1977).

Figure 2.17 Arrhenius plot of rutile thin film deposition from titanium tetrachloride and oxygen after Ghoshtagore and Noreika (1970), at three partial pressures of titanium tetrachloride. 84

Figure 2.18 Schematic representation of preferred rutile crystallite orientation in thin films as a function of substrate material, deposition temperature and orientation, grown from titanium tetrachloride and oxygen, after Ghoshtagore and Noreika (1970). 85

Figure 2.19 Refractive index of titanium dioxide films grown from titanium tetrachloride and water vapour as a function of deposition temperature, after Yeung and Lam (1983). 87

Figure 2.20 Part of the Vanadium-oxygen phase diagram, after Griffiths and Eastwood (1974). 90

Figure 2.21 Temperature dependence of the resistivity of $Ti_xV_{1-x}O$ co-sputtered films, after Balberg et al., (1974). 92

CHAPTER 3 : APPARATUS

Figure 3.1 Schematic diagram of CVD apparatus for oxide growth. 93

Figure 3.2 Diagram illustrating the lead screw mechanism for driving the syringe plunger. 95

Figure 3.3 Circuit diagram of electronic circuit to control stepper motor. 96

Figure 3.4a Atomisation of liquid by application of a high voltage. 98

Figure 3.4b Effect of an electrode on the jet of atomised liquid. 98

Figure 3.5 Schematic diagram of Forward Scattering Spectrometer Probe, after Knollenberg (1976). 99

Figure 3.6 Histogram of atomised droplet diameter sizes. 100

Figure 3.7 Diameter of droplet size as a function of different applied voltages. 100

Figure 3.8 The current of atomised spray as a function of different applied voltages. 101

Figure 3.9 Diagram of vaporisation chamber. 102

Figure 3.10 Diagram of reactor tube. 103

Figure 3.11 Diagram of stainless steel susceptor. 104

Figure 3.12 Diagram to illustrate the geometry of photolytic heating. 105

Figure 3.13 Typical output spectrum from 100W mercury bulb (Oriel Catalogue). 106

Figure 3.14 Calibration curve of temperature of substrate against temperature measured in susceptor block. 107

Figure 3.15 Diagram illustrating the size and position of a 38mm silicon slice relative to the susceptor and the reactor walls. 108

Figure 3.16a-d Photographs demonstrating the uniformity of oxide growth as a function of gas flow rate at a substrate temperature of 200°C. 110

Figure 3.17a-e Photographs demonstrating the uniformity of oxide growth as a function of gas flow rate at a substrate temperature of 350°C. 111

CHAPTER 4 : CHARACTERISATION OF TITANIUM ISOPROPOXIDE AND VANADIUM TRIISOPROPOXIDE OXIDE.

Figure 4.1 Thermal decompostion of titanium isopropoxide as studied by DTA/TGA. 116

Figure 4.2a Debye-Scherrer x-ray of titanium isopropoxide heated to 400°C showing an anatase crystal structure. 118

Figure 4.2b Debye-Scherrer x-ray of titanium isopropoxide heated to 980°C, showing a mixture of anatase and rutile. 118

Figure 4.3 Thermal decomposition of vanadium triisopropoxide oxide. 119

Figure 4.4a Debye Scherrer x-ray of vanadium triisopropoxide oxide heated to 450°C. 118

Figure 4.4b Debye Scherrer x-ray of vanadium triisopropoxide oxide heated to 750°C, showing predominantly V_2O_3 reflections. 118

Figure 4.5 TGA curve showing decomposition of zirconium alkoxide in a nitrogen atmosphere, after Madiyasni et al.,(1965). 121

Figure 4.6 Decomposition steps of zirconium alkoxide after Madiyasni et al., (1965). 122

Figure 4.7 Sample of titanium isopropoxide after illuminating with UV light. 125

Figure 4.8 Sample of vanadium triisopropoxide oxide after illuminating with UV light. 125

CHAPTER 5:INVESTIGATION INTO THE GROWTH RATE DEPENDENCE OF TITANIUM DIOXIDE FILMS ON SUBSTRATE TEMPERATURE, PRECURSOR CONCENTRATION AND GAS FLOW RATE

Figure 5.1 Schematic diagram of Talystep operation. 128

Figure 5.2a-g Photographs of interference colours of titanium dioxide films. 129

Figure 5.3 An Arrhenius plot of ln(Growth Rate) of titanium dioxide against the reciprocal of the absolute temperature for a precursor injection rate of 0.35×10^{-7} moles s^{-1}. and a gas flow rate of $73.3 cm^3 s^{-1}$. 131

Figure 5.4 An Arrhenius plot of ln(Growth rate) of titanium dioxide against the reciprocal of the absolute temperature for two precursor injection rates and showing the effect of illuminating the substrate with UV. 132

Figure 5.5a-e Photographs of titanium dioxide grown onto 30mm diameter silicon slices illustrating the increasing effect of UV illumination with decreasing substrate temperature. 135

Figure 5.6 Ratio of thickness of titanium dioxide films grown under UV illumination to thickness of film grown with no illumination, as a function of substrate temperature. 136

Figure 5.7a-e Growth rate of titanium dioxide films as a function of precursor injection rates at substrate temperatures of 190, 220, 300, 350 and 390°C. 137 -139

Figure 5.8 Best line fits of oxide growth rates at substrate temperatures of 190, 220, 300, 350 and 390°C as a function of precursor injection rates. 141

Figure 5.9 An Arrhenius Plot of ln(Growth Rate) of titanium dioxide against the reciprocal of the absolute temperature 142

for a selection of precursor injection rates.

Figure 5.10 Growth rates of titanium dioxide films as a function of gas flow velocity. 143

CHAPTER 6 : EXPERIMENTAL TECHNIQUES USED IN CHARACTERISATION OF OXIDE FILMS.

Figure 6.1 The composition of the deposited oxide films of titanium and vanadium as a function of precursor solution composition 147

Figure 6.2 Schematic diagram of the FRA after Pugh, (1984). 151

Figure 6.3 Diagram of the sample used for dielectric measurement. 152

CHAPTER 7 : RESULTS OF CHARACTERISATION OF OXIDE FILMS

Figure 7.1 X-ray diffraction results for titanium dioxide films grown at (a) 170, (b) 200, (c) 250, (d) 300 and (e) 350°C. 155

Figure 7.2 Anatase powder diffraction data. 156

Figure 7.3 X-ray diffraction trace of anatase thin film after Wang et al.,(1970). 157

Figure 7.4 Adsorption sites present on a crystal surface after Lewis and Anderson (1978). 159

Figure 7.5 Preferred orientation of titanium dioxide on cleavage steps of sodium chloride substrate at growth temperatures of (a) 100, (b) 180 and (c) 275°C. 160

Figure 7.6a Illustrating the growth if the diffusion length is greater than the separation distance of the cleavage steps. 161

Figure 7.6b Illustrating the growth if the diffusion length is less than the separation distance of the cleavage steps. 162

Figure 7.7a-d Microstructure of titanium dioxide films grown on sodium chloride substrates showing a change in morphology with increasing growth temperature (a)100, (b) 160, (c) 275 and (d) 400°C. 163 - 164

Figure 7.8a-h Electron diffraction patterns for titanium dioxide deposited at growth temperatures of (a) 100, (b) 160, (c) 190, (d) 220, (e) 280, (f) 350, (g) 400 and (h) 400°C. Showing increasing crystallinity and orientation with higher temperatures. 166

Figure 7.9 Calculated diffraction patterns for polycrystalline anatase. 167

Figure 7.10 Illustrating growth with the (001) parallel to the substrate. 169

Figure 7.11 Diffraction pattern for growth with the (001) parallel to the substrate. 169

Figure 7.12 Illustrating growth with (100) or (010) parallel to the substrate. 170

Figure 7.13 The diffraction pattern for the (100) or (010) parallel to the substrate. 170

Figure 7.14 The positions of titanium atoms in the anatase unit cell used for the structure factor determination. 171

Figure 7.15 Diffraction pattern of two orthogonal positions of (100) planes growing parallel to the substrate. 172

Figure 7.16 Diffraction pattern of (100) parallel to the substrate in two orthogonal positions and of (001) parallel to the substrate. 172

Figure 7.17 Illustrating possible epitaxial relationships between sodium chloride and anatase. 173

Figure 7.18 Illustrating the extra reflections observed in figure 7.8f. 174

Figure 7.19 Illustrating the presence of the diffraction pattern due to the (001) parallel to the substrate in samples grown at 400°C. 175

Figure 7.20 Electron diffraction patterns of titanium-vanadium oxide films. 177

Figure 7.21a Values of refractive index as a function of growth temperature for the non-illuminated samples. 178

Figure 7.21b Values of refractive index as a function of growth temperature of illuminated samples. 178

Figure 7.21c Values of refractive index as a function of growth temperature after a post-deposition anneal at 1000°C. 179

Figure 7.22 Refractive index values of titanium dioxide films as a function of deposition temperature. 180

Figure 7.23 Thickness reduction of samples after annealing at 1000°C as a function of original growth temperature. 182

Figure 7.24 Refractive index values of mixed vanadium-titanium oxides as a function of vanadium content. 183

Figure 7.25 The frequency dependence of the real and imaginary components of the complex susceptibility from the ideal Debye response. 187

Figure 7.26 A general classification of all types of dielectric response in the entire range of solids and liquids after Jonscher (1975). 188

Figure 7.27 Potential energy diagram of a many-body two level system representing the energy of a large number of interacting systems. 190

Figure 7.28 The dielectric response as a function of frequency of titanium dioxide grown at 190°C for different measurement temperatures. 193

Figure 7.29 The results of the dielectric response of titanium dioxide grown at 190°C, normalised at 363K. 194

Figure 7.30 Ln[frequency shift] plotted against the reciprocal of the absolute temperature for all oxide samples measured. 195

Figure 7.31 Ln[dc conductivity] plotted against the reciprocal of the absolute temperature for all oxide samples measured. 196

Figure 7.32 Normalised dielectric response of the 20%V film. 198

Figure 7.33 Normalised dielectric response of 53%V film. 199

Figure 7.34 Plot of exponent 'n' against % vanadium. 199

Figure 7.35 Normalised dielectric response of 85%V film. 200

Figure 7.36 Normalised dielectric response of 100%V film. 201

Figure 7.37 Representation of the dielectric sample in terms of parallel capacitor-resistor pairs in series. 202

Figure 7.38 Dielectric response of resistor-capacitor combination illustrated in figure 7.37. 202

Figure 7.39 A computer curve fit of dielectric response of 100%V oxide film (Experimental response shown in figure 7.36). 203

Figure 7.40 Plot of activation energy for dc conductances as a function of atomic %V. 204

Figure 7.41 Plot of ln[dc conductivity] as a function of atomic %V. 205

Figure 7.42 Plot of activation energy for frequency shift as a function of atomic %V. 206

Figure 7.43 Etch rate of titanium dioxide films as a function of deposition temperature in concentrated sulphuric acid at 150°C. 208

Figure 7.44 Etch rate of titanium-vanadium mixed oxide films as a function of vanadium content. 210

CHAPTER 8 : DISCUSSION

Figure 8.1 Plot of calculated maximum growth rate and experimentally observed growth rate as a function of alkoxide injection rate. 212

Figure 8.2 Plot of efficiency of process as a function of alkoxide injection rate. 213

Figure 8.3 Illustrating the change in Arrhenius plot with alkoxide rate. 215

Figure 8.4 Schematic diagram illustrating the change in ln[growth rate] with the reciprocal of the absolute temperature for different alkoxide concentration. 216

Figure 8.5 Schematic diagram summarising results of decomposition and film properties as a function of temperature. 221

Figure 8.6 Schematic diagram of relative free energies of titanium dioxide in the low temperature amorphous structure (ΔG_1), anatase (ΔG_2) and rutile (ΔG_3), compared with the free energy in solution in sulphuric acid etch. 224

CHAPTER 1 : INTRODUCTION

1.1 USES OF OXIDE FILMS

Oxide thin films have numerous uses in modern technology. In the electronics industry thin oxide films are used for the insulated gate of a field effect transistor (FET), for surface passivation, capacitors and masking. With the increasing use of III-V semiconductors such as gallium arsenide (GaAs) and indium phosphide (InP) there is a need to be able to deposit good quality oxide layers at low temperatures. The III-V semiconductors, unlike silicon, do not have good protective native oxides on the surfaces and they begin to decompose at relatively low temperatures.

1.2 METHODS OF PRODUCTION

There are several processes that can be used to grow oxide films and these are briefly described in sections (1.2.1) to (1.2.5).

1.2.1 EVAPORATION

Evaporation is a physical process and many materials can be evaporated in vacuum and allowed to condense on cooled substrates. Titanium dioxide films have been prepared by evaporating titanium metal and subsequently oxidising the layer (Hass, 1952). This method produces good quality titanium dioxide rutile films if the vacuum is better than 10^{-5} mmHg. Evaporation of $TiO_x (0 < x < 2)$ has been carried out (Yamada and Yoshida 1979) and the oxygen content of the film was lower than that of the source material.

1.2.2 SPUTTERING

Sputter deposition is also a physical process and involves the bombardment of the target material with energetic primary particles. The interaction of these particles with the target material can result in a surface atom being ejected and condensing on the substrate. The velocity of the ejected material is an order or more higher than in the evaporation process. Sputtering may be ion beam based (10^{-5} to 10^{-2} Pa) or plasma based (10^{-1} to 10Pa). In ion beam sputtering the ion beam impinges on the target material and ejects target atoms which condense on the substrate. In plasma based sputtering the discharge formed provides the energetic ions that are needed for the ejection. Argon is generally the working gas for sputtering but for oxide deposition, oxygen is often added as a reactive gas. Oxide materials can become depleted of oxygen under ion bombardment due to the preferential sputtering of the more volatile oxygen species and adding a reactive gas compensates for this.

1.2.3 ANODISATION

Anodizing is an aqueous process in which the metal is the anode placed in a suitable electrolyte. When electric current is passed an oxide layer is formed. The oxygen is obtained from the electrolyte and the thickness of the film is limited to the distance the ions can penetrate the oxide under the influence of the applied potential.This technique is obviously limited to growth of oxides on metal substrates.

1.2.4 SOL GEL

The sol gel process for producing oxide films is a chemical process and involves coating the substrate with a solution of metal alkoxide and subsequent processing results in an oxide film on the substrate. The process consists of mixing the alkoxides to the required composition (for mixed oxides) and addition of water to initiate a hydrolysis reaction. Subsequent heating removes the water and organic material. Titanium dioxide layers were deposited on GaAs (Bertrand and Fleischauer, 1983) by imersion in a titanium alkoxide.

1.2.5 CHEMICAL VAPOUR DEPOSITION

Chemical vapour deposition (CVD) is a process where the film is deposited from the vapour phase by means of a chemical reaction. The most common precursor materials for oxide growth are the metal chlorides, the metal alkoxides and the metal alkyls. The chloride route can either use water vapour (Yeung and Lam, 1983) or oxygen (Ghoshtagore and Noreika, 1970), as illustrated in equations (1.1) and (1.2).

$$TiCl_4 + 2H_2O = TiO_2 + 4HCl \quad ---(1.1)$$

$$TiCl_4 + O_2 = TiO_2 + 2Cl_2 \quad ---(1.2)$$

The reaction for growth from the metal alkoxides can be by hydrolysis or thermal decomposition as given in equations (1.3) and (1.4)

$$Ti(OC_3H_7)_4 = TiO_2 + 4C_3H_6 + 2H_2O \quad ---(1.3)$$

$$Ti(OC_3H_7)_4 + 2H_2O = TiO_2 + 4(C_3H_7OH) \quad ---(1.4)$$

The reaction for the metal alkyl deposition of oxides is given by equation (1.5)

$$2MR_3 + O_2 = M_2O_3 + xCO_2 + yH_2O \quad ---(1.5)$$

The technique of oxide growth chosen in this investigation is CVD from the alkoxide precursor. The reasons for this choice are:

(1) The technique can be used to deposit oxides on any substrate.
(2) It is compatible with the growth of semiconductor materials by organo metallic vapour phase epitaxy (OMVPE).
(3) The growth can be carried out at low temperatures which is a requirement for deposition on III-V semiconductors which degrade at higher temperatures.
(4) The alkoxides can be readily purified.
(5) The apparatus is relatively simple compared to the physical deposition techniques which require low pressure conditions.

1.3 ALKOXIDE COMPOUNDS

1.3.1 PROPERTIES OF METAL ALKOXIDES

The metal alkoxides are a class of compounds characterised by the metal-oxygen-carbon bonding system. A comprehensive account of alkoxide chemistry is given by Bradley et al.,(1978) from which the following information has been taken. The basic formula is $M(OR)_n$ where R is an alkyl or aryl group. The elements which can form alkoxides are numerous and a considerable gradation in physical properties ranging from the non-volatile

solid, ionic alkali metal alkoxides to volatile monomeric liquid alkoxides of silicon and germanium is shown.

For use as a precursor for chemical vapour deposition the metal alkoxide needs to be sufficiently volatile to provide a high enough vapour pressure for growth at an acceptable rate. The volatilities of the alkoxides have been investigated and appear to depend mainly on two factors:

(A) Molecular size and shape of the alkoxide group

The volatility of members of an homologous series of monomeric alkoxides $M(OR)_n$ decreases with increasing chain length of R. For an isomeric series the increasing ramification of the chain can lead to an increase in volatility due to reduction in intermolecular forces.

(B) Nature of the Central Atom

The electropositive nature of the central atom exerts a strong influence on the volatility of the alkoxide . The more electropositive metals such as the alkali metals are much less volatile and are solids due to their predominantly ionic character. Less electropositive central atoms such as silicon give volatile liquids. Size of the central atom is also an important factor; a smaller atom is easier to shield by the organic groups thus reducing intermolecular association which reduces volatility.

To grow a metal oxide from a metal alkoxide the compound has to be decomposed in a controlled manner. The presence of the electronegative alkoxy groups makes the metal atom susceptible to nucleophilic attack and a common feature of many alkoxides is their susceptibility to hydrolysis. This feature is utilized to varying extents in oxide production from metal alkoxides. In

some cases water has been added to promote rapid decomposition (Fitzgibbons et al.,1972) and in other cases care has been taken to achieve anhydrous conditions. The particular experimental conditions for deposition are discussed later in chapters 3 and 5.

1.3.2 PYROLYSIS OF METAL ALKOXIDES

The pyrolysis of metal alkoxides has been investigated by Bradley and Faktor (1959)a. Kinetic studies of zirconium tetra-tert-amyloxide showed that despite careful experimental conditions the results displayed a lack of reproducibility. However the reaction, at a temperature of 218.4°C, had a characteristic sigmoid shape of pressure against time curve as shown in figure 1.1.

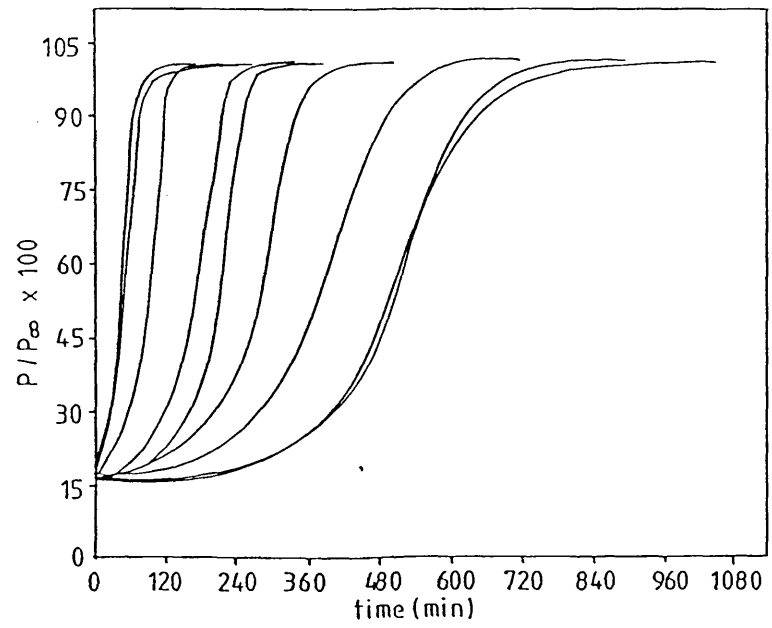


Figure 1.1 Pressure of Zirconium Tetra Tert Amyloxide Samples at 218.4°C as a Function of Time after Bradley and Faktor, (1959)a.

The ratio of the ultimate pressure of the system to the initial pressure of the alkoxide was six which is consistent with the reaction in equation (1.6).

$$Zr(OC_5H_{11}{}^t)_4 = ZrO_2 + 4C_5H_{10} + 2H_2O \quad ---(1.6)$$

Cooling down to room temperature reduced the pressure ratio to four which is in agreement with equation (1.6), with water condensing out.

Irreproducible results from studying the dehydration of alcohol suggested to the authors that this maybe the rate controlling step. The sigmoid shape of the pressure time curves suggested a chain mechanism which is consistent with one molecule of water being produced from one molecule of alcohol which in turn regenerates two molecules of alcohol by hydrolysis of the alkoxide. The sequence of decomposition is given as:

$$C_5H_{11}OH \longrightarrow C_5H_{10} + H_2O \quad ---(1.7)$$

(rate determining)

$$Zr(OC_5H_{11})_4 + H_2O \longrightarrow ZrO(OC_5H_{11})_2 + 2C_5H_{11}OH \quad ---(1.8)$$

(very fast)

$$2ZrO(OC_5H_{11})_2 = Zr(OC_5H_{11})_4 + ZrO_2 \quad ---(1.9)$$

The decomposition of Zr-tert-amyloxide was found to be more rapid at higher temperatures and was also greater when the surface area of the reactor was increased.

Conclusions from the results concerning the thermal

stability of metal alkoxides were:

(1) A metal alkoxide is potentially unstable at any temperature at which the rate of heterogeneous decomposition of the alcohol is appreciable.

(2) The hydrolytic decomposition depends on how easily the alcohol is dehydrated which explains the order of stabilities decreasing from the ethoxide to the isopropoxide to the tertiary butoxide and the amyloxide.

(3) It is possible to retard the hydrolytic decomposition of the alkoxide by removing the alcohol as it is formed. Experiments at constant pressure resulted in a long life of the alkoxide samples. However the presence of oxygen was observed to enhance the decomposition of zirconium tert-pentyloxide and zirconium tert-butoxide (Bradley and Faktor,(1959)b).

1.4 REACTOR DESIGN

To deposit thin films from the precursor a CVD reactor is used. The general requirements of such a system are:

(1) To transport the precursor material into the reactor.

(2) To provide a site for controlled reaction to occur.

(3) To remove waste products.

The design of the reactor is important because it determines the film uniformity, growth rate and efficiency. The chemicals can be metered into the reactor in various ways. If the precursor is a gas e.g. arsine for GaAs growth, the gas flows directly into the reactor and is usually metered by a mass flow controller. If the precursor is a liquid e.g. tri-methyl gallium or titanium

isopropoxide, the most common method is to bubble carrier gas through the liquid which is kept at a constant temperature. An alternative route is to syringe the liquid into a vaporiser. The basic types of conventional epitaxial reactor are shown schematically in figure 1.2a-d.

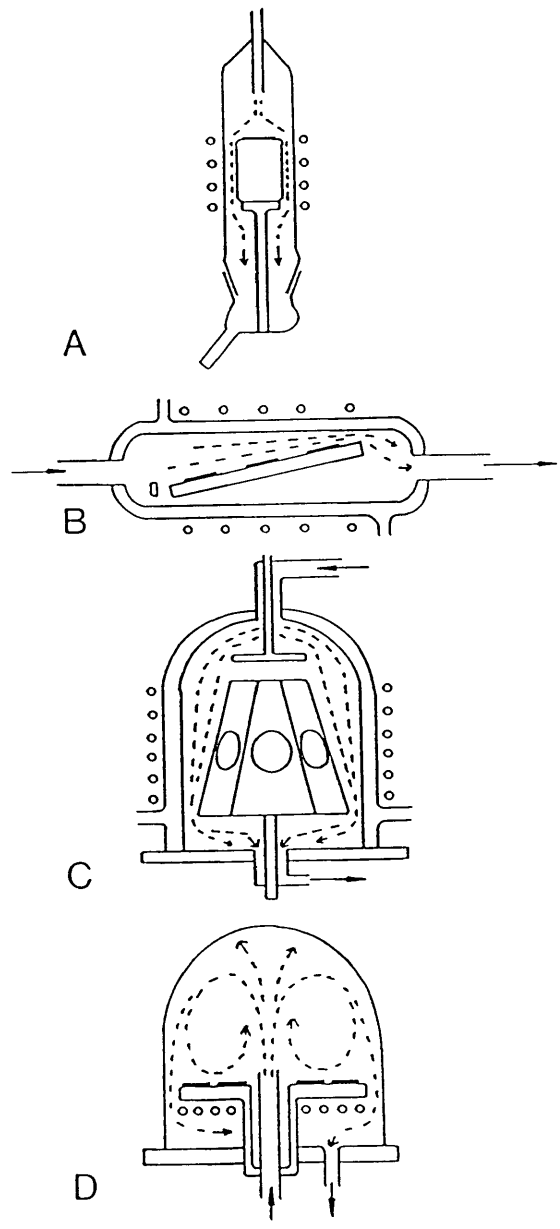


Figure 1.2 Schematic Representation of Conventional Epitaxial Reactors

Figure 1.2a is a single wafer reactor used for research purposes, figure 1.2b is a horizontal reactor, figure 1.2c is a 'barrel' reactor, and figure 1.2d is a 'pancake' reactor. The horizontal and barrel reactors are displacement reactors where the gas entering continually replaces the reacted gases. The gas entering the pancake reactor mixes with the reacted gases. The type of reactor employed in the present work is the horizontal reactor figure 1.2b, and will thus be discussed more extensively.

1.4.1 FLUID DYNAMICS OF A HORIZONTAL REACTOR

1.4.1.1 REYNOLDS NUMBER

The dynamic behaviour of the gas flowing through a tube at constant temperature can be characterised by the dimensionless Reynolds number (Re) as given in equation (1.10)

$$Re = \frac{vh\rho}{\eta} \quad ---(1.10)$$

where v = mean flow rate (ms^{-1})

h = height of tube (m)

ρ = density (Kgm^{-3})

η = coefficient of viscosity ($Kgm^{-1}s^{-1}$)

For values of Re less than 2300 the flow is laminar; the layers of gas move cooperatively through the tube and each layer has a slightly different velocity. For this flow regime the velocity profile across the cross section of the tube is parabolic and the profile remains constant. At higher Re a transition from laminar to turbulent flow can occur; this flattens out the velocity

profile and motion perpendicular to the direction of flow occurs, increasing the mixing of the fluid and the resistance to flow. Hence the value of Re defines the flow regime. Re is temperature dependent and higher temperature can stabilize the flow. The majority of CVD systems operate in the laminar flow regime defined by the value of Re (Giling,1983).

1.4.1.2 RAYLEIGH NUMBER

The presence of a hot susceptor in the reactor requires some consideration of the effect of free convection. Free convection can be characterised by the Rayleigh number (Ra), as given in equation (1.11).

$$Ra = \frac{g C_p \rho^2 \beta h^3 \Delta T}{\eta \kappa} \qquad ---(1.11)$$

where:

β = coefficient of thermal expansion (K^{-1})

g = 9.81 (ms^{-2})

C_p = specific heat ($JKg^{-1}K^{-1}$)

ρ = density (Kgm^{-3})

h = free height above the susceptor (m)

ΔT = T(bottom) - T(top) (K)

η = coefficient of viscosity ($Kgm^{-1}s^{-1}$)

κ = thermal conductivity ($Jm^{-1}s^{-1}K^{-1}$)

For a value of Ra less than approximately 1700, the gas is stable and for Ra greater than 1700 free convection occurs.

1.4.1.3 GRASHOF NUMBER

The Grashof number is often used instead of the Rayleigh number. The Grashof number (Gr), is given by equation (1.12)

$$Gr = \frac{\rho^2 g l^3 \beta \Delta T}{\eta^2} \quad ---(1.12)$$

ρ = density (gcm^{-3})

g = 9.81 (ms^{-2})

l = linear dimension (m)

η = coefficient of viscosity ($Kgm^{-1}s^{-1}$)

β = expansion coefficient (K^{-1})

ΔT = temperature difference (K)

This is actually the Rayleigh number divided by the Prandtl number (Pr), where Pr is given by equation (1.13)

$$Pr = \eta C_p / \kappa \quad ---(1.13)$$

C_p = specific heat ($JKg^{-1}K^{-1}$)

κ = thermal conductivity ($Js^{-1}m^{-1}K^{-1}$)

η = coefficient of viscosity ($Kgm^{-1}s^{-1}$)

The Prandtl number depends only on the properties of the medium and for gases the value lies between 0.4 and 1. The Grashof number is a measure of the force due to the buoyancy caused by heating and this is of the same order of magnitude as the inertia and viscous forces if $Gr \approx Re^2$ (Schlichting, 1955). Sparrow et al., (1959), have used the value of Gr/Re^2 to categorise flow into

forced convection, where the buoyancy effects are negligible, combined flow, where the buoyancy and forced convection contribute and free convection where the buoyancy forces dominate. The flow criteria were derived for a flow around a vertical flat plate and were numerically divided into three classes with respect to heat transfer which are given in equations (1.14), (1.15) and(1.16).

$$Gr/Re^2 > 16 \qquad \text{free convection} \qquad ---(1.14)$$

$$16 > Gr/Re^2 > 0.3 \qquad \text{combined flow} \qquad ---(1.15)$$

$$0.3 > Gr/Re^2 \qquad \text{forced convection} \qquad ---(1.16)$$

These criteria have been used by a number of workers investigating flow in CVD reactors. An analysis using a horizontal flat plate model (Mori, 1961) to investigate the effects of buoyancy forces in a forced laminar convection flow showed that the relevant parameter was $Gr/Re^{2.5}$.

1.4.1.4 ENTRANCE EFFECTS

When the gas enters the reactor both the velocity and temperature profiles have to adjust to the new conditions. This is shown schematically in figure 1.3, (Giling, 1982).

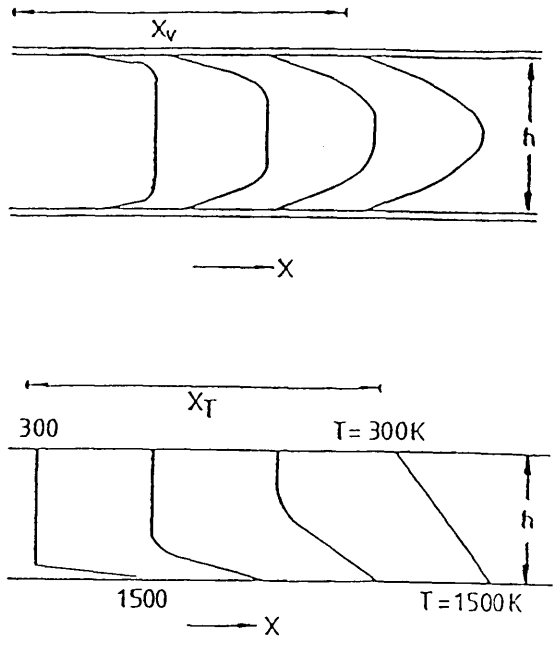


Figure 1.3 Development of Flow and Temperature Profiles entering a Top Cooled CVD Reactor. X_V = entrance length velocity profile, X_T = entrance length temperature profile, after Giling (1983).

The length over which the profiles develop is an entrance effect and the velocity and temperature entrance lengths X_V and X_T respectively are given in equations (1.17) and (1.18).

$$X_V = 0.04hRe \quad ---(1.17)$$

$$X_T = 0.28hRe \quad ---(1.18)$$

These undeveloped profiles produce varying boundary layers. Considering a fluid flowing over a flat plate, the fluid adheres to the plate surface and frictional forces retard the motion of the fluid in a thin layer near the plate. In this layer the velocity increases from zero at the plate surface to the bulk value and the layer is termed the boundary layer. This concept is due to Prandtl(1904). Thermal and diffusion boundary layers also

exist in CVD reactors, but a single boundary layer can be considered because all three layers are of approximately the same thickness (Hitchman,1980).

1.4.1.5 CARRIER GASES

Calculation of the values of Re and Ra for the carrier gases hydrogen, helium, nitrogen and argon at different temperatures has shown that hydrogen and helium are much more stable than nitrogen and argon, (Giling, 1983). The stable laminar flows and smaller entrance effects of the hydrogen and helium compare with the convective behaviour of the nitrogen and argon with an overall motion of two or more convection rolls which spiral through the reactor. However a stable layer can exist close to the hot susceptor because the gas velocity is lower; stable laminar flow exists and convection is depressed because of the high temperature.

1.4.2 REACTOR DESIGN; EXPERIMENTAL OBSERVATIONS

The flow patterns of the gas were first demonstrated by titanium dioxide smoke particles (Eversteyn et al.,1970). The reactor was a rectangular water cooled quartz tube and the effect of increasing gas velocity on the flow patterns was observed with the susceptor at a temperature of 1050^{o}C. At a low gas velocity of 15 cms^{-1}, the streamlines were seen separately but at higher velocities (up to 180 cms^{-1}), a dark layer was observed directly above the substrate and the streamline pattern was confined to the upper region of the reactor. The dark layer was said to be a region of zero velocity and was termed the 'stagnant' layer. This effect was also observed by Ban and Gilbert,(1975), but they

considered the layer next to the susceptor to be in laminar flow.

Further smoke test experiments (Takahashi et al.,1972), observed combined free and forced convection spiral flow of nitrogen and pure forced convection laminar flow as a function of flow rates and pressures. Takahashi et al.,(1972) used the classification of flow criteria developed by Sparrow et al.,(1959) to determine free convection flow, equations (1.14), (1.15) and (1.16). The transition condition from combined to forced convection flow occurred at 0.4-4.1. Ban(1978) also used this criterion and for $Gr/Re^2 \geq 0.5$ a fully developed spiral was observed and for $Gr/Re^2 < 0.5$ upward deflection of the streamline occurred. The validity of this classification has been questioned by Giling (1982) who observed no such correlation in his experiments. Giling (1982) pointed out that although no characteristic differences between the values of Gr/Re^2 existed for nitrogen and hydrogen, the latter gave a stable laminar flow while nitrogen gave a highly unstable and convective flow.

The technique of using smoke tests in CVD reactors to observe the gas flow has received criticism; it was pointed out by Westphal (1983) and Giling (1983) that the presence of a hot surface has a significant influence on the motion of the particles, this is due to a thermal diffusion effect which enhances the diffusion of light molecules and inhibits the diffusion of heavy ones. An alternative technique for observation of gas flow is interference holography which has been comprehensively investigated by Giling (1982). The results give a density map and each interference fringe observed is thus an isotherm. When the flow is turbulent the image will not be

stationary but under stable flow conditions convection can be observed by curved isotherms. When the flow is laminar and not convective, fringes parallel to the hot surface are formed. Experiments investigating the geometry of the reactor cross section (circular or rectangular), whether the reactor was water cooled or air cooled and the type of carrier gas, were carried out. It was concluded that a water cooled top rectangular reactor gave the most uniform condition with helium or hydrogen as a carrier gas. For hydrogen and helium the flow was observed to develop a parabolic velocity profile within a few centimeters of the leading edge of the susceptor and no variation of the boundary layer was present. For velocities less than 10 cms^{-1}, the temperature profile was also completely developed within a few cm of the susceptor. The highly convective flows and severe entrance effects of nitrogen and argon were seen, but under certain conditions the presence of a laminar layer just above the reactor and a convective part in the main stream were evident. The temperature gradient occurred predominantly in the laminar region above the substrate. With an air cooled top the presence of closed concentric rings was evident as shown in figure 1.4.

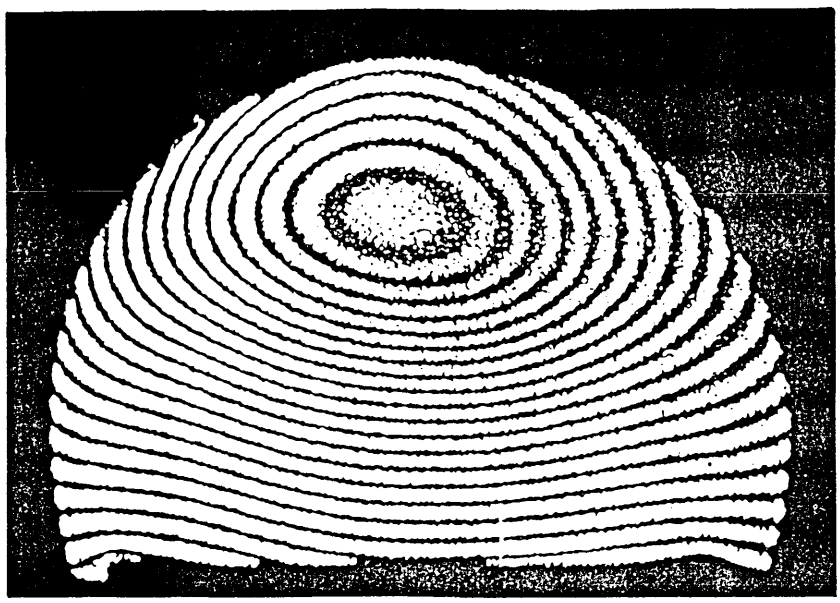


Figure 1.4 Interference Fringes of an air cooled Cylindrical Cell with Helium Carrier Gas, a high flow velocity (70 cms^{-1}) and temperature of susceptor = 1350K, after Giling (1982).

This was termed 'cold finger' and represented a cooler stream of gas flowing through the reactor. These occurred because the wall heating caused expansion of the gas and increase in its viscosity thus increasing the resistance to flow. To maintain the imposed flow rate the velocity in the cooler part of the reactor increased and the temperature dropped.

Experimental measurements of flow (by smoke tests) temperature and concentration were carried out by Ban (1978) for a reactor growing silicon epitaxial layers. The temperature profiles taken along the axis of the reactor for helium carrier gas with a susceptor temperature of 1200^{o}C are shown in figure 1.5.

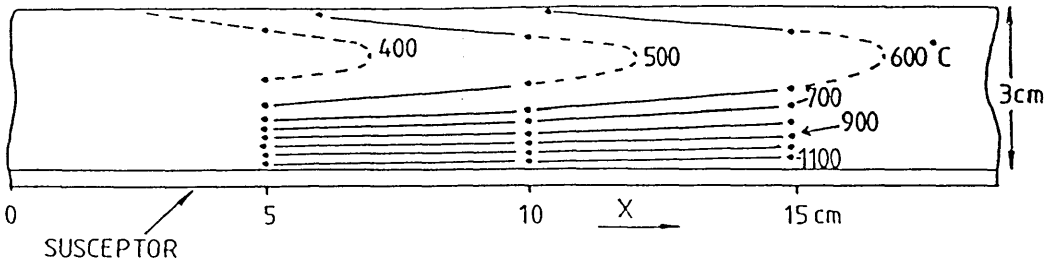


Figure 1.5 Isotherms in a Horizontal Reactor, Flow velocity = 50cms^{-1}, He carrier gas, after Ban (1978).

The temperature gradient is steep close to the susceptor and practically flat further away. Ban (1978) noted that for the same gas velocity and temperature, the gradients were steeper in nitrogen than helium and shallower temperature gradients were present at lower velocities. A more complete model including the concentration profiles, velocity and temperature is shown qualitatively in figure 1.6.

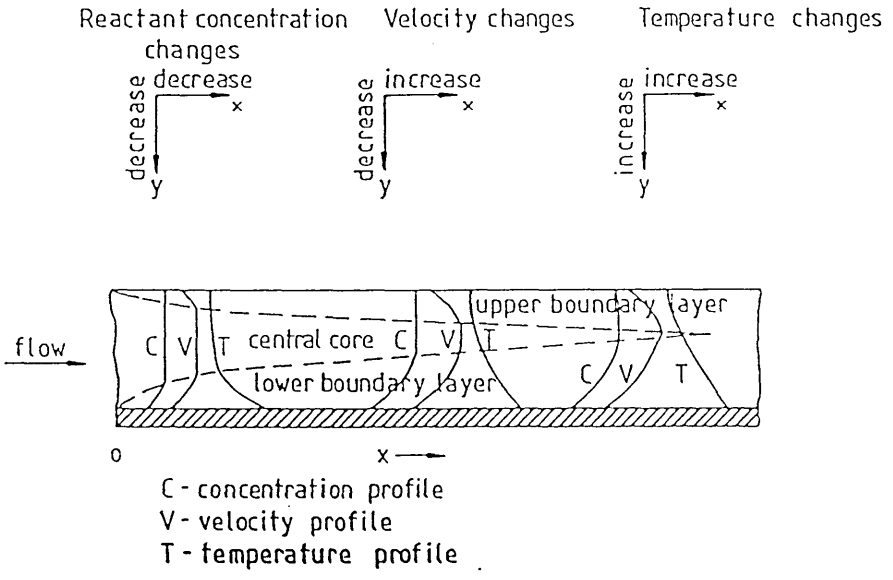


Figure 1.6 A Qualitative Depiction of a Transport Model Suggested by Ban (1978).

The entry effects and the resulting influence on velocity, temperature and partial pressure gradients are shown. The velocity, temperature and diffusion boundary layers are shown to be of the same order of magnitude.

The geometries of the reactor tube used are circular and rectangular. The rectangular geometry has been stated by several authors to provide the most uniform deposition conditions. Considerations into the free height above the susceptor are also important. Andrews et al. (1969), computed growth rates across the width of three reactor tube geometries and the results are shown in figure 1.7. The rectangular tube with the smallest free height gave the most uniform deposition.

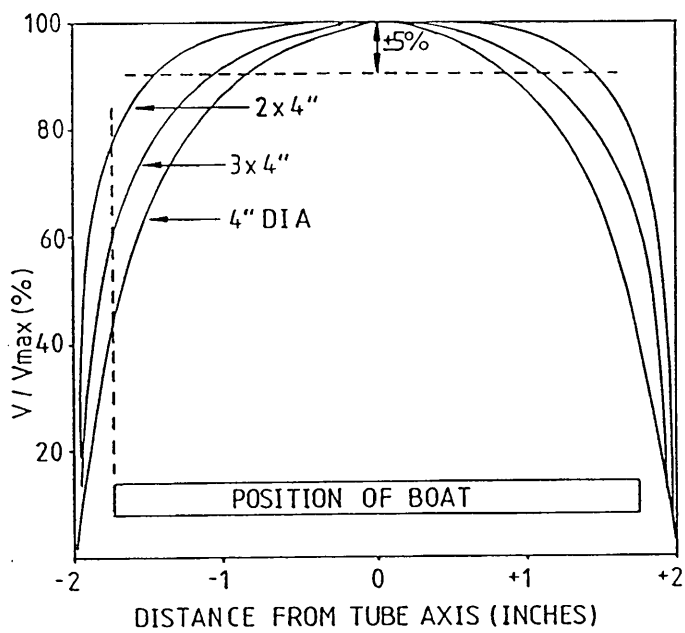


Figure 1.7 Computed Variation in Growth Rate, V, Expressed as a Percentage of the Maximum Growth Rate Across the Width of the Tube for Different Geometries, after Andrews et al.,(1969).

An optimized horizontal reactor suggested by Giling (1982) is shown in figure 1.8.

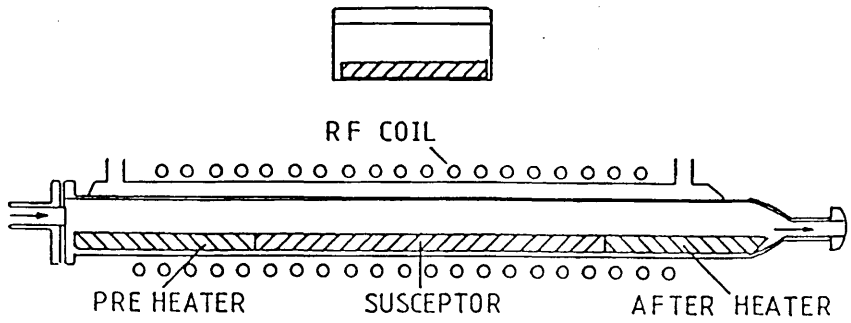


Figure 1.8 Optimized Horizontal Reactor after Giling, (1982).

The cross section is rectangular with a small free height and a water cooled top jacket. Preheaters and a long entrance zone allow full development of velocity and temperature profiles before the deposition zone is reached. The cell has no sudden changes in geometry which encourage vortex formation. The interference hologram (figure 1.9) shows flat horizontal isotherms with no evidence of convection, entrance effects or vortices.

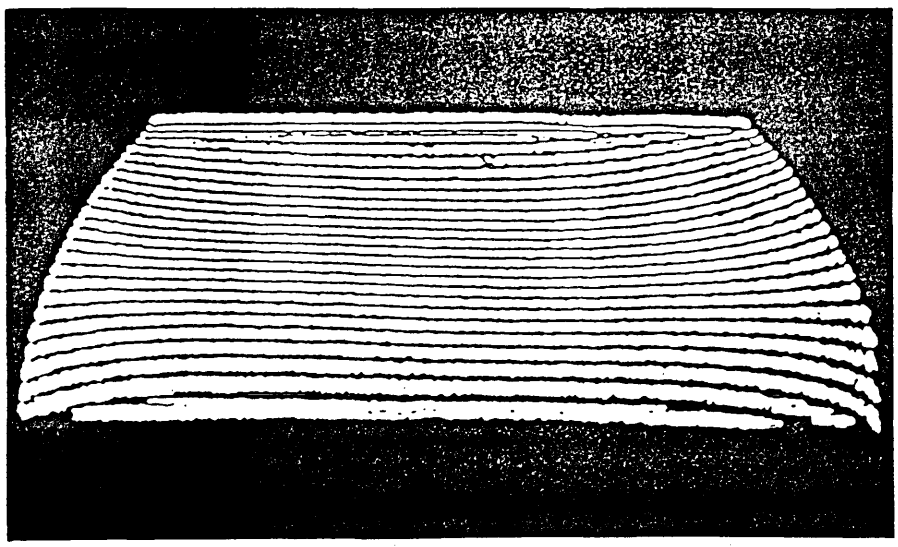


Figure 1.9 Fringe Pattern of Optimized Horizontal Reactor of Figure 1.8.

The growth rate can decrease along the length of the susceptor due to depletion of reactants. The practice of tilting the susceptor compensates for this by reducing the boundary layer (Eversteyn et al.,1970).

1.5 GROWTH OF FILMS

The growth of thin films by CVD is a complex process. A typical sequence of events is:

(1) Transport of reactant materials to the growth surface.
(2) Diffusion of reactants from the gas stream to the substrate surface.
(3) Adsorption of molecules on the surface.
(4) Surface events such as chemical reactions, surface diffusion and lattice incorporation.
(5) Desorption of products from the surface.
(6) Diffusion of products from the surface.

These processes occur sequentially and the slowest one will determine the growth rate and be the rate determining step. If the rate determining step is adsorption, a surface event or desorption, the process is kinetically controlled and can be described by an Arrhenius type equation. Kinetically controlled reactions generally occur in the lower temperature range of the growth process, are strongly temperature dependent and relatively insensitive to flow rate. At higher temperatures the growth rate is often mass transport controlled and it is the diffusion of reactants to, or products from the surface which are the dominating events. The growth rate is less dependent on

temperature and more dependent on flow. The terms diffusional and kinetic control are applied and refer to the resistance offered by each process. In the higher temperatures the observed growth rate may decrease. This can be due to homogeneous nucleation in the vapour phase or deposition on reactor walls; both events deplete the concentration of reactant and reduce growth rate. A typical growth rate dependence on temperature is shown in figure 1.10.

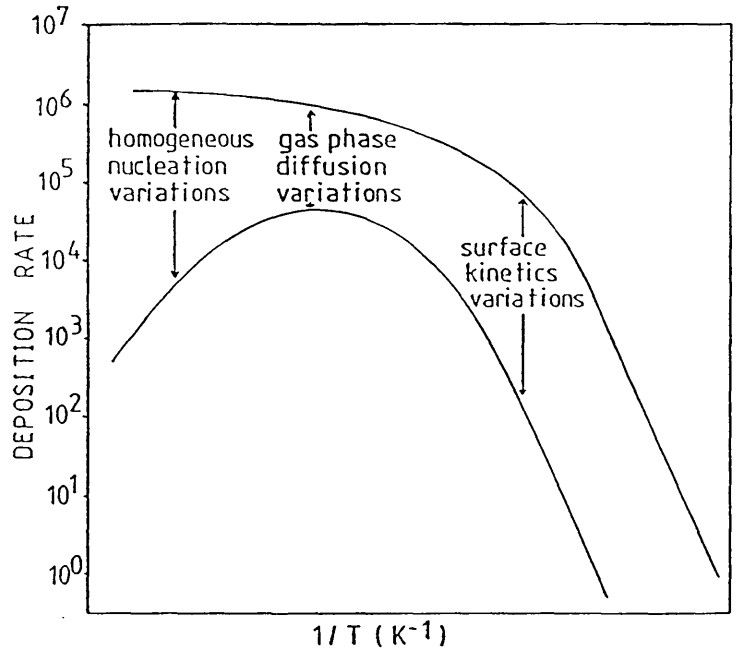


Figure 1.10 Effect of Temperature on Deposition Rate in the Absence of Thermodynamic Limitations after Powell, (1966).

A detailed theoretical discussion on the roles of kinetic and mass transport in heterogeneous growth has been given by Hitchman (1981). A description of the overall growth flux in terms of the kinetic and transport contributions is shown in figure 1.11.

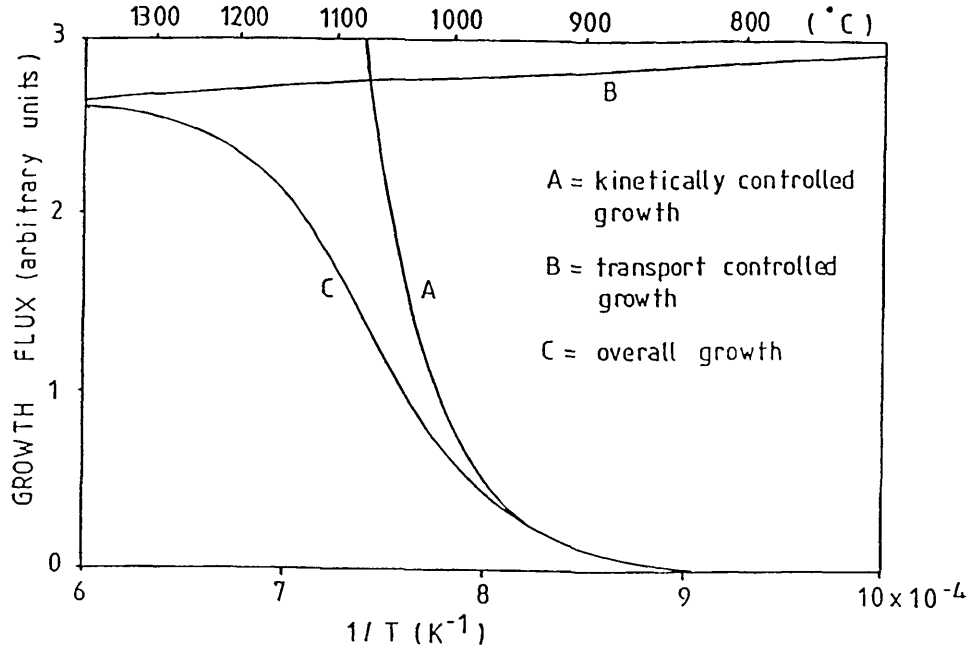


Figure 1.11 Theoretical Curves for Growth as a Function of Temperature for Kinetically Controlled Growth (A), Transport Controlled Growth (B) and Overall Growth (C), after Hitchman (1981).

The transport controlled growth is seen to be only weakly dependent on temperature and the kinetically controlled growth is expontially dependent on temperature. A gradual transition from kinetically controlled to transport controlled growth is evident as the temperature increases. Hitchman (1981) pointed out that erroneous values of activation energy occurred in the literature unless this slow transition from kinetic to diffusion control was taken into account and unless identical conditions of reactant concentration were considered.

1.6 ATOMISATION

The technique of electrostatically atomising a liquid has been utilised in the present work to grow oxide thin films from metal alkoxides. Electrostatic atomisation has many diverse applications and is a well established technology.

When a drop forms at the end of a needle with no applied potential the drop grows until its weight overcomes the net vertical component of the surface tension force. The liquid then forms a neck close to the needle which ruptures causing the majority of the drop to fall. When a voltage is applied to the needle the force due to the interaction of the induced charge and electric field is in the same direction as the gravitational force. Thus the drop size is reduced when a DC potential is applied. When the DC potential is increased from zero to 12kV, several stages of dispersion have been observed (Drozin 1955), as illustrated in figure 1.12.

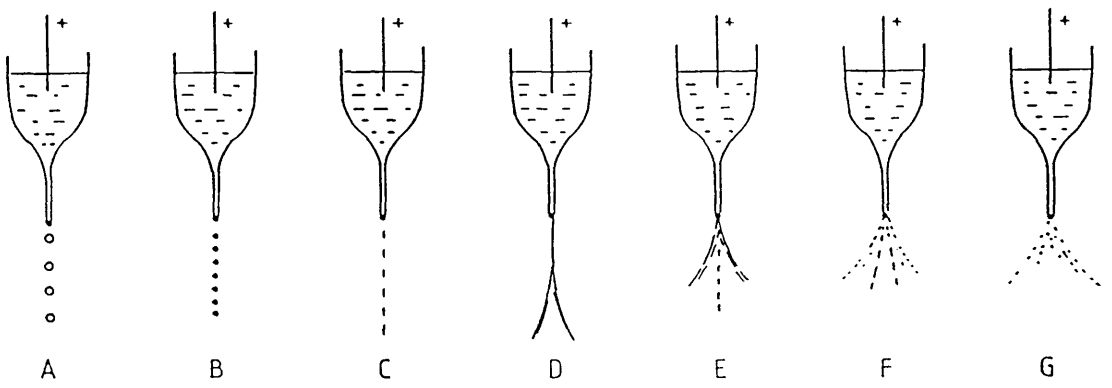


Figure 1.12 Stages of Dispersion of Liquid Observed by Increasing the Applied Potential after Drozin, (1955).

The application of a low potential caused the rate of droplet production to increase (B). Increasing the potential produced elongated droplets (C), then a steady thread (D) which broke up a distance from the capillary tip. The length of the thread reduced in (E) and with further voltage increase fine droplets became the dominant emission (G).

The first recorded investigation of the effect of an electric charge on a liquid was by Bose (1745). The explanation of the effect was put forward by Rayleigh in 1882, who considered a spherical drop of an ideally conducting liquid. The electic charge developed on the droplet is present as a surface charge and thus produces an outward electrostatic force which opposes the surface tension forces acting inwards. The drop becomes unstable when the electrostatic charge just exceeds the inward surface tension pressure, as shown in equation (1.19).

$$\frac{Q^2}{32\pi^2 r^4 \epsilon_0} > \frac{2\sigma}{r} \quad ---(1.19)$$

q = charge

r = radius of drop

σ = surface tension

ϵ_0 = permittivity of free space

The maximum charge to mass ratio is thus given by equation (1.20).

$$q/m = \sqrt{(36\ \epsilon_0\ \sigma / r^3\ \rho^2)} \quad ---(1.20)$$

m = mass

ρ = density

The theoretical charge to mass ratio predicted by Rayleigh's theory has been investigated experimentally by Hendricks (1962) using oil drops. The maximum observed charge to mass ratios of the oil drops at any radius were found to be very close to the Rayleigh limit. This is shown in figure 1.13.

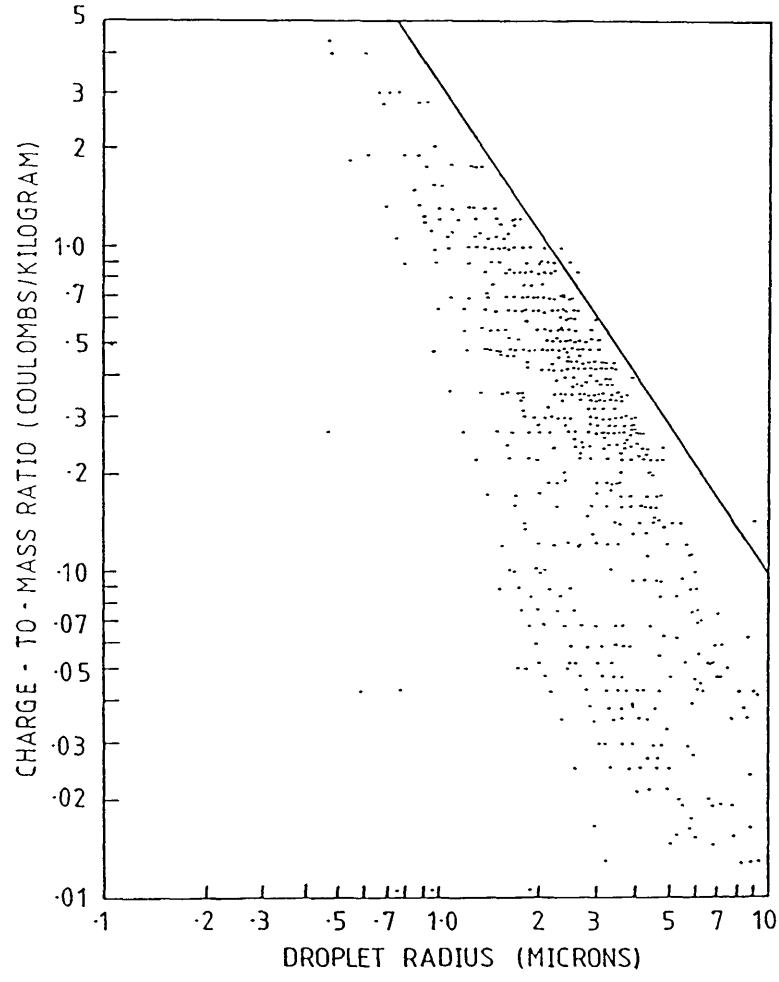


Figure 1.13 The Charge to Mass Ratio of Oil Droplets as a Function of Droplet Radius after Hendricks, (1962).

A droplet with a charge to mass ratio greater than the Rayleigh limit is theoretically unstable and should split up. The disruption of droplets at the Rayleigh limit has been observed by Schweizer and Hanson (1971). A charged droplet was suspended between two charged plates and allowed to evaporate. The charge density on the surface of the drop increased as

evaporation proceeded and when the Rayleigh limit was reached several daughter droplets were ejected. The large droplet remaining retained 77% of the initial charge and 95% of the mass.

When an electrostatically atomised spray is produced the emitting droplets generally consist of a range of sizes and are said to be polydisperse. The distribution of oil droplet radii found by Hendricks (1962), is shown in the histogram in figure 1.14.

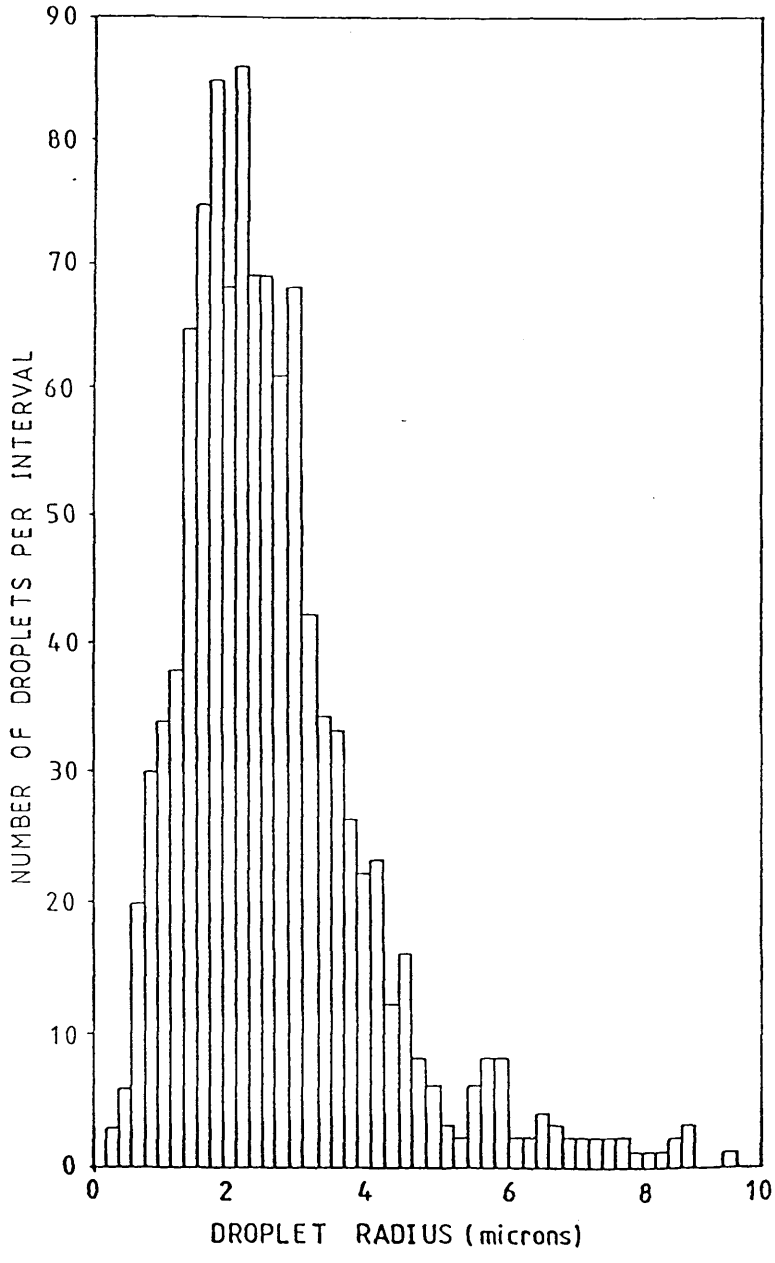


Figure 1.14 Histogram showing Distribution of Droplet Radii in Electrostatically Atomised Spray, after Hendricks (1962).

Monodisperse aerosols have been reported by Vonnegut and Neubauer (1952). The aerosol produced was assessed by the colours in the higher order Tyndall spectra. They put forward the hypothesis of the minimum energy of the system where a charged spherical drop tends to a state in which the surface energy and the energy of coulombic interaction of surface charges is a minimum. This energy state corresponds to the droplets formed when a primary drop breaks up. The equilibrium size and number of particles for the process was derived and Ryce (1964) extended the calculation to an expression for the limiting value of q/m and found it to be half the Rayleigh value. This fitted the majority of Hendricks' (1962) data points (figure 1.13) and was in agreement with the data of Sample and Bollini (1972).

The practical conditions which are relevant in applying electrostatic atomisation to the liquid injection of a precursor for oxide growth are small liquid flow rates (ul/hr) and voltages of up to 10kV at atmospheric pressure. This type of atomisation is termed 'electrohydrodynamic' atomisation (Kozgenkov and Fuks, 1976). The hydrodynamic and gravitational forces are less important because of the small mass flows involved and the charge on the drops increases until the instability point is reached. The theoretical model of an isolated spherical droplet is not an accurate description of the conditions present in emmision from a tube and Hendricks et al.,(1964) modified Rayleigh's theory of stability to consider spraying from a hemispherical meniscus of liquid maintained at the end of a capillary tube. A general expression for the minimum spraying potential was derived as a parametric relationship as given in equation (1.21).

$$U^2_{min} = 20 \sigma \pi (300)^2 a \quad ---(1.21)$$

Umin = minimum spraying potential

σ = surface tension

a = radius

Experimentally this relationship gave an under estimate of the minimum potential but the trend was confirmed. The value of Umin is the capillary potential at which pulsed spraying in a low charge to mass ratio mode commences. For dc spraying a higher value of potential is required and the hemispherical meniscus on which the derivation is based will be replaced by a meniscus which recedes into the bore of the capillary tube (Bailey, 1974).

1.7 PHOTOLYSIS

The use of UV illumination in the field of chemical vapour deposition is at present rapidly expanding. UV light can be used to enhance the growth of materials, to grow at lower temperatures and in selective areas. In addition to deposition the process of photoetching is receiving considerable attention.

1.7.1 SOURCES OF UV LIGHT

Both excimer lasers and mercury arc lamps have been used as a source of UV light. The Hg arc lamp has a broad emission spectrum (figure 3.12), with a UV line at 253.7nm and the wavelength obtainable from the laser sources are 193nm (ArF), or 248nm (KrF). The laser source provides a more powerful light source and can be tightly focussed which is useful in line writing.

1.7.2 EFFECT OF UV LIGHT

The interaction of UV light with the CVD system can influence the deposition of material by several routes:

(1) Local heating.
(2) Electronic excitation of the reactants in the gas phase or in the condensed phase.
(3) Excitation of the solid substrate.

The effect of local heating of the substrate due to the UV illumination is classified as pyrolytic and the mechanism of localised deposition is thermal excitation of the gas phase in the immediate vicinity.

The interaction of light with the reactant molecule can cause electronic excitation. This excited state can promote growth in several ways. The molecular bands are often sufficiently weakened to have a high probability of breaking thermally (Haigh 1983). The sticking coefficient of the excited molecule to the substrate may be enhanced and if the initial chemisorption is non-dissociative UV excitation may cause adsorbed molecules to fragment.

The interaction of light with the solid substrate can effect the growth of a film. The absorption of the light (particularly laser source) can alter the electronic structure of the material which can increase or reduce the degree of absorption. These interactions of light are discussed in detail by Chuang (1982).

1.7.3 GROWTH OF OXIDE LAYERS BY PHOTOLYSIS

Growth of oxide layers at low temperatures is useful in device

production. High temperatures allow dopant profiles to diffuse and III-V compound semiconductors can degrade. The process of photolysis can reduce the temperature of growth of oxide layers and has been used in the present work.

Silicon dioxide has been grown by a photolytic process from a mixture of silane, N_2O and Hg vapour irradiated by a Hg lamp source (253.7nm). The UV activates the mercury atoms which can transfer energy to the SiH_4 and N_2O molecules, (a mercury photosensitized reaction). The reaction is given in equation (1.22),(Peters, 1981).

$$2N_2O^* + SiH_4^* = SiO_2 + 2N_2 + 2H_2 \quad ---(1.22)$$

A direct photolytic reaction to deposit silicon dioxide eliminates the presence of Hg vapour and the UV photons liberate atomic oxygen from the molecular donor molecules (N_2O) by photodissociation (Boyer et al.,1982, Peters, 1981). Boyer et al.,(1982), used an ArF (193nm) laser with the beam parallel to the substrate surface. This created a reaction volume very close to the substrate with a minimal number of UV photons interacting with the substrate. The deposition rate was observed to be proportional to the gas pressure and laser intensity but independent of substrate temperature between 20 and 600°C. At substrate temperatures below 200°C however, the deposited oxide films were milky in appearance and easily scratched. Above 200°C the films were transparent and uniform and above 250°C the films were very adherent and scratch resistant.

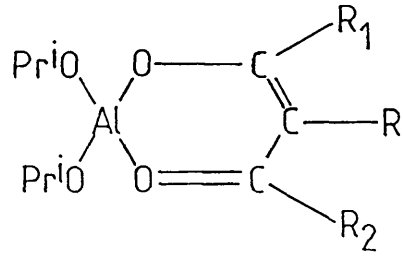
Aluminium oxide has also been grown by photolytic processes. Solanki et al., (1983), used trimethyl aluminium and N_2O as

precursors, and the source of UV was an excimer laser operating at 248nm or 193nm. The detailed mechanism of the reaction was not well understood but as in the growth of silicon dioxide (Boyer et al.,1982) production of excited atomic oxygen from N_2O occurred. The reaction was summarized (equation 1.23):

$$Al(CH)_3 + N_2O + h\nu = Al_2O_3 + \text{products} \quad ---(1.23)$$

In the absence of UV illumination no oxide deposition occurred.

Deposition of aluminium oxide by photolytic processing has been carried out by Brierley, (1987). The precursor for the reaction is a di-isopropoxy aluminium diketonate as shown in figure 1.15.



Pr^i = isopropoxide

Figure 1.15 Di-isopropoxy Aluminium Diketone, after Brierley, (1987).

This family of compounds have absorption peaks in the 250-300nm range.

Chromium oxide films have been grown photolytically from chromyl chloride vapour (CrO_2Cl_2), (Arnone et al.,1986). This system is unusual in that the photochemical deposition is with an

Ar-ion laser operating at 488-515nm. Analysis of the decomposition by a quadrupole mass spectrometer showed a chlorine atom flux and indicated that the photodissociation is via one of two subsequent single photon photolysis reactions (equation 1.24)

$$CrO_2Cl_2 = CrO_2Cl + Cl = CrO_2 + Cl + Cl \quad ---(1.24)$$

CHAPTER 2 LITERATURE SURVEY ON THE GROWTH OF TITANIUM DIOXIDE AND VANADIUM OXIDE FILMS

2.1 INTRODUCTION

An extensive amount of literature exists on the growth of oxide films from metallo organic precursors. The majority of the present work is concerned with the growth of titanium dioxide from titanium isopropoxide and some preliminary work on vanadium oxide from vanadium triisopropoxide oxide has also been carried out. The literature on these two oxide systems is reviewed and includes different precursors, both organic and inorganic.

2.2 TITANIUM DIOXIDE

2.2.1 INTRODUCTION TO TITANIUM DIOXIDE

Titanium dioxide exhibits three polymorhic forms; anatase, brookite and rutile. Brookite is only found as a natural crystal but anatase and rutile can be synthesised. Rutile is the thermodynamically stable structure and both anatase and brookite transform exothermically and irreversibly to rutile when heated to about 1000 and 750^{o}C respectively (Shannon and Pask, 1965). Investigation into the anatase to rutile transformation (Shannon and Pask, 1965) showed that the reaction started with the nucleation of rutile on the anatase surface, followed by growth into the anatase. The reaction as a function of time exhibited a sigmoid curve as shown in figure 2.1, for several temperatures. The initial increasing rate is due to nucleation and decreasing rate is dominated by growth rate.

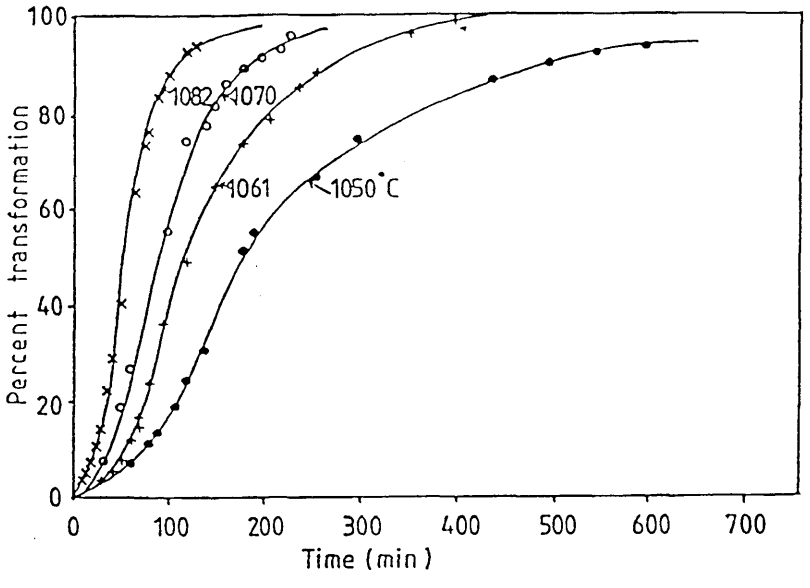


Figure 2.1 Anatase-Rutile Transformation as a Function of Time at Four Temperatures after Shannon and Pask, (1965).

Anatase and rutile are isomeric and both belong to the tetragonal system (Vergard,1916), but they are not isomorphous; rutile has a c:a ratio of 0.644 and anatase has a c:a ratio of 1.777. The crystal structures of anatase and rutile are shown in fig 2.2a and 2.2b respectively.

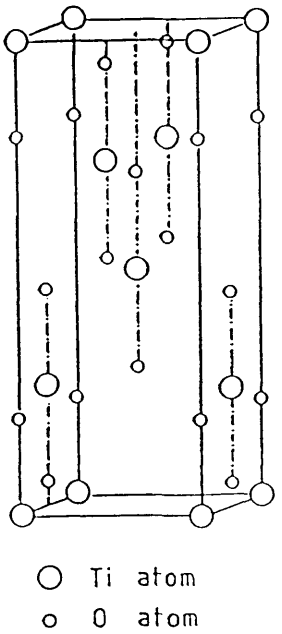


Figure 2.2a Crystal Structure of Anatase

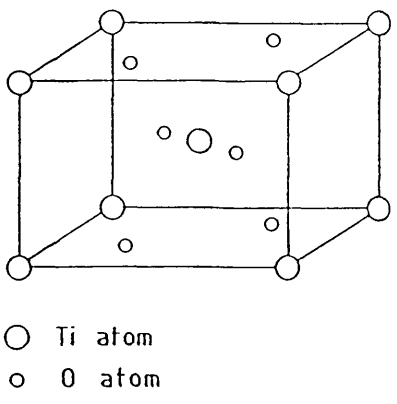


Figure 2.2b Crystal Structure of Rutile

The titanium dioxide films deposited by CVD have been reported to be amorphous, anatase or rutile in form. The conditions under which each have been deposited are summarised in table 2.1.

Table 2.1 Temperatures of growth for Amorphous, Anatase and Rutile Forms of Titanium Dioxide

PRECURSOR	CRYSTAL STRUCTURE OF TITANIUM DIOXIDE DEPOSITED				
	amorphous	anatase	rutile	comment	reference
$Ti(OPr^i)_4$	200	400	-	+water	Fuyuki et al. (1988)
$Ti(OPr^i)_4$	-	400-600	500	rutile grows on anatase	Takahashi et al. (1985)
$Ti(OPr^i)_4$	-	445-565		large gas velocity	Takahashi et al. (1981)
$Ti(OPr^i)_4$	200-300	200-300	-	+water	Hovel (1978)
$Ti(OPr^i)_4$	550	550	-		Balog et al. (1972)
$Ti(OPr^i)_4$	150	anneal 350	anneal 1000	+water	Fitzgibbons et al. (1972)
$Ti(OPr^i)_4$	110	←anneal 1000→			Sladek & Gibert (1972)
$Ti(OPr^i)_4$	-	100-400	800-1000		Wang et al.(1970)
$Ti(OPr^i)_4$	700	700	-	amm. in O_2	Yokozawa et al. (1968)
$TiCl_4$	180	180	-		Yeung & Lam (1983)
$TiCl_4$ + H_2O	100-200	300 A+R	400-900		Hayashi & Hirai (1976)
$TiCl_4$ + O_2	-	-	717-827		Ghoshtagore & Noreika (1970)
$TiCl_4$	280	280	anneal 900		Hass (1952)

$Ti(OPr^i)_4$ = Titanium isopropoxide

2.2.2 CHEMICAL VAPOUR DEPOSITION OF TITANIUM DIOXIDE FILMS GROWN FROM ORGANOMETALLIC PRECURSORS

The use of titanium isopropoxide to deposit titanium dioxide films was mentioned briefly by Haslam (1959). The pyrolysis started at approximately 350°C and the primary decomposition products were tentatively said to be propylene, isopropyl alcohol and titanium dioxide. The pyrolysis was carried out by impinging either an air or nitrogen stream containing a low concentration of titanium isopropoxide onto a surface at 500-600°C. A clear titanium dioxide film was deposited which was considerably harder than the films produced by hydrolysis and were said to contain no residual organic matter.

Titanium dioxide films were grown by Feuersanger (1964) by the hydrolysis of titanium tetrachloride and titanium isopropoxide. The intended use of these films was for integrated electronic applications. Titanium dioxide has a high dielectric constant which is insensitive to temperature and to frequencies into the gigacycle range. The oxide films were grown at a substrate temperature of 150°C and the reactive vapours were passed through a concentric nozzle which was heated to 160°C. This was situated 1.5cm above the substrate placed on a heater in the atmosphere. The apparatus is shown in figure 2.3.

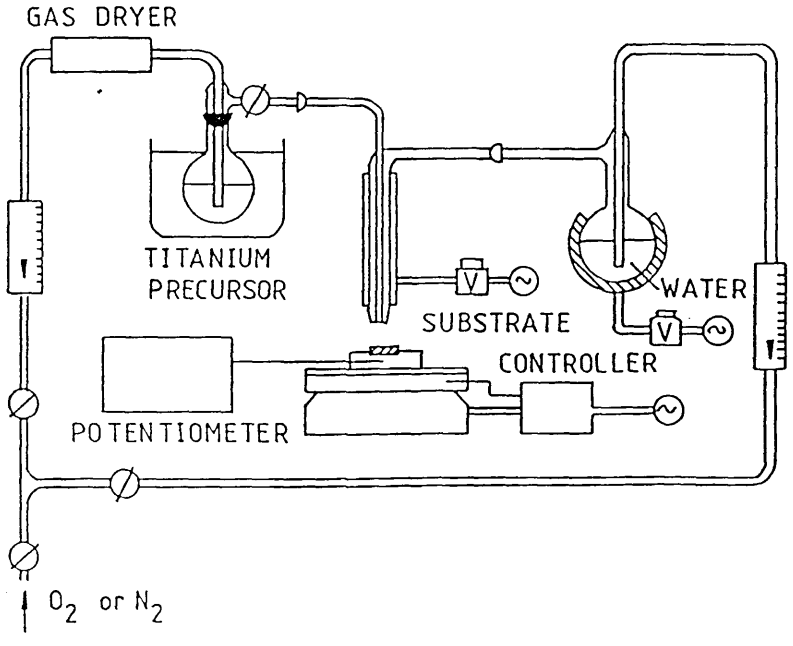


Figure 2.3 Apparatus Used by Feuersanger (1964) to Prepare Oxide Films by Chemical Vapour Deposition

Thin films of titanium dioxide were deposited on a silicon substrate by the thermal decomposition of titanium isopropoxide (Yokozawa et al.,1968). The deposition temperatures were lower than 700°C and the growth was investigated as a function of oxygen content. No water was added in these investigations. The presence of oxygen was found to increase the growth rate at lower temperatures. At higher temperatures the rate became independent of the oxygen content. These results are shown in figure 2.4.

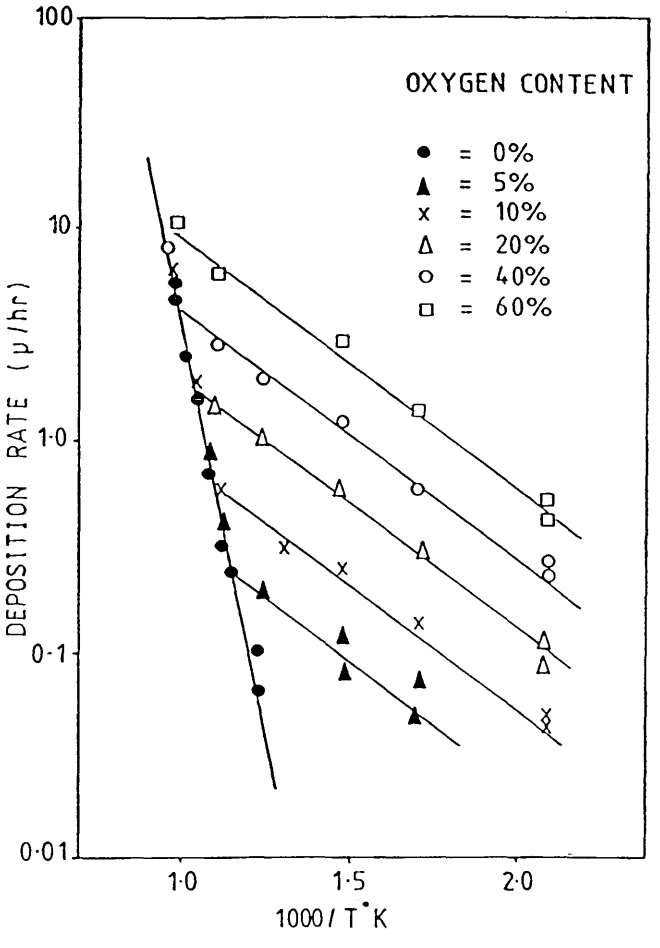


Figure 2.4 Temperature Dependence of Titanium Dioxide Deposition Rate From Titanium Isopropoxide for Various Oxygen Concentrations after Yokozawa et al. (1968)

The activation energies for film formation were calculated to be approximately 36 kcal/mole (150.7kJ/mole) with oxygen concentrations of 5-60%. The films grown in the oxygen free atmosphere were anatase, with a refractive index of 2.10, density 2.55gcm^{-3} and were resistant to etching. The films deposited in an oxidising atmosphere consisted of fine crystallites of anatase of refractive index 2.00 to 2.05, density 2.00 to 2.05 gcm^{-3} and were easily etched by a dilute HF solution.

Oxide films of aluminium, niobium, antimony, zirconium and

titanium were grown at 25-130°C by Sladek and Gibert (1972). Water and alkoxide vapours in nitrogen were passed over a substrate in an isothermal rectangular reactor. The water and alkoxide were syringed into separate heated evaporators. These two streams were kept separate in the reactor by a partition until a suitable distance from the silicon substrate was reached. The equipment is shown in figure 2.5a and 2.5b.

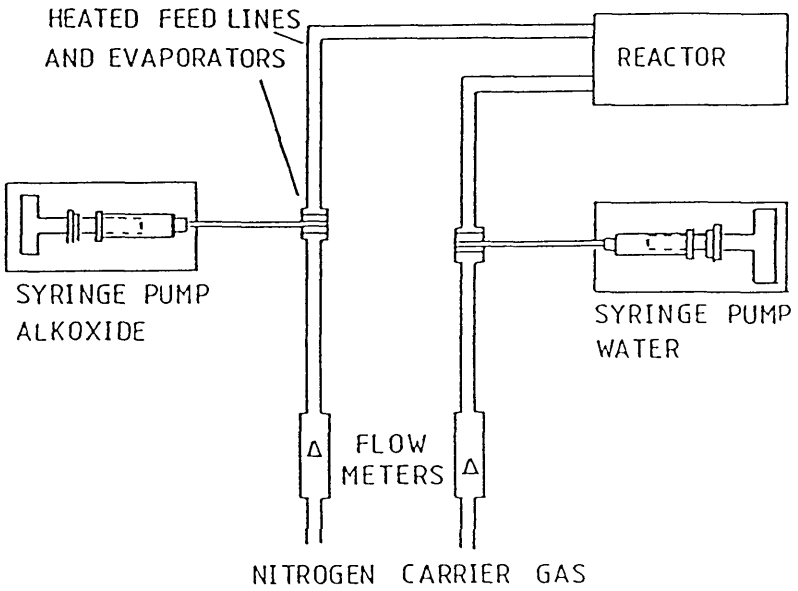


Figure 2.5a Injection System Used by Sladek and Gibert (1972).

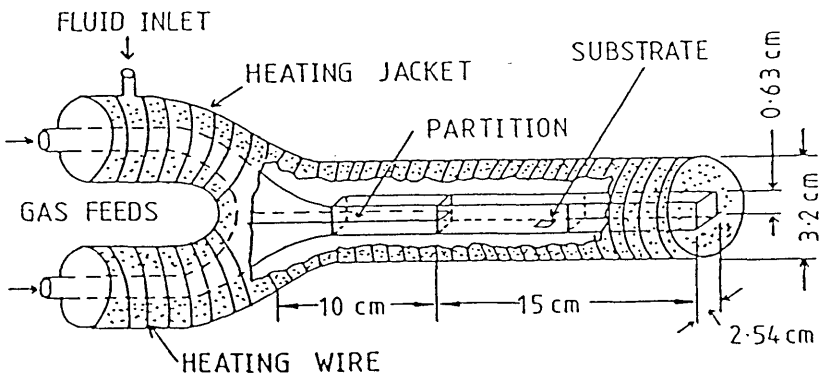


Figure 2.5b Jacketed Rectangular Duct Reactor Used by Sladek and Gibert (1972)

To achieve a reasonable growth rate a high concentration of alkoxide vapour is needed. Sladek and Gibert (1972) state that 0.01 torr is the minium vapour pressure for practical growth and this fixes the minimum reaction temperature. The vapour pressures of the alkoxides used are shown in figure 2.6.

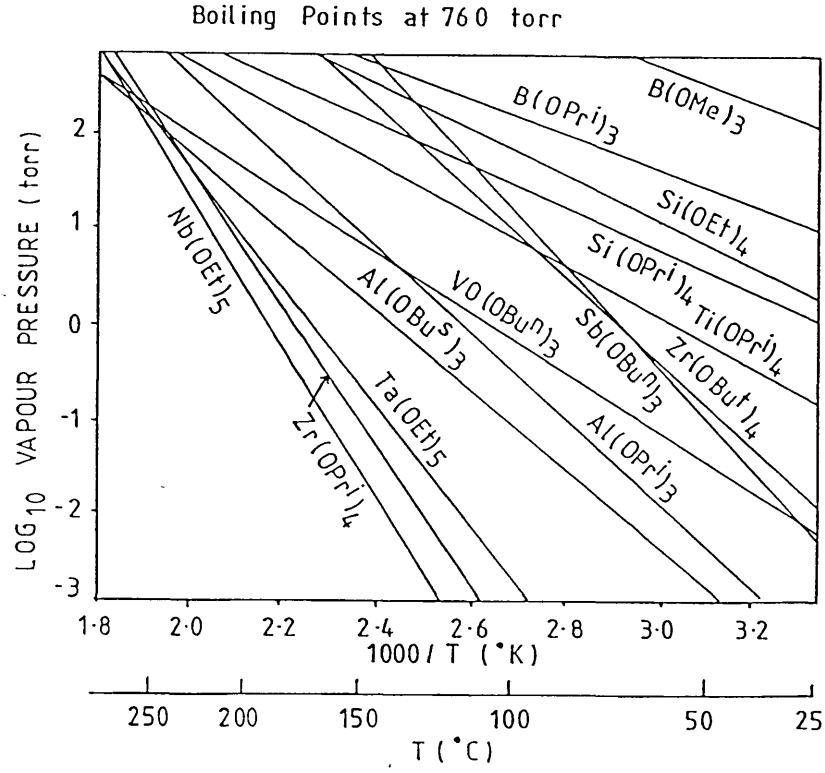


Figure 2.6 Alkoxide Vapour Pressures after Sladek and Gibert, (1972).

If the thickness of the films exceeded 300-600nm, the films fractured. This was attributed to a tensile stress developed in the films during growth, but the cause was not discussed. The films grown were found to be amorphous by x-ray diffraction. Annealing for five minutes at 1000°C in air was found to produce crystalline films. The thickness of the films decreased during annealing and the refractive index increased.

The rate of titanium dioxide deposition was stated to be

insensitive to the substrate temperature. The two temperatures investigated were 110 and 25°C. Due to the insensitivity of the growth rate to temperature the deposition process was thought to be diffusion controlled and a diffusion limited deposition model was developed. The basic assumptions of the model were that the reaction occured at the solid gas interface and the deposition rate was limited by the diffusion rate of alkoxide to the interface. The reaction is thus thought to be so rapid that the alkoxide concentration at the interface is maintained at essentially zero. The insensitivity of growth rate to substrate temperature has not been observed by other investigators (Yokozawa et al., 1968). The limited temperature range investigated and the presence of excess water in the system would probably account for the observations.

Fitzgibbons et al.,(1972) have grown thin films of titanium dioxide with a CVD apparatus similar to that of Feuersanger (1964) as shown in figure 2.3. The films could be grown without using the water source and no changes in the growth dynamics or in the structural, optical or chemical properties of the films were evident. A water vapour in the ambient air appeared to maintain the reaction. The water vapour source however, was found to increase the reproducibility of the electrical properties.

When the thickness of the films exceeded 400-500nm, cracks appeared in the film as reported by Sladek and Gibert (1972). The oxide in the as-grown condition was shown to be amorphous by x-ray diffraction. Annealing the sample at 350°C produced anatase peaks and at 700°C rutile peaks appeared. At 1000°C the diffraction trace was exclusively rutile. The thickness decreased by 35% during annealing at 1000°C and no mass loss

could be detected. The refractive index was increased by annealing.

Hardee and Bard (1975) employed the CVD technique of Fitzgibbons et al. (1972) to grow titanium dioxide electrodes for the photosensitized electrolysis of water. The substrates were titanium metal and thick films of up to 1000nm were required. To overcome the cracking of films thicker than 400-500nm the substrates were annealed in a bunsen flame at suitable thicknesses. This intermediate anneal had been reported by Fitzgibbons et al.,(1972). The oxide films were converted into n-type material by placing in a vacuum at 600°C for 90 miniutes to create oxygen vacancies.

To produce titanium dioxide for antireflection coatings Hovel (1978) utilised the system shown in figure 2.3. The optical properties of the films were investigated as a function of deposition temperature. The refractive index as measured by ellipsometry is shown as a function of temperature in figure 2.7.

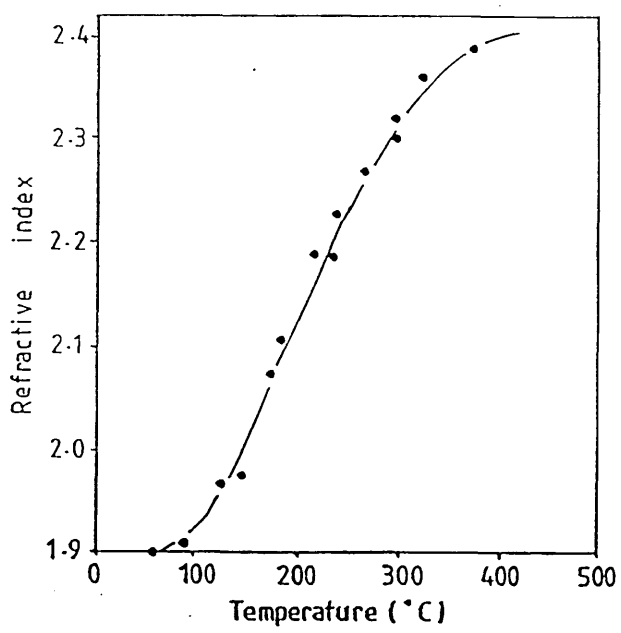


Figure 2.7 Refractive Index at 632.8nm as a Function of Deposition Temperature after Hovel, (1978).

The structure of the films was shown by TEM to transform from an amorphous phase to a polycrystalline phase at a temperature between 200 and 300°C.

Thin films of the transition metal oxides of titanium, tantalum and niobium have been grown by the pyrolysis of metal alkoxides. (Wang et al.,1970). Titanium dioxide was grown by the pyrolysis of titanium isopropoxide in an oxidising ambient in the apparatus shown in figure 2.8.

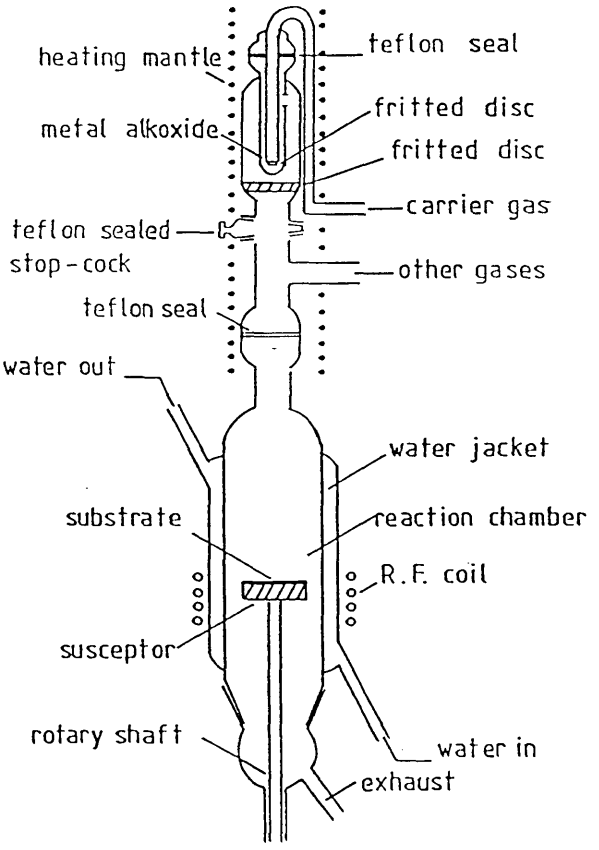


Figure 2.8 Apparatus for Thin Film Deposition of Oxides after Wang et al., (1970).

The vertical quartz reactor was cooled by a water jacket and the graphite susceptor was rotated to provide uniform deposition. The substrate temperature was 450°C and helium carrier gas and oxygen were used. The thickness of the films ranged from 50nm to several μm on a variety of substrates and no

cracking of the films was reported. The structure of the titanium dioxide films were found to be dependent on the deposition temperature. From 100-400°C, the films were polycrystalline anatase with (101) prefered orientation. The anatase transformed to rutile on being annealed at temperatures of 800-1000°C.

Thin oxide films of titanium, zirconium and hafnium were grown to investigate alternative oxides to silicon dioxide in MOS structures (Balog et al.,1979). The oxides were grown in a vertical reactor with a rotating sample holder; the design of which is similar to that of Wang et al.,(1970), figure 2.8.

The titanium organometallics used as precursors were titanium isopropoxide and diisopropoxytitanium bis (acetylacetonate). The films grown below 550°C were found to be amorphous and those grown above 550°C to be polycrystalline anatase. This transition is higher than reported by other workers. The titanium dioxide films were etched by 70% sulphuric acid and the refractive index ranged from 2.05 - 2.26.

Thin films of rutile have been grown by the vapour pyrolysis of ethyl titanate under low pressure conditions at temperatures below 500°C (Takahashi et al.,1981). The deposition of rutile depends on the conditions used; below 450°C formation of rutile is preferred but increasing the substrate temperature suppresses the rutile. A higher linear velocity enabled rutile to form at more elevated temperatures.

The presence of excess oxygen retarded the titanium dioxide deposition. This differs from other investigations where oxygen has been reported to enhance the deposition rates (Yokozawa et al.,1968), and rutile forms at the higher temperatures.

Takahashi et al.,(1981) suggested that the preferred deposition of the more stable rutile phase under conditions of higher linear velocity, rather than the metastable anatase, may be due to the crystal morphology being controlled kinetically, not thermodynamically.

The volatile products were collected in a liquid nitrogen trap and analysed by nmr and mass spectroscopy. With no oxygen in the process the main products were ethanol, ethyl ether and acetaldehyde. With oxygen present the main products were water, ethanol and acetaldehyde with a small amount of ethyl ether.

Takahashi et al.,(1985) grew titanium dioxide from titanium isopropoxide and found that anatase films were formed compared with rutile with the ethyl titanate. Above a film thickness of about 10 μm, rutile was found to grow. The rutile nuclei suppressed the existing anatase and a surface of rutile could be obtained. SEM photographs of anatase and anatase plus rutile films showed that the anatase was columnar in morphology and the rutile was dendritic. The temperature dependence of the deposition from titanium isopropoxide was determined and is shown in figure 2.9.

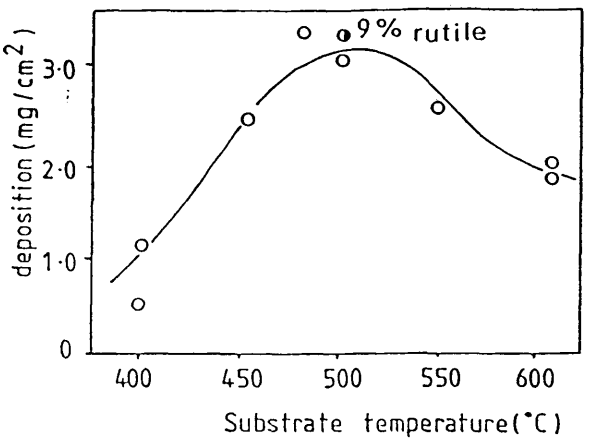


Figure 2.9 Temperature Dependence of Titanium Dioxide Deposition from Titanium Isopropoxide after Takahashi et al.,(1985)

The maximum deposition temperature is shown to be about 500°C. The concentration of oxygen in the vapour was not found to have a great effect on the growth rate of the titanium dioxide films or on the crystal morphology. This is shown in figure 2.10.

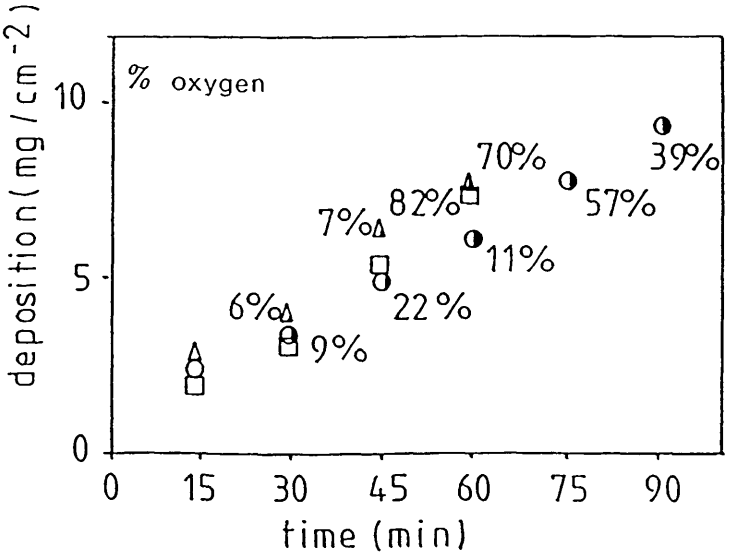


Figure 2.10 Time Dependence of Titanium Dioxide Growth and Rutile Content for Different Oxygen Concentrations after Takahashi et al.,(1985).

The investigations into titanium dioxide growth from titanium isopropoxide can be categorised into pyrolysis and hydrolysis. Generally the hydrolysis promotes the growth rate and deposition at lower temperatures can be carried out. An attempt to quantify the effect of water on the electrical and physical properties of titanium dioxide films produced has been carried out by Fuyuki et al.,(1988).

The dependence of deposition rate on water vapour concentration was determined for two different substrate temperatures of 200 and 400°C and the results are shown in figure 2.11.

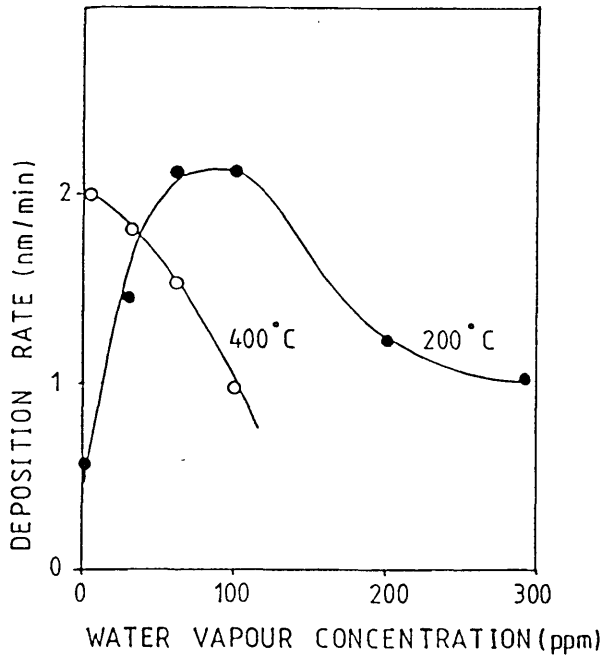


Figure 2.11 The Dependence of Deposition Rate of Titanium Dioxide on Water Vapour Concentration for Temperatures of 200 and 400°C after Fuyuki et al.,(1988)

For the 200°C sample the deposition rate increased rapidly upto 200ppm. The increase was attributed to hydrolysis near the substrate. The decrease in deposition rate for the higher water concentration for the 200°C and for the 400°C sample was due to premature reaction in the region before the substrate, thus reducing the concentration of the reactants and the growth rate.

Values for refractive index were obtained by ellipsometry and plotted as a function of water concentration as shown in figure 2.12.

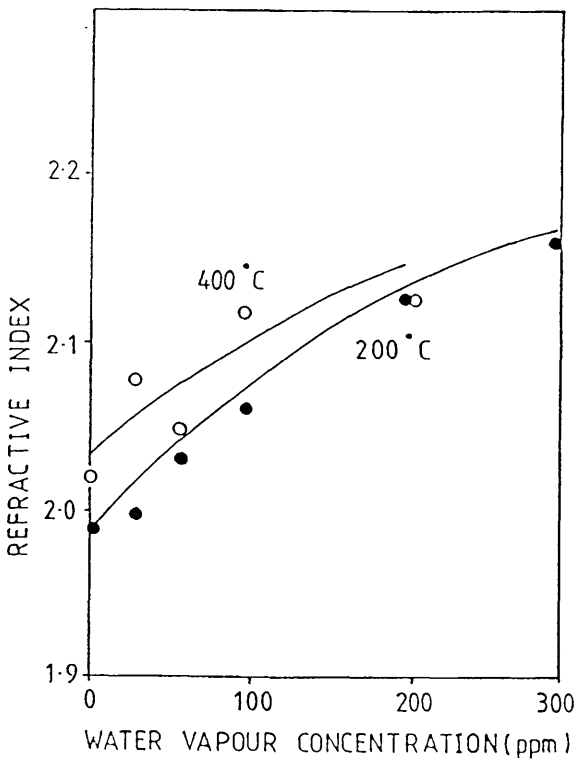


Figure 2.12 The Dependence of Refractive Index of Titanium Dioxide on Water Vapour Concentration at Growth Temperatures of 200 and 400°C after Fuyuki et al.,(1988).

The increase in refractive index with increasing water suggested that the films were of higher density. The etching rates in 10% HF at 20°C were consistent with the higher density indicated by the refractive index values.Figure 2.13 shows the etching behaviour of the films. X-ray diffraction showed that the films deposited at 200°C were amorphous and the films deposited at 400°C were polycrystalline anatase. This is also consistent with the much higher etching rate of the 200°C films.

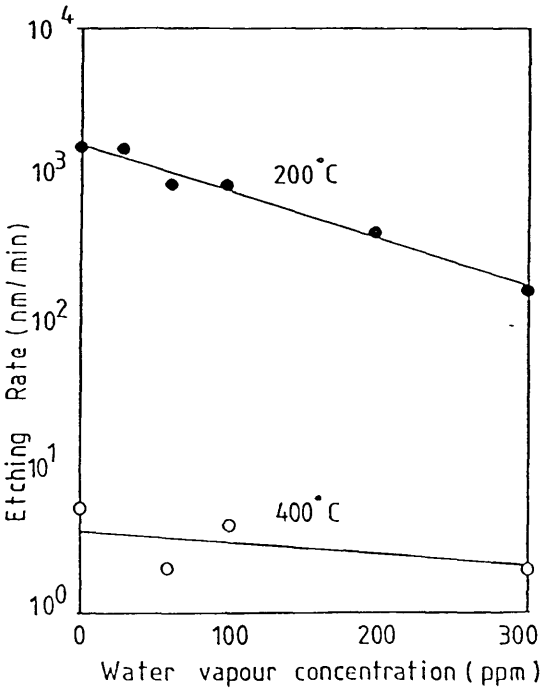


Figure 2.13 The Dependence of Etching Rate of Titanium Dioxide Films on Water Vapour Concentration at Growth Temperatures of 200 and 400°C after Fuyuki et al.,(1988).

Dielectric constants were measured at 1MHz and the results are shown in figure 2.14.

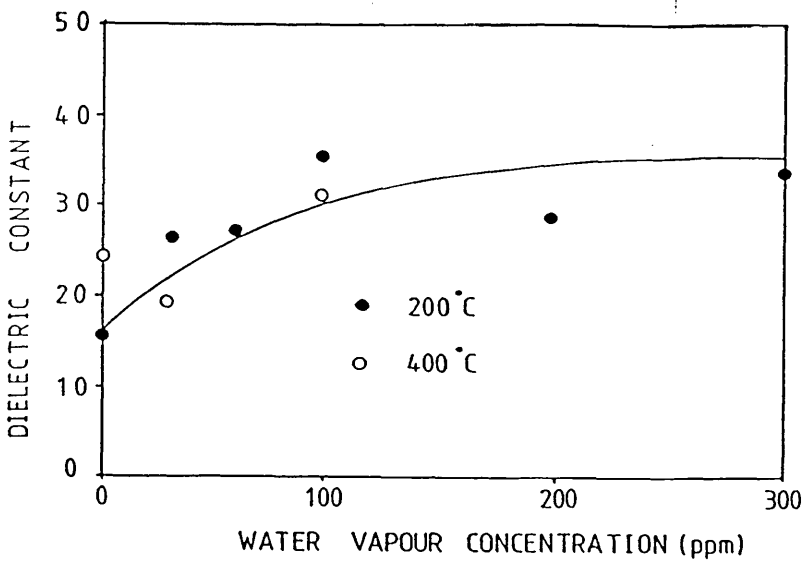


Figure 2.14 The Dependence of Dielectric Constant of Titanium Dioxide Films on Water Vapour Concentration During Growth at Temperatures of 200 and 400°C after Fuyuki et al.,(1988).

With no water present the value was 16 and this increased to about 35 with increasing water concentration. The temperature of deposition did not appear to have a significant effect on the dielectric constant. The current/voltage characteristics of the films were measured. For no added water, ohmic conduction behaviour was exhibited below 4V but the current increased superlinearly above 5V. For films deposited with water concentrations 30-300ppm the behaviour was linear over the whole measurement range of up to 10V. The value of resistivity was 1-2 x 10^9 Ωcm and the breakdown field was greater than 1MVcm^{-1}.

A technique which differs from the conventional CVD technique is the Pyrosol process described by Blandenet et al.,(1981) for depositing metal oxides on glass. The Pyrosol process (pyrolysis of an aerosol) utilizes ultrasonics to produce a spray from the

precursors with a very narrow droplet spectrum. When the aerosol is heated so that it is a vapour when it reaches the substrate it is technically chemical vapour deposition. Titanium dioxide has been grown from butyl orthotitanate at 400°C onto glass and stainless steel.

2.2.3 CHEMICAL VAPOUR DEPOSITION OF TITANIUM DIOXIDE FILMS FROM THE CHLORIDE PRECURSOR.

CVD thin films of metal oxides can be grown by the reaction of a metal chloride with either water or oxygen. There are many similarities between the chloride process and the metal alkoxide process, thus some discussion is valuable. The reactions with water and oxygen of titanium tetrachloride to form the oxide are given in equations (2.1) and (2.2) respectively.

$$TiCl_4 + O_2 = TiO_2 + 2Cl_2 \quad ---(2.1)$$

$$TiCl_4 + 2H_2O = TiO_2 + 4HCl \quad ---(2.2)$$

Titanium tetrachloride is a liquid at room temperature with a relatively high vapour pressure of 10 Torr at room temperature.

Growth of titanium dioxide films was carried out by Hass (1952) using several techniques. One of the techniques was the fuming of titanium tetrachloride onto a heated substrate. The structure of the films prepared by this method were found to depend strongly on the substrate temperature. A room temperature substrate resulted in a soft film being formed and hardness, density and refractive index of the films increased with increasing temperature. Below 280°C, the films were amorphous

and at higher temperatures the anatase structure was formed. A long anneal at 900°C was required to convert the anatase to rutile. The system developed by Feuersanger (1964) was used for both the chloride and alkoxide precursors (figure 2.3) and has been described previously. Hayashi and Hirai (1976) deposited titanium dioxide films from the reaction of the water vapour with the titanium tetrachloride (equation 2.2) at temperatures of 100-900°C in a horizontal reactor. The films grown at 100-200°C exhibited no x-ray diffraction peaks whereas the ones grown at 300°C indicated broad peaks of anatase (85%) and rutile (15%). The x-ray diffraction patterns of the deposits grown at 400-900°C showed a rutile structure which had a preferred orientation of (301) in the 400-500°C temperature range and (100) in the 600-900°C range. The titanium dioxide in contact with the substrate contained a small amount of anatase. This initial growth of anatase prior to rutile has been observed in the alkoxide system (Takahashi et al.,1981). The surface morphologies of the oxide films varied with deposition temperature. At low temperatures of 100-300°C the surfaces exhibited a 'pebble' structure. At 400°C small crystalline grains less than 10 μm were observed. At 900°C small grains of about 5 μm were observed on larger 50 μm grains. The films grown in the temperature region 100-300°C fractured above a certain thickness during deposition. This is similar to cracking reported by Sladek and Gibert (1972). For the higher temperature films (400-900°C) cracks were rarely observed up to about 300 μm thick on the silicon substrate during deposition but the films grown on fused quartz cracked during cooling. This was attributed to the thermal expansion mismatch between quartz and

titanium dioxide. The density of the deposited films was investigated as a function of temperature and was compared with the results of other workers. This is shown in figure 2.15.

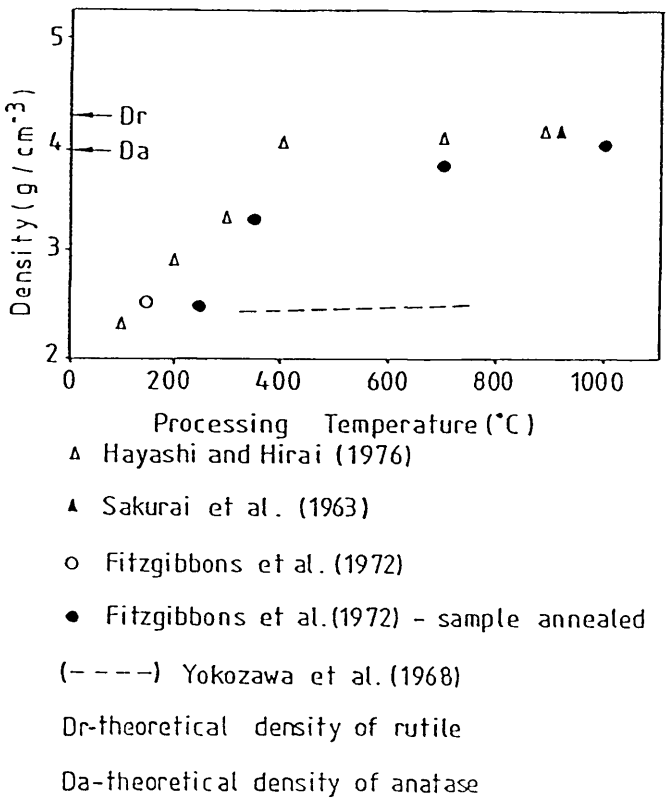


Figure 2.15 Densities of Titanium Dioxide Films Deposited by CVD after Hayashi and Hirai., (1976), Compared with Results of Other Workers.

The density can be seen to increase substantially from the temperature 100-300°C corresponding to the change from amorphous to crystalline state. The deposition rate as a function of temperature was investigated and the results are shown in figure 2.16.

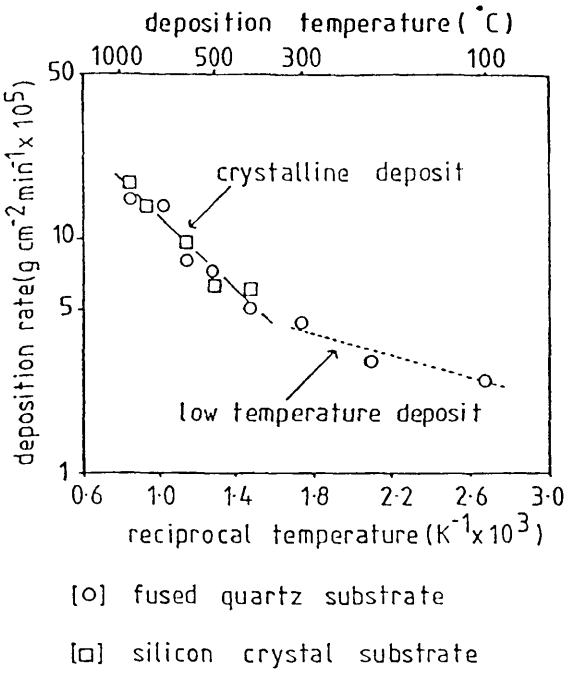


Figure 2.16 The Temperature Dependence of Deposition Rate of Titanium Dioxide from Titanium Tetrachloride and Water after Hayashi and Hirai, (1977).

The change in slope from the low temperature deposit of less crystalline material to the higher temperature deposit of the crystalline material should be compared with figure 2.4 of Yokozawa et al.,(1968). The oxygen assisted growth produced a less dense, less crystalline structure with a lower activation energy and unassisted growth had a higher activation energy but was more crystalline and denser. The lower temperature structures of Hayashi and Hirai (1976) suffered a weight loss of as much as 30.4% when annealed at 400°C. This weight loss was thought to be due to the incorporation of volatile components into the film. Despite substantial reduction in thickness on annealing films grown from organometallics at low deposition

temperatures, weight loss could not be detected (Fitzgibbons et al.,1972).

Extensive investigations into the growth behaviour of titanium dioxide from the reaction of titanium tetrachoride with oxygen have been carried out by Ghoshtagore and Noreika (1970). A selection of substrates were used and the temperature range investigated was 400- 1047°C. The structure of the films was mainly rutile. Figure 2.17 shows an Arrhenius plot relating the deposition rate to substrate temperature at three constant partial pressures of titanium tetrachloride.

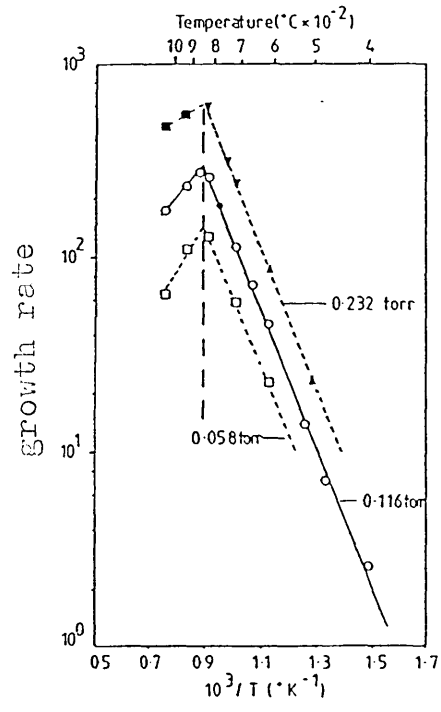


Figure 2.17 Arrhenius Plot of Rutile Thin Film Deposition from Titanium Tetrachloride and Oxygen at three constant Partial Pressures of Titanium Tetrachloride after Ghoshtagore and Noreika.,(1970).

Homogenous nucleation in the vapour phase became predominant at about 850°C and the growth rate declines at temperatures higher than this due to the effective reduction of titanium tetrachloride concentration. The same trend in results was obtained for a plot of the density of nuclei as a function of 1/T. Variations in the crystallographic orientation of the titanium dioxide films were observed on the different substrate materials. The films grown on different orientations of silicon, (111), (110) and (100), were found to be independent of substrate orientation. However the orientation of the film was dependent on substrate temperature. Varying degrees of epitaxial growth were observed on rutile and MgO substrates. The various orientations of the films as a function of substrate material and temperature are summarised in figure 2.18.

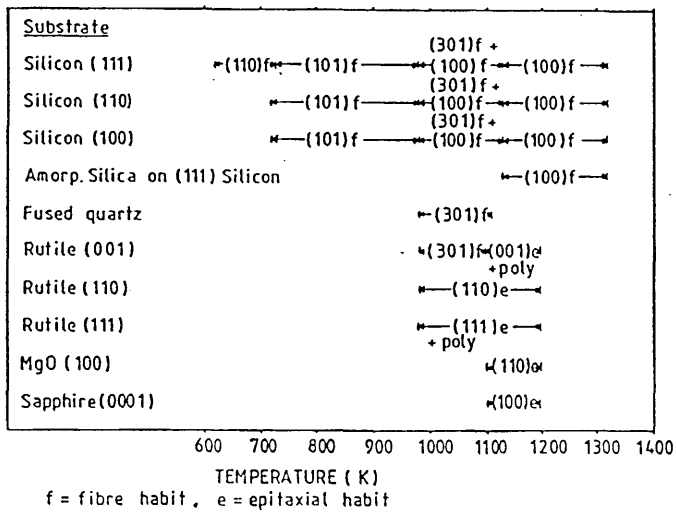


Figure 2.18 Schematic Representation of Preferred Rutile Crystallite Orientation in Thin Films as a Function of Substrate Material, Temperature and Orientation Grown from titanium Tetrachloride and Oxygen after Ghoshtagore and Noreika, (1970).

TEM studies were carried out on the oxide films deposited on silicon. All films exhibited platelet morphology. Electron diffraction results revealed the presence of anatase in deposits prepared above 850°C. It was suggested that the appearance of anatase in the films may be due to the homogeneous nucleation which occurred in growth above 850°C.

Refractive index measurements of films grown on silicon were determined by ellipsometry. For films in the thickness range 20-150nm an average value of 2.83 was obtained. No reproducible behaviour of change in refractive index as a function of either film thickness or deposition temperature was detected. Increasing refractive index values have been reported for amorphous - anatase titanium dioxide films with increasing substrate temperature but the films in this investigation were predominantly rutile.

Thin films of titanium dioxide were grown in the lower temperature range of 130-250°C by the hydrolysis of titanium tetrachloride (Yeung and Lam, 1983). The application for these films was as an antireflection coating in silicon solar cells. The refractive index of the deposited films was determined by ellipsometry and a strong dependance on deposition temperature was observed as shown in figure 2.19. The steep rise of the refractive index at about 180°C was correlated with an amorphous - anatase crystalline transition. At thicknesses greater than 400nm, cracks started to appear in the films.

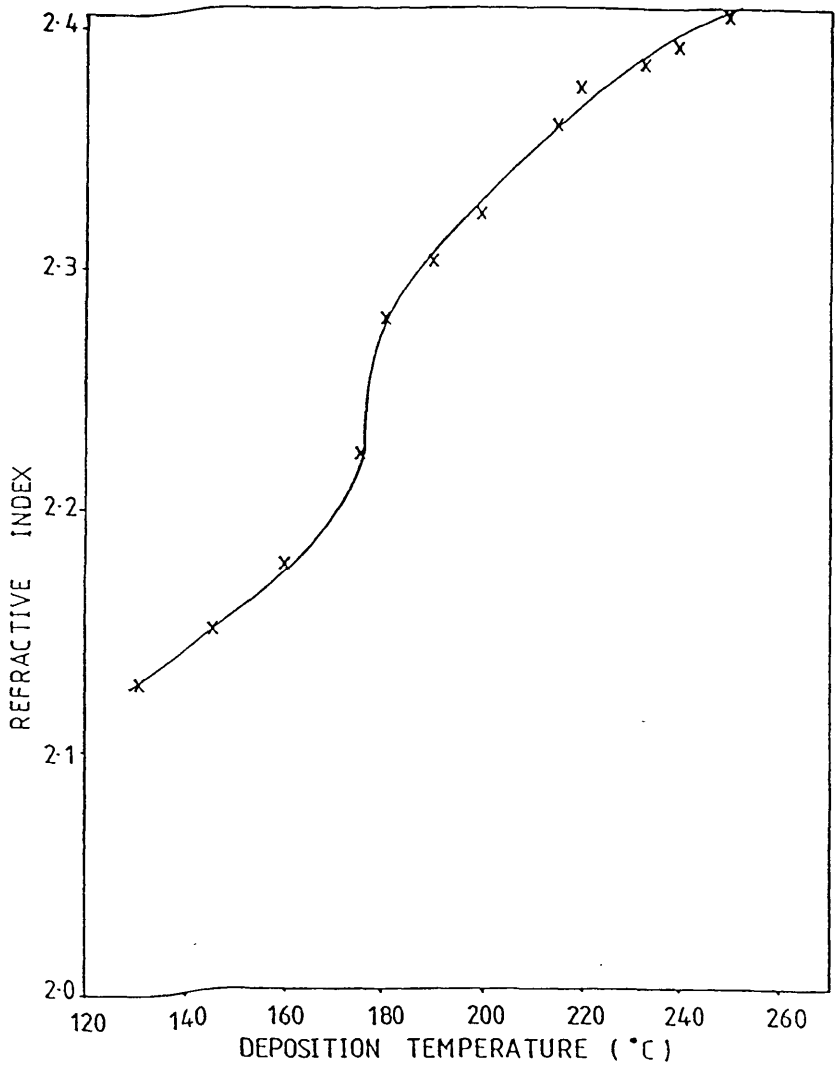


Figure 2.19 Refractive Index of Titanium Dioxide Films Grown From Titanium Tetrachloride and Water as a Function of Deposition Temperature after Yeung and Lam, (1983).

Considering the literature discussed in section (2.2.2) and (2.2.3), general trends can be noted:

(1) Low temperature growth favours amorphous oxide deposition with properties of low refractive index, low density, high etching rate and a tendency for cracking above a certain thickness.

(2) Higher growth temperatures result in a crystalline oxide with higher refractive index, higher density and lower etching rate. Cracking is less prevelant at the higher growth temperatures and annealing can be used to obtain thicker films. Some problems of powder formation have been reported at the higher temperatures.

(3) The change in refractive index with substrate temperature for the amorphous-anatase films has been observed in several investigations.

(4) The growth rate of oxide deposition in most cases increases with increasing substrate temperature.

(5) The growth rate of titanium dioxide is generally found to be dependent on the water concentration in the environment.

2.3 VANADIUM OXIDE

Interest in vanadium oxides was generated with the discovery by Morin (1959) that VO, V_2O_3, and VO_2 undergo a metal to insulator transition with change in temperature. Vanadium dioxide has received much attention because it has a switching temperature of 68°C which is closer to room temperature than for other compounds. At 68°C a change in crystal structure from monoclinic to tetragonal symmetry occurs which is accompanied by a change in electrical conductivity which can be as large as 10^5.

The driving force for growing thin films of vanadium oxides has been first, for use in device applications and secondly, because single crystals have not been found to survive the cycling through the transition temperature (Balberg, 1971). Several techniques have been employed in depositing thin films. Steensel et al.,(1967) grew films by the reactive evaporation of vanadium in a residual gas atmosphere of oxygen. Subsequent annealing of the films in an oxygen atmosphere was necessary to form the dioxide form. Numerous phases in the vanadium-oxygen system exist as shown in figure 2.20.

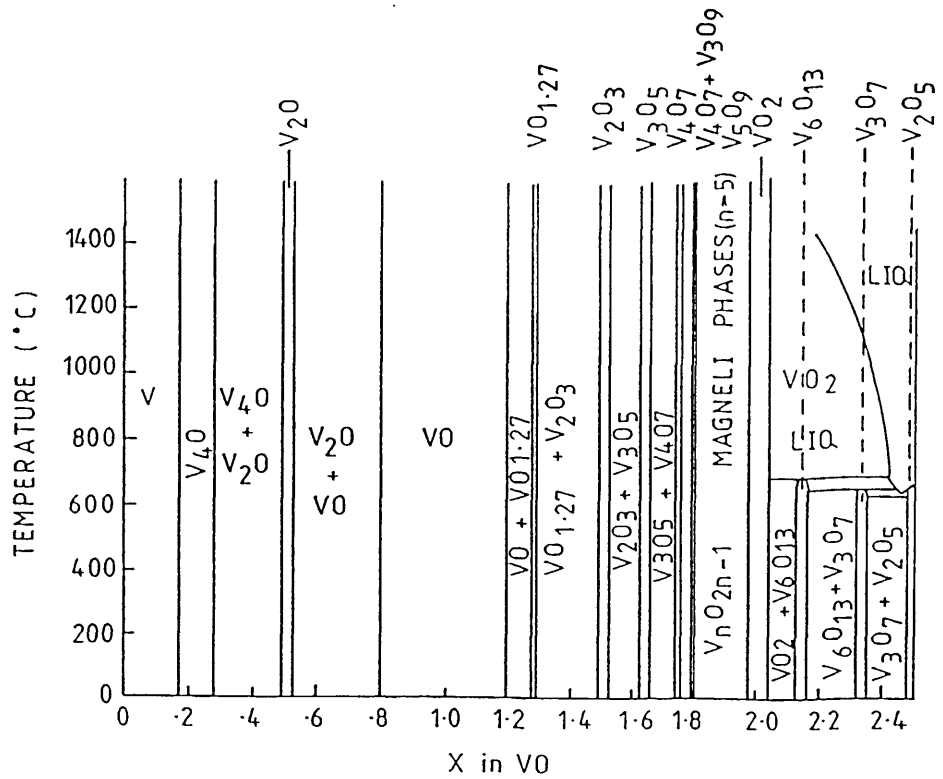


Figure 2.20 Part of the Vanadium-Oxygen Phase Diagram after Griffiths and Eastwood, (1974).

Reactive sputtering was used by Rozgonyi and Hensler (1968), to grow vanadium dioxide films on a variety of substrates. The deposited films varied in structure and conductivity with the substrate material. On amorphous substrates the films were polycrystalline with conductivity ratios between the two states of approximately 10^2 with a broad transition centred at 68°C. Highly textured films grew on sapphire substrates and on rutile the films were epitaxial. Higher conductivity ratios of 3.5 x 10^3 were obtained in both cases.

Growth of vanadium oxides by the chemical vapour deposition route has been achieved from both inorganic and organometallic precursors. MacChesney et al., (1968) grew V_2O_5 from vanadyl trichoride at temperatures below 127°C in a carbon dioxide

atmosphere. Reduction of these films to VO_2 was carried out by heating in controlled atmospheres of oxygen between 500 and 550°C.

Vanadium acetylacetonate $(C_5H_7O_2)_4V$ was the precursor used by Ryabova (1972) to deposit vanadium oxides. The film composition was found to be sensitive to the carrier gas composition. In pure nitrogen at 420°C the V_2O_5 grew (with some intermediate phase present), with a 10:1 ratio of nitrogen to oxygen at 400°C VO_2 grew and with equal volumes of oxygen and nitrogen at 340°C V_2O_5 grew.

The precursor of most interest to the present work is vanadyl tri-isopropoxide and has been used by Greenberg (1983) to grow VO_2 containing films. Films were prepared directly by CVD, by reduction of films grown by CVD and by room temperature gelation-hydrolysis followed by reduction. In the CVD system the furnace tube was open ended and the glass substrates were fed through. A substrate temperature of 530°C was used and a nitrogen gas flow carried the vanadyl tri-isopropoxide vapours to the hot substrate. After moving through the deposition zone the substrate entered a conveyor furnace which was flushed with forming gas. For samples prepared for subsequent reduction the latter stage contained ambient air rather than forming gas to promote the growth of V_2O_5. The largest switch in resistance of $10^3\Omega$ was obtained from the films which had undergone post-reduction of the V_2O_5.

Doping of the vanadium dioxide films has been carried out with the aim of changing the switching temperature. Balberg et al.,(1974), investigated mixed oxides of vanadium and titanium grown by reactive co-sputtering. The addition of titanium

dioxide to vanadium dioxide was found to increase the transition temperature and broaden the temperature range over which it occurred. No transition was apparent for more than 50 vol% titanium dioxide. These results are shown in figure 2.21.

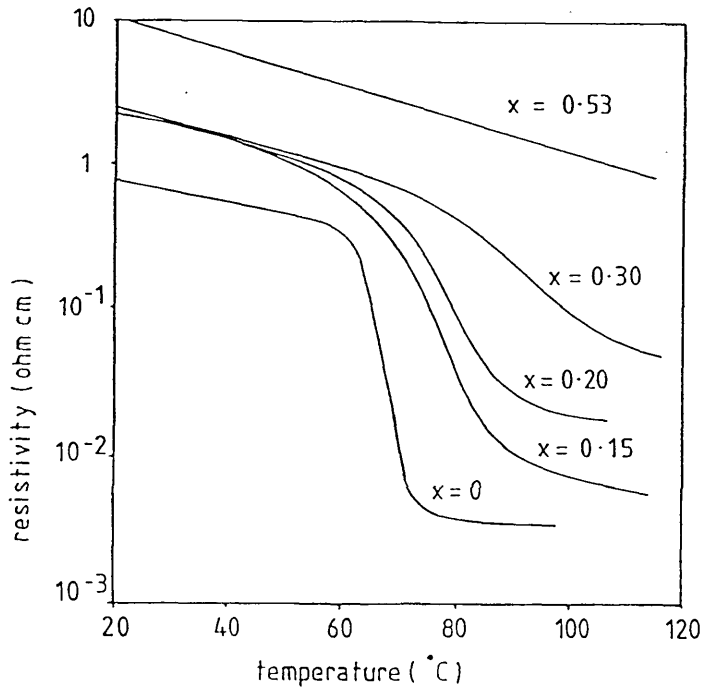


Figure 2.21 Temperature Dependence of the Resistivity of $Ti_xV_{1-x}O$ Co-sputtered Films, after Balberg et al., (1974).

CHAPTER 3 : APPARATUS

3.1 INTRODUCTION

The apparatus built for deposition of oxide films from liquid metal alkoxide precursors is shown in figure 3.1. Transport of the metal alkoxide into the reactor is by liquid injection from a syringe; the liquid is atomised and vaporised, before being swept into the reactor chamber by dry nitrogen carrier gas. Thermal decomposition to the oxide occurs in the heated zone of the susceptor and the waste products are swept out through the exhaust. To enhance the growth at lower temperatures a 100W mercury arc lamp provides a source of UV radiation. The different sections are described in greater detail in (3.2) to (3.7).

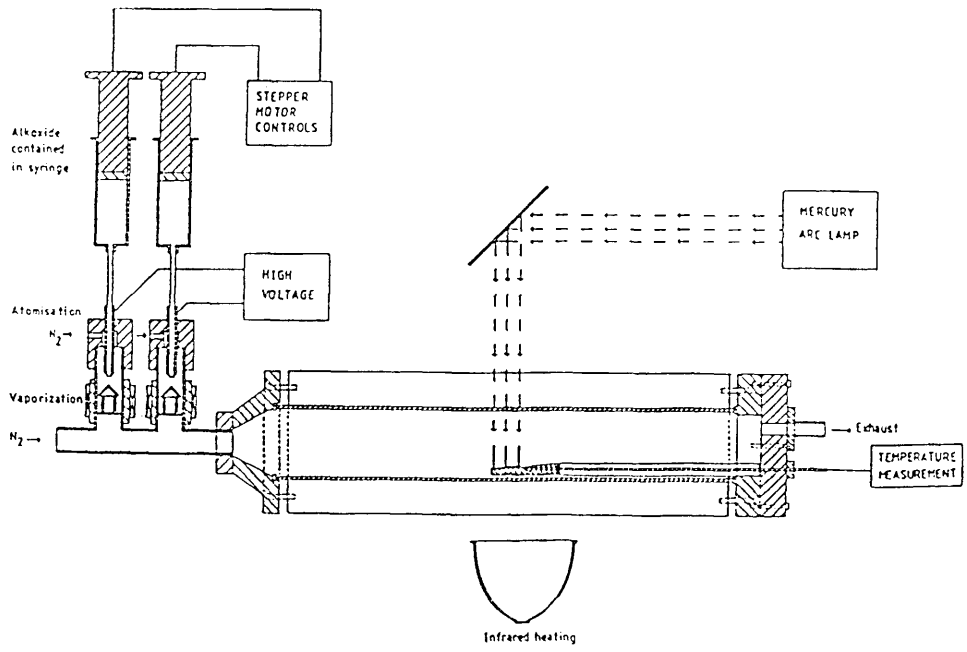


Figure 3.1 Schematic Diagram of Chemical Vapour Deposition Apparatus for Oxide Growth

3.2 LIQUID INJECTION

In the process of liquid injection the precursor is introduced directly into the reactor and vaporized at the point of entry. The metal alkoxide is contained in a syringe and the rate of injection depends on the speed of travel of the plunger. This can be accurately controlled and hence a precise metering of the precursor is achieved. This technique is inherently simpler than bubbler technology with respect to calculating the input rate of precursor. Mass flow from a bubbler depends on factors such as the temperature, carrier gas flow rate, bubble size and path length through the liquid. Calibration of a bubbler is generally required prior to use. Further advantages of injecting the liquid directly are apparent when the precursor is thermally unstable or a solution of more than one precursor is to be injected. A thermally unstable precursor is zirconium tertiary amyl oxide and Hough (1978) stored this metal alkoxide in an aspirator at room temperature and vaporized it only when required in order to minimize premature thermal decomposition. Liquid injection of a miscible solution of tetra ethyl ortho silicate, trimethylborate and trimethyl phosphite to grow borophosphosilicate glasses was used to maintain the ratio of species in the liquid and gas phases (Levy, 1987). If the solution were contained in a single bubbler depletion of the most volatile component would occur and compositional changes with time would be a problem.

3.2.1 PRACTICAL DETAILS

3.2.1.1 Syringe Operation

The syringes used to contain the metal alkoxide are Hamilton

'1000' series, of either 5ml or 10ml capacity. These are high performance gas tight syringes with a teflon plunger tip which protects the precursor from atmospheric moisture. A CTFE removable needle connects the syringe to the reactor. The plunger is operated by a lead screw mechanism which is illustrated in figure 3.2.

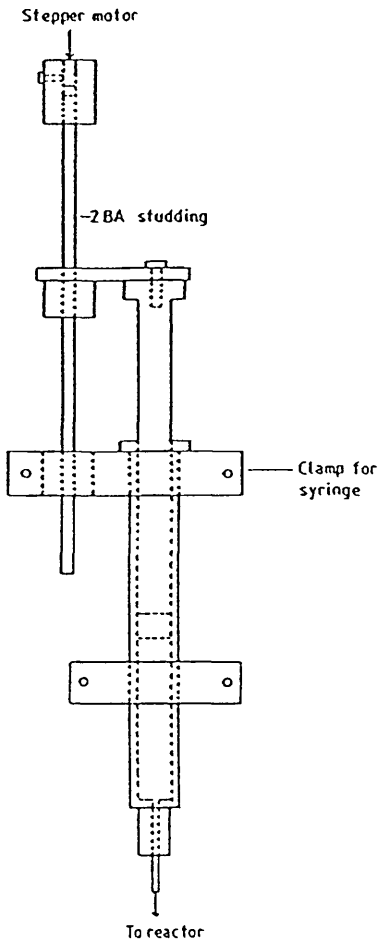


Figure 3.2 Diagram Illustrating the Lead Screw Mechanism for Driving the Syringe Plunger.

As indicated in figure 3.2, the syringe is driven by a stepper motor. The circuit built to control the stepper motor is shown in figure 3.3.

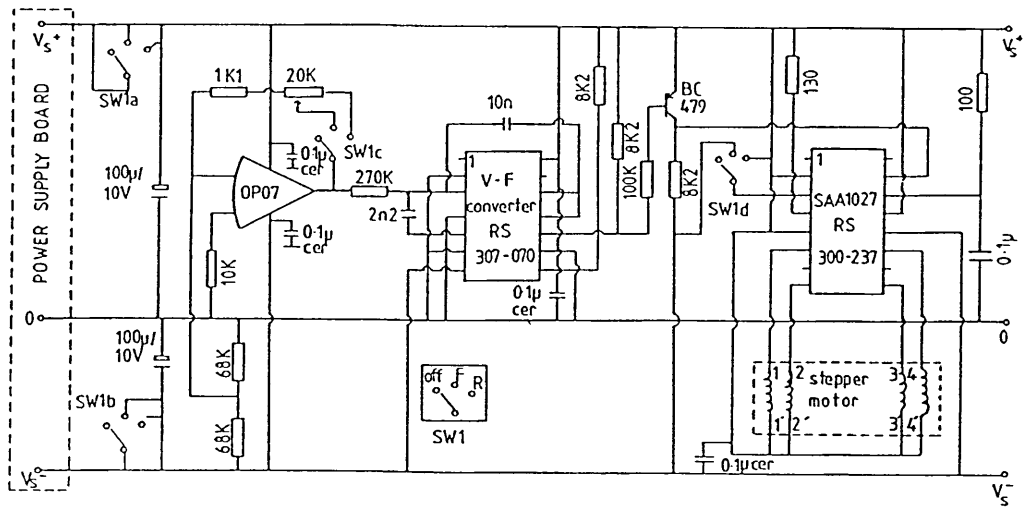


Figure 3.3 Circuit Diagram of Electronic Circuit to Control Stepper Motor

A stepper motor works on the principle of a rotating field, generated by the control electronics, pulling a magnetic rotor along. The SAA 1027 is a stepper motor driver IC and provides the switching sequence required for driving the stepper motor. The voltage to frequency converter (V-F) IC generates a step input to the SAA 1027 which determines both the frequency of the output to the stepper motor (the rate of alkoxide injection) and the sequence of output signals (the direction of rotation). The frequency of the V-F output depends on the input voltage and this is varied by the 20K potentiometer. The stepper motor is connected to the syringe mechanism via a gearbox of ratio 250:1 and the injection rate range available with a 5ml syringe varies from 1.042×10^{-5} to $1.923 \times 10^{-3} cm^3 s^{-1}$.

3.2.1.2 ATOMISATION

Using the lowest injection rate of 0.35×10^{-7} moles s^{-1}, a drop is injected into the vaporisation chamber at a rate of approximately $10^{-2} s^{-1}$. This can lead to a fluctuating concentration of alkoxide vapour entering the reactor. To overcome this problem the liquid is atomised electrostatically on leaving the needle producing a continuous spray of small droplets. The effect of applying a high voltage to a drop is shown in figure 3.4a. The droplets are charged on leaving the needle and the spray can be manipulated by an electrode as shown in figure 3.4b. During atomisation all parts of the apparatus need to properly earthed, to prevent arcing and damage of the electronic components.

The large reduction in drop size increases the surface to volume ratio of the liquid which facilitates vaporisation. An added effect is the increase in vapour pressure of small drops as given by equation (3.1), (Perry, 1953).

$$P = Po[1+(2\sigma M)/rdRT] \quad ---(3.1)$$

Po = bulk vapour pressure,

σ = surface tension $= 25 \times 10^{-3} Nm^{-1}$

M = molecular weight = 284.25kg

d = density $0.955 Kgm^{-3}$

R = 8.314×10^{3} J $mol^{-1} K^{-1}$

T = temperature = 323K

r = radius of droplet = 2×10^{-6} m

P = vapour pressure of the droplet.

For titanium isopropoxide with an average droplet radius of 2μm,

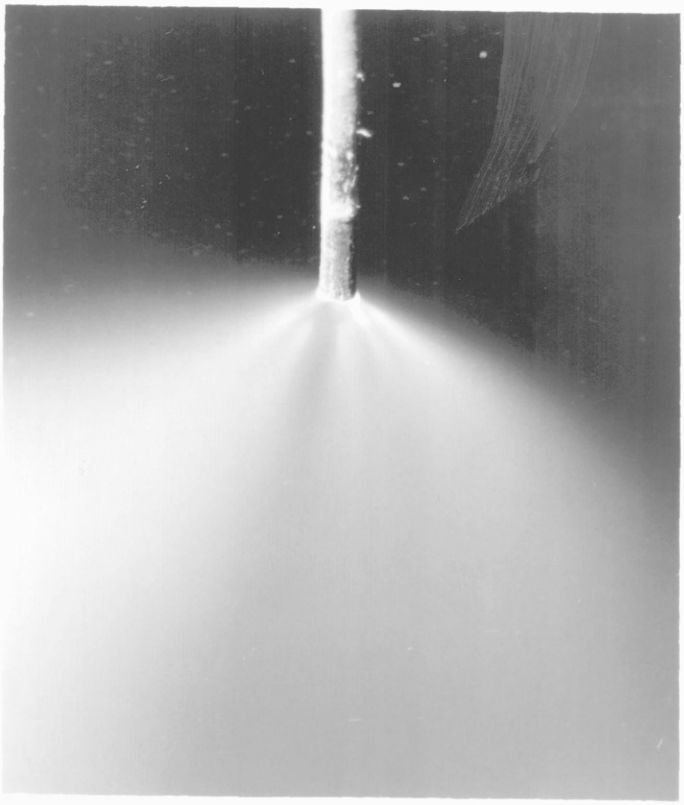


Figure 3.4a Atomisation of Liquid by Application of a High Voltage.

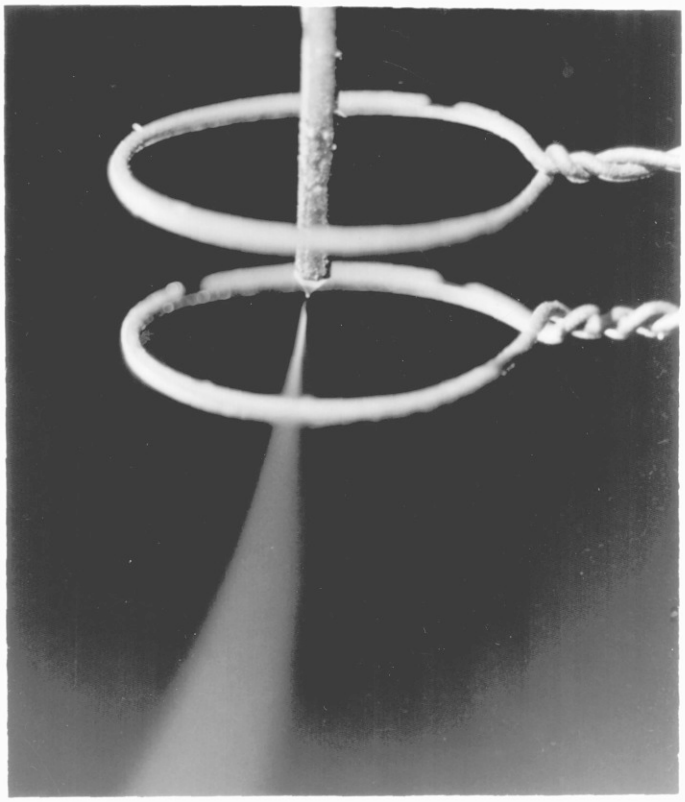


Figure 3.4b Effect of an Electrode on the Jet of Atomised Liquid.

the vapour pressure is increased by 0.3%.

The size of the atomised droplets was investigated by a Forward Scattering Spectrometer Probe (FSSP) as shown in figure 3.5,(Knollenberg 1976).

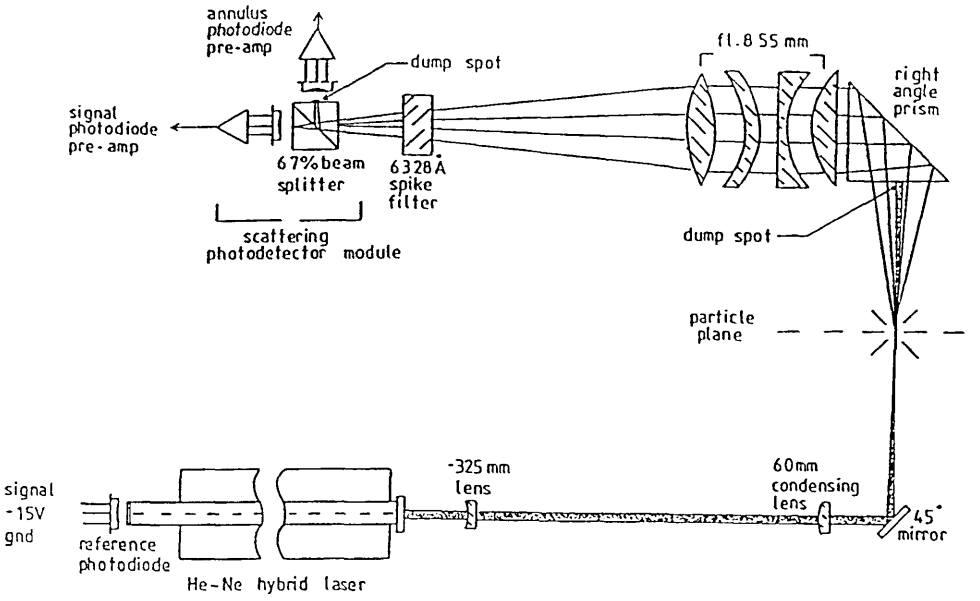


Figure 3.5 Schematic Diagram of a Forward Scattering Spectrometer Probe, after Knollenberg, (1976).

This is an optical technique and the droplets are measured by the amount of light scattered into the collecting optics during particle interaction through a focussed laser beam. The scattered energy is relayed from the object plane by a right angle prism to a collecting lens and focussed onto a masked beam splitting prism. A dump spot on the right angle prism stops the transmitted laser beam going through. Particles of sizes 0.5-45μm diameter can be measured in four switchable size ranges e.g. 0.5-8μm, 1-16μm etc. This work was carried out at the Plant Protection Division, ICI. Figure 3.6 is a typical histogram of droplet diameters of titanium isopropoxide.

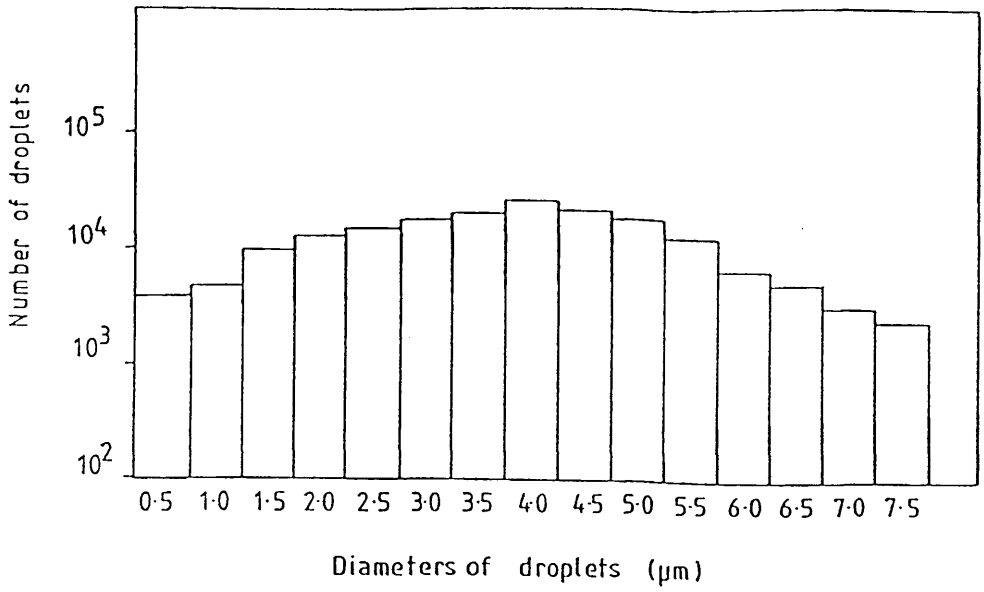


Figure 3.6 Histogram of Droplet Diameter Sizes Measured by a FSSP.

An average droplet diameter for this flow rate and voltage was about 4μm. The average droplet size was found to vary with applied potential (figure 3.7) but not noticeably with the range of flow rates used.

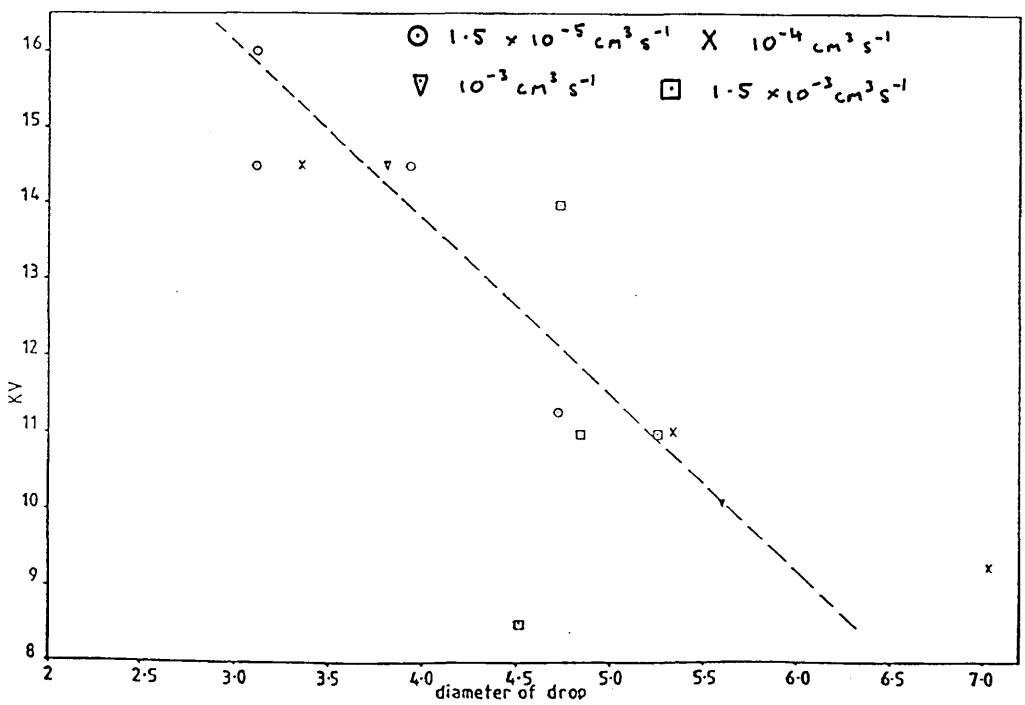


Figure 3.7 Diameter of Droplet Size as a Function of Different Applied Voltages.

The current of the atomised spray was measured by an avometer connected to a metal collecting plate. At a flow rate of $2x10^{-4}cm^3s^{-1}$, the current was measured at different applied kV, as shown in figure 3.8. A typical value of charge/drop was estimated to be 10^{-8} coulombs.

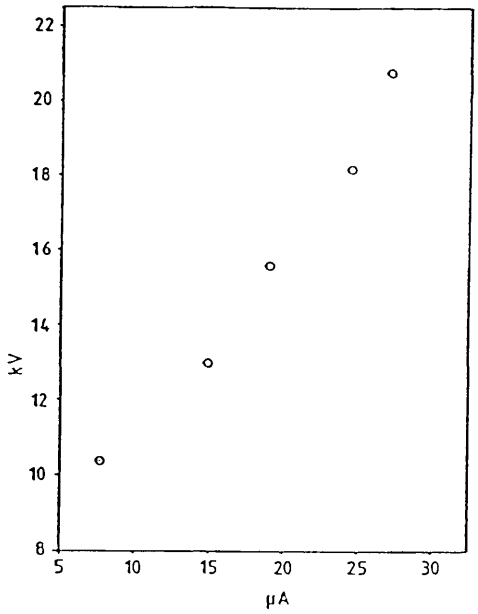


Figure 3.8 The Current of the Atomised Spray as a Function of Applied Voltage

3.3 VAPORISATION

The atomised droplets are vaporised in a heated chamber as illustrated in figure 3.9. A resistance 'collar' heater is clamped around an aluminium tube and the temperature is maintained at the required temperature by a Eurotherm temperature controller with a Pt-PtRh thermocouple. The inlet tube is pyrex and designed to prevent droplets from entering the

main reactor tube before vaporising. Dry nitrogen is flushed through all the inlet ports of the reactor and two vaporisation chambers provide the facility for simultaneous injection of two precursors. The inlet tubes are maintained at a temperature sufficient to prevent condensation of the vaporised metal alkoxide by a resistance heating tape.

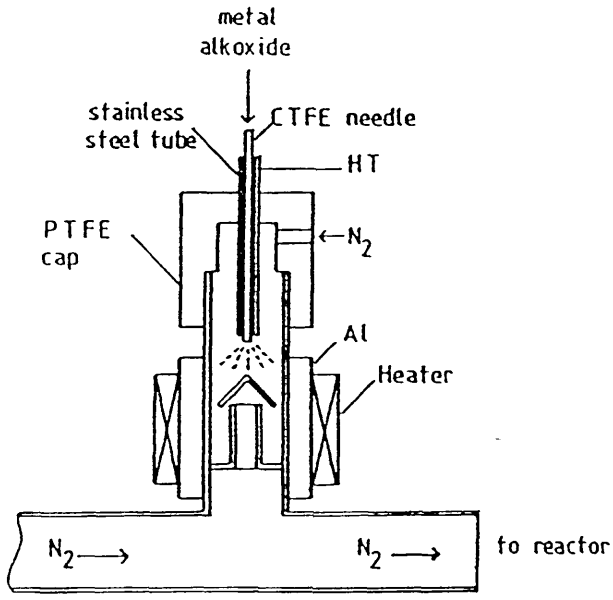


Figure 3.9 Diagram of Vaporisation Chamber

3.4 REACTION CHAMBER

The main reactor chamber is a rectangular quartz tube with cross sectional dimensions of 39 x 49mm and is 250mm long. This tube is clamped between aluminium endpieces and sealed with silicone rubber gaskets as shown in figure 3.10.

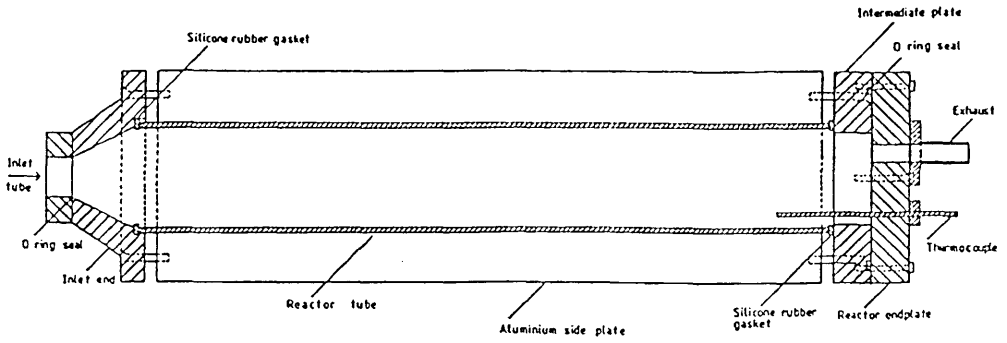


Figure 3.10 Diagram of Reactor Tube

The aluminium inlet is tapered to provide a gradual increase in cross sectional area from the inlet tube to the reactor tube in order to reduce vortex formation occurring in the gases. At the exhaust end of the reactor there are two aluminium plates; the purpose of the intermediate plate is to clamp the quartz tube in place while the endplate with attached susceptor is screwed into position. This design of reactor was used by Wojcik (1985), and requires minimal quartz glasswork, is easy to dismantle and clean and the reactor tubes can be easily interchanged.

3.5 SUSCEPTOR

The alkoxide vapour thermally decomposes to the oxide film on reaching the hot substrate. The substrate is placed on a stainless steel susceptor as illustrated in figure 3.11.

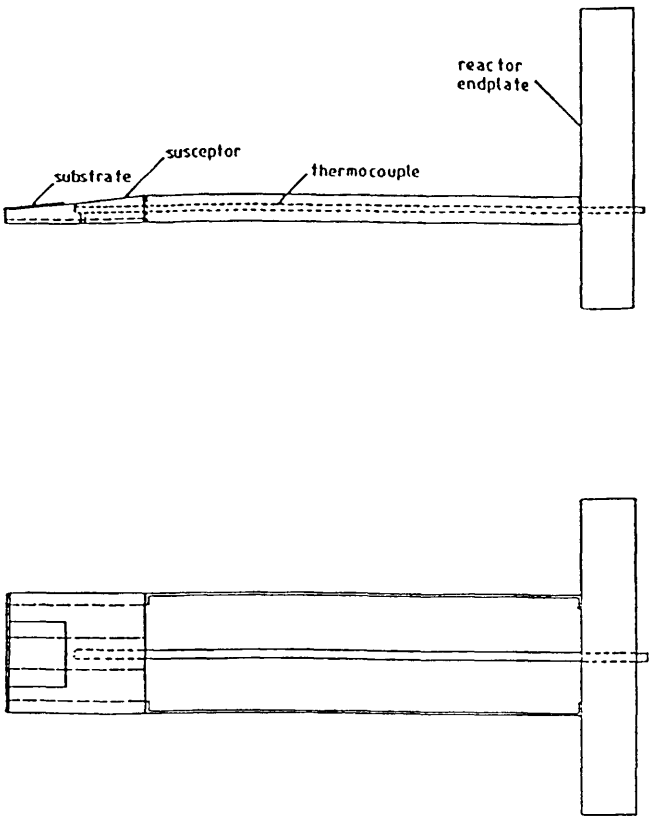


Figure 3.11 Diagram of the Stainless Steel Susceptor

To allow easy insertion and withdrawl from the reactor and to maintain an identical position in the reactor the susceptor is attached to the exhaust endplate. A thermocouple is positioned in a hole in the susceptor to measure the temperature. To compensate for possible depletion of the precursor along the length of the substrate it is inclined at an angle. The purpose of the front ledge is to locate the substrate. In the underside, grooves have been machined to allow gas flow underneath the susceptor and thus reduce the turbulence which can originate from the front ledge.

3.6 SUSCEPTOR HEATING

Radiant heating is used to heat the substrate and temperatures up to a maximum of 600^{o}C in the susceptor block are obtainable.

This method of heating is quite rapid, does not heat up the reactor walls significantly and is external to the reactor. A 1000W bulb (Philips, model T/4) has been used and is positioned as shown in figure 3.12.

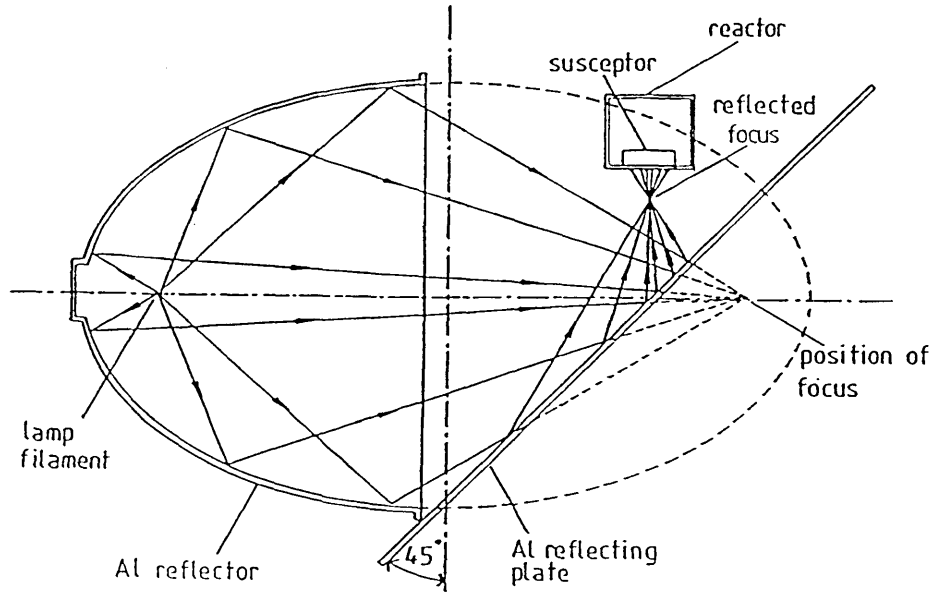


Figure 3.12 Diagram to Illustrate the Geometry of Heating.

It is a requirement of the bulb to be suspended vertically with the base up. The bulb is at one focus of the elliptical reflector and the second focus is slightly below the susceptor thus spreading the heating area on the susceptor. There are two fans attached to the heating assembly to provide the necessary ventilation for cooling the bulb. The temperature was controlled manually. The voltage of the thermocouple (type K) was fed into an amplifier and then into a panel meter. The temperature could be read to better than $1^{o}C$ and once the temperature had stabilised it did not vary by more than $\pm 5^{o}C$.

3.7 PHOTOLYSIS

To enhance the oxide growth at lower temperatures the

substrate was illuminated with ultraviolet radiation. A 100W high pressure mercury arc lamp (Cathodeon) was used as a source of UV and a typical output spectrum is shown in figure 3.13. The UV light was reflected into the reactor by a mirror inclined at 45^{o} as shown in figure 3.12 The quartz reactor tube is essentially transparent to the UV radiation. Partial masking of the substrates could be easily achieved by placing an opaque mask in the path of the light. The power intensity on the substrate was estimated to be of the order of mW cm^{-2}.

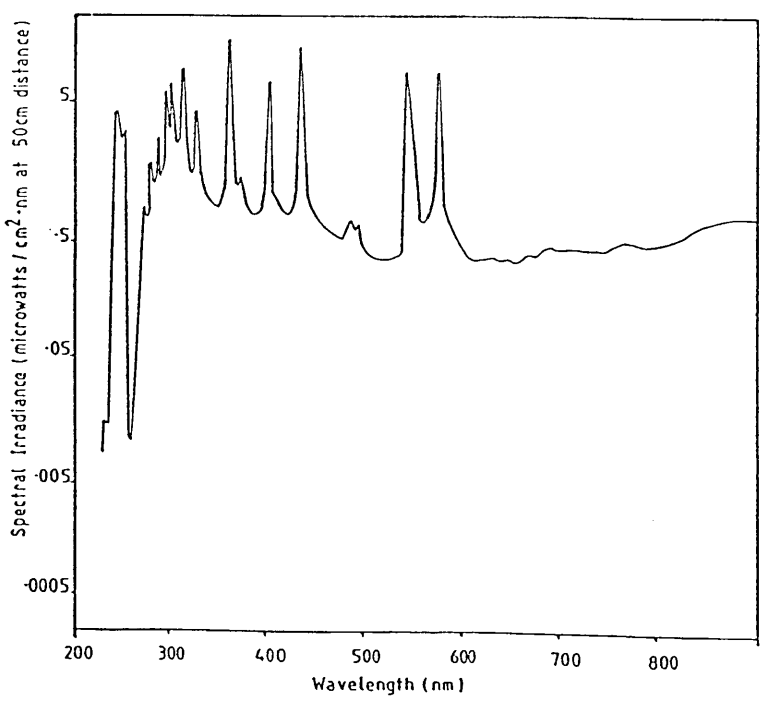


Figure 3.13 Typical Output Spectrum from 100W Mercury Bulb

3.8 CHARACTERISATION OF REACTOR

3.8.1 SUBSTRATE TEMPERATURE MEASUREMENT

The measuring thermocouple is positioned in a hole in the stainless steel susceptor as shown in figure 3.11. To check the temperature of the substrate surface a second thermocouple was placed in a simulation experiment in contact with the silicon slice and a simultaneous reading taken. The effect of illuminating the surface was also investigated. Measurements were taken over the whole temperature range with a gas flow rate of 73.3 $cm^3 s^{-1}$ and the results are plotted in figure 3.14. The temperature of the reactor wall directly above the susceptor was also measured and is plotted in figure 3.14.

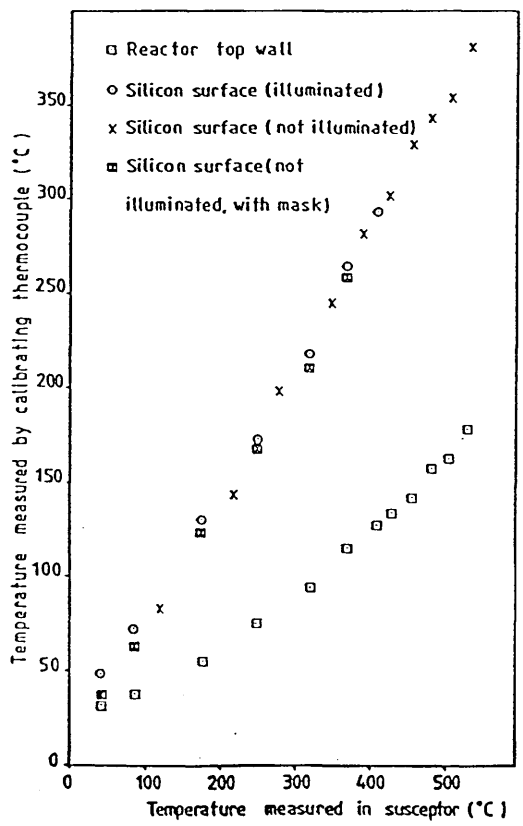


Figure 3.14 Calibration of Substrate Temperature

3.8.2 FILM UNIFORMITY AS A FUNCTION OF GAS FLOW RATE

To investigate the uniformity of growth with increasing gas flow rates, 38mm diameter silicon slices were used as substrates. This size of slice relative to the susceptor and the reactor width is shown in figure 3.15.

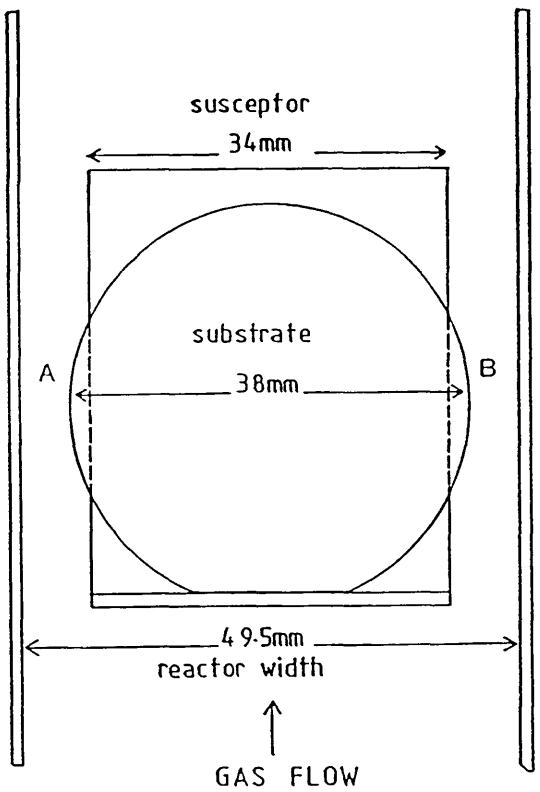


Figure 3.15 Illustrating the Size and Position of a 38mm Silicon Slice relative to the Susceptor and Reactor Walls

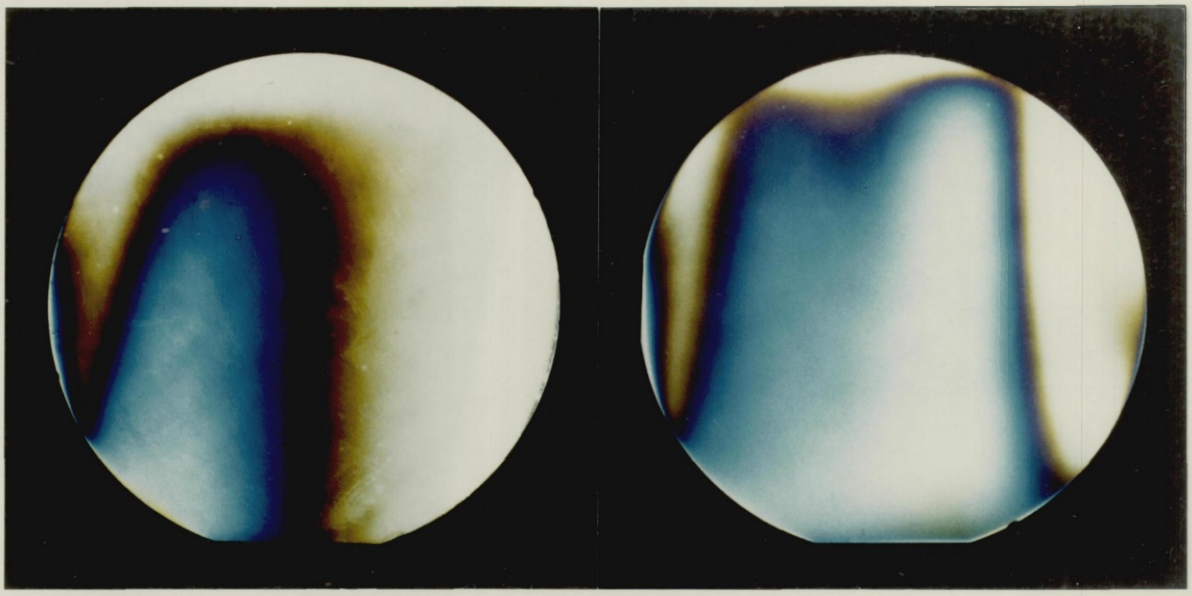
The close proximity of the slices to the reactor walls and the small overhang of the slice over the susceptor edge will inevitably lead to a lower temperature at regions A and B of the

slice as shown in figure 3.15. For this characterisation two substrate temperatures of 200 and 350°C were investigated and gas flow rates of 6.667, 20, 46.7, and 73.3 $cm^3 s^{-1}$ were used for both temperatures. The alkoxide injection rate was maintained at 1.575×10^{-7} moles s^{-1} throughout and the results of these growth runs are given in figures 3.16a-d and 3.17a-e for 200 and 350°C respectively. The thickness of the films is indicated by the interference colours as discussed later in section (5.2.1). For both temperature conditions the gas flow rate of 6.667$cm^3 s^{-1}$ produced a very non-uniform film (figures 3.16 a and 3.17 a). During the growth run at this flow rate extensive wall deposition occurred which exhibited patterns associated with convective flow. Increasing the gas flow rate to 20$cm^3 s^{-1}$ improved the uniformity in the centre region of the slices (figures 3.16b and 3.17b) and a reduction in wall deposition was observed. For the 200°C samples, gas flow rates of 46.7 and 73.3$cm^3 s^{-1}$ produced a reasonably uniform film (figures 3.16c and d). The corresponding films grown at 350°C (3.17c and d) were less uniform at the edges of the slices close to the reactor wall. This could be due to a higher thermal gradient at the higher substrate temperature.

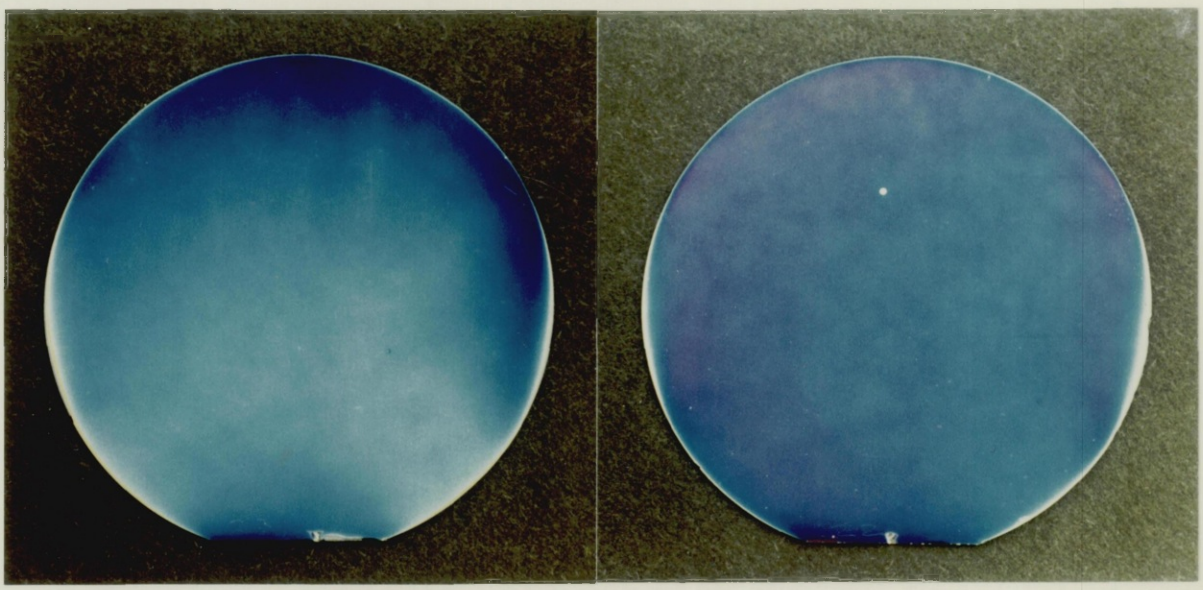
For the majority of growth runs in subsequent experiments smaller size substrates have been used; typically 15mm square in area. These have been placed centrally on the susceptor to obtain the best uniformity and the majority of deposition has been carried out with a gas flow rate of 73.3$cm^3 s^{-1}$.

3.8.3 CALCULATION OF DIMENSIONLESS NUMBERS

The uniformity of oxide deposition for this particular apparatus has been investigated experimentally. To compare the

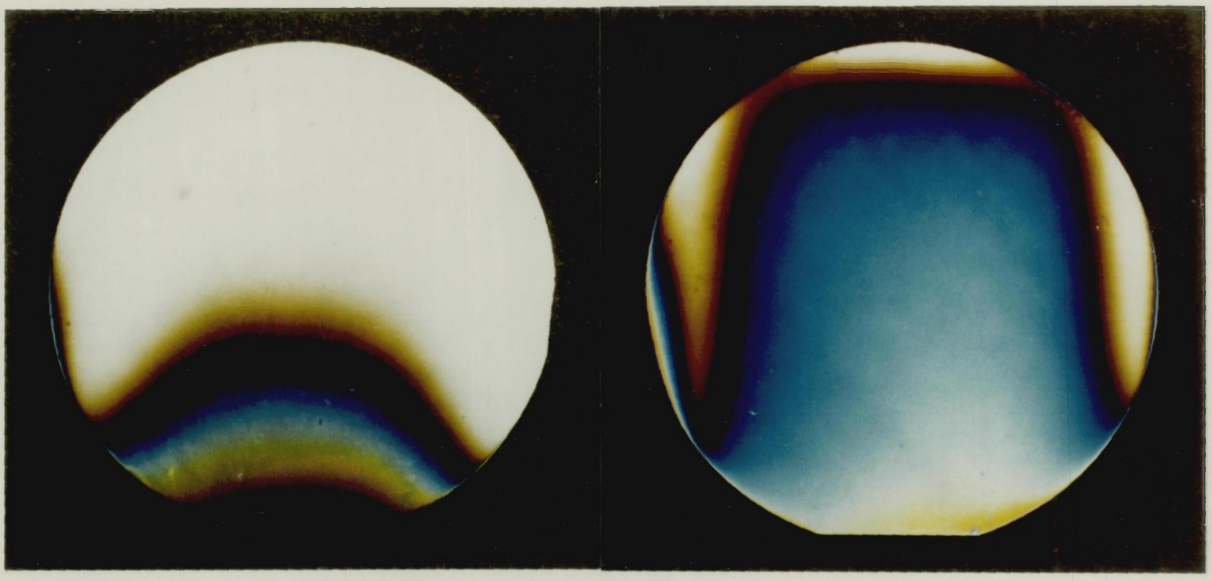


(a) gas flow = $6.7 cm^3 s^{-1}$ (b) gas flow = $20 cm^3 s^{-1}$

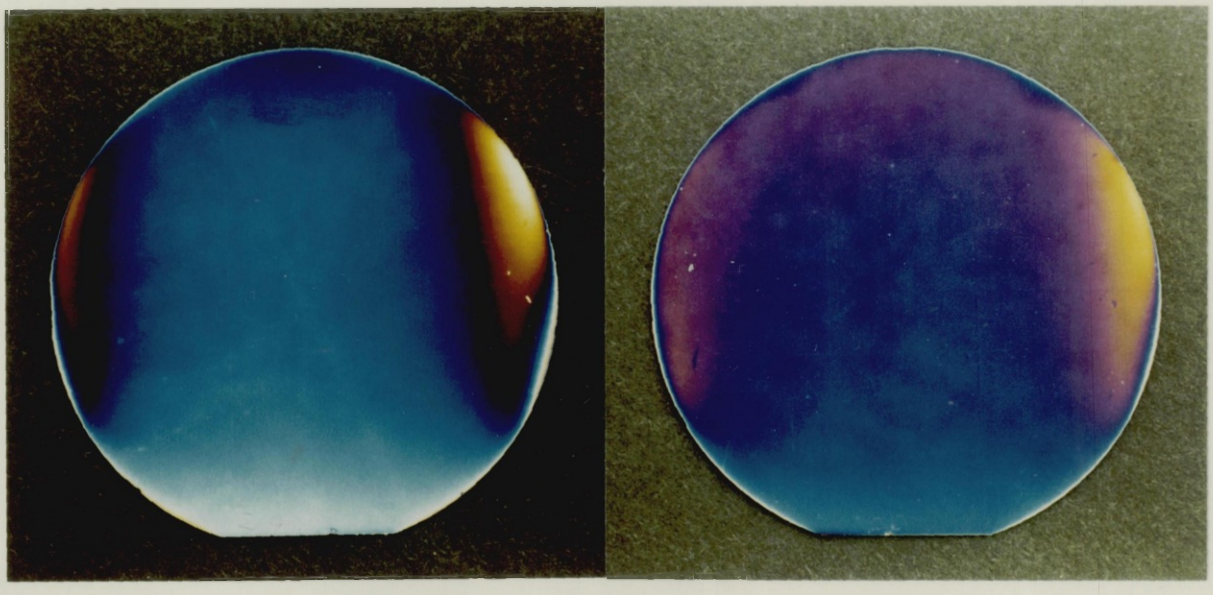


(c) gas flow = $46.7 cm^3 s^{-1}$ (d) gas flow = $73.3 cm^3 s^{-1}$

Figure 3.16a-d Illustrating the uniformity of titanium dioxide growth at 200 C as a function of gas flow rate.



(a) gas flow = $6.7 cm^3 s^{-1}$ (b) gas flow = $20 cm^3 s^{-1}$



(c) gas flow = $46.7 cm^3 s^{-1}$ (d) gas flow = $73.3 cm^3 s^{-1}$

Figure 3.17a-d Illustrating the uniformity of titanium dioxide Growth at 350 C as a function of gas flow rate.

results with the theoretical analysis discussed in section 1.4.1 the values of the Reynolds, Rayleigh and Grashof numbers are estimated. The mean velocity of the gas passing through the reactor immediately above the susceptor has been varied from $0.412 cms^{-1}$ to $6.185\ cms^{-1}$ in the present set of experiments.

3.8.3.1 CALCULATION OF REYNOLDS NUMBER

Taking equation (1.10) for Reynolds number

$$Re = vh\rho/\eta$$

with a free height of 3.3cm above the susceptor and ρ/η as 6.39 (calculated from Giling 1983) for a velocity of $0.412\ cms^{-1}$ the Reynolds number is 8.69 and for a velocity of $6.185\ cms^{-1}$ the Reynolds number is 130. Hence the maximum Reynolds number of 130 is well below the critical value of 2300 for the transition to turbulent flow and the reactor is operating in the laminar regime.

3.8.3.2 RAYLEIGH NUMBER

To estimate the value of the Rayleigh number the susceptor temperature has been taken as 500K, the top reactor wall as 300K and the free height above the susceptor as 0.033m. From Giling(1983), for nitrogen at 500K, the relevent numbers are:

$\beta = 1/T$, $g = 9.81 ms^{-2}$, $C_p = 1056.6\ JKg^{-1}K^{-1}$, $\rho = 682.8 \times 10^{-3}\ Kgm^{-3}$

$\Delta T = 200K$, $\eta = 25.59 \times 10^{-6} Kgm^{-1}s^{-1}$ $\kappa = 38.4 \times 10^{-3} Jm^{-1}s^{-1}K^{-1}$.

Using the equation (1.11) for Rayleighs number :

$$Ra = \frac{g\, Cp\, \rho^2 \beta h^3 \Delta T}{\eta \kappa}$$

yields a value of 70700 which indicates that the gas is not stable with respect to convection.

3.8.3.3 ENTRANCE LENGTHS

Using equations (1.17) and (1.18) for the velocity and temperature entrance lengths respectively, and using the minimum and maximum values of Reynolds numbers occurring in the present reactor, gives velocity entrance lengths of:

(1) Re = 130, $X_V = 0.04hRe = 0.04 \times 0.033 \times 130 = 0.17m$

(2) Re = 8.69, $X_V = 0.04hRe = 0.04 \times 0.033 \times 8.69 = 0.01m$

and thermal entrance lengths of:

(1) Re = 130, $X_T = 0.28hRe = 0.28 \times 0.033 \times 130 = 1.20m$

(2) Re = 8.69, $X_T = 0.28hRe = 0.28 \times 0.033 \times 8.69 = 0.08m$

The actual length of the susceptor used is 0.049m and the substrate is typically placed in the first two cm. Hence from these calculations the substrate is positioned in a developing velocity and temperature profile.

3.8.3.4 RATIO OF Gr/Re^2

The Grashof number is given by Ra/Pr where Pr is typically 0.7. Hence for Ra of about 70000, Gr = 100000. Taking the maximum and minimum values of the Reynolds number gives ratios of Gr/Re^2 of

(1) Re = 130, $Gr/Re^2 = 5.92$

(2) Re = 8.69, $Gr/Re^2 = 1324$

These ratios are classified as (1) combined flow and (2) free flow, according to Sparrow et al., (1959). Considering experimental results (figures 3.16 & 3.17), the minimum gas flow velocity resulted in very non-uniform growth (figures 3.16 & 3.17a), as expected from free flow conditions and increasing the gas velocity into the combined flow regime improved the uniformity (figure 3.16b-d & 3.17 b-d).

3.9 COMPARISON WITH CVD GROWTH OF TITANIUM DIOXIDE BY OTHER WORKERS

Much of the literature analysing the flow in CVD reactors has been concerned with silicon growth which involves higher substrate temperatures and often higher gas flow velocities than used in oxide deposition. It is difficult to to compare the present apparatus with the reactors used to grow titanium dioxide by other workers because of the lack of data presented and the variety of reactor designs. The reactors used have been described in chapter 2 and can be categorised into three main types:

(1) Vertical reactors with rotating substrates used by Wang et al.,(1970), Balog et al., (1972) and Takahashi et al., (1985), as shown in figure 2.8.

(2) A cruder version of vertical reactor where the vapour stream of reactants impinges on the substrate often placed on a hotplate in the atmosphere, used by Hovel, (1978), Feuersanger,(1964) and Fitzgibbons et al.,(1972), as shown in figure 2.3.

(3) Horizontal reactor, used by Ghoshtagore and Noreika,(1970), Sladek and Gibert, (1972) and Fuyuki et al.,(1988). Sladek and Gibert reported that the spatial variation in oxide thickness of

films grown in a circular cross section reactor was improved by using a rectangular cross section reactor (figure 2.5b)

Values of flow rate have been reported by some workers; Balog et al.,(1972) and Yokozawa et al.,(1968) used 16.7 $cm^3 s^{-1}$ and Wang et al.,(1970) used 60.75 $cm^3 s^{-1}$ and the carrier gases were either nitrogen or helium, with oxygen being added by some workers as a reactive gas. The carrier gases used are summarised in table 3.1

TABLE 3.1 SUMMARY OF CARRIER GASES AND REACTOR TYPES

GAS	REACTOR CATEGORY	REFERENCE
$N_2 + O_2$	3	Fuyuki et al (1988)
$N_2 + O_2$	vertical furnace	Takahashi et al. (1981)
N_2	2	Hovel (1978)
N_2	2	Hardee & Bard (1975)
$He + O_2$	1	Balog et al. (1972)
$He + CO_2$	2	Fitzgibbons et al (1972)
N_2	3	Sladek & Gibert (1972)
$He + O_2$	1	Wang et al. (1970)
$N_2 + O_2$	-	Yokozawa et al. (1968)
O_2 or N_2	2	Feuersanger (1964)
N_2 ($TiCl_4$)	2 (modified)	Yeung & Lam (1983)
O_2 ($TiCl_4$)	3	Ghoshtagore & Noreika (1970)

In the present work a rectangular horizontal reactor of type 3 was used with nitrogen carrier gas operating a flow rate range of 6.667 to 100 $cm^3 s^{-1}$.

CHAPTER 4 CHARACTERISATION OF TITANIUM ISOPROPOXIDE AND VANADIUM (V) TRIISOPROPOXIDE OXIDE

4.1 THERMAL CHARACTERISATION

In the process of growing the metal oxide films from the metal alkoxide precursor compounds the molecule thermally decomposes to the oxide plus volatile waste products. This decomposition has been investigated by differential thermal analysis (DTA) and thermogravimetric analysis (TGA) in a Stanton Redcroft DTA/TGA. A drop of the precursor liquid was placed in a platinum crucible which was heated at a rate of $10^{o}Cmin^{-1}$ from $20^{o}C$ to $1000^{o}C$ in a nitrogen atmosphere; alumina was used in the reference crucible.

4.1.2 THERMAL DECOMPOSITION OF TITANIUM ISOPROPOXIDE

The DTA/TGA results for titanium isopropoxide are shown in figure 4.1.

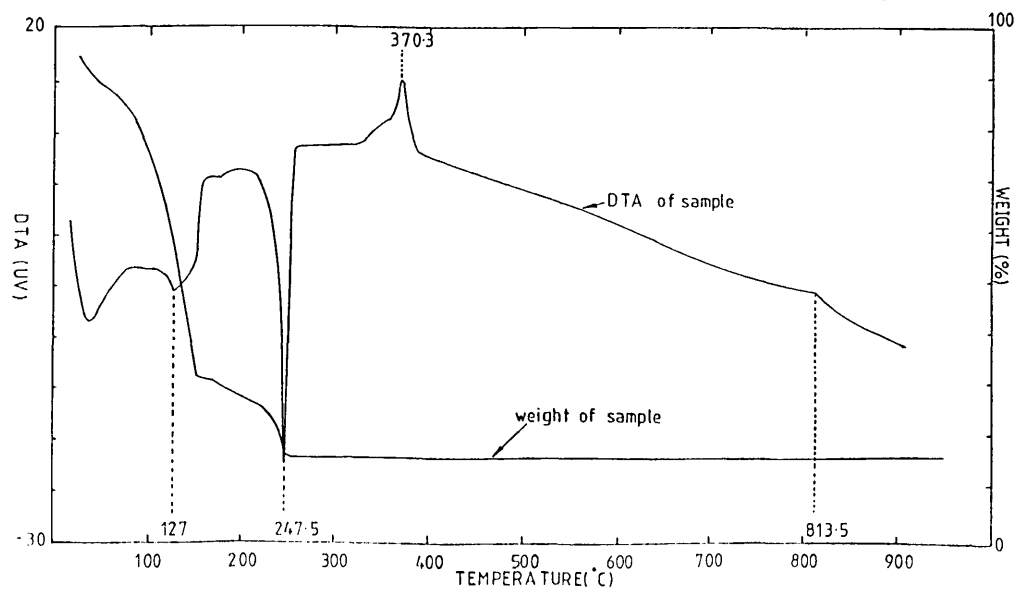


Figure 4.1 Thermal Decomposition of Titanium Isopropoxide as studied by DTA/TGA

Considering the TGA response which monitors weight loss, two distinct stages are present; the first stage below about 150°C exhibits quite rapid weight loss and the second stage from 150 to 250°C is a more gradual weight loss. The DTA behaviour showed two endothermic reactions corresponding to the two stages; the temperatures of the DTA peaks being 127 and 247.5°C respectively. The second endothermic peak at 247.5°C was particularly pronounced and it corresponds to the complete decomposition to the oxide as no subsequent weight loss is observed as the temperature is increased to 1000°C. Further changes however do occur in the DTA curve above 250°C. A significant exothermic peak is present at 370°C and a smaller peak at 813.5°C. To investigate the nature of these reactions samples were taken which had been heated to 300°C, 400°C and 980°C and Debye-Scherrer x-ray diffraction was carried out on the powders. The sample heated to 300°C gave a diffuse halo pattern indicating an amorphous structure; heating to 400°C produced an anatase pattern as shown in figure 4.2a and heating to 980°C produced a mixture of anatase and rutile as shown in figure 4.2b. These identifications were made by comparing the film to standards in the Department of Mineralogy, Natural History Museum. Hence the peak at 370°C was identified as a crystallisation reaction and the peak at 813.5°C indicated the transition from anatase to rutile. This transition is not an instantaneous one as discussed in section (2.2.1).

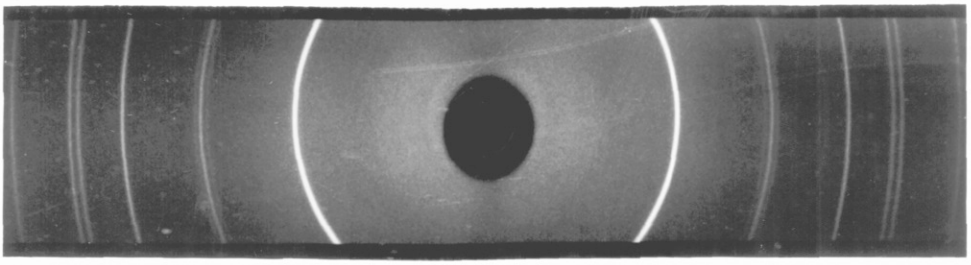


Figure 4.2a Debye Scherrer X-ray of Titanium Isopropoxide Heated to 400°C showing an Anatase Crystal Structure.

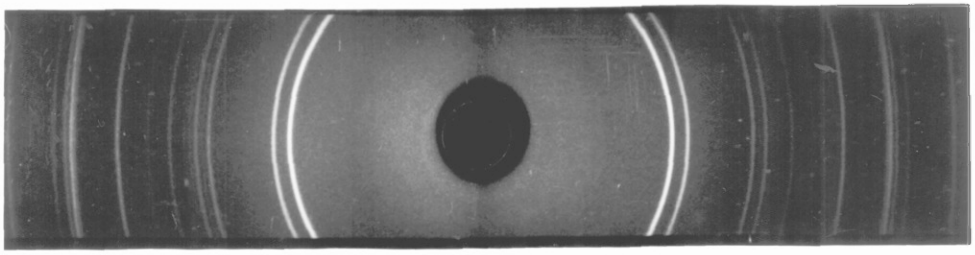


Figure 4.2b Debye Scherrer X-ray of Titanium Isopropoxide Heated to 980°C showing a mixture of Anatase and Rutile.

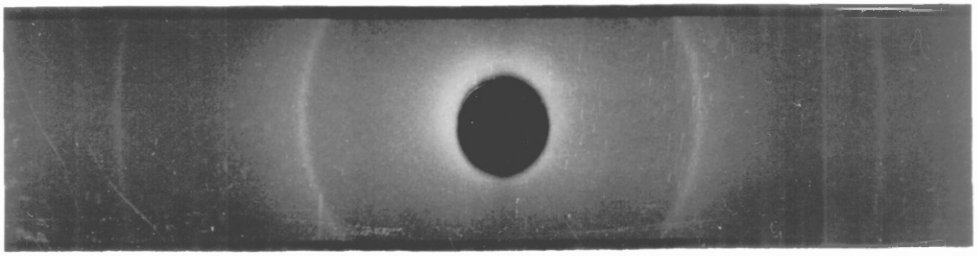


Figure 4.4a Debye Scherrer X-ray of Vanadium (V) Triisopropoxide Oxide Heated to 400°C.

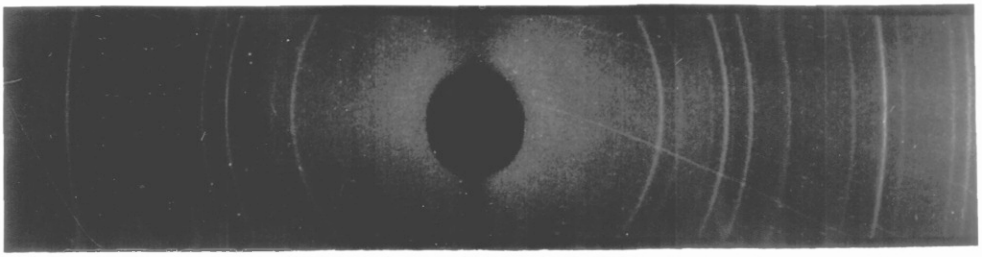


Figure 4.4b Debye Scherrer X-ray of Vanadium (V) Triisopropoxide Oxide Heated to 750°C, showing predominantly V_2O_3 reflections.

4.1.3 THERMAL DECOMPOSITION OF VANADIUM (V) TRIISOPROPOXIDE OXIDE

The DTA/TGA response for vanadium (V) triisopropoxide oxide is given in figure 4.3.

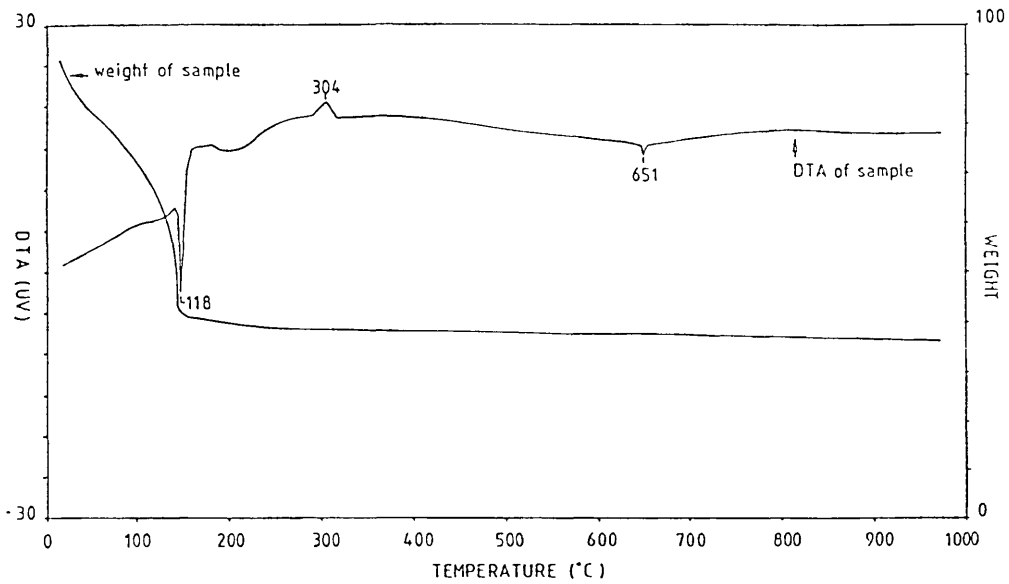


Figure 4.3 Thermal Decomposition of Vanadium (V) Triisopropoxide Oxide as studied by DTA/TGA

The behaviour of the vanadium (V) triisopropoxide oxide given by the TGA curve shows a continuous and significant weight loss upto a temperature of approximately 120°C. A sharp endothermic peak in the DTA curve occurs at 118°C which is similar to the titanium isopropoxide peak at 247.5°C. Above approximately 120°C the TGA curve flattens out but careful examination reveals that a small continuous weight loss occurs over the whole temperature range. The small exothermic peak at 304°C and the

small endothermic peak at 651°C were investigated by Debye-Scherrer x-ray of powders heated to 250, 450 and 750°C in a nitrogen atmosphere. The x-ray photographs are shown in figures 4.4. The powder heated to 250°C and to 450°C both contained two reflections as shown in figure 4.4 a the sample heated to 750°C produced numerous reflections. The colour of the powder changed from dark green at 450°C to black after heating to 750°C which indicates a change in oxidation state of the vanadium oxide.

The lower temperature vanadium oxide was difficult to identify because only two x-ray reflections were present. Numerous vanadium oxides form as indicated by the phase diagram shown in figure 2.20. The two reflections correspond to lattice spacings of approximately 3.4 and 1.8Å; several vanadium oxides have strong reflections at lattice spacings close to these values and these include V_6O_{13}, V_3O_7 and a VO_2 which forms above 220 and below 330°C. The diffuse nature of the reflections and the fact that only two were present suggests that a certain amount of 'amorphous' structure was present in the sample.

The oxide heated to 750°C was of a much more crystalline nature, giving numerous sharp relections. The strongest reflections have been identified as V_2O_3. This oxide is black and the lower oxygen content of this oxide compared to the possible candidates for the lower temperature sample is consistent with the weight loss observed in the TGA trace of figure 4.3. The DTA peaks cannot be conclusively identified for the vanadium (V) triisopropoxide oxide trace. The peak at 651°C is probably a transition to V_2O_3 but the peak at 304°C showed no difference in the x-ray results.

4.2 DISCUSSION OF RESULTS

The two stage weight loss of the titanium isopropoxide was also observed by Mazdiyasni et al. (1965) for zirconium alkoxides as shown in figure 4.5.

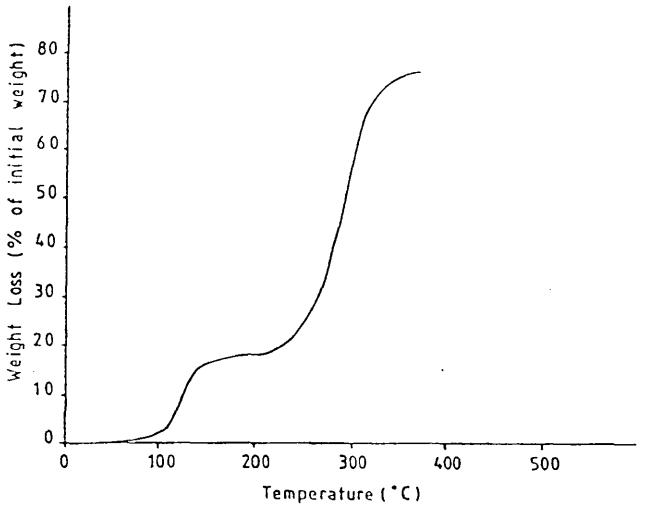


Figure 4.5 TGA Curve showing Decomposition of Zirconium Alkoxide in a Nitrogen Atmosphere, after Madiyasni et al.,(1965).

The reaction mechanism of the pyrolysis of the zirconium akloxide was discussed by Mazdiyasni et al.(1965) and the successive steps are shown in figure 4.6.

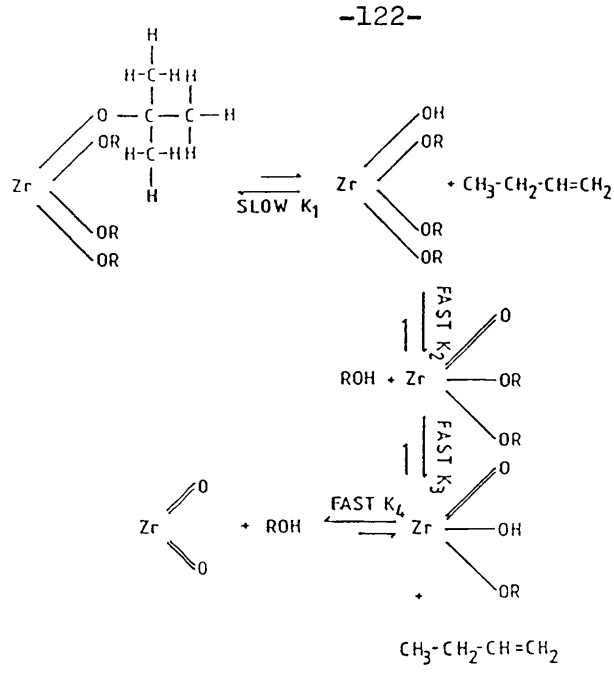


Figure 4.6 Decomposition Steps of Zirconium Alkoxide after Maziyasni et al. (1965)

The initial decomposition step in which an alkene is split out was slow and this is the step that Mazdiyasni et al.(1965) attributed to the first stage of decomposition between 100 and 125°C in the TGA curve. The subsequent more rapid stages occurred in the 250 to 300°C temperature range.

The reaction mechanism proposed by Mazdiyasni et al. (1965) differs from the mechanism of Bradley and Faktor (1959)a who suggested that the rate controlling process is the dehydration of the alchol. The water produced by the dehydration immediately hydrolysed the Zr-OR groups.

The alkoxide in this experiment was placed into the platinum crucible and then heated in a stream of nitrogen. The exposure of the compound to the atmosphere and to a nitrogen stream which probably contained some moisture is likely to have caused some hydrolysis of the sample. A partially hydrolysed compound could explain the two stage decomposition observed in figure 4.1 for the titanium isopropoxide (Prof. Bradley, private communication). The first large weight loss can be attributed to

the vaporisation of the alkoxide which has not undergone hydrolysis, and the second weight loss to the thermal decomposition of the alkoxide which has suffered partial hydrolysis.

The vanadium (V) triisopropoxide oxide was seen to have a single decomposition stage (figure 4.3). The susceptibility of this compound to hydrolysis and its volatility are unknown. There was some vanadium oxide left in the crucible after the experiment had finished which indicated that the weight loss did not correspond to all the compound vaporising. It is possible that the thermal decomposition of this compound is much more facile than the titanium isopropoxide and the weight loss is actually a decomposition to the oxide. It does not appear to be an intermediate or partially hydrolysed product because no further weight loss is observed.

The technique of DTA/TGA gives useful information on how the liquid alkoxide decomposes as a function of temperature. Direct comparison with the conditions present in the CVD reactor however cannot be fully justified. In CVD the alkoxide is vaporised and decomposition occurs in a controlled manner on a heated surface from the vapour phase. It is likely that some water molecules are present in the reactor and hydrolysis can occur. As discussed in chapter 2, water has been deliberately added to promote the reaction in some cases. Any surface catalytic contribution to the decomposition cannot be investigated by DTA/TGA and the heating rate of $10^{o}Cmin^{-1}$ employed differs from a molecule of the alkoxide reacting on the substrate surface maintained at a constant temperature. The solid state reactions of crystallisation and transformation

from anatase to rutile do occur in CVD but the temperatures can significantly differ due to the more controlled decomposition conditions on the substrate surface where rearrangement can permit a more ordered structure. The concentration of alkoxide decomposing can also influence the structure; rapid decomposition from a high concentration is more likely to produce an amorphous structure because time for the atoms to arrange into a crystalline state is limited.

4.3 RESPONSE OF LIQUID ALKOXIDE TO UV ILLUMINATION

To investigate the response of the liquid precursor to the UV light of the Mercury lamp a sample was contained in a quartz tube and irradiated. The titanium isopropoxide was observed to turn from a colourless liquid to a dark blue colour as shown in figure 4.7. This reaction proved to be slowly reversible if left in the quartz container and reverted quickly if exposed to air. The dark blue colour indicates a change from Ti^{4+} to Ti^{3+}.

Illuminating the vanadium (V) triisopropoxide oxide under the same conditions produced a dark brown colour from the clear liquid as shown in figure 4.8. The vanadium (V) triisopropoxide oxide was much slower to revert to the clear liquid than the titanium isopropoxide and examination of the quartz tube showed that a film had formed in the most intense region of illumination.

The exposure of the liquid titanium isopropoxide and vanadium (V) triisopropoxide oxide to UV demonstrates that the compounds interact with the illumination from the mercury arc lamp. As with the DTA/TGA experiment described in section 4.1, a direct correlation with the situation in the reactor cannot be made. The

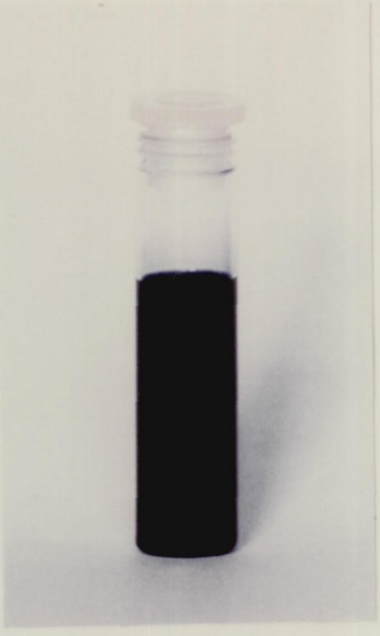


Figure 4.7 Sample of Titanium Isopropoxide after Illuminating with UV Light.

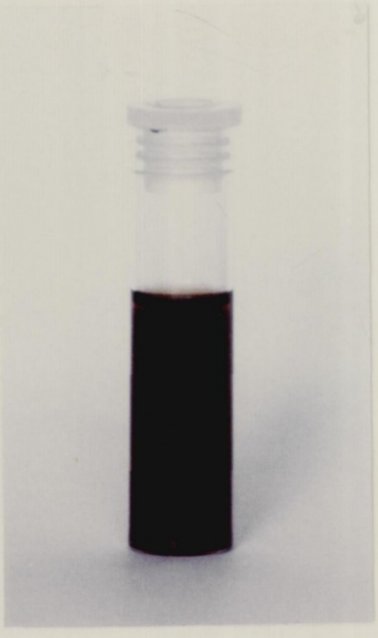


Figure 4.8 Sample of Vanadyl Propoxide after Illuminating with UV Light.

exact nature of the interaction of the precursor molecule is unknown; it may occur in the vapour phase before the molecule reaches the substrate or it may occur in the adsorbed state on the substrate surface. The experiment shows the response of a large volume of liquid alkoxide to the illumination at room temperature. In the reactor the molecules are thermally excited, have a greater nearest neighbour distance and are either in a nitrogen gas stream or an adsorbed state on the substrate; the latter being more like a thin 'liquid' layer on the surface.

CHAPTER 5 : EXPERIMENTAL SECTION

INVESTIGATION INTO THE DEPENDENCE OF TITANIUM DIOXIDE GROWTH RATE ON SUBSTRATE TEMPERATURE, CONCENTRATION OF TITANIUM ISOPROPOXIDE AND GAS FLOW RATES

5.1 INTRODUCTION

Experiments have been carried out to determine the growth rate of the oxide films under differing conditions of substrate temperature, alkoxide concentration, gas flow rate and illumination with UV radiation. These results are unique to the particular apparatus used in this work and identical results are unlikely to be obtained for a reactor of different design. However the general behaviour of growth with the parameters studied should be reproducible in other systems.

5.2 EXPERIMENTAL DETAILS

The growth rate of the titanium dioxide films has been investigated as a function of:

(1) Substrate temperature (room temperature to 400^{o}C).
(2) Alkoxide injection rate (0.35×10^{-7} moles s^{-1} to 6.505×10^{-7} moles s^{-1}).
(3) Gas flow rates (at 350^{o}C and 250^{o}C substrate temperatures).

5.2.1 THICKNESS MEASUREMENT

Three techniques were employed to evaluate the thickness of the oxide films; (1) Talystep measurements, (2) ellipsometry, (3) film colour.

5.2.1.1 TALYSTEP

Talystep measurement involves the surface profile of the film being mapped by the movement of a stylus across the surface. A requirement of this technique is that a step the height of film thickness is present on the surface. This is shown in figure 5.1.

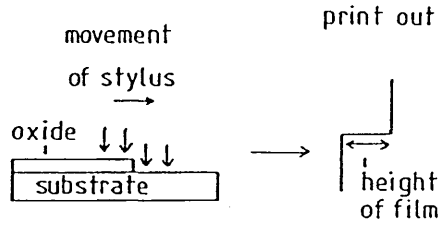


Figure 5.1 Schematic Diagram of Talystep Operation

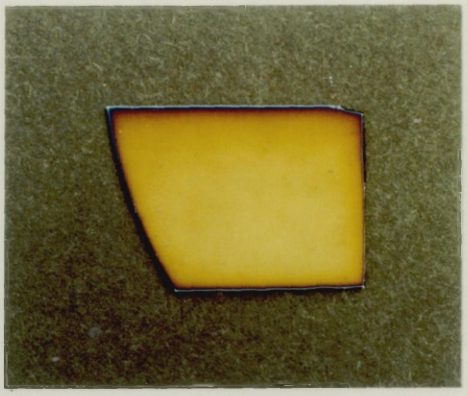
During growth the silicon substrate was partially masked by a second piece of silicon thus producing a step with the height of the film thickness.

5.2.1.2 ELLIPSOMETRY

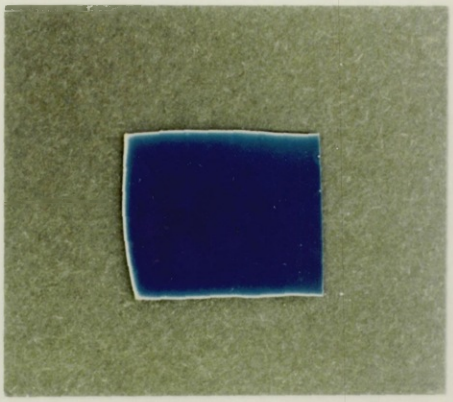
Ellipsometry is a technique that allows the optical properties and thickness of a thin film on a reflecting substrate to be determined by measuring the change in ellipticity of polarised light reflected. The ellipsometer used was a Rudolph Research model with a He-Ne laser of wavelength 632.8nm.

5.2.1.3 INTERFERENCE COLOURS

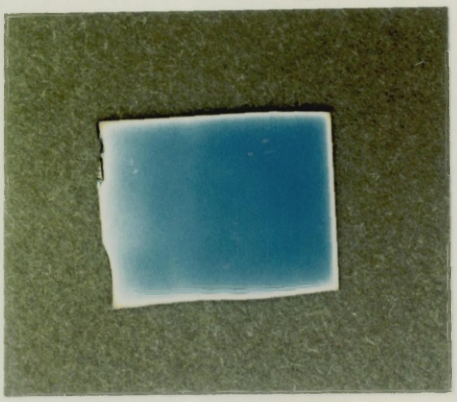
The oxide films changed colour with increasing thickness due to interference effects. A typical series of colours is shown in figure 5.21a-g. The colour is due to interference occurring between the light beams reflected from the upper and lower surfaces of the oxide films. Reflection of specific wavelengths



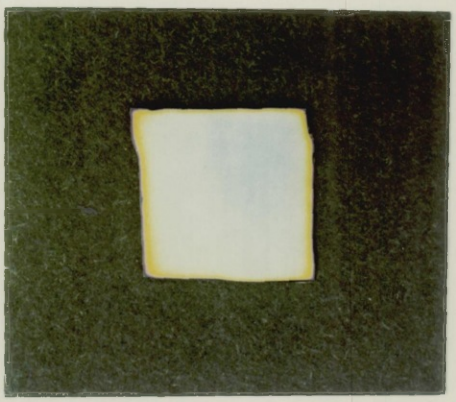
(a) brown



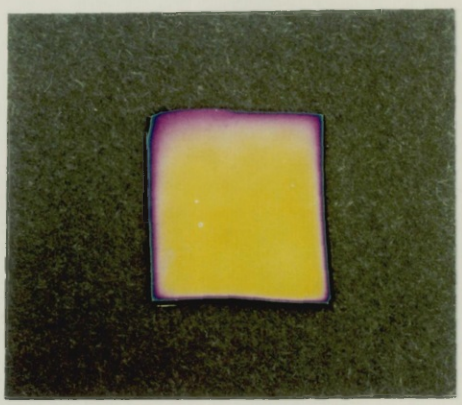
(b) purple



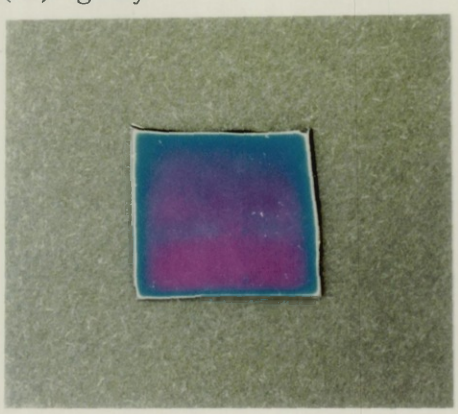
(c) blue



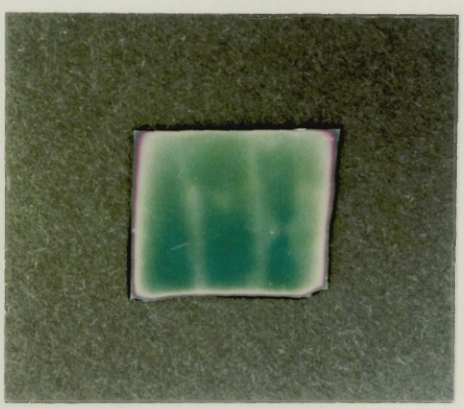
(d) grey



(e) gold



(f) pink



(g) green

Figure 5.2a-g Photographs of Interference colours of Titanium Dioxide Films.

interfere destructively and the remaining wavelengths combine to give a characteristic colour.

Talystep measurements were used for the majority of the film thickness values, with the interference colour being used as a check. Ellipsometry was found to be valuable in determining the thickness of the thinner films where inaccuracies in the Talystep were more appreciable.

5.2.2 PREPARATION FOR GROWTH

Due to the dependence of growth rate on moisture content of the environment (Fuyuki et al., 1988), the apparatus was dried prior to growth and the nitrogen carrier gas was passed through molecular sieves. The silicon substrates were degreased in trichloroethylene and rinsed in distilled water before deposition.

5.3.1 GROWTH RATE AS A FUNCTION OF SUBSTRATE TEMPERATURE AND UV ILLUMINATION

The growth rate of titanium dioxide has been investigated as a function of substrate temperature in the temperature range of 25 - 400^{o}C. A constant gas flow rate of 73.3 $cm^3 s^{-1}$ was used for all of these growth runs. An injection rate of 0.35×10^{-7} moles s^{-1} was employed over the whole temperature range and at higher temperatures an injection rate of 5.30×10^{-7} moles s^{-1} was also investigated. Using the higher injection rate at lower temperatures resulted in condensation of alkoxide on the reactor walls. The effect on growth rate of illuminating the substrate with UV illumination from a 100W mercury arc lamp was also

monitored. During growth, part of the reactor tube was masked off to allow both illuminated and non-illuminated samples to be grown simultaneously.

5.3.2 RESULTS OF GROWTH RATE AS A FUNCTION OF SUBSTRATE TEMPERATURE AND UV ILLUMINATION

Considering a precursor injection rate of 0.35×10^{-7} moles s^{-1} and no photolysis, the growth rate of the oxide film varies with substrate temperature as shown in the Arrhenius plot of figure 5.3.

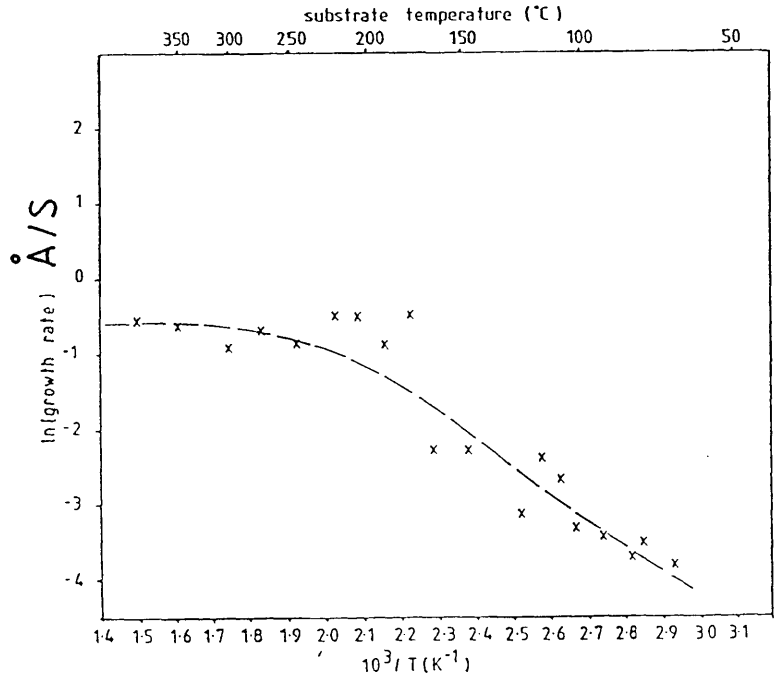


Figure 5.3 An Arrhenius Plot of ln(growth rate) of Titanium Dioxide Against the Reciprocal of the Absolute Temperature for an Injection Rate of 3.5×10^{-7} moles s^{-1}, Gas Flow Velocity of $73.3 cm^3 s^{-1}$.

The general shape of the curve is similar to figures 1.10 and 1.11; at lower temperatures the growth is kinetically limited With increasing temperature, mass transport limitation becomes

LEAST SQUARES FITTING OF DATA SHOWN IN FIGURE 5.4.

The errors in the temperature measurement are small compared with the errors in growth rate and the line of regression of ln(growth rate) on 1/T has been calculated. The least squares fitting provides the best line through the data points assuming a straight line with gradient of (activation energy/Boltzmann's constant). The uncertainty of the values of ln(growth rate), σ_y, has been calculated from equation A.

$$\sigma_y^2 = \frac{1}{N-2} \sum_{i=1}^{N} (Y_i - A - BX_i)^2 \quad ---(A)$$

Where y_i = measured ln(growth rate)

x_i = measured 1/T

A = intercept on y axis

B = gradient

N = number of measurements.

The uncertainty of the gradient B, σ_B , has been calculated from equation B

$$\sigma_B^2 = N\sigma_y^2 / N(\sum X_i^2) - (\sum X_i)^2 \quad ---(B)$$

CALCULATED VALUES

sample (moles/s)	eqn. of line	σ_y	σ_B
0.35×10^{-7}	3.998-2626/T	0.33	864
0.35×10^{-7}(i11)	0.040-635.5/T	0.17	442
5.30×10^{-7}	15.00-7084/T	0.52	2499
5.30x10-7(i11)	16.30-7185/T	0.35	1618

the controlling process.

Figure 5.4 illustrates the effect of both UV illumination and a higher injection rate on the curve of figure 5.3.

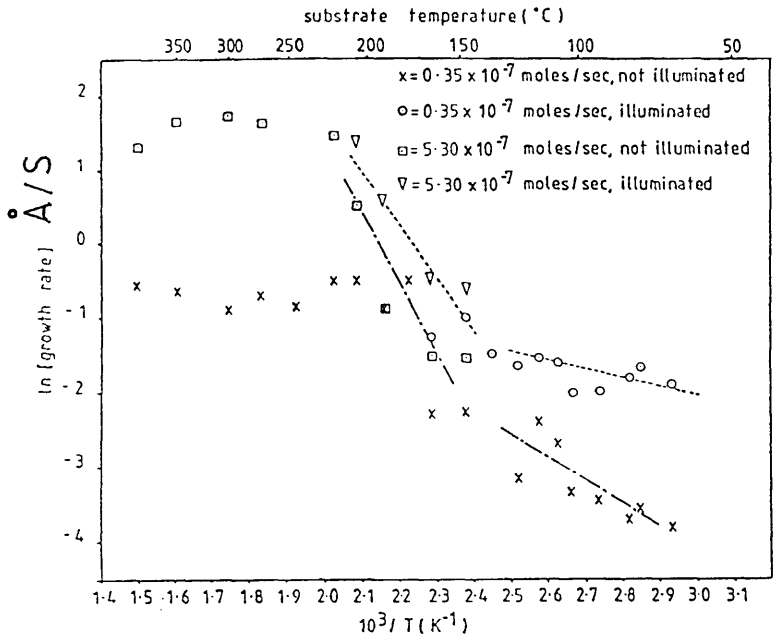


Figure 5.4 An Arrhenius Plot of Titanium Dioxide Growth Rates at Two Different Alkoxide Injection Rates and Showing the Effect of Illuminating the Substrate with UV.

Illuminating the substrate enhances the growth rate at lower temperatures and the activation energy for the process is reduced as indicated by the change in slope. The photolysis appears only to enhance the growth rate in the kinetically controlled region; no difference in growth rate was observed in the mass transport controlled region. Increasing the injection rate of the precursor increases the growth rate in the mass transport controlled region and increases the gradient of the kinetically controlled region. The maximum temperature at which photolysis can be visually observed is greater for the higher injection rate runs than for the lower injection rate runs.

AMENDMENT TO TABLE 5.1

Activation energy values calculated from the least squares analysis (p132).

0.35×10^{-7}	moles/s (P)	0.06 ± 0.04eV
0.35×10^{-7}	moles/s	0.23 ± 0.08eV
5.30×10^{-7}	moles/s (P)	0.60 ± 0.20eV
5.30×10^{-7}	moles/s	0.60 ± 0.20eV

As a result of this analysis it can be seen that in the first case, at low flow rates, there is a small but insignificant effect on the activation energy by illumination. In the second case, at the larger flow rates, there does not seem to be any noticeable effect of illumination.

Estimates of the activation energies have been made from figure 5.4 for the kinetically controlled regions of both alkoxide concentrations and these are given in Table 5.1 along with values of temperature below which photolysis operates.

TABLE 5.1 Activation Energies of Titanium Dioxide Growth

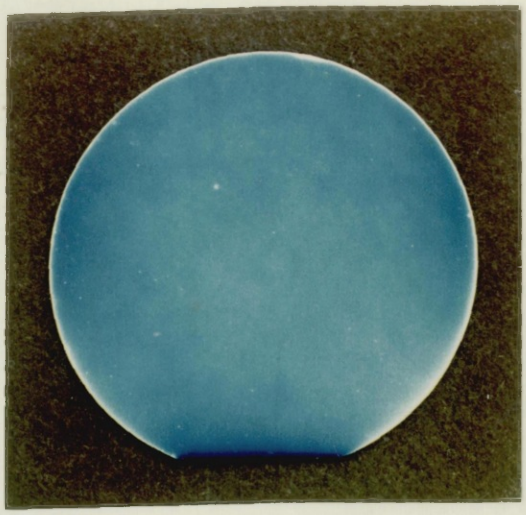
ALKOXIDE INJECTION RATE	TEMPERATURE PHOTOLYSIS OPERATES BELOW(^{o}C)	ACTIVATION ENERGY (eV)
0.35×10^{-7} moles/s	190	0.10(P)
0.35×10^{-7} moles/s		0.26
5.30×10^{-7} moles/s	215	0.62(P)
5.30×10^{-7} moles/s		0.78

From table 5.1 the concentration of the alkoxide molecules in the reactor effects the activation energy as stated by Hitchman (1981). The illumination of the substrate decreases the activation energy in both cases by 0.16eV. These two results are not sufficient to firmly establish the change in activation energy with illumination because only two measurements have been taken and there is some experimental scatter of results presented in figure 5.4. The maximum energy of the light from the mercury lamp of wavelength 253.7nm is 4.9eV which is greater than the change in activation energy observed. It is possible that either a longer wavelength is sufficient to promote growth or only a proportion of the energy input is seen in the change in activation energy of the process.

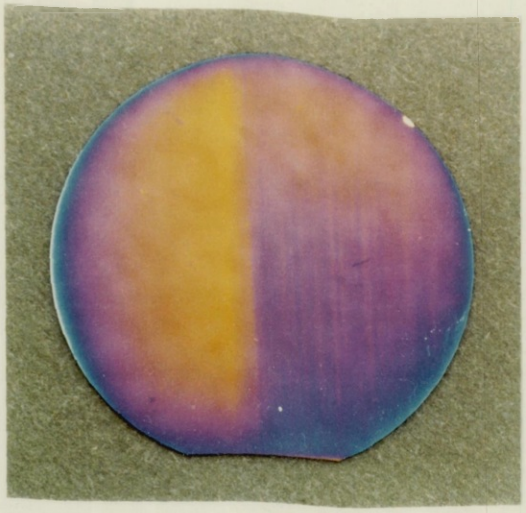
From the Arrhenius plot of figure 5.4, it is evident that the illumination of the substrate sith UV light has an increasingly

important contribution as the substrate temperature is lowered. This is illustrated by figure 5.5a-e, which is a series of five 30mm diameter silicon slices with titanium dioxide grown at temperatures of 70, 100, 130, 160 and 190°C. During deposition the alkoxide injection rate was maintained at 0.35×10^{-7} moles s^{-1} and the gas flow rate at 73.3 $cm^3 s^{-1}$; only the right hand side of the substrate was exposed to UV illumination. The oxide layer grown under illumination has a variation in thickness which is due to the intensity variation of the focussed light beam. the vertical textured appearance is due to the quartz reactor tube which has a longitudinal striated texture.

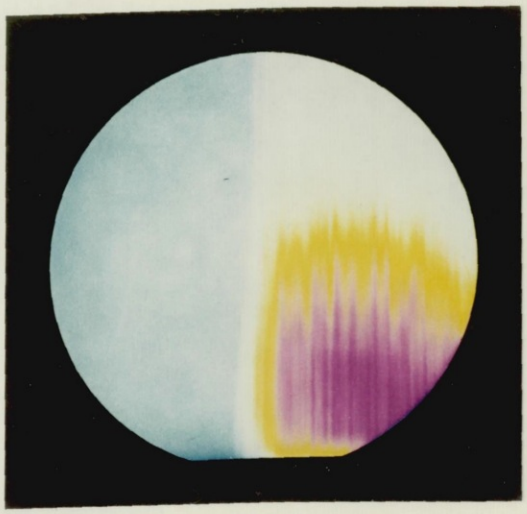
As the substrate temperature is increased from 70 to 190°C the difference in thickness of the oxide grown with and without illumination decreases. In figure 5.5 e a very faint line on the oxide layer can be seen at the point where the substrate was masked; above this temperature, for these growth conditions photolysis would have no visual effect on the oxide layer. The ratio of the thickness of the illuminated layer in the thickest region to the thickness of the non-illuminated layer is plotted in figure 5.6. (The thickness has been estimated from the interference colour of the film).



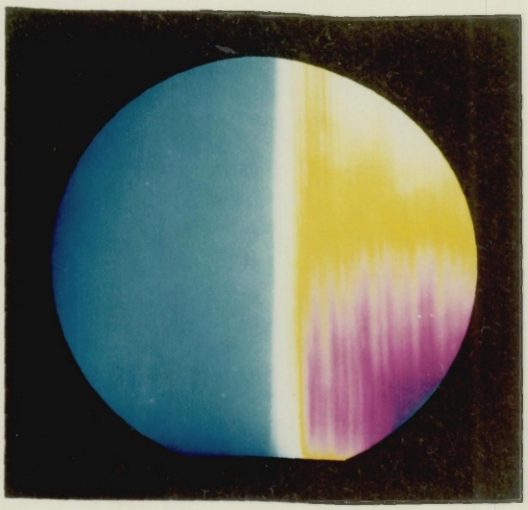
(a) 190°C



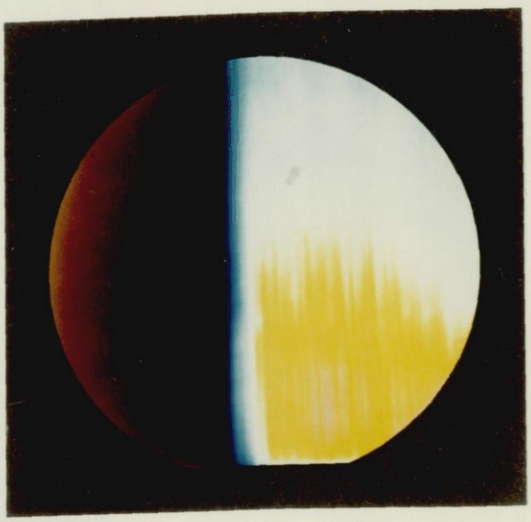
(b) 160°C



(c) 130°C



(d) 100°C



(e) 70°C

Figure 5.5 Illustrating the Increasing Effect of UV Illumination on Titanium Dioxide Growth with Decreasing Substrate Temperature.

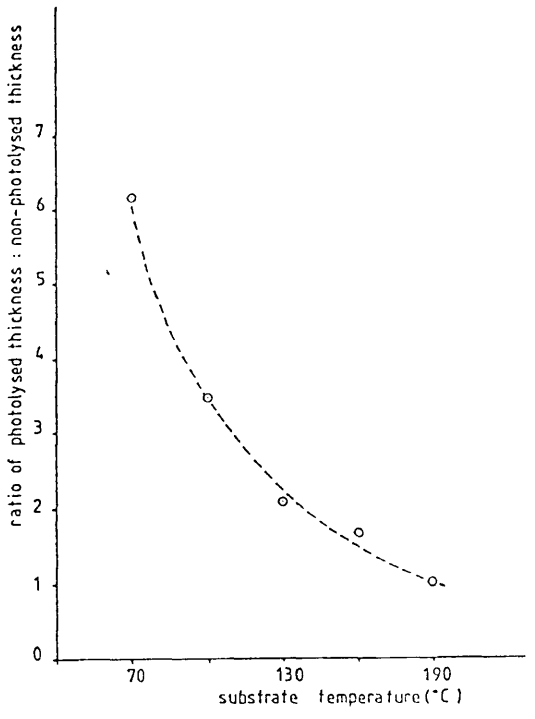


Figure 5.6 Ratio of Thickness of Oxide Film Grown Under UV Illumination to Thickness of Film with no Illumination as a Function of Temperature

5.4.1 GROWTH RATE AS A FUNCTION OF PRECURSOR INJECTION RATE

In this set of experiments the effect of increasing the alkoxide injection rate from 0.35×10^{-7} moles s^{-1} to 6.505×10^{-7} moles s^{-1} was investigated. Substrate temperatures of 190, 220, 300, 350 and 390°C were used and at least ten different injection rates were taken for each temperature condition. The gas flow rate was maintained at $73.3 cm^3 s^{-1}$ as in section (5.3.1). With increasing concentration of alkoxide vapour in the reactor, wall deposition and some homogeneous nucleation were observed and these resulted in a lower vapour concentration of alkoxide at the

substrate than calculated from the input value. Lower temperatures than 190°C were not investigated in this set of experiments because of condensation on the reactor walls. The occurrence of condensation means that the saturated vapour pressure has been exceeded and increasing the input rate would not necessarily increase the vapour phase concentration of the alkoxide.

5.4.2.1 RESULTS OF GROWTH RATE AS A FUNCTION OF PRECURSOR INJECTION RATE

The growth rate of titanium dioxide as a function of injection rate is plotted in figures 5.7a-e for substrate temperatures of 190, 220, 300, 350 and 390°C.

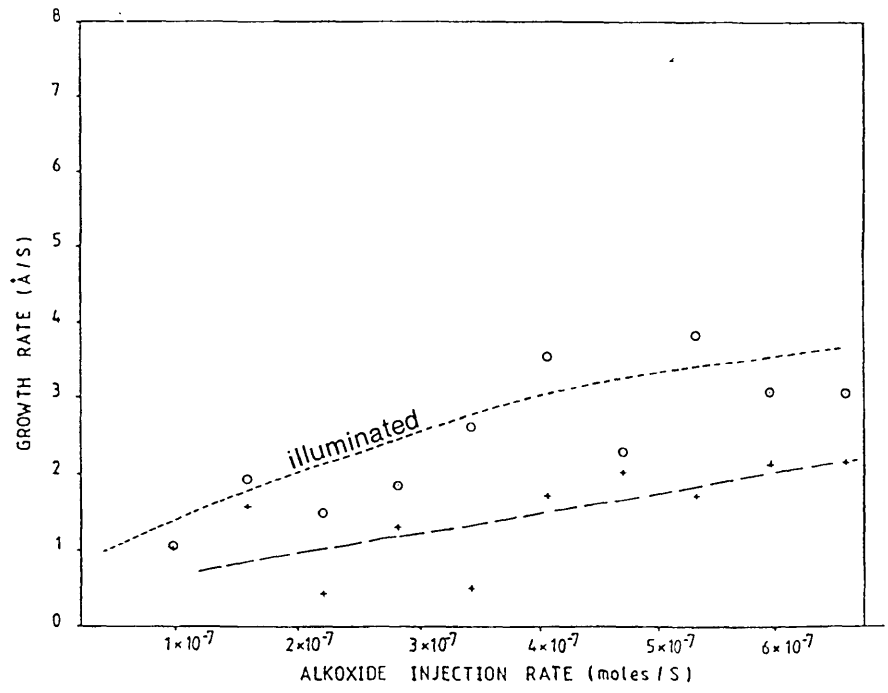


Figure 5.7a Growth Rate of Titanium Dioxide as a Function of Injection Rate at 190°C.

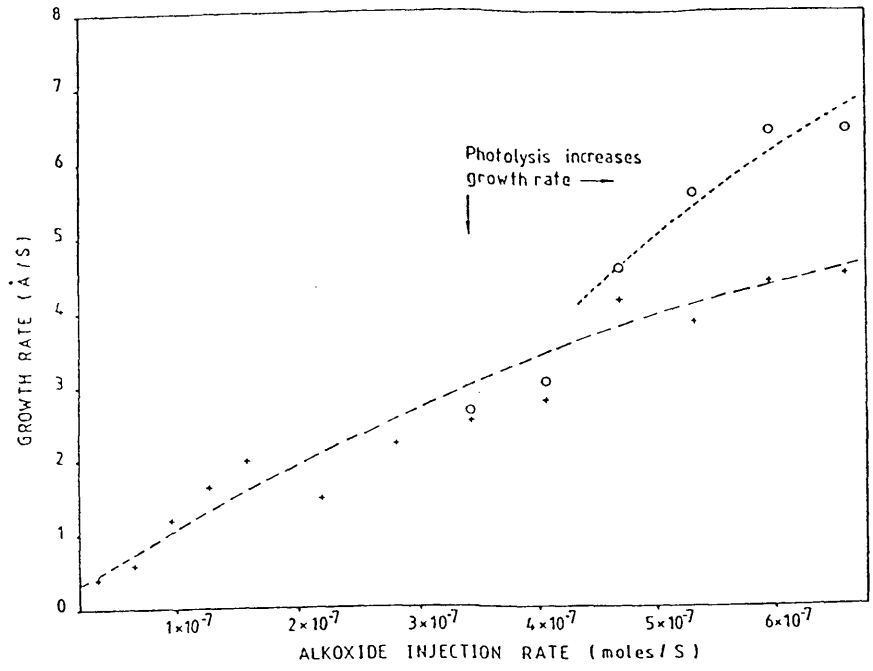


Figure 5.7b Growth Rate of Titanium Dioxide as a Function of Injection Rate at 220°C.

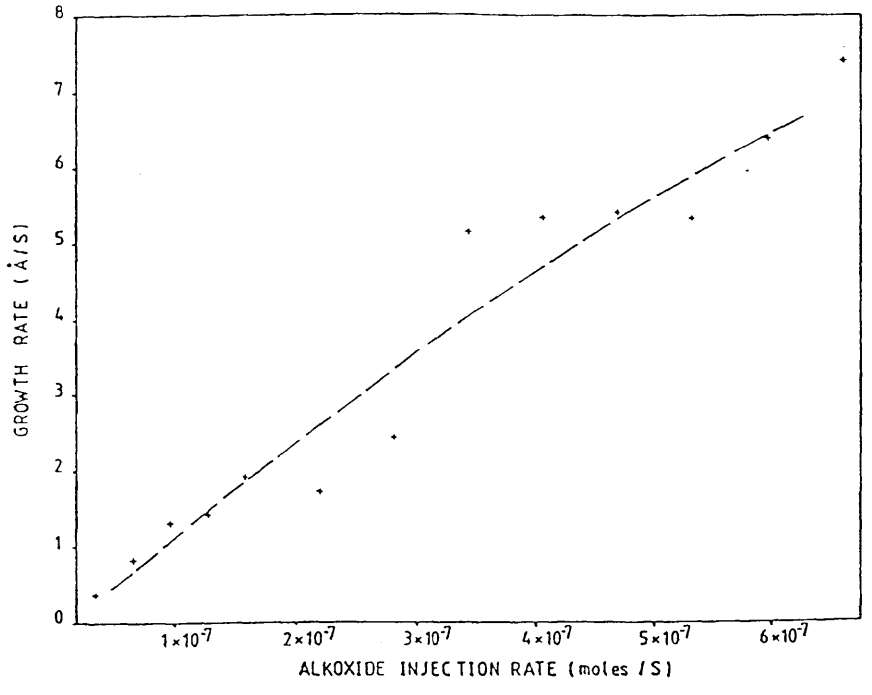


Figure 5.7c Growth Rate of Titanium Dioxide as a Function of Injection Rate at 300°C.

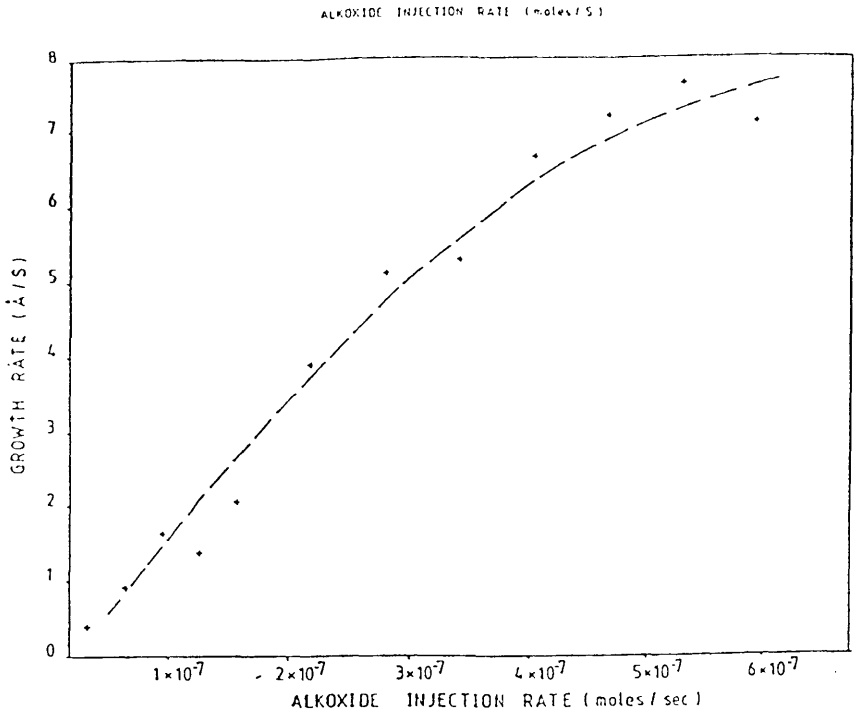


Figure 5.7d Growth Rate of Titanium Dioxide as a Function of Injection Rate at 350°C

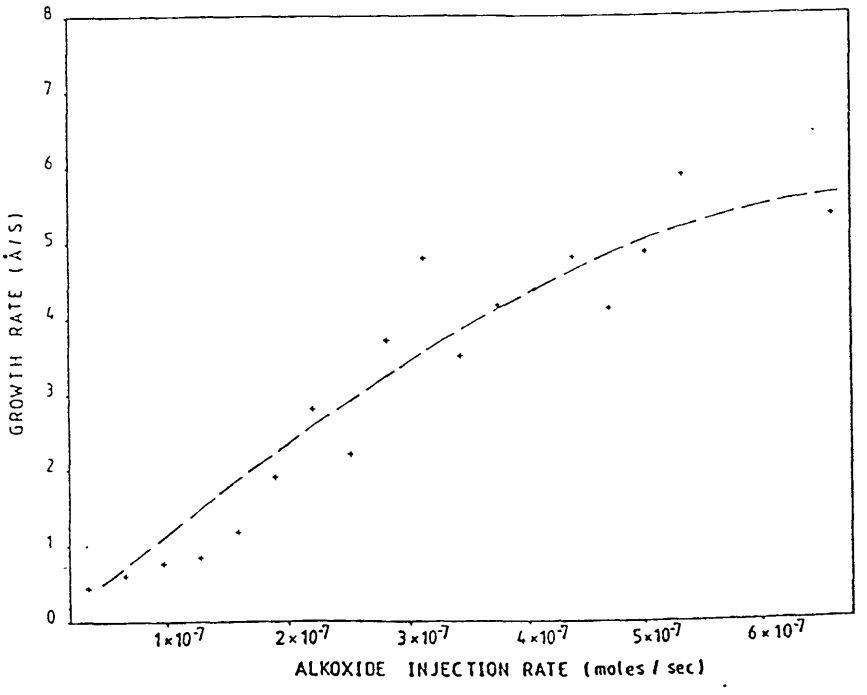


Figure 5.7e Growth Rate of Titanium Dioxide as a Function of Injection Rate at 390°C.

For all the substrate temperatures investigated, the growth rate increased with increasing alkoxide injection rate. However the magnitude of increase in growth rate did vary with the substrate temperature and this is shown more clearly in figure 5.8 which shows plots of all the best line fits of the non-illuminated growth rates on the same graph. The lowest substrate temperature of 190^{o}C has the smallest increase in growth rate with increasing injection rate. Considering the higher substrate temperatures of 220, 300 and 350^{o}C, a progressively larger response in growth rate with increasing alkoxide injection rate is observed. A further increase in temperature to 390^{o}C reverses the trend. At this temperature, substantial oxide deposition on the reactor walls was observed and this would deplete the precursor concentration in the vicinity of the substrate. The growth rate at the lowest alkoxide injection rate of 0.35×10^{-7} moles s^{-1} is approximately the same value for all the temperatures considered and considering figure 5.3 of the Arrhenius plot for 0.35×10^{-7} moles s^{-1}, the temperature range lies in the mass transport limited region for this concentration; the alkoxide molecules have sufficient time to decompose and they are not kinetically limited. Increasing the concentration of alkoxide molecules in the reactor results in the growth rate becoming dependent on temperature, indicating some kinetic limitation to the process.

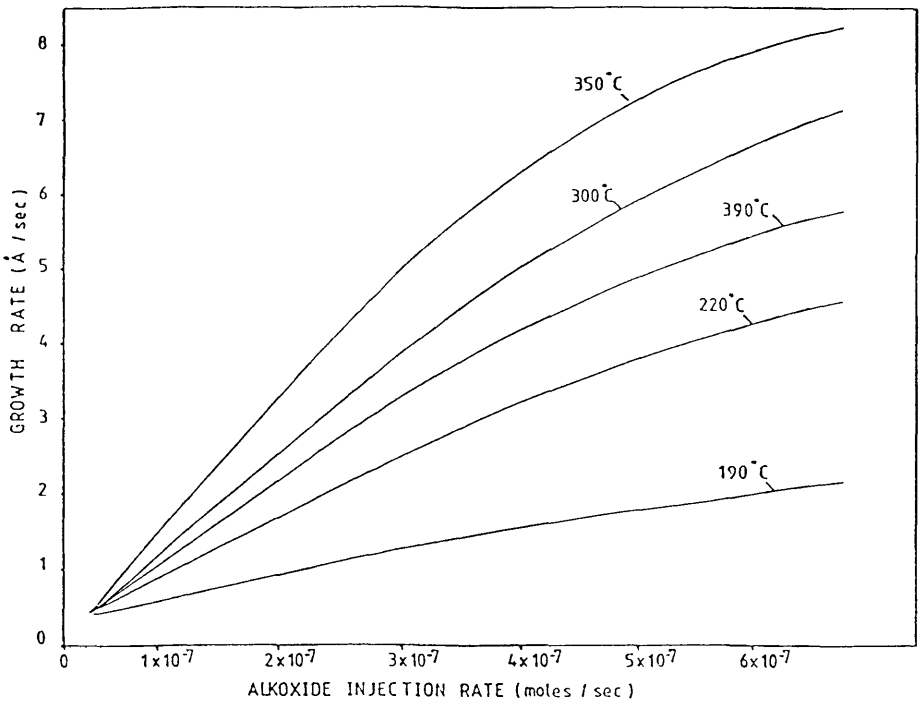


Figure 5.8 Growth Rate of Titanium Dioxide Films as a Function of Alkoxide Injection Rate for Several Substrate Temperatures.

From figure 5.8 values of growth rate at several injection rates have been taken and for these an Arrhenius plot has been made as shown in figure 5.9. The lowest concentration of 0.35 x 10^{-7} moles s^{-1} is a straight line but the higher concentrations can be seen to vary with temperature.

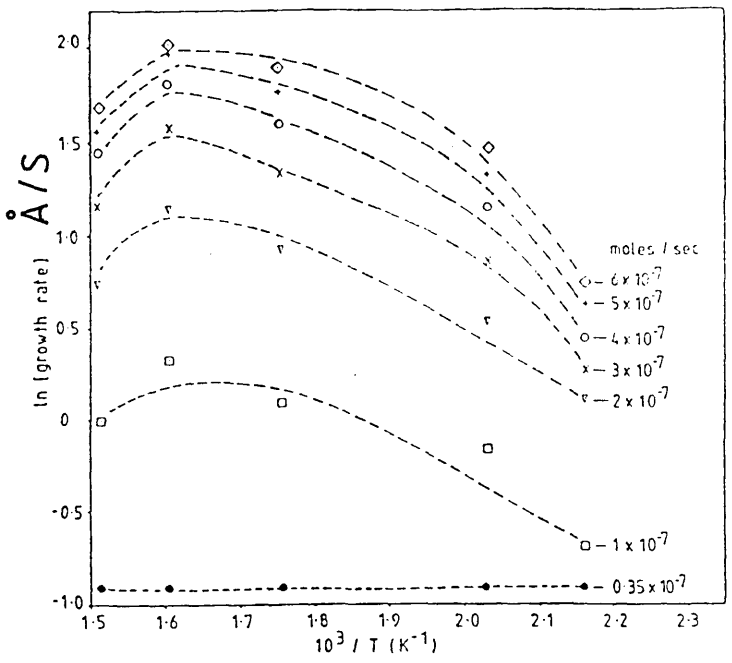


Figure 5.9 Arrhenius Plot of ln(Growth Rate) against the Reciprocal of the Absolute Temperature for Different Alkoxide Concentrations.

5.4.2.2 EFFECT OF UV ILLUMINATION

The conditions under which photolysis enhances the growth rate of oxide films have been found to be both temperature and concentration dependent, (section 5.4.2.1). At the lowest temperature of 190°C, photolysis operates above an injection rate of 0.35×10^{-7} moles s^{-1} at 190°C and only a very faint line can be observed. Increasing the substrate temperature to 220°C increases the injection rate at which photolysis is effective to approximately 3.3×10^{-7} moles s^{-1}.

5.5.1 GROWTH RATE AS A FUNCTION OF GAS FLOW RATE

The growth rate of oxide at a constant substrate temperature and precursor injection rate was investigated as a function of

gas flow rate. At 350°C injection rates of 1.575×10^{-7} and 5.3×10^{-7} moles s^{-1} were employed and at 200°C an injection rate of 1.575×10^{-7} moles s^{-1} was used. From the results of uniformity of growth shown in figure 3.16 and 3.17a-e, it was decided to investigate the gas flow rate from 15.0 to 100$cm^3 s^{-1}$. At a gas flow rate of 6.67$cm^3 s^{-1}$, the deposition was extremely non-uniform and extensive wall deposition occurred. The films were all grown to the same interference colour in these experiments.

5.5.2 RESULTS OF GROWTH RATE AS A FUNCTION OF GAS FLOW RATE

The growth rates of the titanium dioxide films as a function of mean gas velocity are plotted in figure 5.10.

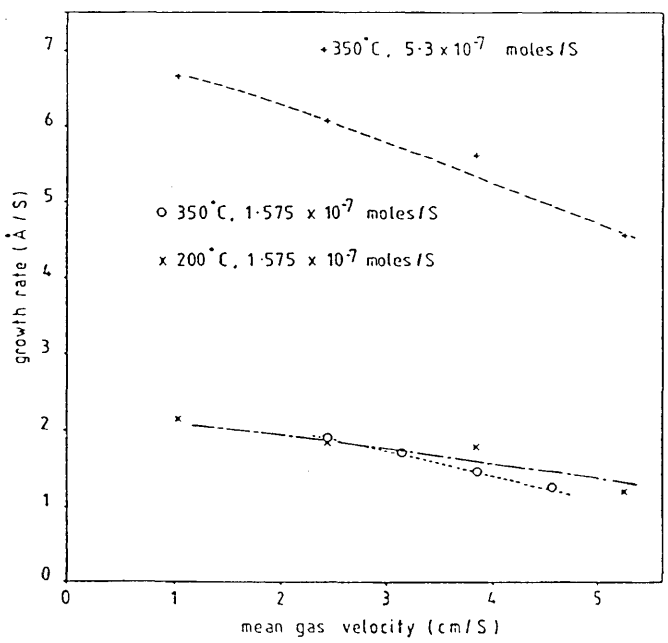


Figure 5.10 Growth Rate of the Titanium Dioxide Films as a Function of Gas Flow Velocity Through the Reactor.

For both temperatures and injection rates the growth rate can be seen to decrease as the mean gas velocity is increased. Despite only four values being taken for each growth condition it

appears that there is a greater decrease in growth rate with increasing gas velocity for the higher temperature deposition than for the lower temperature. This maybe due to the greater expansion of the gas at the higher temperature which results in a higher mean velocity than calculated from the input flow rate at room temperature. The concentration of alkoxide in the reactor is reduced with an increase in nitrogen flow rate and the residence time in the vapour stream is reduced; these factors are probably responsible for the decrease in growth rate observed.

CHAPTER 6 EXPERIMENTAL TECHNIQUES USED IN CHARACTERISATION OF OXIDE FILMS

6.1 INTRODUCTION

In addition to knowing the growth rate of the oxide films deposited, the properties of the oxide layer need to be determined for use in electronic devices. For example a low density amorphous film provides less resistance to etching and mobile ion migration and is less mechanically durable than a higher density crystalline film of the same composition. The refractive index is important for use of the films in antireflective layers and the electrical resistivity and capacitance are important for their use as capacitors or gate oxides. The characterisation techniques employed in the present study were:

(1) X-ray diffraction.
(2) Transmission electron microscopy.
(3) Ellipsometry.
(4) Frequency response analysis.
(5) Etching.

X-ray diffraction and electron diffraction provide information about the crystal structure and orientation of the films. Transmission electron microscopy (TEM) allows detailed observation of the grain size and morphology of the microstructure. Values of refractive index at a wavelength of 632.8nm are obtained by ellipsometry. The value of refractive index can vary with density, crystal structure and orientation

of the films. Measurement of capacitance and conductance as a function of frequency and temperature provides information about impurities in the films. For example mobile impurities can increase the conductance, polarising molecules can produce a dispersion in the response and the presence of pinholes leads to an anomalously high conduction value. The change in behaviour of a process with temperature allows an activation energy to be calculated. A knowledge of the etching behaviour of oxide layers is important in some semiconductor processing where selected areas are etched away.

6.2 OXIDE LAYERS ANALYSED

The oxide layers studied by the characterisation techniques listed in section 6.1 fall into the two categories: titanium dioxide films and mixed oxide films of titanium and vanadium.

6.2.1 TITANIUM DIOXIDE FILMS

The titanium dioxide layers were grown over a substrate temperature range from 25 to 400^{o}C with a precursor injection rate of 0.35×10^{-7} moles s^{-1} and a gas flow rate of 73.3$cm^{3}s^{-1}$; photolysed and non-photolysed samples were examined. The growth rate behaviour of these layers as a function of temperature is given in figure 5.4.

6.2.2 MIXED OXIDE FILMS OF TITANIUM AND VANADIUM

Titanium and vanadium mixed oxide films were grown from a solution of titanium isopropoxide and vanadium triisopropoxide oxide ($VO(OC_3H_7)_3$, obtained from Alfa), in anhydrous cyclohexane. The growth temperature was maintained at 250^{o}C and

investigation into the variation of the film properties with change in composition was carried out. Ten solution compositions were used, ranging from 100% vanadium triisopropoxide oxide to 100% Titanium isopropoxide in anhydrous cyclohexane.

6.2.2.1 ANALYSIS OF THE TITANIUM AND VANADIUM CONTENTS IN THE MIXED OXIDE FILMS

To investigate the composition of the oxide films with respect to the titanium and vanadium content an energy dispersive analysis with ZAF correction (i.e. signal corrected for atomic number, absorption and florescence) was carried out in a JEOL JSM 35 microscope. The oxide films were grown on a silicon substrate and this element was excluded from the analysis. The ratio of titanium to vanadium in the oxide film was compared to the ratio present in the liquid precursor and the results are presented in figure 6.1.

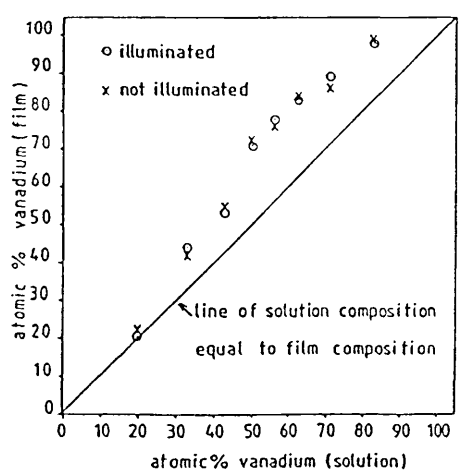


Figure 6.1 The Composition of Deposited Oxide Films of Titanium and Vanadium as a Function of Precursor Solution Composition.

From figure 6.1 all the film compositions were found to contain a greater atomic percent of vanadium than the precursor solution, and illumination of the substrate during growth did not change the composition of the oxide film. Hence from a vapour stream containing both the titanium isopropoxide and the vanadium triisopropoxide oxide molecules, a greater proportion of the vanadium triisopropoxide oxide molecules decompose to produce vanadium oxide than titanium isopropoxide to form titanium dioxide, under these growth conditions. In the results presented in chapter 7 the composition is stated in % vanadium and this relates to the relative percent of vanadium to titanium in the films with out taking the oxygen content into consideration.

6.3 EXPERIMENTAL DETAILS

6.3.1 X-RAY DIFFRACTION

The samples prepared for x-ray diffraction were grown onto silicon substrates and a Philips diffractometer was used with a scan speed of $0.033^{o}s^{-1}$; the radiation was CuK_{α} of wavelength 0.154nm.

The oxide films were only approximately 100nm thick and a strong substrate contribution was present in the x-ray traces; the silicon peaks were subtracted from the results. The x-ray diffraction results of the titanium dioxide films deposited at substrate temperatures of 170, 200, 250, 300 and $350^{o}C$ are shown in figure 7.1 a-e respectively. Mixed oxide films of titanium and vanadium were investigated by x-ray diffraction over the whole composition range.

This analysis technique is quick, non-destructive and

convenient to use, but its sensitivity on these samples is low as shown by the limited number of peaks in figure 7.1. To achieve greater sensitivity and more detailed information electron diffraction has been employed. Electron diffraction is a more sensitive technique because the intensity of a typical electron reflection is 10^8 times larger than the intensity of an x-ray reflection; electrons are scattered much more easily than x-rays. A film of 5nm, for example diffracts an electron beam sufficiently to give a recordable diffraction pattern whereas the same film does not have enough scattering power for x-rays. A film thicker than several 100nm however absorbs most electrons but can give good x-ray results.

6.3.2 TRANSMISSION ELECTRON MICROSCOPY

To observe samples in the TEM with a beam voltage of 100kV, the thickness of the films is limited to about 100nm. Oxide films were grown on a substrate of single crystal sodium choride (IR window, Buck Inst.) which was cleaved along (100) just before growth. A short deposition time of typically 1-5 min, was used and the films were coated with 10-20nm of amorphous carbon in a carbon coater. This served to keep the thin and sometimes discontinuous films intact during preparation and observation in the 100kV Philips microscope. During preparation, the sodium chloride substrate was sandwiched between two copper grids and immersed in distilled water. Several rinsings in distilled water completely dissolved the sodium chloride and left the carbon coated oxide films suspended on the copper grids.

The titanium dioxide films were examined as a function of

substrate temperature and a selection of microstructures and a series of electron diffraction patterns are presented in section 7.2.1 and 7.2.2

Mixed oxide films were examined in a similar manner and the results are presented in section 7.2.3.

6.3.3 ELLIPSOMETRY

Ellipsometry measurements were carried out on oxide films grown on silicon substrates. The choice of silicon was made because of its good surface quality and the ellipsometer had a data analysis programme for films grown on silicon. Each sample was measured three times and the average value taken. The refractive index was measured for photolysed and non-photolysed films. The results for titanium dioxide samples grown with and without UV illumination are plotted against growth temperature in figures 7.21a & b respectively. A selection of samples annealed at 1000^{o}C for three hours in an argon atmosphere were remeasured and these results are presented in figure 7.21c.

The refractive indices of the mixed titanium and vanadium oxide films were measured and are plotted against atomic % vanadium in figure 7.24. The surface quality of the mixed oxide films was poorer than the 'mirror'like titanium dioxide films and some problems were encountered when measuring due to scattering.

6.3.4 ELECTRICAL MEASUREMENT OF SAMPLES USING A FREQUENCY RESPONSE ANALYSER

The electrical properties of a selection of oxide films have been investigated by measurement with a Frequency Response

Analyser. This technique is capable of measuring a wide frequency range extending from 10^{-4} Hz to 10^{4} Hz and with computer control a large number of data points can be processed and recorded (Pugh, 1984). A schematic diagram of the instrument is shown in figure 6.2.

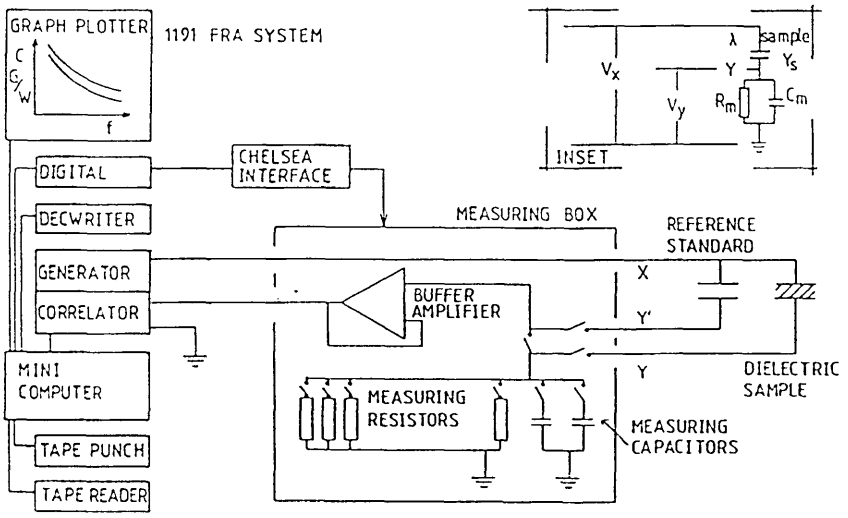


Figure 6.2 Schematic Diagram of the FRA after Pugh, (1984).

The equipment has been developed by the dielectrics group, Kings College, (formerlly at Chelsea College) from the 1191 FRA system, commercially available from the Solartron Electronic Group. To take a measurement the generator applies a sine wave signal to the sample from 0.01V to 9.99V in the frequency range 10^{-4} to 10^{4} Hz. The applied potential is measured at points X and Y in the circuit (see figure 6.2) and compares the sample reading with a known reference. The computer controls the selection of measuring resistor and capacitor combinations for each frequency and the results are continuously recorded. At each

frequency a minimum of three measurements was taken and if consecutive readings showed a phase difference of more than 10μ radians additional measurements were carried out; a maximum of ten readings was used. The data is presented in the form of log-log plots of real and imaginary components of the complex susceptibility, because the frequency dependence obeys a power law which will be discussed in section 7.4.

To measure the electrical properties of the titanium dioxide samples oxide films were grown on polished stainless steel samples. A top contact of a six mm diameter area of silver dag was used and figure 6.3 illustrates the geometry of the sample.

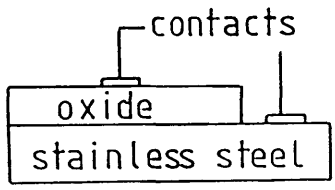


Figure 6.3 Diagram of the Sample used for Dielectric Measurement.

During measurement the sample was placed in a cryostat and the temperature could be varied from 77K to 373K. The cryostat was evacuated during measurement to prevent any condensation on the sample at low temperatures. An ac voltage of 0.01V was applied to the sample and four measurements per decade of frequency were

taken. This low ac voltage was used because the films were only approximately 100 nm thick and a high electic field can easily damage the film if the breakdown field is reached. A field of the order of 10^3 Vcm^{-1} is produced with a 0.01V applied signal.

A series of titanium dioxide films grown at different substrate temperatures and a selection of mixed titanium-vanadium oxide films were measured. The results are presented in section 7.4.

6.3.5 ETCHING

The etching rate of oxide films was measured in concentrated sulphuric acid maintained at a temperature of 150°C for the titanium dioxide films and at 100°C for the mixed oxide films. This reduction in temperature to 100°C was necessary for the mixed oxide films because the dissolution rate was much quicker than for the titanium dioxide films and could not be determined with sufficient accuracy at 150°C. Oxide films grown on silicon substrates were used because of the inertness of silicon and the good visibility of the oxide films on the reflecting substrate. The time for the colour to completely disappear was measured to one second, however, this technique has limitations in accuracy due to this method of thickness measurement. The interference colours are only visible above a certain thickness and measurement of the oxide thickness below this value is not possible by visual inspection. However, these experiments do show the comparative rates of etching of the different oxide films and distinct trends in behaviour are observed.

Titanium dioxide films deposited at substrate temperatures ranging from 25 - 400°C were etched and the results are given in

figure 7.43. Five samples annealed at 1000^{o}C for 3 hours in an argon atmosphere were etched for comparison. The etching rates of the titanium vanadium mixed oxide films are plotted in figure 7.44 as a function of atomic % vanadium.

CHAPTER 7 RESULTS OF CHARACTERISATION OF OXIDE FILMS

7.1 X-RAY DIFFRACTION

The x-ray diffraction traces of the titanium dioxide samples grown at 170, 200, 250, 300 and 350°C are shown in figure 7.1a-e respectively. At substrate temperatures of less than 170°C no diffraction peaks were observed indicating an amorphous structure. At 170°C, three diffraction peaks are observed which have been identified as the {101}, {200} and {211} reflections of anatase. The intensity of the {101} and {200} reflections increase at substrate temperatures of 200 and 250°C. Increasing the temperature to 300 and 350°C results in the disappearance of the {200} peak, a reduction in intensity of the {101} peak and the apperance of the {112} and {220} reflections of anatase.

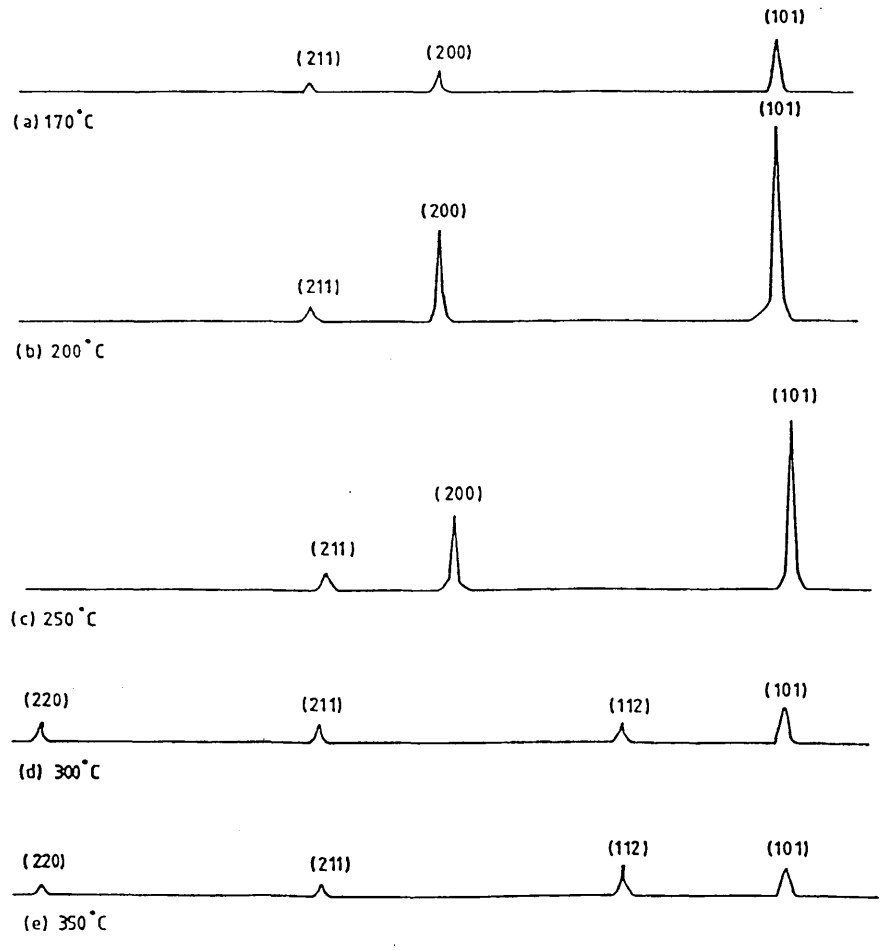


Figure 7.1 X-ray diffraction Results for Titanium Dioxide Films Grown at (a) 170, (b) 200, (c) 250, (d) 300, and (e) 350°C.

The changes in intensities of the anatase reflections with substrate temperature are due to varying orientations in the deposited oxide. A completely random deposition of anatase would have a diffraction pattern with the reflection intensities correlating to the intensities given by the standard powder diffraction data as shown in figure 7.2.

21-1272

d	3.52	1.89	2.38	3.52	$(TiO_2)12O$
I/I_1	100	35	20	100	Titanium Oxide (Anatase)

Rad. CuK_{α_1} λ 1.54055 Filter Mono. Dia.
Cut off I/I_1 Diffractometer $I/I_{cor.}$ =4.3
Ref. National Bureau of Standards, Mono. 25, Sec. 7, 82 (1969)

Sys. Tetragonal S.G. $I4_1/amd$ (141)
a_0 3.7852 b_0 c_0 9.5139 A C 2.5134
α β γ Z 4 Dx 3.893
Ref. Ibid.

ωα nωβ εγ Sign
2V D mp Color Colorless
Ref. Ibid.

Pattern at 25°C. Internal standard: W.
Sample obtained from National Lead Co., South Amboy, New Jersey, USA.
Anatase and another polymorph brookite (orthorhoebic) are converted to rutile (tetragonal) by heating above 700°C.
Merck Index, 8th Ed., p. 1054.

d A	I/I_1	hkl	d A	I/I_1	hkl
3.52	100	101	1.0436	4	321
2.431	10	103	1.0182	2	399
2.378	20	004	1.0070	2	208
2.332	10	112	0.9967	2	325
1.892	35	200	.9555	4	316
1.6999	20	105	.9361	4	400
1.6655	20	211	.9246	<2	307
1.4930	4	213	.9192	2	335
1.4805	14	204	.9138	2	411
1.3641	6	116	.8966	6	215,1110
1.3373	6	220	.8830	2	228
1.2795	<2	107	.8819	<2	413
1.2649	10	215	.8795	2	404
1.2509	4	301	.8461	2	420
1.1894	<2	008	.8308	<2	327
1.1725	2	303	.8268	4	415
1.1664	6	224	.8102	2	309
1.1608	4	312	.7974	4	424
1.0600	2	217	.7928	2	0012
1.0517	4	305			

Figure 7.2 Anatase Powder diffraction Data.

From figure 7.2 the order of comparative reflection intensities of anatase is:

(1) {101} =100%

(2) {200} = 35%

(3) {004}, {105}, {211} = 20%

(4) {204} = 14%

(5) {103}, {112}, {215} = 10%

Considering the x-ray diffraction traces of the oxides grown at 170, 200 and 250°C (figures 7.1a,b and c) the presence of the {101}, {200} and {211} in decreasing order of intensity is consistent with a random orientation. The absence of the {004} and {105} reflections which have the same intensity as the {211}

may indicate a preference for the 'c' axis to be positioned parallel to the substrate and hence the {004} and {105} planes would not be in a reflecting position. The disappearance of the {200} reflection and the reduction of the intensity of the {101} at higher growth temperatures suggests that the orientation changes and the planes prefer not to be parallel to the surface in the diffracting condition. The {112} and {220} reflections which are normally of low intensity in a random orientation are present in the diffraction pattern of figure (7.1 d-e) in addition to the {101} and {211} . These four reflections indicate that more than one preferred orientation is present in the film grown at substrate temperatures of 300-350°C

X-ray diffraction of titanium dioxide films grown at 100-400°C was carried out by Wang et al.,(1970) and a typical x-ray trace is shown in figure 7.3.

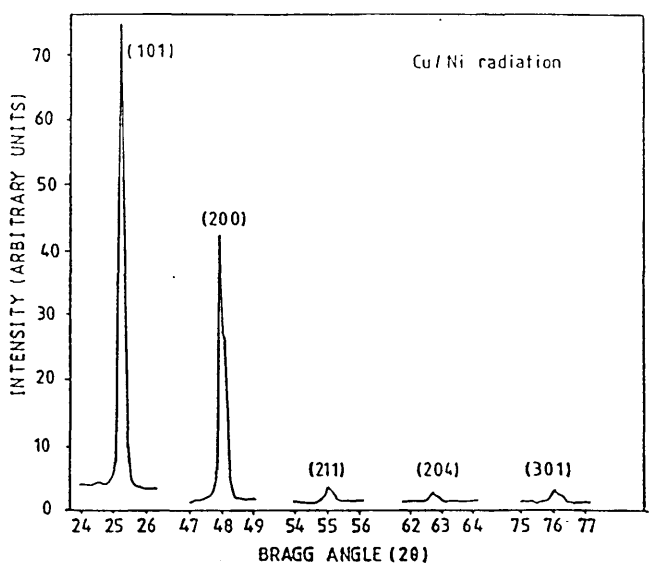


Figure 7.3 X-ray Diffraction Trace of Anatase Thin Film after Wang et al., (1970).

The substrate used by Wang et al., (1970) was fused quartz and figure 7.3 was stated to be a typical diffraction trace for a substrate temperature of 100 -400°C. The precursor was titanium isopropoxide and the deposition was carried out in an oxidising atmosphere. The x-ray results differ from the present work where below 170°C no anatase was identified and the intensity and presence of reflections was dependent on the substrate temperature.

The x-ray diffraction results of the mixed titanium-vanadium oxide films grown an 250°C showed no reflections other than those of the silicon substrate and the structure of the mixed oxide films was concluded to be of an amorphous nature.

7.2 TRANSMISSION ELECTRON MICROSCOPY

7.2.1 MICROSTRUCTURES OF TITANIUM DIOXIDE FILMS GROWN ON SODIUM CHLORIDE SUBSTRATES

The microstructures of titanium dioxide films grown on sodium chloride substrates have been investigated by transmission electron microscopy as described in section 6.3.2. The microstructures observed are probably somewhat different from the microstructures that would be seen for titanium dioxide grown on a silicon substrate. Sodium chloride is an ionic crystal and a precursor molecule or fragment will experience some electrostatic interaction with the substrate surface. The sodium chloride is cleaved in air just before inserting into the reactor and the surface will inevitably be contaminated. On cleaving the crystal, cleavage steps will be produced in which an incomplete plane of atoms is left on the surface. A silicon substrate in comparison is much smoother atomically; it does not have the same electrostatic interaction with the impinging

molecules; and the surface is covered with a thin layer of oxide. The types of defects present on a crystal surface that promote adsorption of atoms are illustrated in figure 7.4.

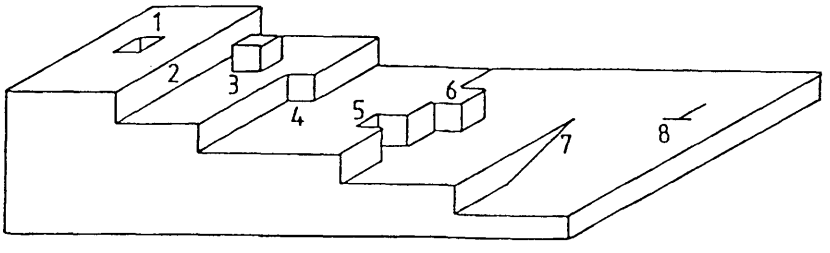
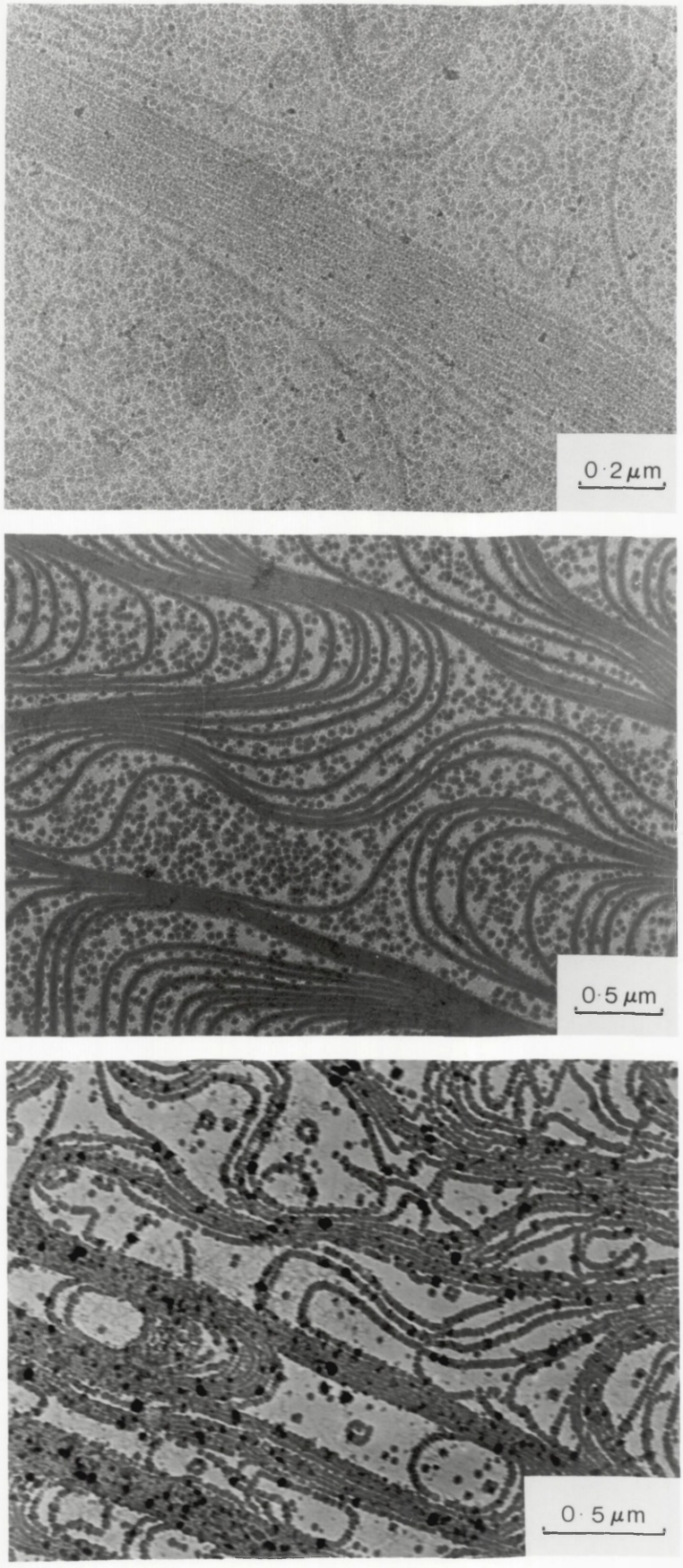


Figure 7.4 Adsorption Sites Present on a Crystal Surface, after Lewis and Anderson, (1978)

The defects illustrated in figure 7.4 are (1) vacancy (2) step (3) self-adsorbed atom (4) kink (5) double kink (6) atom self-adsorbed at step (7) screw dislocations emerging in surface (8) edge dislocation emerging in surface.

The adsorption of an atom at a site where the number of nearest-neighbour atoms is increased, is favourable compared with adsorption on a perfect surface with only one nearest-neighbour atom. For example the adsorption at a step (site 2) provides two nearest neighbours and adsorption at a kink (site 4) provides three nearest neighbours. Defects are thus generally preferred sites for adsorption and this can be seen in the numerous examples of "decoration" effects observed in **nucleation stages of thin film growth, where a higher density of nuclei occur at the cleavage steps on the substrate surface.**

Preferential growth at cleavage steps has been observed in the present work for titanium dioxide deposition as shown in



(a)100°C

(b)180°C

(c) 275°C

Figure 7.5 Illustrating the Preferential Growth of Titanium Dioxide at Sodium Chloride Cleavage Steps at different growth Temperatures.

figure 7.5a-c for substrate temperatures of 100, 180, and 275°C.

From figure 7.5a-c it can be seen that at the highest temperature of 275°C, nucleation occurs almost exclusively at the cleavage steps; at 180°C, nucleation occurs at the steps but also randomly in the regions between the steps and at the lowest temperature of 100°C, a more uniform distribution of nuclei is present but with a higher than average density at the steps. If growth occurs only at steps which are a distance 'W' apart as illustrated in figure 7.6a, the diffusion length, λ, of the precursor molecule is greater than 'W' and all the adsorbed species can reach a step. On lowering the temperature, the diffusion length, λ, of the precursor molecule decreases and when $\lambda < W$ growth between the steps occurs as shown in figure 7.6b.

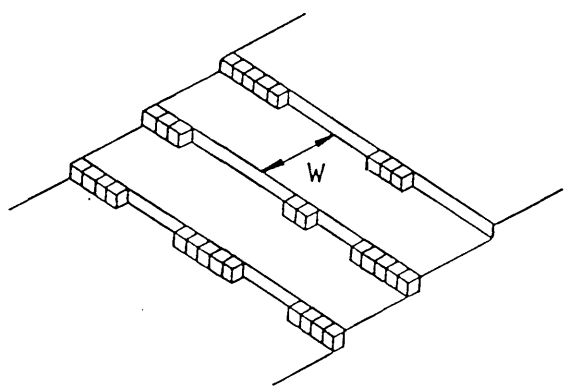


Figure 7.6a Illustrating the Growth if the Diffusion Distance is Greater than the Cleavage Separation.

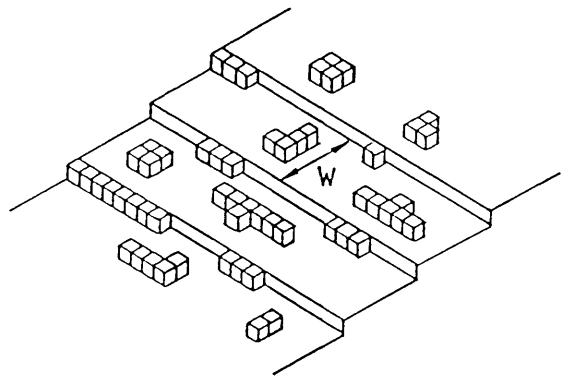
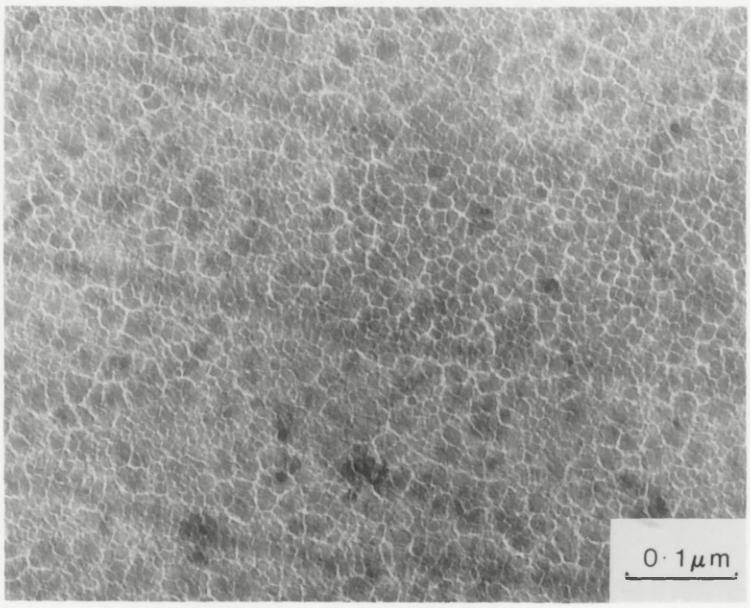


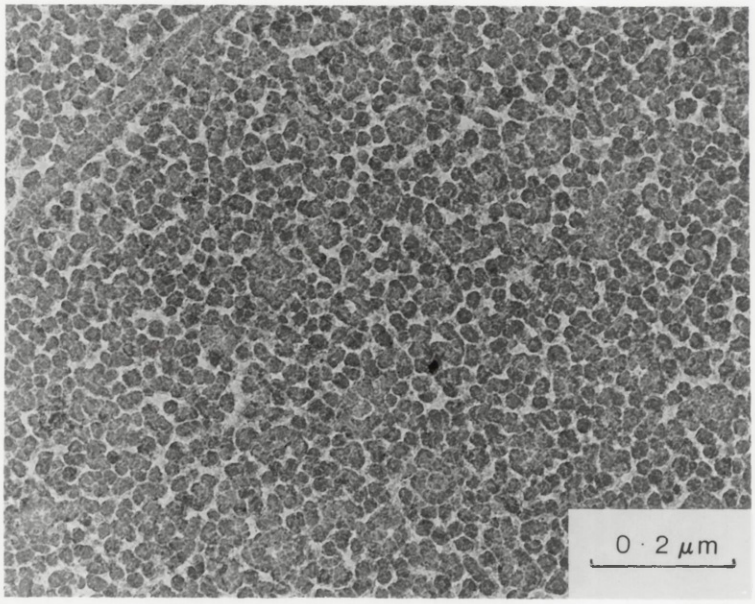
Figure 7.6 b Illustrating the Growth if the Diffusion length is less than the separation Distance of the Cleavage Steps

The microstructure of thicker oxide films is shown in figure 7.7a-d for samples grown at temperatures of 100, 160, 275 and 400°C respectively. All samples show polycrystalline microstructures and the grains of the samples shown in figures 7.7a-c are reasonably equiaxed. As the substrate temperature decreases the grain boundaries appear less well defined; this suggests a 'rougher' grain surface occurring at lower temperatures. The highest temperature sample grown at 400°C contains grains which exhibit a rectangular shape and lie in positions with the major axis both 'vertical' and 'horizontal' and inclined at 45°.

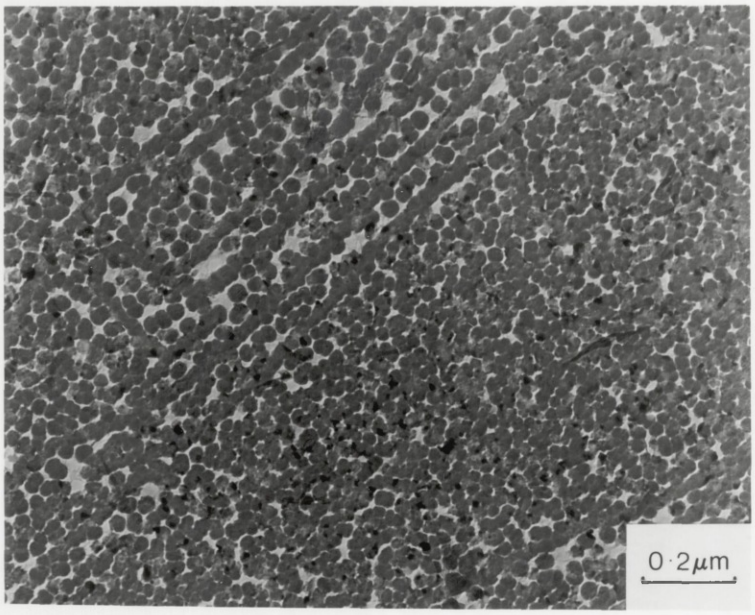
The morphology changes seen in figures 7.7a-d as a function of substrate temperature are similar to those reported by Lewis and Stirland (1968), for growth of lead telluride on sodium chloride at temperatures from 20 to 200°C. At lower temperatures a dendritic type morphology is observed which changes to squares with $\langle 100 \rangle$ edges at 200°C.The explanation given for the morphological change with temperature is based on the stability



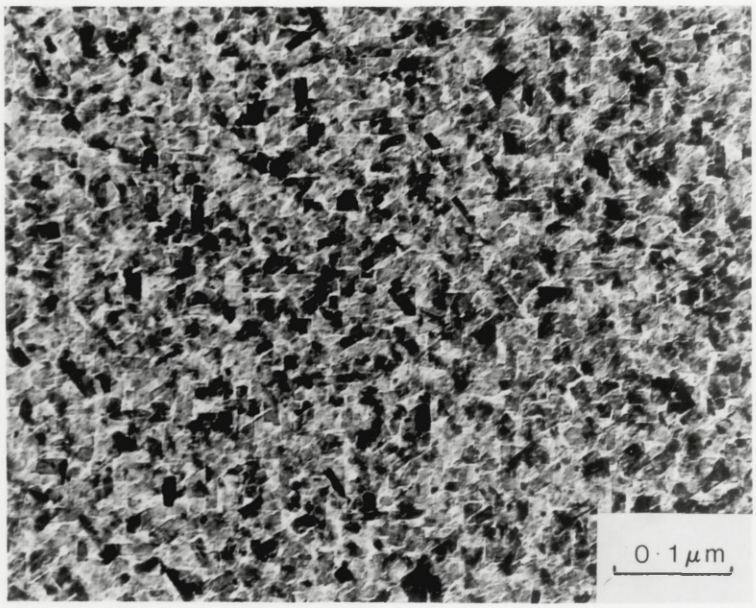
(a) 100°C



(b) 160°C



(c) 275°C



(d) 400°C

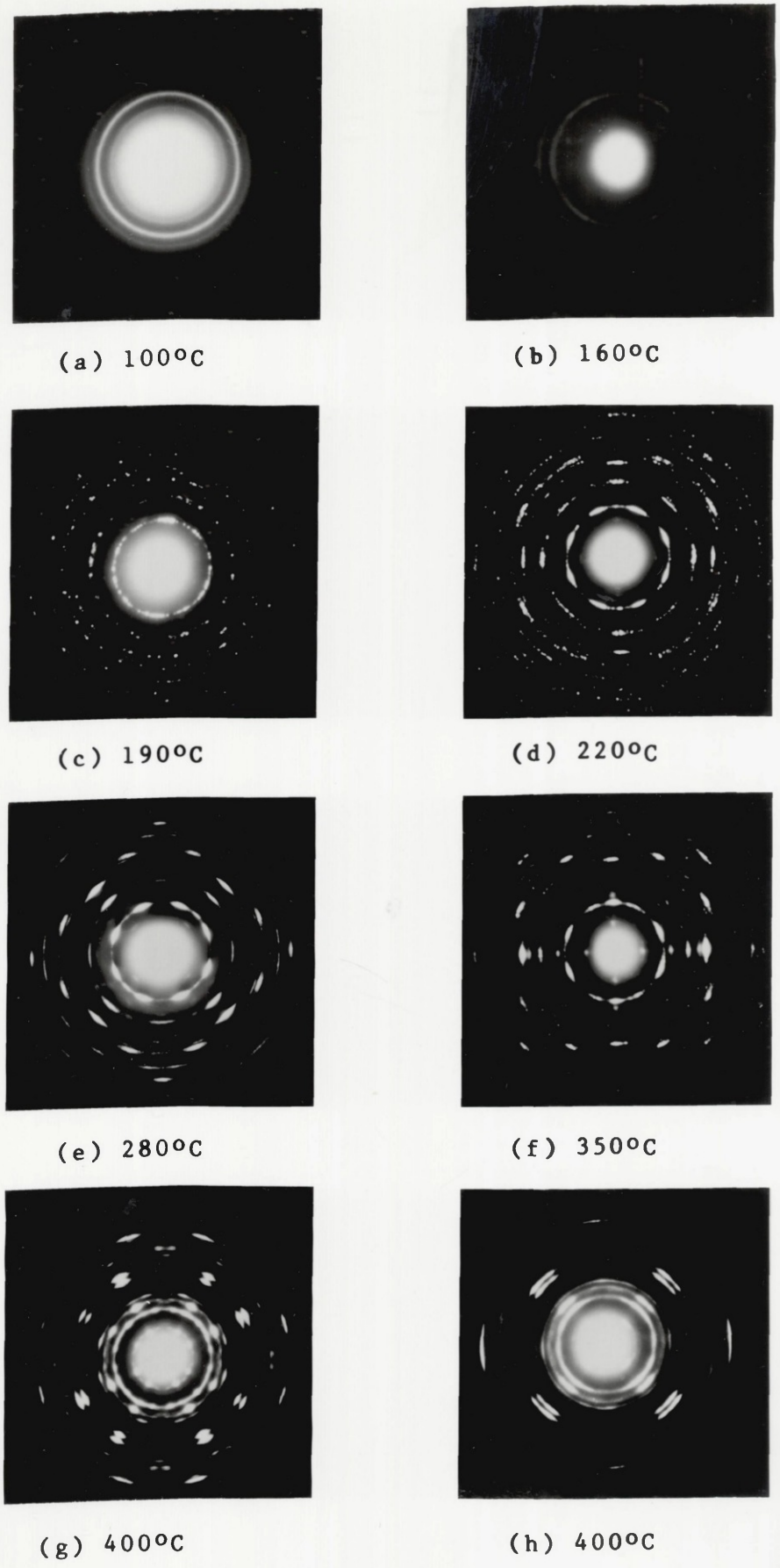
Figure 7.7a-d Microstructures of Titanium Dioxide Films as a Function of Growth Temperature.

of molecules arriving either at an incomplete $\langle 100 \rangle$ edge which is a kink site or on a complete $\langle 100 \rangle$ edge which is a step site (e.g. positions 4 and 2 in figure 7.4). If the molecules are unstable on a complete $\langle 100 \rangle$ edge, they can be stabilized by the capture of another molecule, but this process is slow compared with the umimpeded growth on a kink site (which is a $\langle 110 \rangle$ edge), and the resulting nuclei are square. When molecules are stable on both sites, growth is unimpeded. At the lower temperatures the nuclei were of high enough density to capture all the incident molecules. Morphological instability occurred with growth being faster in $\langle 110 \rangle$ directions and at the corners and tips of growing nuclei because the flux of available material was higher. This led to dendritic growth with branches in the $\langle 110 \rangle$ direction.

7.2.2 ELECTRON DIFFRACTION OF TITANIUM DIOXIDE FILMS

From the x-ray diffraction results of oxide films grown on a silicon substrate (figure 7.1), the anatase modification of titanium dioxide has been identified. The electron diffraction patterns for oxide films grown on a sodium chloride substrate are shown in figure 7.8a-h for substrate temperatures increasing from 100 to 400°C. From the diffraction patterns in figure 7.8 a trend of increasing crystallinity and orientation with increasing substrate temperature can be observed.

The lower temperature samples of 100 and 160°C have some amorphous nature as indicated by the diffuse rings; at 180°C sharper rings are present which are evidence of a polycrystalline microstructure with no preferred orientation. Figure 7.8d shows a preferred orientation beginning to develop



(a) 100°C (b) 160°C

(c) 190°C (d) 220°C

(e) 280°C (f) 350°C

(g) 400°C (h) 400°C

Figure 7.8a-h Electron diffraction Patterns for Titanium Dioxide Grown on Sodium Chloride as a Function of Growth Temperature.

and this is further developed at higher temperatures. The diffraction pattern changes at the highest temperature considered.

7.2.2.1 ANALYSIS OF DIFFRACTION PATTERNS

The diffraction pattern of polycrystalline, randomly oriented anatase has been drawn in figure 7.9.

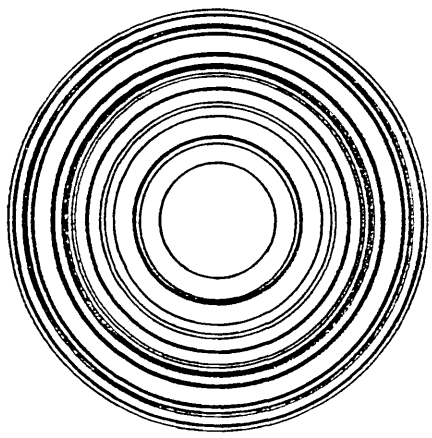


Figure 7.9 Calculated Electron Diffraction Pattern of Randomly Oriented Anatase.

The ring diameters have been calculated from the known lattice spacings of anatase (d) (as given in figure 7.2) and for electron diffraction, equation (7.1) can be used.

$$rd = \lambda L \qquad ---(7.1)$$

r = radius of diffraction ring

d = lattice spacing

λL = the camera constant of the microscope

In the present work the diameter of the diffraction ring (2r) in mm is given by equation (7.2).

$$2r = 51.9/d \quad ---(7.2)$$

Figure 7.8a shows the oxide deposited at 100°C had two diffraction rings that cannot by identified as anatase; these have lattice spacings of 2.88Å (18mm ring) and 2.12Å (24.5 mm ring), and the sample grown at 160°C had the 24.5mm ring. At such low growth temperatures it is likely that intermediate compounds in the decomposition process are present and this is the most probable origin of the extra diffraction rings.

Increasing the temperature to 180°C (figure 7.8c) produced a deposit which gave a more crystalline diffraction pattern which is identified as anatase. There is no evidence of preferred orientation in this sample. A faint ring at 24.5mm is still present as in figures 7.8a&b, which indicates that some intermediate compound may still be present at this growth temperature.

At 220°C (figure 7.8d) the electron diffraction pattern shows some developing orientation with positional variation in intensity of the ring. For example the {101} and the {103} reflections show eight more intense regions and the {004} shows four.

At a higher substrate temperature of 280°C the diffraction pattern shows a higher degree of orientation. From the reflection present in figure 7.8e it is evident that more than one orientation of anatase is present; for example there is a {004} reflection at 21.83mm and a {101} reflection at 14.74mm. These planes would not both diffract from the same orientation.

Consider first that the (001) is parallel to the substrate as illustrated in figure 7.10.

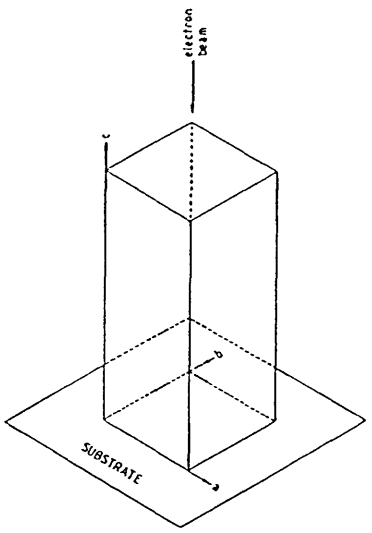


Figure 7.10 Illustrating growth with the (001) parallel to the substrate

The electron beam is in the [001] direction and the resulting diffraction pattern is the (001) reciprocal lattice plane as drawn in figure 7.11.

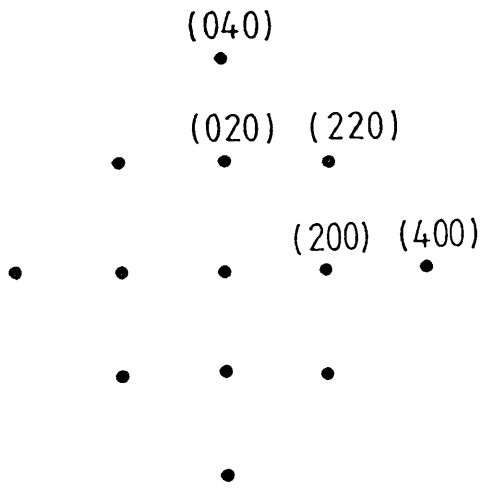


Figure 7.11 Diffraction Pattern for Growth with the (001) parallel to the substrate.

This diffraction pattern is present in figure 7.8e.

The second orientation to consider is the (100) of (010) parallel to the substrate as illustrated in figure 7.12.

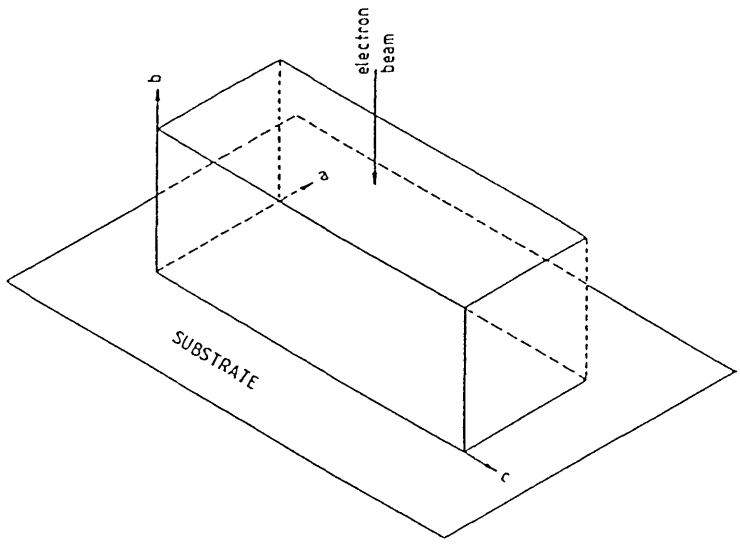


Figure 7.12 Illustrating growth with (100) or (010) parallel to the substrate.

The diffraction pattern in this orientation is the reciprocal lattice plane of the (100) or the (010) of anatase as drawn in figure 7.13.

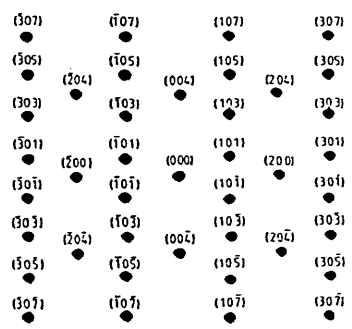


Figure 7.13 The Diffraction Pattern for the (100) or (010) Parallel to the Substrate.

The electron diffraction pattern shown in figure 7.13 has missing or forbidden reflections due to the structure factor of anatase.

Considering the titanium atom positions 1, 2, 3 and 4 as marked in figure 7.14, the atom positions are given by:

$1 = 000$, $2 = 0\,\frac{1}{2}\,\frac{1}{4}$, $3 = \frac{1}{2}\,\frac{1}{2}\,\frac{1}{2}$, $4 = \frac{1}{2}\,1\,\frac{3}{4}$.

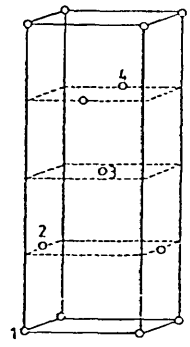


Figure 7.14 The Positions of Titanium Atoms in the Anatase Unit Cell Used for the Structure Factor Determination.

Hence the structure factor is given by equation (7.3).

$$F_{hkl} = f\left\{\exp 2\pi i(0+0+0) + \exp 2\pi i\left(0+\frac{k}{2}+\frac{l}{4}\right) + \exp 2\pi i\left(\frac{h}{2}+\frac{k}{2}+\frac{l}{2}\right) + \exp 2\pi i\left(\frac{h}{2}+k+\frac{3}{4}l\right)\right\} \quad ---(7.3)$$

($\exp 2\pi i = +1$ for n = even integer and -1 for n = odd integer. Factorising equation (7.3) gives:

$$F_{hkl} = \left\{1 + \exp \pi i\,(h+k+l)\right\}\left\{1 + \exp \pi i\left(k+\frac{l}{2}\right)\right\} \quad ---(7.4)$$

If $|F_{hkl}|^2 = 0$, the (hkl) reflection has zero intensity and is a forbidden reflection. Hence for anatase the conditions for forbidden reflections are:

(1) if h+k+l = odd integer (this is the body centred rule)

(2) if h+l/2 (or k+l/2) = odd integer

From the diffraction pattern in figure 7.8e, there are extra reflections present due to more than one positioning of the (100) on the sodium chloride, e.g. there are eight intense {101} reflections instead of four, with the second position being a rotation of 90° of the unit cell. The diffraction pattern of both positions is illustrated in figure 7.15.

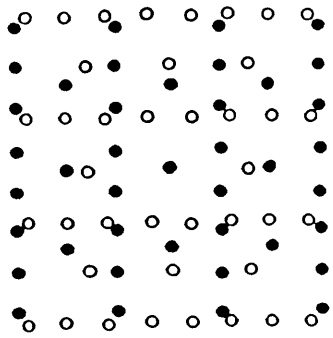


Figure 7.15 Diffraction Pattern of two Orthogonal Positions of (100) Planes Growing Parallel to the Substrate.

The total diffraction pattern consisting of the two (100) parallel positions on the substrate and the (001) parallel on the substrate is drawn in figure 7.16. The square symmetry of the diffraction patterns of figure 7.8 d-f is apparent.

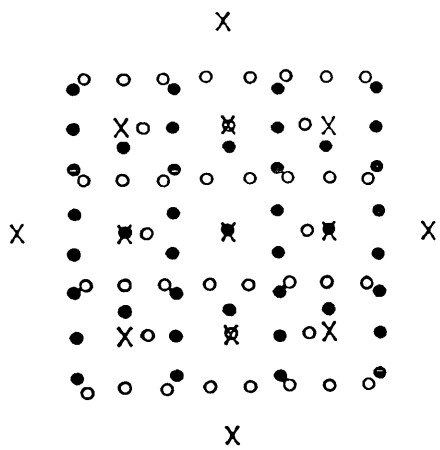


Figure 7.16 Diffraction Pattern of (100) parallel to the substrate in two Orthogonal Positions and of (001) Parallel to the Substrate.

In the diffraction pattern of figure 7.8d&e four faint reflections are present inside the $\{101\}$ ring, which could be identified as $\{002\}$. In accordance with the structure factor this is a forbidden reflection because $(h + 1/2) = 1$ = odd integer and hence F_{hkl} = zero. However the reflection could be present by double diffraction of for example the $(\bar{1}01)$ and (101) reflections which add vectorially to give the (002). (Prof. Pashley, private communication).

Considering the orientations of the anatase with the (001) and (100) being parallel to the substrate, possible relationships between the anatase crystal and the (100) sodium chloride are shown in figure 7.17.

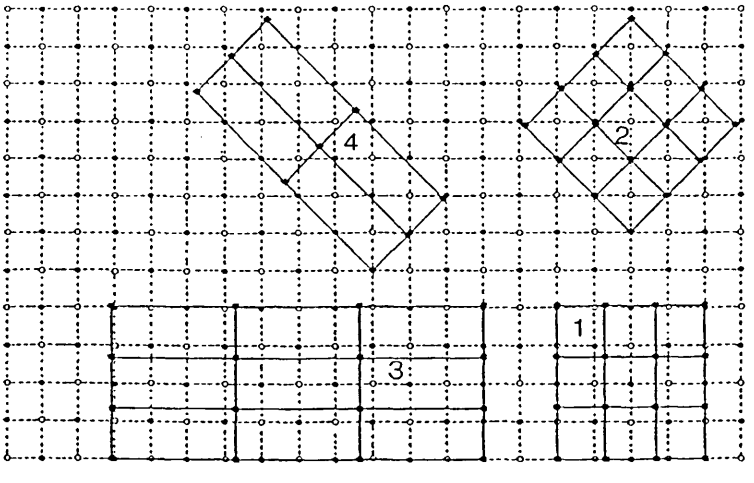


Figure 7.17 Illustrating Possible Epitaxial Relationships between Sodium Choride and Anatase.

Considering position (1) in figure 7.17, a good fit is achieved when two sodium chloride [100] match three titanium dioxide [100] with a difference of only 0.08Å. Position (2) matches with twice the [110] sodium chloride for four [100] titanium dioxide, with a difference of 0.8Å. From most of the

diffraction patterns observed only one of these positions occurred; position (1) is the position of less elastic strain but in position (2), the titanium ions are positioned at greater distances from the sodium ions. Considering positions (3) and (4) with the (100) plane parallel to the substrate, in position (3) considering the [001] direction of the titanium dioxide, three units of titanium dioxide on five units of sodium chloride give a difference of 0.38Å and in position (4) six units of sodium chloride for five units of titanium dioxide gives 0.203Å difference.

Increasing the growth temperature further to 350°C, figure 7.8f, resulted in the appearance of reflections at 9mm, 17mm and 26mm (lattice spacings of 5.8, 3.0 and 2.0Å) in a four fold symmetry as shown in figure 7.18.

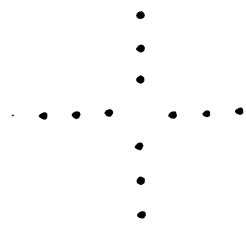


Figure 7.18 Illustrating the Extra Reflections Observed in Figure 7.8f.

The origin of these reflections is unknown; the lattice spacings do not match any titanium oxide powder difraction file, but it is possible that a reaction with the sodium chloride could have taken place.

Diffraction patterns of films grown at 400°C are shown in figures 7.8g&h. On comparison with the patterns worked out in

figures 7.11 and 7.13, the diffraction pattern of figure 7.11 with the (001) parallel to the substrate can be seen as highlighted in figure 7.19a&b for the patterns of figures 7.8g&h.

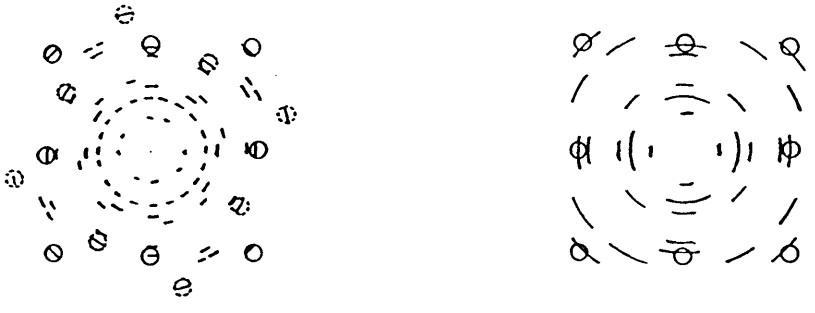


Figure 7.19 Illustrating the Presence of the Diffraction Pattern due to the (001) Parallel to the Substrate in Samples Grown at 400°C.

Figure 7.8g shows the presence of two diffraction patterns oriented at 30°. The {101} reflections are also present in the patterns indicating some orientation of the (100) parallel to the substrate. The reflections shown in figure 7.18 are also present.

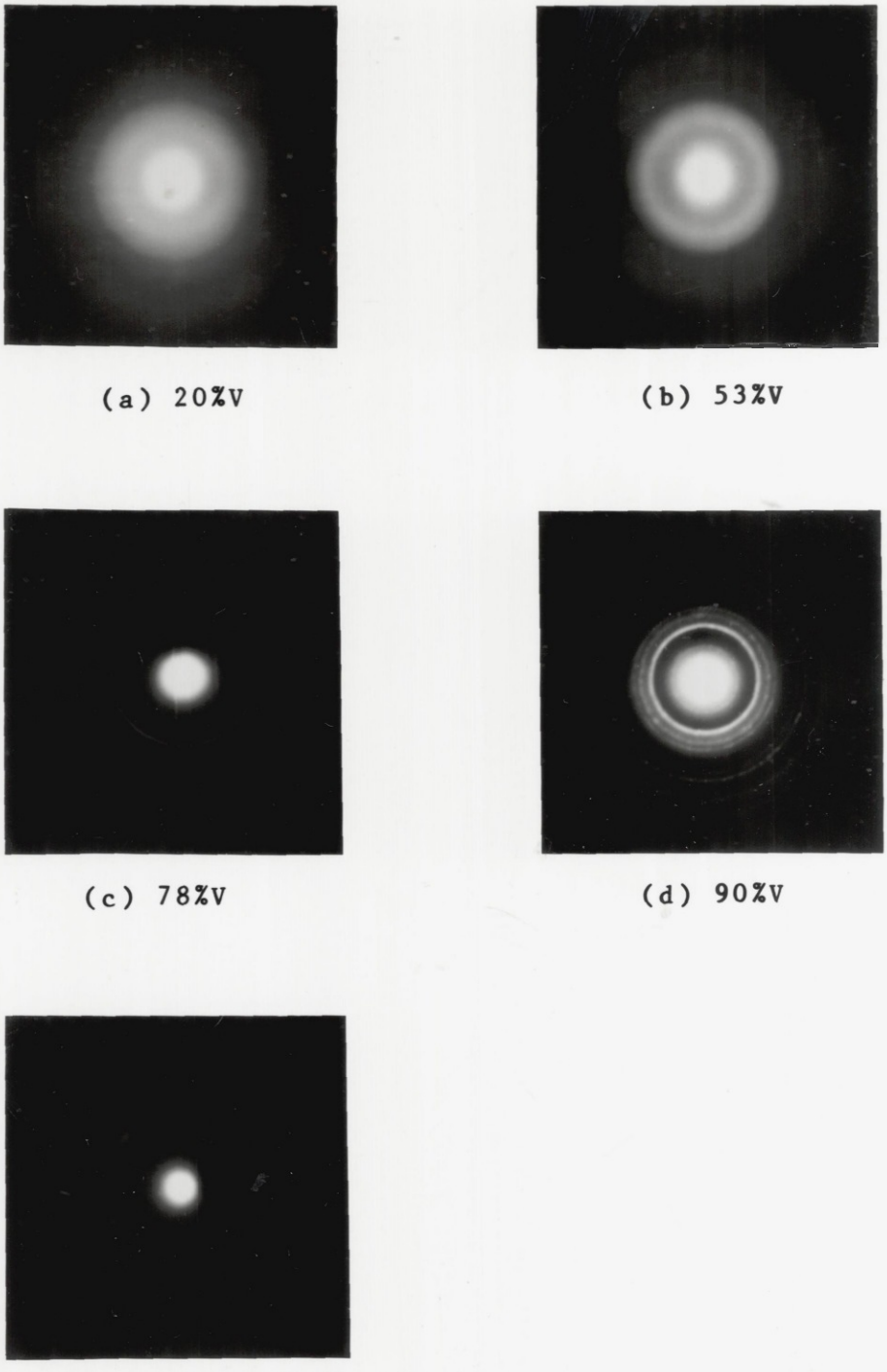
From the diffraction patterns shown in figure 7.8 a change of structure with deposition temperature is apparent. At low deposition temperatures the films probably contained partially decomposed titanium isopropoxide and were less crystalline. Increasing the deposition temperature showed that anatase was grown with preferred orientations of the (001) and two orthogonal positions of the (100) parallel to the substrate. At temperatures of 350°C and higher extra reflections were present which did not belong to anatase. These reflections were not identified as a titanium oxide and a possible cause was a compound formed by reaction of the sodium chloride substate with

the titanium dioxide film.

7.2.3 DIFFRACTION PATTERNS OF MIXED TITANIUM-VANADIUM OXIDE FILMS

The diffraction patterns obtained from the mixed oxides of vanadium and titanium are shown in figure 7.20a-e. The electron diffraction patterns of the two oxides containing the smallest amount of vanadium, 20% and 53 %, give diffuse halos which indicate an amorphous crystal structure. A composition of 78% vanadium (figure 7.20c) gives a ring pattern with only two lattice parameters; 2.66 and 1.57Å, however a composition of 90%V produces several rings as shown in figure 7.20d. The vanadium oxide gives a very weak pattern as shown in figure 7.20e which has two lattice parameters of 2.53 and 1.55Å.

Considering the mixed titanium oxide-vanadium oxide system the diffraction files for two mixed oxide compounds of $V_2Ti_3O_7$ and TiV_4O_{10} were found. These did not however match the lattice parameters of the present samples. The two reflections of figure 7.20c&e give similar lattice spacings considering the accuracy of measurement and the width of the reflection and these two reflections may also be present in figure 7.20d (90%V). Considering the 90%V sample and comparing the reflections with the diffraction files for the vanadium oxides the most similar were two types of vanadium dioxide with file numbers 31-1439 and 31-1438. The colour of the VO_2 of 31-1439 was black and reactor wall deposits showed the oxide grown to be green. Hence the most likely candidate was deduced to be a tetragonal form of VO_2; the deposit produced is a solid solution of titanium dioxide in vanadium dioxide.



(a) 20%V

(b) 53%V

(c) 78%V

(d) 90%V

(e) 100%V

Figure 7.20 Diffraction Patterns of Mixed Titanium-Vanadium Oxide Films Grown at 250°C for different Compositions.

7.3 ELLIPSOMETRY

7.3.1 TITANIUM DIOXIDE FILMS

The variations of refractive index of the titanium dioxide films with substrate growth temperature for (1) non-illuminated samples, (2) illuminated samples and (3) annealed samples are shown in figures 7.21 a,b,and c respectively.

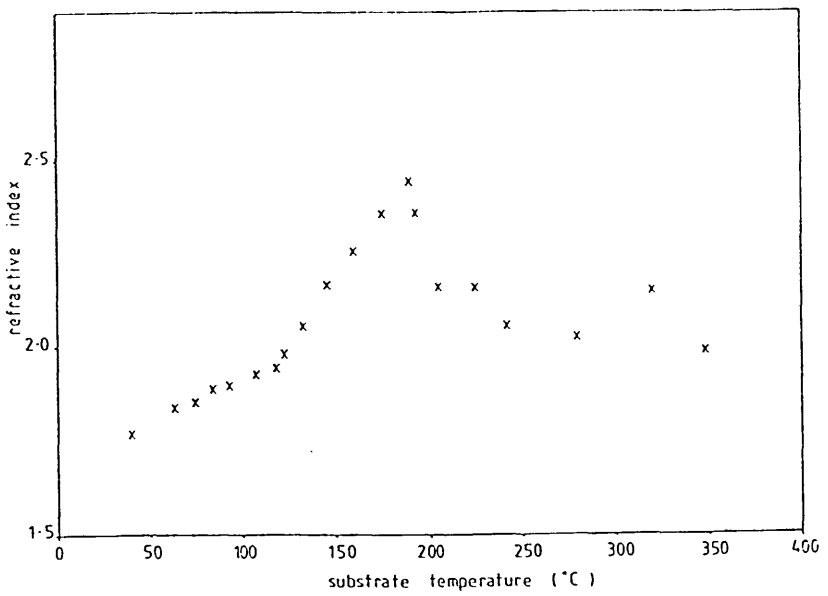


Figure 7.21a Values of Refractive Index as a Function of Growth Temperature for the non-illuminated samples.

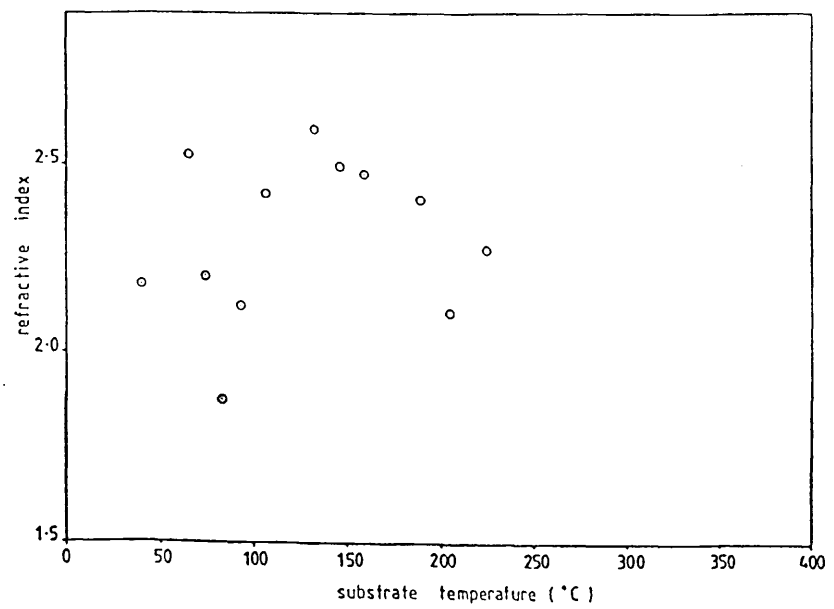


Figure 7.21b Values of Refractive Index as a Function of Growth Temperature for Illuminated Samples.

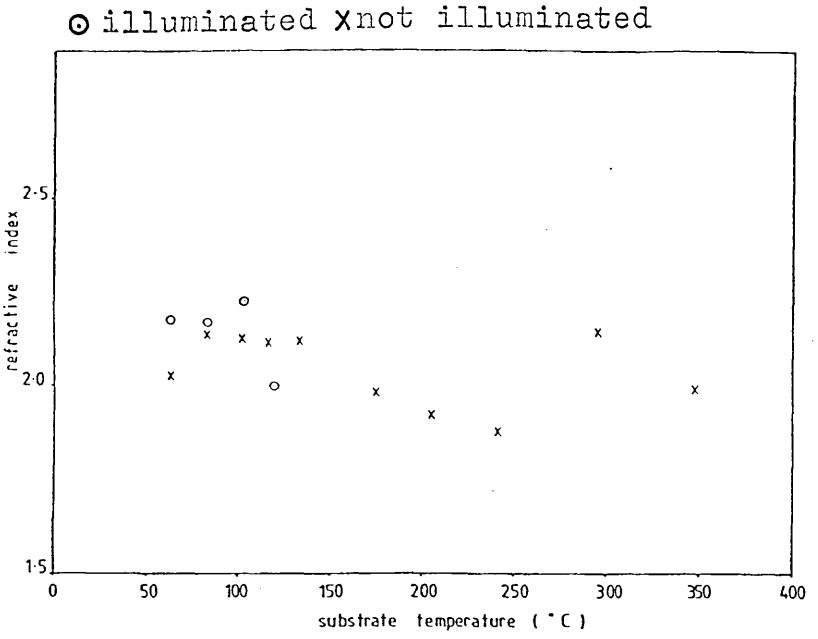


Figure 7.21c Values of Refractive Index as a Function of Growth Temperature after a Post-Deposition anneal at 1000°C.

The non-illuminated oxide films show considerable change in refractive index with growth temperature. In the temperature range from room temperature to approximately 120°C a gradual increase in refractive index with increasing substrate temperature is observed. From 120 to 200°C there is a greater rate of increase of refractive index with increasing growth temperature and above 200°C the value of refractive index does not change significantly but it is below the maximum value observed at 200°C.

The refractive index values of oxide films grown under UV illumination are shown in figure 7.21b and a large scatter is apparent. The cause of scatter could be the less homogeneous

nature of the films as shown by the striated appearance of the illuminated films in figure 5.5. The average value of the refractive index is greater than for the non-illuminated films.

Annealing both the illuminated and the non-illuminated films results in a value of refractive index of approximately 2.1; this is similar to the refractive index of the oxide films grown above 200°C shown in figure 7.21a.

The values of refractive index measured in the present work for as-grown non-illuminated samples are plotted in figure 7.22, along with results from other workers, as a function of growth temperature.

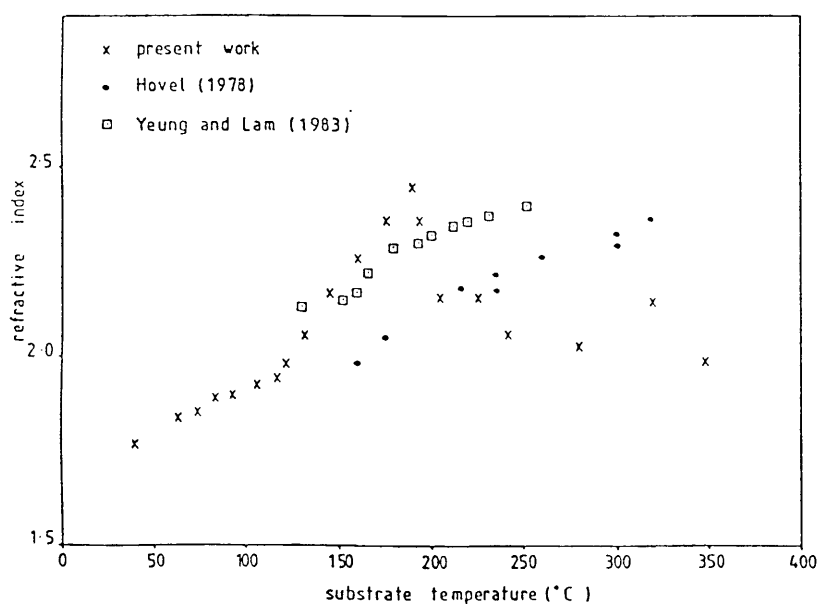


Figure 7.22 Refractive Index Values of Titanium Dioxide Films as a Function of Deposition Temperature.

The values of refractive index of both Hovel (1978) and Yeung and Lam (1983) increase with increasing substrate temperature, but unlike the results of the present work no decrease is observed above 200°C. A more comprehensive list of refractive index values from the literature is given in table 7.1.

TABLE 7.1 VALUES OF REFRACTIVE INDEX OF TITANIUM DIOXIDE THIN FILMS

PRECURSOR	REFRACTIVE INDEX (632.8nm)	TEMPERATURE OF GROWTH	REFERENCE
$TiCl_4$	2.55(540nm)	150	Feuersanger
$+H_2O$			(1964)
$Ti(OPr^i)_4$	2.08-2.13	410-750	Yokozawa et
$+O_2$	2.00-2.05(O_2)	320-540	al.,(1968)
$TiCl_4 + O_2$	2.83	400-1047	Ghoshtagore & Noreika(1970)
$Ti(OPr^i)_4$	2.02	550	Balog et al.,
$+ O_2$	2.26	650	(1972)
$Ti(OPr^i)_4$	2.0/2.1	150	Fitzgibbons et
$+H_2O$	2.4/2.6	1000(ann)	al.,(1972)
$Ti(OPr^i)_4$	1.82	110	Sladek & Gibert
$+ H_2O$	2.26	1000(ann)	(1972)
$Ti(OPr^i)_4$	1.9	100	Hovel (1978)
$+ H_2O$	2.4	400	
$TiCl_4$	2.13	130	Yeung & Lam
$+ H_2O$	2.4	250	(1983)
$Ti(OPr^i)_4$	2-2.15	200	Fuyuki et al.,
$+ H_2O$			(1988)

The refractive indices of anatase and rutile single crystal at 632.8nm have been taken from Hass (1952) to be approximately 2.5 and 2.64 respectively. Hence the value for single crystal anatase is higher than any result for as-grown anatase thin films, (table 7.1). Annealing the films at 1000°C should allow the anatase to convert to the rutile form, however figure 7.21c showed that the annealed films had a refractive index of approximately 2.1 which is much lower than the single crystal rutile. Sladek and Gibert (1972) and Fitzgibbons et al. (1972) annealed samples at 1000°C and measured the refractive indices to be 2.26 and 2.4/2.6 respectively.

The ellipsometer provided values of thickness as well as refractive index and all samples showed a reduction in thickness on annealing, as shown in figure 7.23. The average reduction in thickness is 26% and no trend with substrate temperature was evident. Assuming no mass loss from the oxide sample during annealing means that the density has increased by an average of 35%.

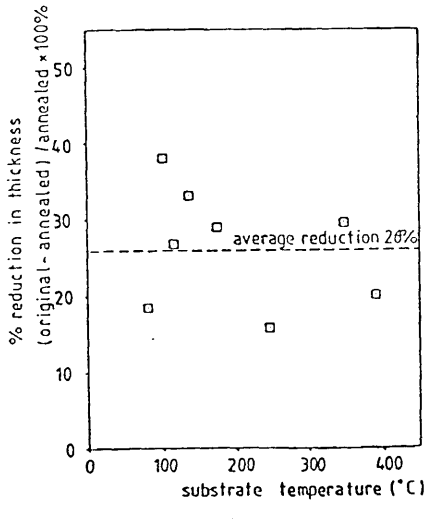


Figure 7.23 Thickness Reduction of Samples after Annealing at 1000°C as a Function of Original Growth Temperature.

A thickness reduction of 35% has been reported by Fitzgibbons et al. (1972), for titanium dioxide films grown from titanium isopropoxide and water at 150°C. Despite careful weighing while annealing no mass loss was detected and the low density of the as grown films was attributed to voids of less than 10nm in size; these disappeared on annealing causing the shrinkage in thickness and increase in density.

A decrease in thickness of 40% was also observed by Sladek and Gibert (1972) for titanium dioxide films grown from titanium isopropoxide and water at 110°C and annealed for five minutes in air at 1000°C.

7.3.2 MIXED VANADIUM-TITANIUM OXIDE FILMS

The values of refractive index of mixed titanium-vanadium oxides as a function of film composition in atomic % vanadium are plotted in figure 7.24. The single oxides of titanium and vanadium are approximately 2.3 and 2.2 respectively but all the mixed oxides have a much higher value in the range 2.8-3.2. Within experimental error, illuminating the substrate did not have any effect on the value of refractive index.

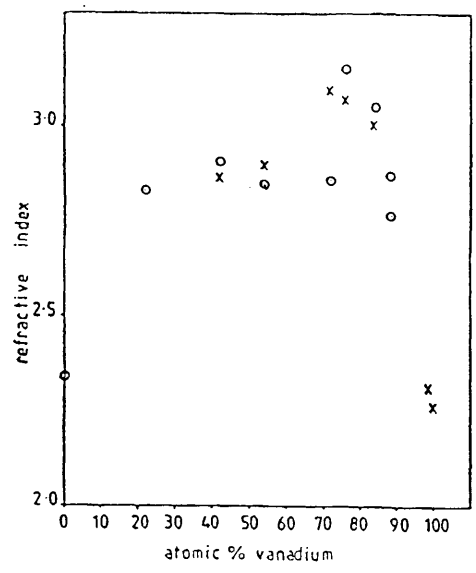


Figure 7.24 Refractive Index Values of Mixed Vanadium-Titanium Films as a Function of Vanadium Content.

7.4 DIELECTRIC MEASUREMENTS OF OXIDE FILMS

7.4.1 INTRODUCTION TO DIELECTRIC BEHAVIOUR

Many applications of dielectric materials involve the use of time varying electric fields and experimentally the behaviour of the material as a function of frequency can provide information concerning the structure and presence of dipoles and charge carriers.

The purpose of this section is to introduce information relevant to the results presented in section 7.4.2; it is not intended to be a detailed analysis, the majority of the information has been taken from Jonscher (1983).

7.4.1.1 DEFINITIONS

The application of an electric field to a material causes a shift of the positive and negative charges which is termed dielectric polarisation. The general relation between the polarisation, P, and the field, E, is given by equation (7.5)

$$P = \epsilon_0 \chi E \quad ---(7.5)$$

ϵ_0 = permittivity of free space = $8.854 \times 10^{-12} Fm^{-1}$

χ = susceptibility.

The polarisation is related to the surface charge on a material; the total charge being the sum of the contribution from free space ($\epsilon_0 E$) and from the material of susceptibility χ, ($\epsilon_0 \chi E$), giving a total charge of Q as in equation (7.6)

$$Q = \epsilon_0(1+\chi)E \equiv \epsilon(o)E \quad ---(7.6)$$

$\epsilon(o)$ = the static permittivity of the material.

Considering the response of a material with a time dependent electric field; the induced charge due to free space can follow the field instantaneously but the material has a delayed response and lags behind the driving field. The frequency dependent susceptibility is a complex function of frequency as given in equation (7.7).

$$\chi(\omega) = \chi'(\omega) - i\chi''(\omega) \qquad ---(7.7)$$

This provides information about both the amplitude and phase angle of the components of polarisation. The dielectric response of a sample is usually measured in terms of the complex capacitance. If the sample exhibits a dc conductivity, this is in phase with the measuring ac voltage and contributes to the imaginary component of the capacitance, the dielectric loss. Considering one particular process in a system, the capacitance can be expressed as the sum of a dispersive component and the effective "infinite" frequency contribution which is real and is the summation of the incremental capacitive dispersions which occur at higher frequencies. The complex capacitance is given by equation (7.8).

$$C(\omega) = C'(\omega) - iC''(\omega) \qquad ---(7.8)$$

$$= \epsilon_o \frac{A}{d}\left[\epsilon'(\omega) - i\epsilon''(\omega)\right] - i\frac{\sigma}{\omega}\frac{A}{d}$$

$$= \epsilon_o \frac{A}{d}\left[\chi'(\omega) + \epsilon(\infty) - i\chi''(\omega)\right] - i\frac{\sigma}{\omega}\frac{A}{d}$$

ϵ_0 = absolute permittivity ($8.85 \times 10^{-12} Fm^{-1}$ A=area, d=sample thickness, $\epsilon'(\omega) - i\epsilon''(\omega)$ = frequency dependent permittivity, $\epsilon(\infty)$= "infinite" frequency permittivity, σ = conductivity.

The real part of the permittivity consists of the contributions of free space and of the real part of the material and the imaginary component is entirely due to the medium.

7.4.1.2 THE DEBYE MODEL

When considering the dielectric behaviour of a material as a function of frequency the model derived by Debye (1912, 1945) is most commonly used.

This model considered the response of a charged dipole embedded in a viscous medium and is a good description of a single particle, non-interacting system. The Debye spectral response of susceptibility in the frequency domain is given by equation (7.9).

$$\chi(\omega) = \chi(o)\left(\frac{1}{1+\omega^2\tau^2} - \frac{i\omega\tau}{1+\omega^2\tau^2}\right) \qquad ---(7.9)$$

where ω is the angular frequency $\omega = 2\pi f$ (Hz), τ is the relaxation time for the polarisation and is related to the viscosity of the medium, $\chi(0)$ is the magnitude of the real part of the susceptibility at zero frequency.

The susceptibility is a complex function of frequency because it contains information about the amplitude and the phase angle; the response of the material is not instantaneous. From equation (7.9) both the real and imaginary susceptibilities exhibit power law behaviour and this is illustrated in log-log plots of $\chi(\omega)$ against ω ,figure 7.25 (Hill and Jonscher, 1983)

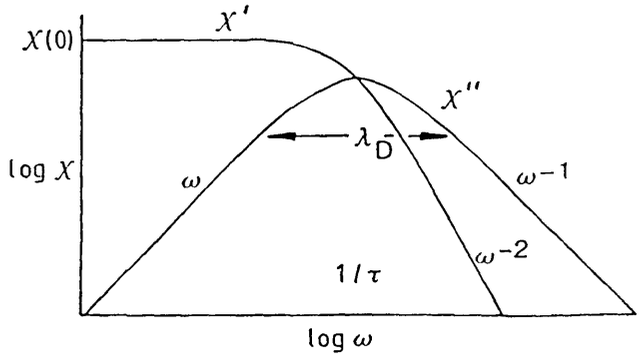


Figure 7.25 The Frequency Dependence of the Real and Imaginary Components of the Complex Susceptibility from the Ideal Debye Response.

7.4.1.3 LIMITATIONS OF DEBYE MODEL

The Debye model is strictly a single particle model and each dipole is considered to act independently of the other dipoles. In practice this model is applicable to systems such as gases at low pressures, but for the majority of experimental data a broader response is observed (Jonscher, 1975, 1980, Hill, 1981). Plotting $\log \chi(\omega)$ against $\log \omega$ for a large number of experimental results has shown a power law behaviour with exponents always having values of between zero and unity (Jonscher, 1983). Empirically the frequency dependence can be represented by combining two power laws which are respectively less than and greater than the peak frequency ω_p. (equation 7.10).

$$\chi''(\omega) \propto \frac{1}{(\omega/\omega_p)^{-m} + (\omega/\omega_p)^{1-n}} \qquad ---(7.10)$$

The exponents m and (1-n) have values between 0 and 1 (Jonscher, 1975).

The origin of the departure of the dielectric response from the Debye model lies in the assumption that the dipoles are non-interactive. This assumption may be valid for a system such as a gas at low pressure, but for condensed matter the rotation of one dipole affects both the surrounding environment and the forces acting on other dipoles. Experimentally an average of the interactions and dipole rotations is observed. The relaxation process needs to be interpreted as a many-body problem.

Experimental observation has led to a general classification of dielectric response as shown in figure 7.26, (Jonscher, 1980).

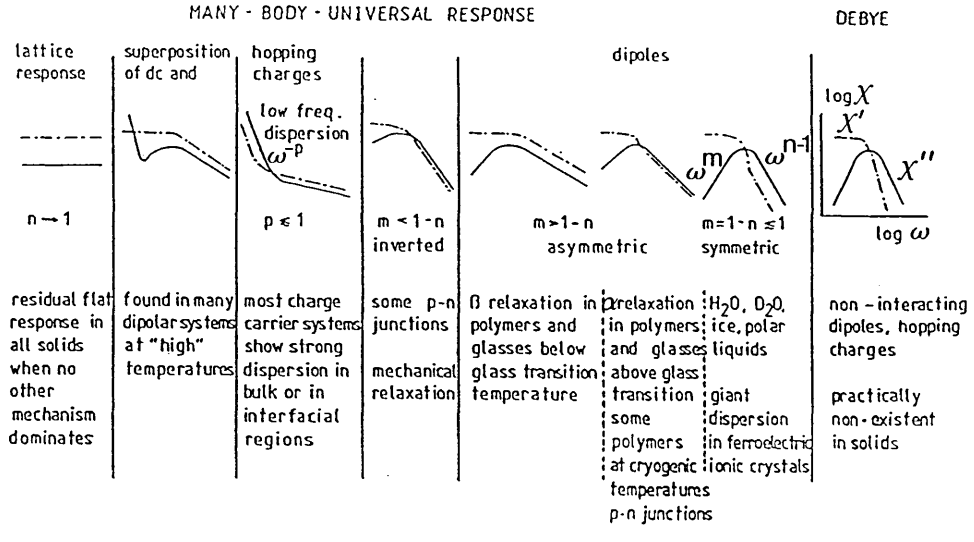


Figure 7.26 A General Classification of all Types of Dielectric Response in the Entire Range of Solids and Liquids. (The plots of log $\chi'(\omega)$ as a function of log ω are dotted lines and log $\chi''(\omega)$ as a function of log ω are solid lines).

7.4.1.4 BEHAVIOUR OF DIELECTRIC RESPONSE AS A FUNCTION OF TEMPERATURE

The dielectric permittivity is a function of temperature as well as frequency; commonly a loss peak moves to a higher frequency with increasing temperature. Generally, the magnitude of the response has not been found to change very significantly with temperature (Jonscher, 1983). Data obtained at different temperatures can be normalised by shifting the frequency spectra laterally and vertically until the data for both measurements coincide as closely as possible. The curve constructed from several temperature measurements has an extended effective frequency range and a higher density of data points; it is called the master curve. During the process of normalisation a reference point (A) is marked at certain coordinates and the new positions of A are marked at different temperatures. The locus of A provides information about the frequency dependence in the horizontal translation and the amplitude dependence in the vertical translation of the loss spectra.

The normalisation of experimental data into a master curve is possible because the spectral shape of the loss characteristics remains invariant with temperature. Because of this property the complete frequency and temperature dependence of loss may be represented by a product rule as given in equation (7.11).

$$\chi''(\omega,T) = A(T)F[\omega/\omega_p(T)] \qquad ---(7.11)$$

where A(T) is an amplitude term which is generally weakly dependent on temperature and $F[\omega/\omega_p(T)]$ is the spectral shape function of the normalised frequency. $\omega_p(T)$ is the temperature

dependent loss peak frequency which is usually temperature dependent and can show an Arrhenius behaviour (equation 7.12).

$$\omega_p(T) = \nu_o \exp(-W/kT) \quad ---(7.12)$$

W = activation energy

k = Boltzmann's constant

T = absolute temperature

ν_o = typical lattice vibration frequency (e.g. 10^{12} Hz)

If the spectral shape of the loss characteristic does change with temperature it can be concluded that structural changes in the material have taken place. These can be phase transitions or slowly evolving structural processes (Jonscher 1983).

7.4.1.5 MANY BODY MODEL

The importance of many-body interactions led to the Dissado-Hill model (Dissado and Hill, 1979). An outline is given in this section.

The Dissado-Hill model considers three types of transitions to be occurring during relaxation as illustrated in figure 7.27.

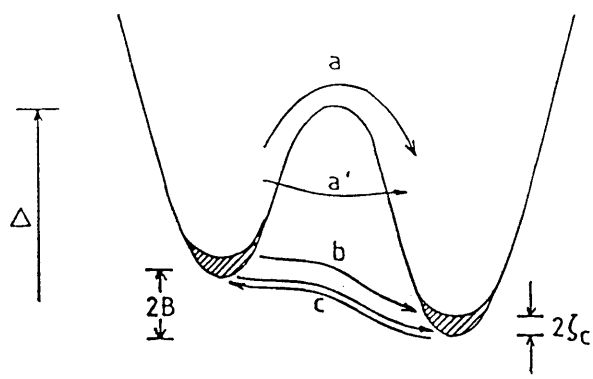


Figure 7.27 Potential Energy Diagram of a Many-Body Two Level System Representing the Energy of a Large Number of Interacting Systems

a = large thermally assisted transition over the barrier .

a' = thermally + tunnel assisted process.

b & c = configurational tunnelling transitions of flip and flip-flop types respectively.

2ζ = width of correlated states.

The correlated states are energy levels resulting from weak interactions which cause small variations in the energies of interacting particles as the result of other particles, i.e. they are of a many-body type. The energies involved with the correlated states are less than milli-eV in magnitude and are inaccessible to thermal excitations because they represent interactions between particles and not excitations of individual particles. Because the small transitions in the correlated states require negligible energy, they are referred to as configurational tunnelling.

The three fundamental processes denoted by a, b and c govern different stages of the dielectric relaxation. The large thermally assisted process (a) governs the response in the immediate neighbourhood of the loss peak frequency (ω_p) and the loss peak remains closely associated with the Debye process. The "wings" of the response on both sides of the loss peak frequency are governed by the many-body processes b and c. Processes b are denoted as small flip transitions and they represent a tunnelling mode between different configurations giving a net change in dipole moment. These flip transitions are the dominant relaxation mechanism at relatively short times and govern the response at frequencies higher than ω_p, i.e. the (n-1) index. The flip transition can operate before the Debye process of large transitions has time to develop.

At frequencies lower than the loss peak the flip-flop processes, denoted c in figure 7.27 govern the response i.e. the m exponent. These transitions do not change the value of total polarisations, they distribute the energy of the system.

The relaxation process occurring after removal of a polarising field can be considered as a succession of four stages, each being dominated by a particular type of transition. First, at times less than approximately 10^{-12}s, there is a delay necessary to establish the flip processes. Secondly the flip transitions dominate. The probability of the flip transitions occurring at this stage is greater than the flip-flop transitions because a large number of dipoles need to make a transition in the early stages of relaxation. The flip transitions dominate up to times of the order of $1/\omega_p$ which is the delay time for the onset of the Debye-like large transitions. In the third stage both the dominating Debye-like large transitions and the flip transitons cause a relaxation of the dipole moment. The fourth stage sets in at times greater than $1/\omega_p$ in which the state of polarisation approaches equilibrium and the 'directional' processes of the second and third stages become less important and flip-flop transitions become the dominating mechanism. This process redistributes the energy locally and slows down the transitions which change the dipole moment.

7.4.2 RESULTS OF DIELECTRIC MEASUREMENTS

7.4.2.1 TITANIUM DIOXIDE FILMS

Titanium dioxide films grown on polished stainless substrates at temperatures of 70, 150, 190, 275 and 350^{o}C were

measured by the FRA. The samples typically exhibited a very broad loss peak and a slowly varying value of the real part of the susceptibility with frequency. The onset of dc conductivity was observed in some of the samples as the frequency decreased; this is manifested by a slope of -1 in the imaginary susceptibility curve. The oxide films grown at the lower temperatures of 70 and 150°C did not give reproducible results when remeasured. This may be due to the oxide containing decomposition products or to the amorphous nature of the low temperature films. The dielectric response of the oxide grown at 190°C is shown in figure 7.28 for five temperatures ranging from 243 to 363K, and the results normalised into a master curve are plotted in figure 7.29.

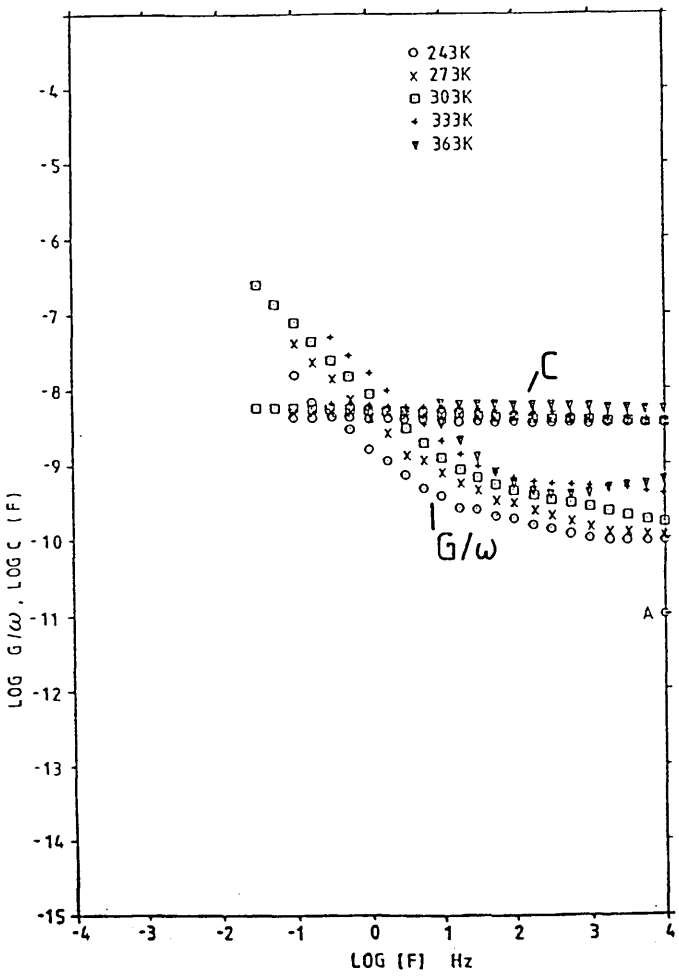


Figure 7.28 The Dielectric Response as a Function of Frequency of Titanium Dioxide Grown at 190°C for different Measurement Temperatures.

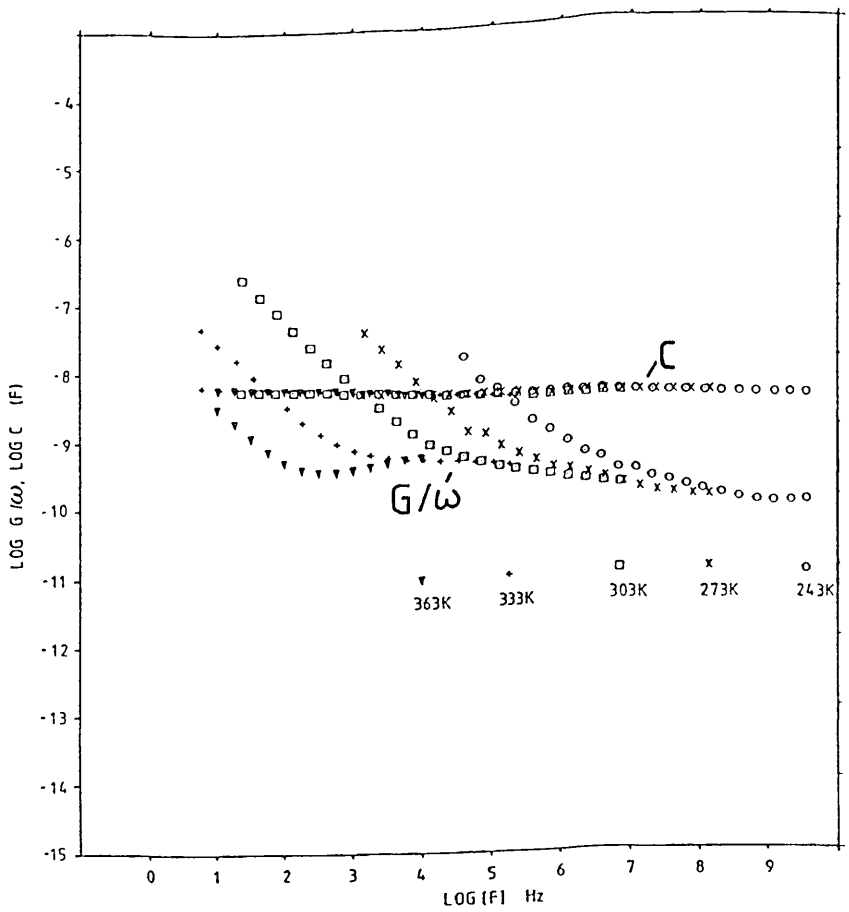


Figure 7.29 The Results of the Dielectric Response of Titanium Dioxide Grown at 190°C , Normalised at 363K.

From figure 7.29 the lateral shift of the reference point A provides the frequency shift with changing temperature. In figure 7.30 the ln(frequency shift) is plotted for a number of samples against the reciprocal of the absolute temperature in order to investigate whether an Arrhenius dependence on temperature is present.

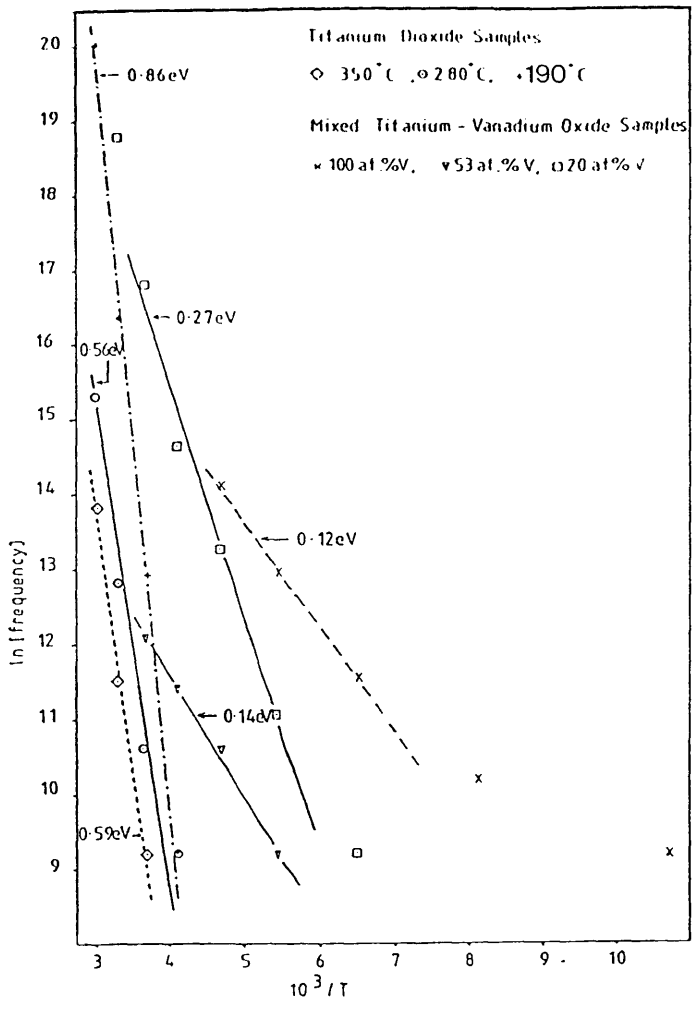


Figure 7.30 Ln[frequency shift] Plotted Against the Reciprocal of the Absolute Temperature for all Oxide Samples Measured.

From figure 7.30 a straight line is observed and the activation energy for the process is 0.86 eV. Plots of both the samples grown at 275 and 350^{o}C are also shown in figure 7.30 and the activation energies calculated.

LEAST SQUARES FIT TO DATA OF FIGURE 7.31

(The method and symbols are explained on page 132)

Sample	Eqn. of line	σ_y	σ_B	act. energy
TiO_2				
190°C	-14.73-2199/T	0.043	9.8	0.19 ± 0.001eV
350°C	-20.06-1452/T	0.269	623	0.13 ± 0.05eV
TI-V-O				
20%V	-5.18-2613/T	0.692	24.3	0.225±0.002eV
53%V	-5.85-2989/T	0.247	151	0.26 ±0.015eV
85%V	-5.41-899.7/T	0.267	47.8	0.078±0.004eV
100%V	-3.59-1130/T	0.516	115	0.1 ± 0.01eV

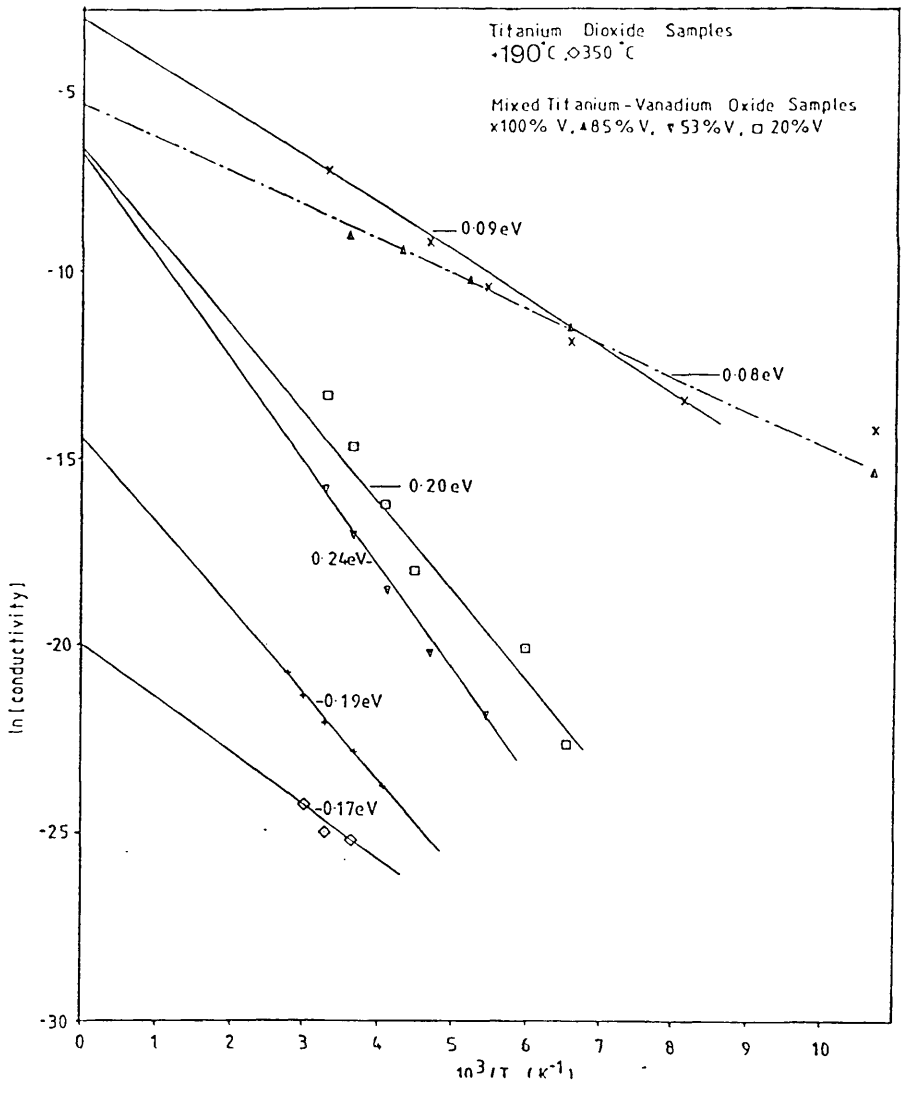


Figure 7.31 Ln[dc conductivity] Plotted Against the Reciprocal of the Absolute Temperature for all Oxide Samples Measured.

The values of dc conductivity of the sample grown at 190°C are dependent on the measurement temperature and an Arrhenius plot (figure 7.31) shows the process to be thermally activated with an activation energy of 0.195 eV. The activation energy for dc conduction for the sample grown at 350°C has been calculated from the plot in figure 7.31; the sample grown at 275°C did not exhibit dc conductivity in the frequency and temperature range measured. All activation energies for frequency shift and dc conductance are given in table 7.1 along with estimated values of conductivities.

From the limited number of titanium dioxide samples measured

no trends in conductivity, activation energies or values of relative permittivity can be concluded. Repeated measurements of several samples grown under identical conditions and a greater number of different growth condition need to be investigated. From the present results the following points can be noted:

(1) The value of the exponent n and the shape of the response is similar to that of a glassy material as shown in figure 7.26.
(2) The activation energy of the dc conductivity is of the order of 0.15 to 0.2eV which indicates that the mechanism is electronic not ionic (Prof. Hill, private commumincation).
(3) The activation energy of the frequency shift is greater than that for dc conduction and hence a different process is responsible (e.g. dipoles).
(4) The dc conductivity of the materials at room temperature ranges from 10^{-10} to 10^{-12} Ωm^{-1}.

7.4.2.2 MIXED OXIDE FILMS OF TITANIUM AND VANADIUM

Mixed oxide films of compositions 20, 53, 85 and 100 atomic % vanadium (compared to titanium) were measured. These films were all measured at lower temperatures than the titanium dioxide films because of their higher dc conductivity at temperatures above room temperature. Figure 7.32 shows the master curve of the 20% film.

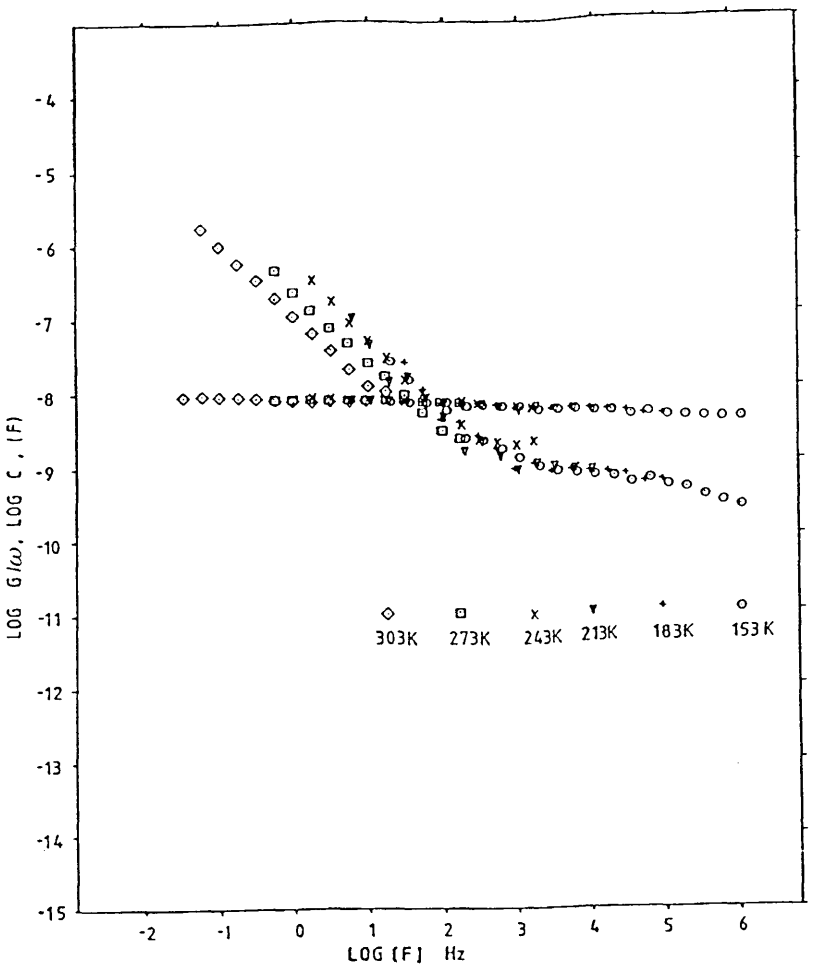


Figure 7.32 Normalised Dielectric Response of the 20%V Film.

The response is similar in shape to the titanium dioxide samples with a slowly varying real part of the susceptibility and a loss peak with dc conduction occurring as the frequency decreases. Careful inspection of both responses shows that the dispersion is slightly greater in the 20% vanadium sample and the loss peak has a smaller value of the index n, than the titanium dioxide sample. Increasing the vanadium content to 53% produces a dielectric response shown in figure 7.33.

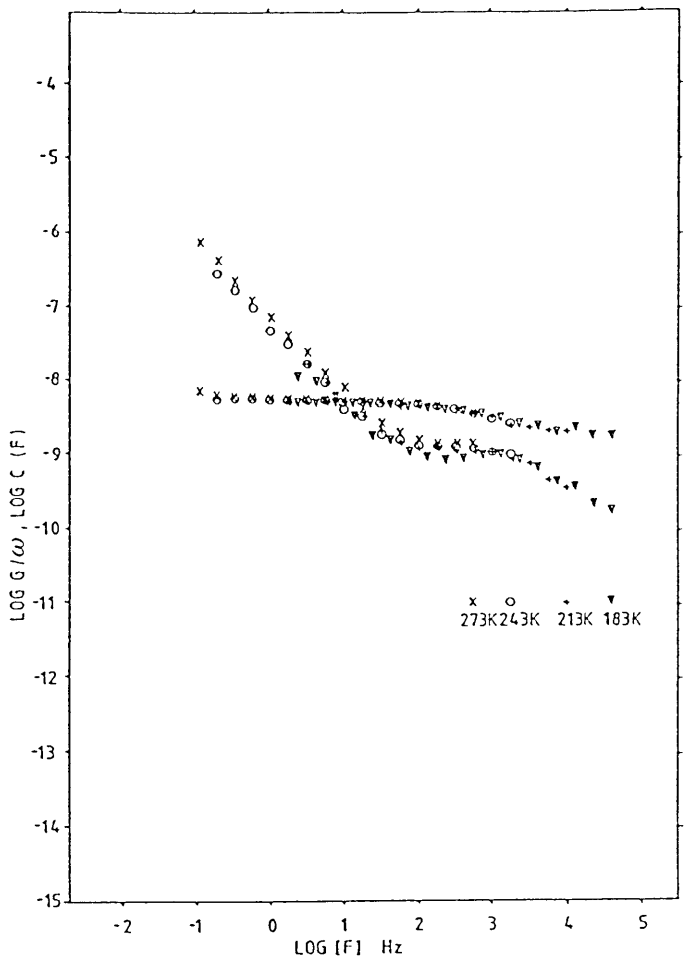


Figure 7.33 Normalised Dielectric Response of 53%V Film.

The size of the dispersion is larger than the one observed in the 20% vanadium and the loss peak is narrower with a smaller value of index n. A plot of the value of n against atomic % vanadium is given in figure 7.34.

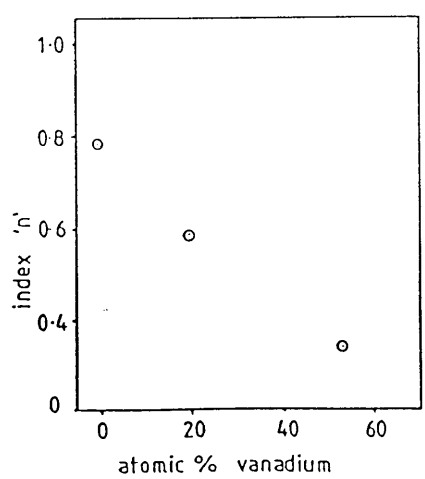


Figure 7.34 Plot of Exponent 'n' Against % Vanadium.

The normalised dielectric response of the 85 and 100% vanadium oxide films are shown in figures 7.35 and 7.36 respectively.

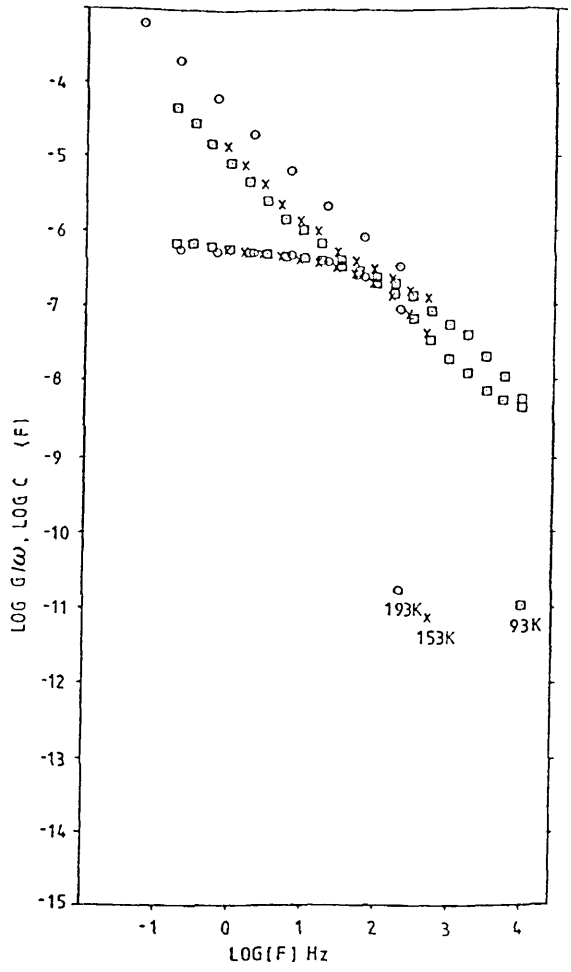


Figure 7.35 Normalised Dielectric Response of 85%V Film.

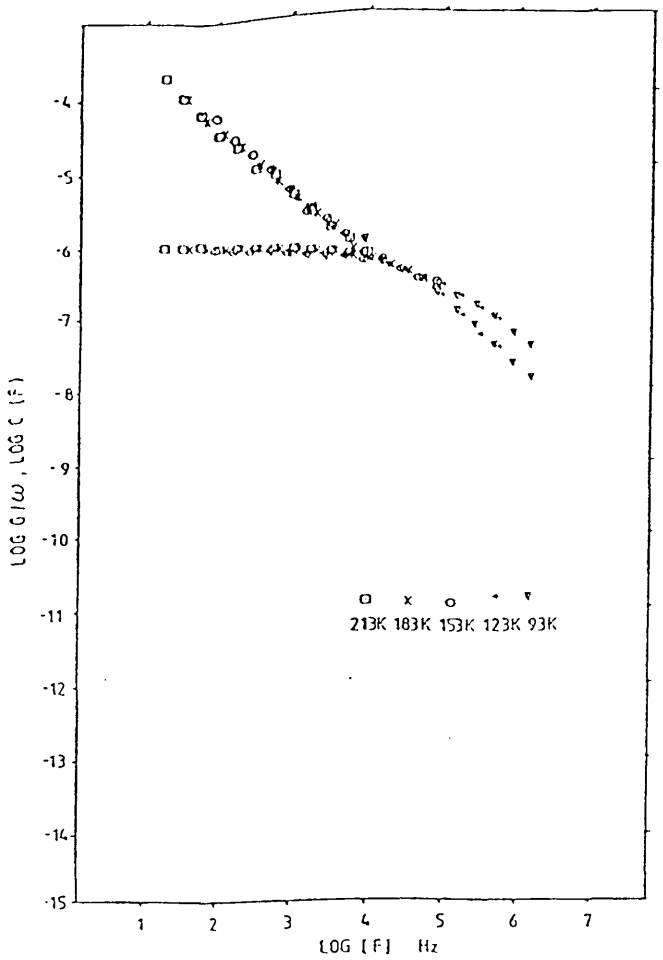


Figure 7.36 Normalised Dielectric Response of 100ÅV Film.

These responses differ considerably from the other dielectric responses measured as shown in figure 7.29, 7.32 and 7.33. The difference is associated with the electrodes on the sample creating a high capacitance barrier layer which is observed in the dielectric response at low frequencies. The barrier layer is in series with the sample and both the barrier layer and sample can be represented as a capacitor and resistor in parallel as shown in figure 7.37.

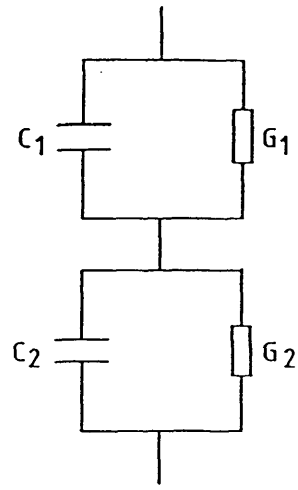


Figure 7.37 Representation of the Dielectric Sample in Terms of Parallel Capacitor-Resistor Pairs in Series.

The response of this combination is shown in figure 7.38.

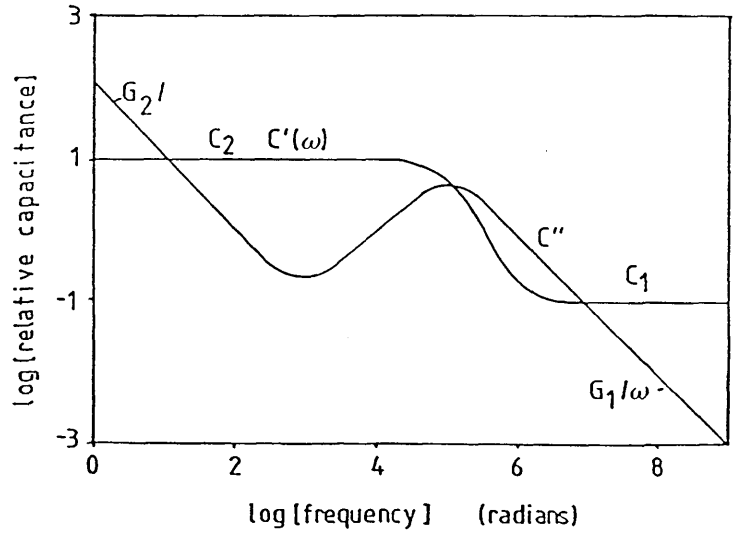


Figure 7.38 Dielectric Response of Resistor-Capacitor Combination Illustrated in Figure 7.37, after Hill and Pickup, (1983).

Where $C_1 = 0.1$, $C_2 = 10$, $G_1 = 10^6$, $G_2 = 10^2$.

The characteristic shows that G_1 and C_1 dominate at high frequencies and G_2 and C_2 dominate at low frequencies. The structure of this plot can be understood in terms of the transfer of the effective impedance within the complete system from one element in the series pair e.g. C_1, G_1 to the other, e.g. C_2, G_2 as the frequency is varied.

This effect is observed in the 85%V and the 100%V samples because of the higher value of conductivity. The titanium dioxide samples and lower vanadium content samples have a higher resistance which dominates the response at all frequencies i.e. even if a barrier layer is present it is insignificant to the total response because the bulk dominates.

A computer curve fitting has been carried out on the 100% vanadium oxide sample to extend the frequency range of the response up to 10^8 Hz. This is shown in figure 7.39 and shows the real part of the bulk capacitance levelling off at the higher frequencies.

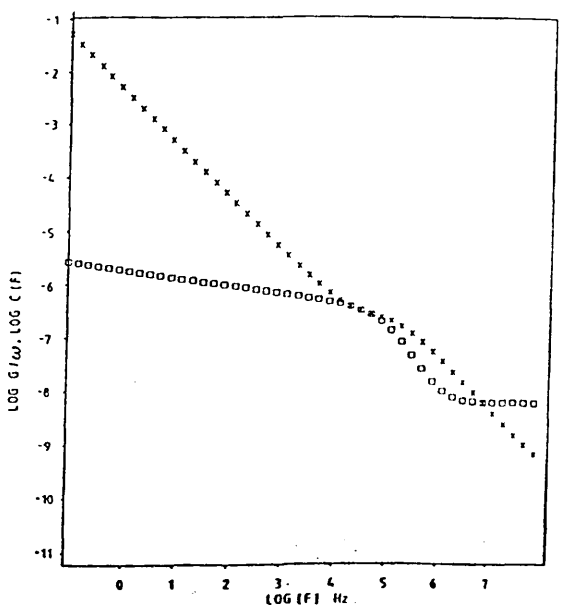


Figure 7.39 A Computer Curve Fit of Dielectric Response of 100%V Oxide Film. (Experimental Response Shown in Figure 7.36).

At lower frequencies the real part of the susceptibility increases with a small gradient which indicates that the barrier layer is dispersive. The increase in capacitance is of the order of 100 times which for a film of 100nm would give a barrier layer of about 1nm.

From the dielectric responses of the mixed oxide films (figures 7.32-7.36), Arrhenius plots of the shifts in frequency and the conductivities have been carried out and are presented in figures 7.30 and 7.31 respectively. Considering the activation energies for dc conductivity, the values lie between 0.08eV and 0.24eV compared to 0.19eV and 0.17eV for titanium dioxide, and no obvious correlation with composition is observed as shown in figure 7.40.

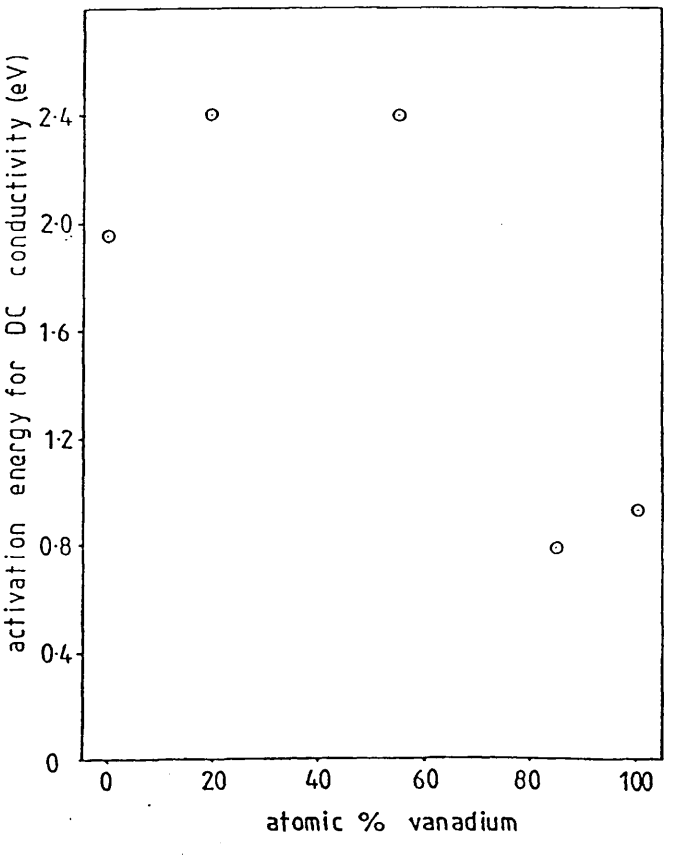


Figure 7.40 Plot of Activation Energy for dc Conductances as a Function of Atomic %V.

A plot of the ln(conductivity) at infinite temperature against the % vanadium however, does show an increasing value with higher vanadium content, (figure 7.41).

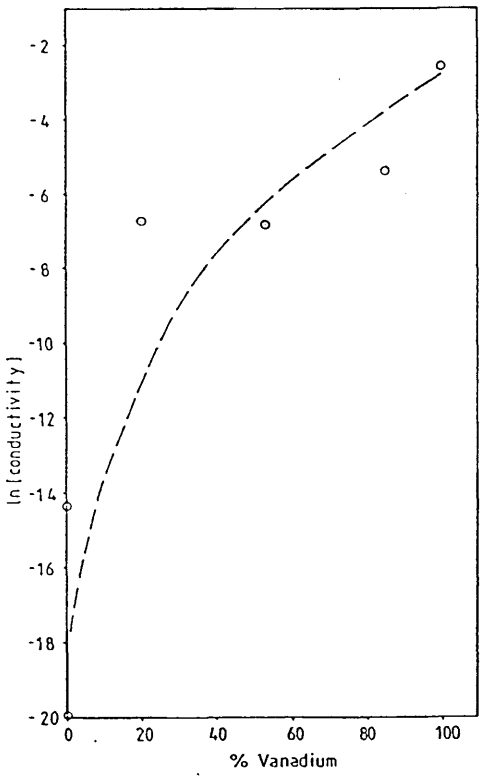


Figure 7.41 Plot of ln[dc conductivity] as a Function of Atomic %V.

Considering the activation energies of the frequency shifts shown in figure 7.30, a trend of decreasing activation energy with increasing vanadium content was noted and the activation energy as a function of vanadium content is plotted in figure 7.42.

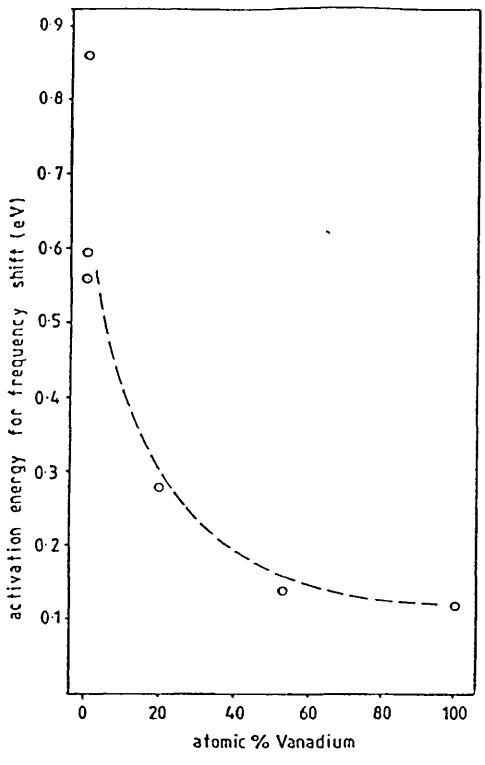


Figure 7.42 Plot of Activation Energy for Frequency Shift as a Function of Atomic %V.

As in the case of the titanium dioxide samples a greater number of measurements and samples need to be considered before drawing firm conclusions from the results. However, certain trends have been observed and these are:

(1) The loss peak observed for three samples of composition 100% titanium dioxide, 20% vanadium and 53% vanadium was found to decrease the index n with increasing vanadium composition and the magnitude of the corresponding dispersion in the real part of the susceptibility increased with increasing vanadium composition.

(2) The value of dc conductivity increased with increasing vanadium content (figure 7.41).

(3) The activation energy for dc conductivity ranged from 0.08 to 0.24eV with no obvious correlation with vanadium content. The magnitude of the activation energy indicates that the conductivity mechanism is electronic, not ionic, as with the

titanium dioxide films.

(4) The activation energy for the shift in frequency response showed a decrease with increasing vanadium content.

(5) The 85 and 100% vanadium oxide films exhibited evidence of a barrier layer in the frequency responses.

TABLE 7.1 SUMMARISING DIELECTRIC RESULTS

Sample	Conductivity at 303K (Ω m)	Energy (cond) (eV)	Energy (freq) (eV)	'n'
TiO_2				
350°C	1.48×10^{-11}	0.166	0.59	-
275°C	-	-	0.56	-
190°C	2.64×10^{-10}	0.195	0.86	0.79
Ti-V-O				
250°C				
20%V	1.24×10^{-6}	0.20	0.27	0.58
53%V	1.37×10^{-7}	0.24	0.14	0.33
85%V	2.03×10^{-4}	0.08	-	-
100%V	6.75×10^{-4}	0.09	0.12	-

AMENDMENT TO TABLE 7.1

TiO_2	act. energy (cond.)
190°C	0.19 ± 0.001eV
350°C	0.13 ± 0.05eV
Ti-V-O	
20%V	0.225 ± 0.002eV
53%V	0.26 ± 0.015
85%V	0.078 ± 0.004eV
100%V	0.1 ± 0.01eV

7.5. ETCHING

7.5.1 ETCHING OF TITANIUM DIOXIDE FILMS

The etch rate of the oxide films in sulphuric acid at 150°C as a function of substrate temperature is plotted in figure 7.43.

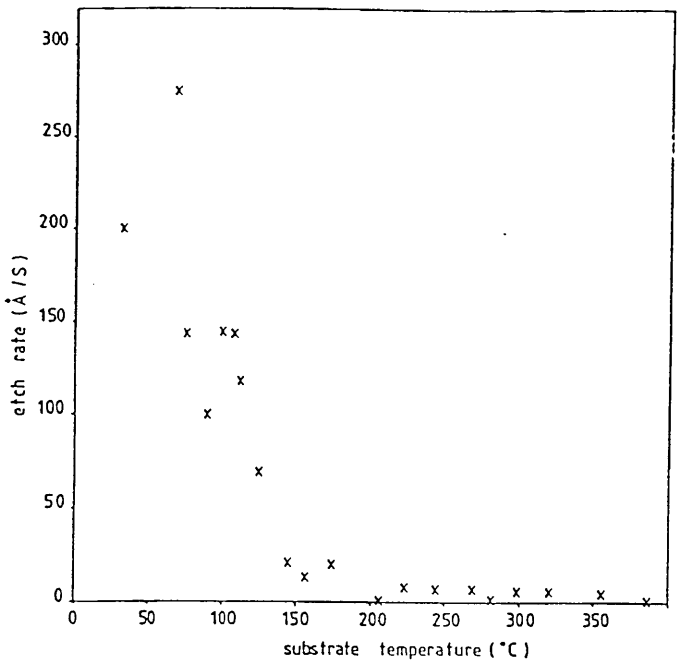


Figure 7.43 Etch Rate of Titanium Dioxide Films as a Function of Deposition Rate in Concentrated Sulphuric Acid at 150°C.

The etch rate can be seen to be reasonably constant for substrate temperatures of greater than 200°C. At substrate temperatures less than 200°C the etch rate increases rapidly with decreasing temperature.

A selection of samples annealed at 1000°C were etched in the same manner and had an etch rate at least an order of magnitude less than any of the as grown films.

It is difficult to compare the etch rates found in the present work with the values in the literature because different etches, concentrations and temperatures are used and the often qualitative descriptions such as 'easily etched' do not allow for accurate comparison. However the results of etching are summarised in table 7.2.

TABLE 7.2 SUMMARY OF ETCHING BEHAVIOUR OF TITANIUM DIOXIDE FILMS

PRECURSOR	SUBSTRATE TEMPERATURE	ETCHANT	ETCH RATE	REFERENCE
$TiCl_4$ $+H_2O$	150	10%HF	-	Feuersanger (1964)
$Ti(OPr^i)_4$	410-750	conc.HF	0.3Å/S	*Yokozawa et al.
$Ti(OPr^i)_4$ $+O_2$	320-540	dil.HF	4-60Å/S	(1968)
$Ti(OPr^i)_4$ $+O_2$	550	70%H_2SO_4	easily etched	Balog et al. (1972)
$Ti(OPr^i)_4$ $+H_2O$	150	0.5%HF	70-78Å/S	Fitzgibbons et al.(1972)
		48%HF	v.rapid	
		100% H_2SO_4	25-40Å/S	
	ann. 350	0.5%HF	v.slow	
		48%HF	slow	
		100% H_2SO_4 (50-100C)	15Å/S	
	ann. 1000	0.5%HF	none	
		48%HF	slow	
		100% H_2SO_4 (120C)	1000Å/S	
$Ti(OPr^i)_4$	200	10%HF	10^3nm/min	Fuyuki et al.
$+H_2O$	400	10%HF	10nm/min	(1988)

*** Etch rate increases with decreasing deposition temperature and with increasing oxygen content.**

A general trend of etching which is consistent with the present work is decrease in etching rate with increasing substrate temperature.

7.5.2 ETCHING OF VANADIUM-TITANIUM MIXED OXIDE FILMS

The etch rate of titanium-vanadium oxide films in concentrated sulphuric acid at 100°C as a function of atomic % vanadium is plotted in figure 7.44. The etch rate increases by more than three orders of magnitude from the 100% titanium dioxide film to the 100% vanadium oxide film. There may be an increased etching rate for the samples grown under UV illumination but the experimental scatter is too great to definitely conclude this.

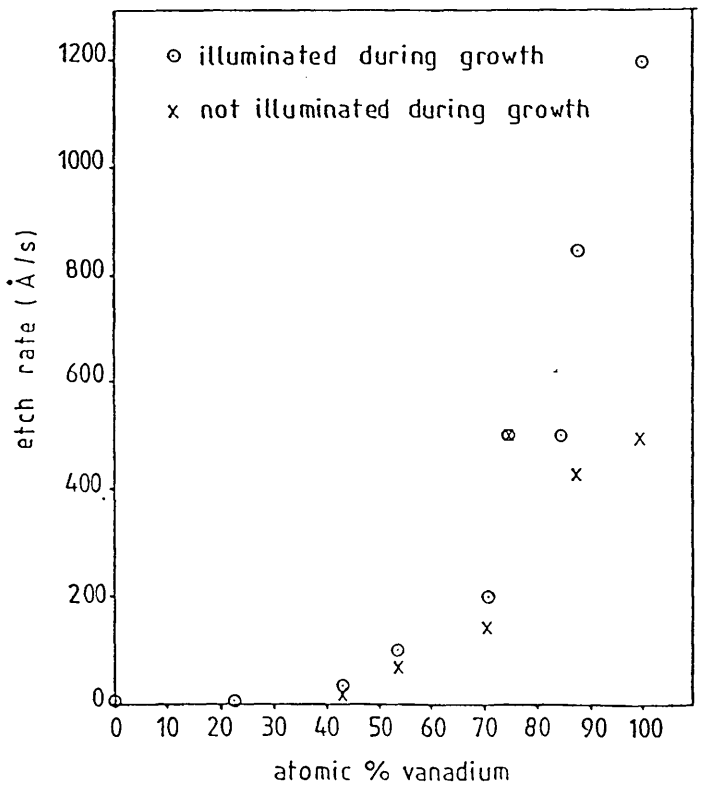


Figure 7.44 Etch Rate of Titanium-Vanadium Oxide Films as a Function of Vanadium Content.

CHAPTER 8 DISCUSSION

8.1 INTRODUCTION

The experimental work described in chapters 4,5,6 and 7 is concerned with the decomposition of the metal alkoxide precursors, the resulting growth rates and properties of the deposited films. The results indicate that the process can yield titanium dioxide films over a range of temperatures and growth rates, resulting in layers which have shown large variations in crystallinity, refractive index and resistance to etching. The growth of mixed oxides is another route for varying the properties of the oxide layers and the addition of vanadium oxide to titanium dioxide has a very large effect especially on the etching and the electrical properties. In this chapter a discussion of the overall view of the process is intended, correlating the results from chapters 4-7.

8.2 PROCESS DETAILS

8.2.1 EFFICIENCY OF PROCESS

A simple calculation has been carried out to determine the efficiency of the process, i.e. to give an indication of the proportion of precursor that actually decomposes to oxide on the substrate. This value is unique to the particular design of reactor used in the present experiments and a higher efficiency could be achieved if this was an important design consideration, e.g, if the precursor chemical were particularly expensive or the process were commercial.

Taking the area of deposition as $15cm^2$, i.e. the area of the susceptor, and a typical value of density of deposited oxide as $3gcm^{-3}$ (Fitzgibbons et al., 1972), from the volume of precursor

injected (of density 0.955 gcm^{-3}) the maximum growth rate of titanium dioxide occurs when every molecule of injected alkoxide decomposes to titanium dioxide on the substrate. This growth rate has been calculated as a function of alkoxide injection rate and is plotted in figure 8.1. For comparison the growth rate of titanium dioxide at 350°C (figure 5.7d) which was the highest growth rate determined experimentally, has also been plotted in figure 8.1 and is considerably less than the calculated maximum.

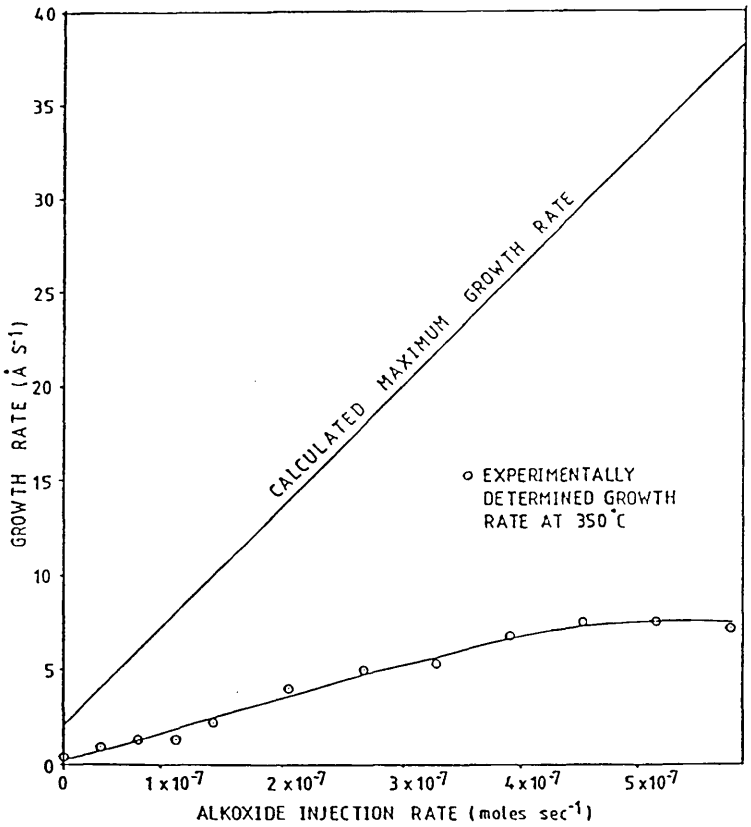


Figure 8.1 Plot of Calculated Maximum Growth Rate and **Experimentally Observed Growth Rate as a Function of Alkoxide Injection Rate.**

The efficiency of the process is taken as (growth rate observed experimentally/maximum calculated) x 100%, and this is

plotted against the alkoxide injection rate in figure 8.2.

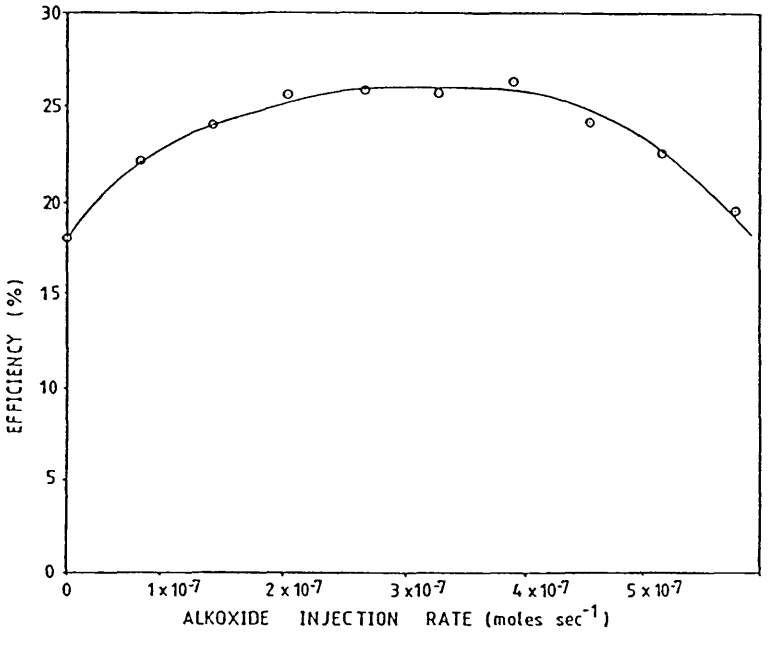


Figure 8.2 Plot of Efficiency of Process as a Function of Alkoxide Injection Rate.

FIgure 8.2 shows a quite narrow range of efficiency values ranging from approximately 18% to 26%. The losses in the process include deposition on the inside of the reactor and some molecules are swept through the reactor without decomposing; the residence time over the substrate is not sufficient for all molecules to diffuse to the substrate. From figure 5.10, the growth rate was observed to decrease with increasing gas velocity, which reduced the residence time of the molecules above the substrate.

8.2.2 EFFECT OF ILLUMINATING THE SUBSTRATE DURING GROWTH

The growth rate in the lower temperature range is enhanced by illuminating the surface with UV as shown in figure 5.4. In this

temperature regime the growth rate is limited by kinetics and the Arrhenius plot of figure 5.4 is a straight line (with some experimental scatter). Values of activation energies have been calculated for the conditions used (table 5.1) and a decrease in activation energy of 0.16eV was found for both alkoxide concentrations when the growth surface was illuminated. The decrease of activation energy of 0.16eV was less than the maximum photon energy input (4.9eV for a wavelength of 253.7nm). A decrease in activation energy in the growth of silicon from silicon tetrachloride was noted by Kumagawa et al.(1968). A 500W high pressure mercury lamp irradiated the substrate during growth and a decrease of 2.1kcal/mole (0.091eV) was observed. As with the present work the decrease in activation energy was much less than the maximum energy input from the mercury lamp.

At all growth temperatures used some thermal deposition occurred. Hence photolysis is not capable of selected area deposition by a masking process. An interesting feature of the interaction of irradiation on the growth process is the dependance of growth on alkoxide concentration (figures 5.4 and 5.7b). For example, at lower alkoxide concentrations no enhancement of growth was observed but on increasing the alkoxide injection rate photolysis did increase the oxide growth rate.

There are insufficient results presented in chapter 5 to draw any firm conclusions about the concentration dependence of photolytic enhancement of growth rate in this system; a series of experiments is necessary to determine more accurately the conditions for the onset of photolysis. However tentative explanations can be put forward on the basis of the present

observations. It can be seen from the results of chapter 5 that there is a change in the Arrhenius curve with alkoxide injection rate, as illustrated in figure 8.3.

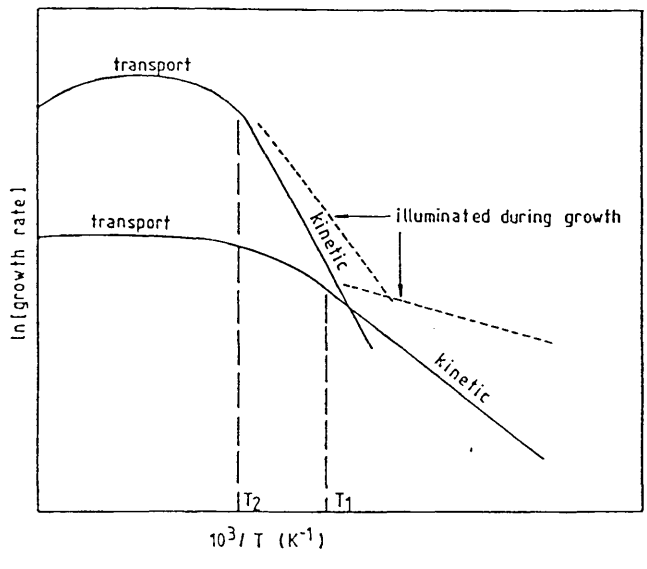


Figure 8.3 Illustrating the Change in Arrhenius Plot with Alkoxide Injection Rate.

At the lower alkoxide injection rate of 0.35×10^{-7} moles s^{-1} the growth rate indicates a change from a kinetically dominated regime to a mass transport dominated regime at a temperature of T_1. (This is an arbitrary value because the change from kinetic to mass transport control is a continuous process as illustrated in figure 1.11). The change from kinetic to mass transport control occurs at a higher temperature for the alkoxide injection rate of 5.30×10^{-7}, T_2 in figure 8.3. This increase in transition occurs because the number of impinging precursor molecules on the substrate surface is larger for the higher concentration and hence mass transport does not become limiting until a higher temperature is reached. Another observation

from figure 5.4 is that photolysis only appears to operate in the kinetically controlled regime. The exact nature of the interaction of light with the titanium isopropoxide molecule is not known but it is possible that the light excites the molecule into a state from which thermal decomposition is easier than from the unexcited molecule; this would account for the lower activation energy which is observed. In a growth regime which is not kinetically controlled, the thermal energy is sufficient to decompose the molecules that arrive at the surface; the rate is determined by the supply from the vapour and the contribution from the UV would not be observed i.e. it is not operating on the rate controlling step any more.

With the two considerations of (1) concentration dependence of transition temperature from kinetic to mass transport control, and (2) Photolysis being effective in the kinetic regime only, the concentration dependence of photolysis can be explained with the aid of figure 8.4.

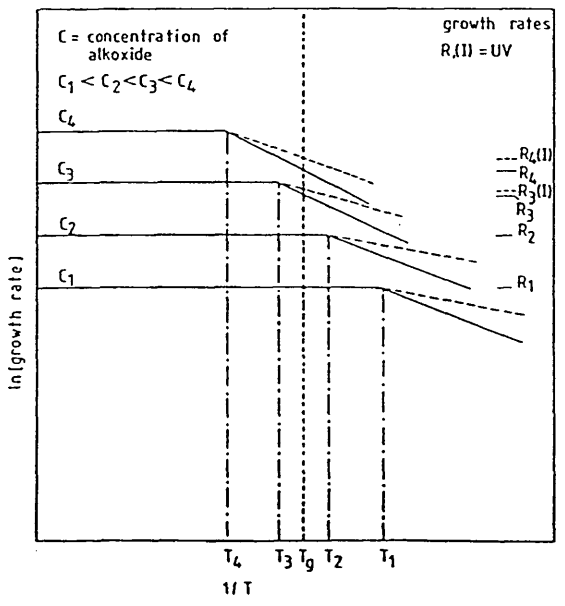


Figure 8.4 Schematic Diagram Illustrating the Change in ln[Growth Rate] vs 1/T ,for Different Alkoxide Concentrations.

Considering a temperature T_g as indicated in figure 8.4, growth at this temperature from concentrations C_1 and C_2 are in the mass flow regime and photolysis does not enhance to the growth rates R_1 and R_2. However increasing the concentration to C_3, would put the growth into the kinetically controlled regime and different growth rates of $R_3(I)$ and R_3 would be observed for photolysed and non-photolysed samples respectively. Hence the photolysis is concentration dependent.

Growth in the kinetic regime is favourable for obtaining good uniformity of deposition, for example the films shown in figure 5.5 are very uniform in the non-illuminated regions. Growing in the kinetically controlled region can however produce a less dense structure with partially decomposed compounds and poorer properties; this will be discussed in section 8.3.

8.3 PROPERTIES OF TITANIUM DIOXIDE FILMS AS A FUNCTION OF GROWTH CONDITIONS

The titanium dioxide films have been grown over a temperature range from 25 to 400°C. The thermal decomposition of titanium isopropoxide (figure 4.1) investigated by DTA/TGA, is only complete at temperatures higher than about 250°C.

The information gained from the DTA/TGA measurements can be used as a guide to the decomposition of precursor in the reactor; as discussed in chapter 4 a direct comparison cannot be made due to the different conditions. Hence the guidelines that figure 4.1 provides are :

(1) The oxide formed is only free from partially decomposed products above temperatures of 250°C,

(2) Between 250 and 370°C the structure is amorphous,

(3) Between 370 and 800°C the titanium dioxide is anatase. Above 800°C transformation to rutile occurs.

The maximum growth temperature used in the present work is 400°C so the presence of the rutile modification of titanium dioxide is unlikely.

8.3.1 CRYSTAL STRUCTURE OF TITANIUM DIOXIDE FILMS

The crystal structure of the deposited films has been investigated by both x-ray and electron diffraction and the results are presented in figures 7.1 and 7.8 respectively. The x-ray diffraction results did not provide detailed information because the technique is not sensitive enough for thin film analysis ; however it did indicate that below 170°C no observable crystalline structure was present and on increasing the temperature, the anatase reflections developed and a change in orientation was observed. Electron diffraction results gave a much more detailed view of the crystal structure. The lower temperature deposits (7.8a&b) had a more diffuse diffraction pattern which indicated an amorphous nature to the deposit and reflections were present which could not be attributed to anatase. The most probable origin of these unidentified reflections was the presence of partially decomposed titanium isopropoxide in the film; this would correlate with the DTA/TGA response which showed incomplete decomposition at these temperatures.

The sample grown at 190°C showed a predominantly anatase structure which was randomly oriented but a faint reflection which was attributed to incomplete decomposition or an intermediate compound was observed. The presence of the latter

reflection correlates with figure 4.1 but the crystalline anatase does not. The DTA/TGA results indicate that anatase forms at temperatures greater than 300°C and below this temperature the titanium dioxide is amorphous. The crystalline structure probably forms from the vapour deposition because the molecules have time to find a site on the existing titanium dioxide film (when a monolayer has grown). The molecules in the vapour deposition process have greater nearest neighbour distances which would reduce molecular interaction which could inhibit mobility. The presence of a surface may also catalyse the reaction.

The electron diffraction pattern of the sample grown at 220°C showed no evidence of incomplete decomposition and the anatase was crystalline with some developing preferred orientation. Hence in the vapour growth of titanium dioxide from titanium isopropoxide the decomposition is complete at a lower temperature than indicated by the DTA and TGA and the titanium dioxide is crystalline.

The growth of titanium dioxide at higher temperatures results in development of preferred orientation of the anatase film with both the (100) and (001) parallel to the substrate. At deposition temperatures of greater than 350°C extra reflections are present which may be due to interaction with the substrate.

If the trend in crystal structure changes with temperature are compared with the Arrhenius plot of figure 5.4, it can be seen that the kinetic region for an injection rate of 0.35×10^{-7} moles s^{-1} extends to approximately 200°C and at higher temperatures the mass transport processes become more important. The films deposited in the kinetic region are shown to contain

unidentified compounds and are randomly oriented polycrystalline structures. The kinetic step is probably concerned with the decomposition of the partially decomposed alkoxide molecules. In this growth regime more molecules impinge on the growth surface than can be accommodated in the lattice. This probably inhibits the rearrangement on the surface because of the large population of partially decomposed species which are constantly being replenished.

In the mass flow controlled regime the molecular dissociation is much easier due to the higher thermal energy and the growth is restricted by the supply of precursor molecules. Hence the adsorbed species have more chance of fully decomposing before impinging molecules are adsorbed and due to the increased mobility with higher temperature, the chances of occupying a preferred lattice site are greater. Hence the structure is more ordered.

8.3.2 THE CHANGE IN FILM PROPERTIES WITH GROWTH TEMPERATURE

The strong dependence of crystal structure on growth temperatures has been discussed in section 8.3. The structure of the deposited film is reflected in the changes in properties observed. In the present work, the characterisation techniques employed have been ellipsometry, dielectric measurements and etching as described in chapters 6 and 7. The results of the changes in properties as a function of growth temperature are summarised in figure 8.5 together with the thermal decompostion of titanium isopropoxide.

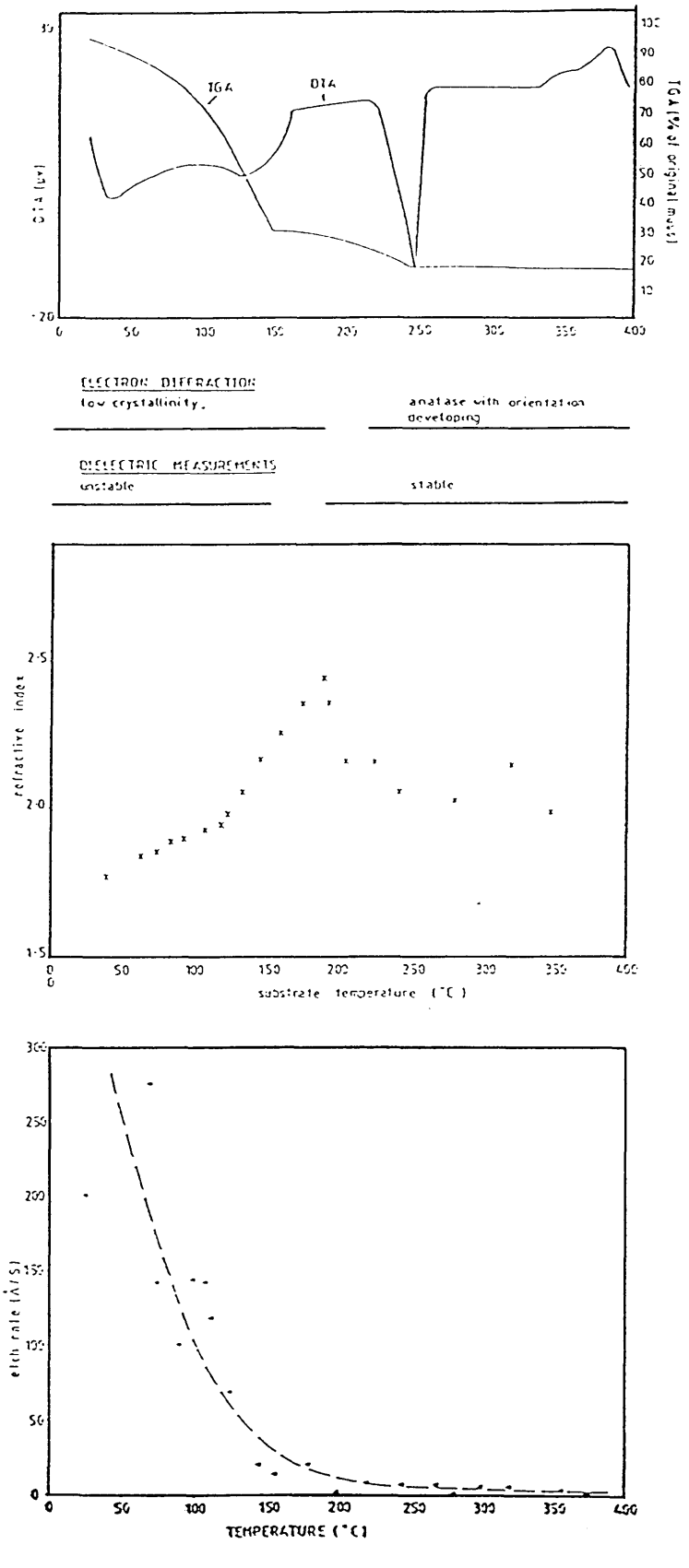


Figure 8.5 Schematic Diagram Summarising Results of Decomposition and Film Properties as a Function of Temperature.

Considering figure 8.5, both the refractive index and the etching rate of the titanium dioxide exhibit features which can be correlated to some extent with the crystal structure and decomposition of titanium isopropoxide. First, the refractive index response shows a distinct change in slope at approximately 120°C; this may be correlated with the end of the first decomposition stage observed in the DTA/TGA. The evidence from electron diffraction is that extraneous matter is probably incorporated in the films up to temperatures of approximately 200°C; however the patterns of 7.8a and 7.8b show an extra unidentified ring of 2.88Å present in the sample grown at 100°C. Hence the two-stage decomposition process observed by DTA/TGA may result in films containing different intermediate compounds, depending on the growth temperature. From a growth temperature of 120°C, to approximately 200°C the refractive index increases and the structure in this temperature range is becoming progressively more crystalline and the proportion of intermediate compounds is decreasing. Above 200°C the refractive index decreases sharply to a value of about 2.1 which remains reasonably constant with further increase in temperature. The structure in this temperature region is anatase which increases its orientation with increasing growth temperature.

The etching rate of the titanium dioxide films shows a strong dependence on the growth temperature. In the range 25 to 200°C, the etching rate decreases from approximately 250Ås^{-1} to less than 10Ås^{-1} and at higher growth temperatures the etch rate remains relatively constant. Thus the lower temperature films which contain intermediate compounds, have a less crystalline

structure and are almost certainly of lower density, etch more rapidly. The reasons for this could be chemical, e.g. the films containing intermediate compounds are more chemically reactive with the sulphuric acid; or structural, e.g. the lower density and crystalline order of the oxide makes it more prone to attack from the etchant. Some etchants used in metallographic preparation preferentially attack the grain boundaries of a structure which are areas of lower order and density. The oxide films grown at temperatures in the range 200 - 400°C had a reasonably constant etch rate and corresponded to an oriented crystalline anatase structure. These films were denser and hence for the same number of molecules dissolved by the etchant, a lower etch rate is observed. The structure is also thermodynamically more stable than the amorphous structure, which increases its chemical stability.

Annealing some of the titanium dioxide samples at 1000°C resulted in the refractive index being approximately the same as that of the oriented anatase but the etching rate was reduced by an order of magnitude. From the DTA/TGA results, at 1000°C the rutile modification of titanium dioxide should be formed. Rutile is the thermodynamically stable form and hence is more difficult to etch than the anatase. This is shown schematically in figure 8.6.

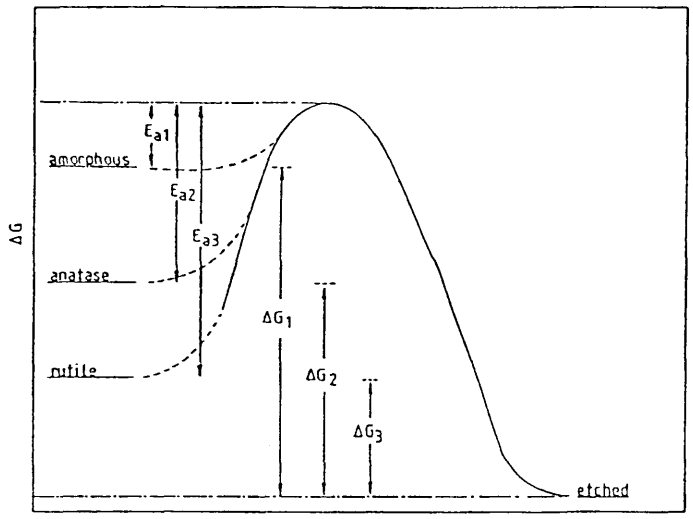


Figure 8.6 Schematic Diagram of Relative Free Energies of Titanium Dioxide in the Low Temperature Amorphous Structure, ΔG_1, Anatase, ΔG_2 and Rutile, ΔG_3 compared with the Free Energy in Solution in Sulphuric Acid Etch.

The activation energies Ea_1, Ea_2 and Ea_3 increase from the low temperature amorphous structure, anatase to rutile respectively as shown in figure 8.6 and the driving force for the reaction ΔG_1, ΔG_2 and ΔG_3 decreases respectively. Hence etching becomes progressively more difficult as the growing temperature increases because the titanium dioxide is able to grow in a more stable form.

The increase in density observed after annealing the samples was approximately 35% as shown in figure 7.23. If the annealed oxide is assumed to be rutile of density $4.2 gcm^{-3}$, then a rough estimate of the density of the as grown film is $3.1 gcm^{-3}$. This is approximately the same value observed by other workers (Fitzgibbons et al.,1972).

The dielectric measurements of the oxides were made on only a small number of samples. However, from the measurements, the two titanium dioxide films grown at 70 and 150°C were found to be unstable and a repeat measurement gave a different response, e.g. with much higher conductivity. The behaviour of the films was probably due to the impurities trapped in the structure because of incomplete decomposition. These impurities may be irreversibly changed by the measurement making a reproducible measurement impossible. Only room temperature measurements were carried out on these samples. Three titanium dioxide films grown at temperatures of 190, 275 and 350°C were measured and these all gave reasonably similar results. The capacitance did not change very much over the whole frequency range and a very broad loss peak was observed. The dc conductivity of the material was of the order of 10^{-10} Ωm, however the activation energy for conduction was less than 0.2eV. The value of activation energy is typical of electronic rather than ionic conducting species and the low value of conductivity observed could be due to trapping centres in the oxide reducing the electron mobility and thus the number of charges reaching the electrodes.

The characterisation of the titanium dioxide films has shown that although the uniformity of growth is better at lower deposition temperatures, the properties are less reproducible. The higher temperature films are more stable electrically, have a lower and more constant etching rate, a reasonably constant refractive index and a higher density. These films are also mechanically superior and more resistant to scratching than the lower temperature films. However in some circumstances the variation in properties could be utilized. For example if a low

temperature film were deposited, a laser or electron beam could selectively anneal areas into the higher temperature form and the lower temperature deposit could be easily etched away.

The ability to deposit materials with different refractive indices from the same precursor could be useful e.g. a graded refractive index could be manufactured.

8.4 TITANIUM-VANADIUM MIXED OXIDE FILMS.

8.4.1 INTRODUCTION

Oxide films containing different proportions of titanium and vanadium oxide have been grown and characterised as described in chapters 6 and 7. The thermal decomposition of the vanadium triisopropoxide oxide was observed to differ from that of the titanium isopropoxide as shown in figures 4.3 and 4.1 respectively. The mass loss of the vanadium triisopropoxide oxide occurred in one distinct stage and was complete by about 120^{o}C; the titanium isopropoxide decomposed in two distinct stages and the decomposition was only completed by 250^{o}C. Hence the two precursors used in these experiments differed in their decomposition behaviour. The apparently more facile decomposition of the vanadium triisopropoxide oxide was probably the reason for a higher proportion of vanadium oxide being deposited in the solid film than was present in the precursor solution (figure 6.1). The precursor solution contained both titanium isopropoxide and vanadium triisopropoxide oxide in anhydrous cyclohexane. No visible interaction occurred between the two precursors but it would have been interesting to observe the thermal decomposition of mixtures of both compounds by DTA/TGA because some interaction

during decomposition could occur. The vanadium triisopropoxide oxide appeared to have a stronger interaction than the titanium isoproproxide with the irradiation from the mercury arc lamp and a solid deposit was observed on the liquid quartz interface where the solution had been illuminated. As with the titanium isopropoxide, the exact nature of the light interaction is unknown. The DTA/TGA results for the decomposition of the vanadium triisopropoxide oxide (figure 4.3) showed a small but continuous weight loss of the vanadium oxide which suggested a loss of oxygen content. Heating the oxide in a nitrogen atmosphere caused the colour to change from green to black; the green oxide was tentatively identified as vanadium dioxide and the black oxide as V_2O_3.

All deposition of mixed oxides was carried out at a substrate temperature of 250°C. At this deposition temperature the titanium dioxide films were anatase and decomposition of both precursors should be complete. Only one decomposition temperature was investigated due to lack of time.

8.4.2 STRUCTURE OF TITANIUM-VANADIUM MIXED OXIDE FILMS

The structure of some of the titanium-vanadium mixed oxide films was investigated by electron diffraction as reported in section 7.2. None of the films containing vanadium oxide were as highly crystalline as titanium dioxide films grown at the same temperature. The 20% and 53% vanadium oxide films produced amorphous diffraction patterns (figures 7.20a&b), but sharper reflections were obtained with the 78%, 90% and 100% vanadium samples (figures 7.20c-e). These reflections were tentatively identified as vanadium dioxide which appeared to be the closest

match. Mixed vanadium-titanium oxide films grown by sputtering (Balberg et al.,1974), were also found to be of low crystallinity with the vanadium dioxide lines becoming weaker with increasing titanium content and the titanium dioxide lines being too weak to be observed.

The crystallinity of the titanium dioxide is reduced on addition of vanadium oxide. This may be due to the presence of the vanadium oxide species on the surface may inhibiting the mobility of the titanium oxide species and the chances of finding a lattice site could be lowered.

8.4.3 PROPERTIES OF VANADIUM-TITANIUM MIXED OXIDE FILMS.

The properties of mixed vanadium-titanium oxide films have been investigated as described in chapters 6 and 7. In the case of the titanium dioxide films, the properties were found to be strongly dependent on the crystal structure of the deposit, however in this series of specimens a strong dependence on chemical composition was observed.

The refractive index values of the mixed oxide films were higher than those of the single titanium or vanadium oxides (figure 7.44). The reason for this increase is unclear but the property could be useful if a higher refractive index is required.

A large change in dielectric properties was observed with varying composition of the oxide films (section 7.4.2.2). The dc conductivity was higher with increasing vanadium content (figure 7.41). The exact nature of the conduction mechanism is unknown but the value of activation energy for the process was of the order of 10^{-1}eV, which is typical of electronic rather than

ionic conducting species. Films of reactively sputtered vanadium dioxide films grown at 400°C (Fuls et al.,1967) had an activation energy of 0.28eV below 336K which is higher than the value for vanadium oxide measured in the present work. Electrical conductivity measurements on single crystals of the system $V_{1-x}W_xO_2$ in the composition range 0.006 x 0.052 (Horlin et al.,1972), gave an activation energy of 0.096eV, but the activation energy of vanadium dioxide was 0.46eV. Hence a range of activation energies have been measured. The difference in values may be due to the variations in crystal quality, impurity or stoichiometry resulting from the preparation technique.

The magnitude of electrical conductivity depends on the number of charge carriers and on the mobility of the carriers in the material; these two contributions cannot be separated in the present results. The increasing value of conductivity of the oxide sample with vanadium content led to the observation of barrier effects in the 85 and 100% vanadium films as explained in section 7.4.2.2.

The shifts in frequency response of the samples were measured as a function of testing temperature and the activation energies calculated. The value of activation energy was found to decrease with increasing vanadium content from typically 0.6eV for titanium dioxide to 0.12eV for vanadium dioxide as shown in figure 7.42. The thermally activated part of the dielectric response is due to large transitions e.g. transition 'a' in figure 7.27, which is typically a dipole. The reduction in activation energy with increasing vanadium content indicates that the dipole movement becomes easier, the opposing forces

from the environment are lower.

The loss peaks of the titanium dioxide, 20% and 53% vanadium samples became narrower and the value of the exponent 'n' decreased with increasing vanadium content. The value of the 'n' exponent is concerned with the efficiency of structural re-ordering on a local scale after dipole movement. A value of zero is the Debye response with no interactions; as the interaction between the dipoles is increased and many-body interactions become important, the value of 'n' increases and the dipole movement becomes progressively more dissipated.

The etching rate of the titanium-vanadium mixed oxide films was measured in concentrated sulphuric acid maintained at 100°C as described in section 7.5.2. From the results presented in figure 7.44, the etch rate can be seen to increase by three orders of magnitude from titanium dioxide to vanadium dioxide; this is a far greater difference than the change in etching rate of titanium dioxide with change in growth temperature as shown in figure 7.43. In the case of titanium dioxide the changes were predominantly structural rather than chemical (although some compositional change may be considered with the incorporation of intermediate compounds in the lattice at low temperatures). With the mixed oxide films the difference in chemical composition is the major contribution to the variation in etching rate with vanadium oxide being much more reactive with the sulphuric acid than the titanium dioxide. Certain structural changes in the lattice will occur due to incorporation of ions of a different size and this may contribute to a lesser extent to the enhanced etching rate observed. The results plotted in figure 7.44 indicate that the photolysed samples have a higher etch rate than

the non-photolysed samples. To confirm this trend, further measurements need to be carried out. From the experiments with irradiating the vanadium triisopropoxide oxide in chapter 4, the compound was found to actually decompose on exposure to the UV and it might be expected that an increased vanadium content could be deposited due to the irradiation which would enhance the etch rate; however the compositional analysis of the films (figure 6.1) did not show this to be the case in the deposition conditions investigated.

The investigation into the Ti-V-O system has been of a preliminary nature with only one deposition temperature being studied. To thoroughly characterise the system a range of temperature and growth rates needs to be used and a greater number of samples measured. The sudden change of electrical conductivity of the vanadium oxide with temperature, which was the original driving force for much of the research into the system as discussed in section 2.3 has not been investigated in the present study. However, it has been demonstrated that the reactor can be used to deposit mixed oxides.

The full potential of the reactor however, has not been utilized in the present work; it is capable of injecting precursors with different volatilities because the vaporisation heaters can be individually controlled and a graded oxide layer could be grown by varying the injection rate of one or more precursors (computer control would be required for this).

There is a lot of potential for depositing oxides by this technique which has the flexibility to accomodate higher temperatures, lower pressures and deposition of many other materials.

CONCLUSIONS

The work presented in this thesis has progressed from the design and development of the reactor and a simple investigation into the decomposition of the precursor compounds used, to a study of the parameters influencing the titanium dioxide growth rate and the properties of the films grown under different conditions and with varying titanium- vanadium compositions. The conclusions that can be drawn from the investigation are:

(1) The design of reactor incorporating a liquid injection system and atomisation unit has worked successfully and oxide films of titanium dioxide have been grown at different substrate temperatures and with different precursor injection rates. The use of the reactor for growing mixed oxide films has been shown for the Ti-V-O system using titanium isopropoxide and vanadium triisopropoxide oxide as precursors.

(2) The thermal decomposition of the precursors studied by DTA/TGA provided a rough guide to the growth temperatures which would give complete decomposition.

(3) The alkoxides showed some reaction to the emmission from the 100W mercury arc lamp in the liquid state and enhanced growth of titanium dioxide was observed at the lower growth temperatures when the process was kinetically dominated.

(4) The growth rate of titanium dioxide increased with increase in substrate temperature; at the lower temperatures decomposition was kinetically controlled, and at the higher temperatures, mass transport controlled. Irradiation of the growth surface enhanced the growth in the kinetically controlled regime and reduced the activation energy by 0.16eV for both the injection rates investigated. Photolysis did not affect the

growth rate when mass transport was the rate controlling step and this led to effective photolysis at high precursor concentrations, but not at low concentration for the same growth temperature.

(5) Growth rate increased for increasing precursor concentrations especially in the mass transport controlled conditions. The efficiency of the process was calculated for growth of titanium dioxide at 350°C and varied from 18 to 26% with changing alkoxide injection rate.

(6) A few measurements of growth rate as a function of carrier gas flow rate showed that growth rate decreased with increasing gas flow rate. This was probably due to the decrease in time a molecule spent in the reactor with increasing gas velocity.

(7) The crystal structure of titanium dioxide varied from amorphous to oriented anatase with substrate temperature increasing from 100 to 400°C. There was evidence for the presence of intermediate compounds in the films up to approximately 200°C. The crystal structure was reflected in the properties of the films. The lower temperature deposits which were more amorphous showed a varying refractive index (increasing with higher substrate temperature), unstable dielectric properties and higher etch rates, whereas the higher temperature deposits had a reasonably stable refractive index and dielectric properties and the etching rate was much lower.

(8) The mixed vanadium-titanium oxide films were grown over the whole composition range at 250°C and a higher vanadium content was present in the deposited film than in the precursor solution. The properties of the mixed oxide films were strongly dependent on composition. The crystal structures were less crystalline

than the titanium dioxide films grown at the same temperatures. Refractive index measurements indicated a higher value for the mixed composition films than for either of the single oxides, the electrical conductivity was increased and dipole movement easier as the vanadium content increased, and the etching rate increased by three orders of magnitude from titanium dioxide to vanadium dioxide.

SUGGESTIONS FOR FURTHER WORK

The work carried out in the thesis has characterised the titanium dioxide films grown from titanium isopropoxide and preliminary investigation into the properties of the mixed titanium-vanadium oxide films has been carried out. There is a lot of interesting work that can be undertaken in this field, both on the development of the reactor to a more sophisticated level and on the materials deposited.

The present reactor reaches a maximum substrate temperature of 400°C. This is satisfactory if only low temperature growth of oxides is required, but there are occasions where a higher temperature may be needed. In the titanium dioxide system for example, the rutile modification would probably be deposited if the substrate temperature were higher.

The electrostatic atomisation utilized in the liquid injection of the precursor produced a spray that was electrically charged. Fully charging the incoming vapour to the main reactor chamber could provide a way of 'switching' growth on and off by using electrodes to attract or repel the charged species. This would be useful if sharp compositional changes or very thin layers were required.

Automatic control of the stepper motor rates to grow a graded oxide layer could be developed. Automating all the growth runs would provide a greater degree of control and reproducibility over the process.

There are numerous uses for thin oxide layers of various types at the present time, which include the superconducting oxides, ferroelectric oxides, oxides for passivation, capacitor films, gas sensors and hard coatings. Hence many diverse research

interests are concerned with the production of thin oxide films. Considering just the area of electronics, there is a need for high quality thin oxide layers to be grown at a low temperature. Further work into different oxide systems, perhaps attempting to grow epitaxially onto the single crystal semiconductor would be interesting as would growing the semiconductor, oxide and metallic layers in the one reactor.

Andrews, R.W., Rynne, D.M. & Wright, E.G.(1969) Solid State Tech. 10 61.

Arnone, C., Rothschild, M., Black, J.G. & Ehrlich, D.J.(1986) Appl. Phys. Lett. 48 (15) 1018.

Bailey, A.G. (1974) Sci. Progr. 61 555.

Balberg, I., Abeles, B. & Arie, Y.(1974) Thin Solid Films, 24 307.

Balberg, I. & Roach, W.R.(1971) Proc. Int. Conf. on Conductivity in Low Mobility Materials, Taylor & Francis, London p.77. (ref. taken from Greenberg, (1983)).

Balog, M., Schieber, M., Patai, S. & Michman, M.(1972) J. Cryst. Growth 17 298.

Ban, V.S.(1978) J. Electrochem. Soc. 125 317.

Ban, V.S. & Gilbert, S.L.(1975) J. Cryst. Growth 31 284.

Bertrand, P.A.& Fleischauer, P.D.(1983) Thin Solid Films 103 167.

Blandenet, G., Count, M. & Lagarde, Y.(1981) Thin Solid Films 77 81.

Bose, G.M. (1745)'Recherches sur la cause et sur la veritable theorie de l'electricite', Wittenberg.

Boyer, P.K., Roche, G.A., Ritchie, W.H. & Collins, G.J. (1982) Appl. Phys. Lett. 40(8) 716.

Bradley, D.C., Mehrotra, R.C. & Gaur, D.P. (1978) 'Metal Alkoxides' Academic Press.

Bradley, D.C. & Faktor, M.M. (1959a) Trans. Faraday Soc. 55 2117.

Bradley, D.C. & Faktor, M.M. (1959b) J. Appl. Chem. 9 435.

Brierley, C. (1987) BACG Newsletter Sept. p.3.

Chuang, T.J. (1982) J. Vac. Sci. Tech. 21 798.

Debye, P. (1912) Z.Phys. 13 97.

Debye, P. (1945) 'Polar Molecules' (New York:Dover).

Dissado, L.A. & Hill, R.M. (1979) Nature 279 685.

Drozin, V.G. (1955) J. Colloid Sci. 10 158.

Eversteyn, F.C., Severin, P.J.W., v.d.Brekel, C.H.J. & Peek, H.L. (1970) J. Electrochem. Soc. 117 925.

Feuersanger, A.E. (1964) Proc. IEEE 52 1463.

Fitzgibbons, E.T., Sladek, K.J.& Hartwig, W.H. (1972) J. Electrochem. Soc. 119 735.

Fuls, E.N., Hensler, D.H. and Ross, A.R. (1967) Appl. Phys. Lett. 10 199.

Fuyuki, T., Kobayashi, T. & Matsunami, H. (1988) J. Electrochem. Soc. 135 248.

Ghoshtagore, R.N. & Noreika, A.J. (1970) J. Electrochem. Soc. 117 1310.

Giling, L.J. (1982) J. Electrochem. Soc. 129 634.

Giling, L.J. (1983) Lecture Notes for Fifth International Summer School on Crystal Growth, Dagos.

Greenberg, C.B. (1983) Thin Solid Films, 110 73.

Griffith, C.H. & Eastwood, H.K. (1974) J. Appl. Phys. 45 2201.

Haigh, J. (1983) J. Materials Sci. 18 1072.

Hardee,. K.L. & Bard, A.J. (1975) J. Electochem. Soc. 122 739.

Haslam, J.H. (1959) 'Metal Organic Compounds', Advances in Chemistry Series, 23 Am. Chem. Soc. Washington DC.

Hass, G. (1952) Vacuum 11(4) 331.

Hayashi, S. & Hirai, T. (1976) J. Cryst. Growth 36 157.

Hendricks, C.D. (1962) J. Colloid Sci. 17 249.

Hendricks, C.D., Carson, R.S., Hogan, J.J. & Schreider, J.M. (1964) AIAA JL 4 733. - taken from Bailey (1974).

Hill, R.M. (1981) J. Mater. Sci. 16 118.

Hill, R.M. & Jonscher, A.K. (1983) Contemp. Phys. 24 75.

Hill, R.M. & Pickup, C. (1985) J. Mater. Sci. 20 4431.

Hitchman, M.L. (1980) J. Cryst. Growth 48 394.

Hitchman, M.L. (1981) Progress in Cryst. Growth and Characterisation, Ed. B.R. Pamplin, Pergamon Press. Oxford.

Hough, R.L. (1972) CVD Third International Conference (F.A.Glaski ed.) Am. Nucl. Soc., Hinsdale Illinois.

Horlin, T., Niklewski, T. & Nygren, M. (1972) Mat. Res. Bull. 7 1515.

Hovel, H.J. (1978) J. Electrochem. Soc. 125 983.

Jonscher, A.K. (1975) Colloid. Polym. Sci. 253 231.

Jonscher, A.K. (1980) Phys. Thin Films 11 205.

Jonscher, A.K. (1983) 'Dielectric Relaxation in Solids' Chelsea Dielectric Press, London.

Knollenberg, R.G. (1976) Preprint Vol. International Conference on Cloud Physics July 26-30 Boulder Colo. American Meteorological Soc. Boston Mass.

Kozhenkov, V.I. & Fuks, N.A. (1976) Russ. Chem. Rev. 45 12.

Kumagawa, M., Sunami, H., Terasaki, T. & Nishizawa, J. (1968) Jpn. J. Appl. Phys. 7 1332.

Levy, R.A., Gallagher, P.K. & Schrey, F. (1987) J. Electrochem. Soc. 134 430.

Lewis, B. & Anderson, J.C. (1978) 'Nucleation and Growth of Thin Films'. Academic Press.

Lewis, B. & Stirland, D.J. (1968) J. Cryst. Growth 3,4 200.

MacChesney, J.B., Potter, J.F. & Guggenheim, H.J. (1968) J. Electrochem. Soc. 115 52.

Mazdiyasni, K.S., Lynch, C.T. & Smith, J.S. (1965) J. Am. Cer. Soc. 48(7), 372.

Mori, Y. (1961) J. Heat Trans. 83 479.

Morin, F.J. (1959) Phys. Rev. Lett. 3 34.

Perry (1953) 'Chemical Enginneers' Handbook. Third Edition p.293.

Pugh,J (1984) IEE Conf. DMMA Lancaster, Autumn.

Pugh, J. & Ryan, J.T. (1979) IEE Conf. Pub. No. 177 404.

Prandtl, L. (1904) 'Uber Flussigkeitsbewegung bei sehr kleiner Reibung. Proc.III Intern. Math. Cong. Heidelberg. -taken from Schlichting (1955).

Peters, J.W. (1981) Proc. IEDM Washington p.240.

Powell, C.F., Oxley, J.H. & Blocher Jr. J.M. (1966) ' Vapour Deposition' (Wiley, New York/Sidney).

Lord Rayleigh (1882) Phil. Mag. Series 5 14 184.

Rozgonyi, G.A. & Hensler, D.H. (1968) J. Vac. Sci and Tech. 5 194.

Ryabova, L.A., Servinov, I.A. & Darevsky, A.S. (1972) J. Electrochem. Soc. 119 427.

Ryce, S.A. (1964) J. Colloid Sci. 19 490.

Sample, S.B. & Bollini, R.(1972), J. Colloid Interface Sci. 41(2) 185.

Schlichting, H. (1955) 'Boundary Layer Theory' Pergamon Press Ltd.

Schweizer, J.W. & Hanson, D.N. (1971) J. Colloid Interface Sci. 35 417.

Shannon, R.D. & Pask, J.A. (1965) J. Am. Cer. Soc. 48 391.

Sladek, K.J. & Gibert, W.W.(1972) Proc. Third Intern. Conf. on CVD, Ed. F.A. Glaski, Am. Nucl. Soc. 215.

Solanki, R., Ritchie, W.H. & Collins, G.J. (1983) Appl. Phys. Lett. 43(5), 454.

Sparrow, E.M., Eichhorn, R. & Gregg, J.L. (1959) Phys. Fluids 2 319.

van Steensel, K., van de Berg, F. & Koof, C. (1967) Philips Res. Repts. 22, 170.

Takahashi, R., Koga, Y. & Sagawara, K. (1972) J. Electrocham. Soc. 119, 1406.

Takahashi, Y., Suzuki, H. & Nasu, M. (1985) J. Chem. Soc. Faraday Trans. 1 81 3117.

Takahashi, Y., Tsuda, K., Sugiyama, K., Minoura, H., Makino, D. & Tsuiki, M. (1981) J. Chem. Soc. Faraday Trans. 1 77 1051.

Vergard, L. (1916) Phil. Mag. 32 505.

Vonnegut, B. & Neubauer, R.L. (1952) J. Colloid Sci. 7 616.

Wang, C.C., Zaininger, K.H. & Duffy, M.T. (1970) RCA Rev. 728.

Westphal, G.H. (1983), J. Cryst. Growth 65 105.

Wojcik, A.G. (1985) Private Communication.

Yamada, Y. & Yoshida, K. (1979) Sur. Sci. 86 161.

Yeung, K.S. & Lam, Y.W. (1983) Thin Solid Films 103 167.

Yokozawa, M., Iwasa, H.& Teramoto, I. (1968) Jpn. J. Appl. Phys. 7, 96.